

Exploring Plant Responses to Changing Environments: Integrating Phenotyping and Modeling Across Scales

Dissertation

zur Erlangung des Grades

Doktor der Ingenieurwissenschaften (Dr.-Ing.)

der Agrar-, Ernährungs- und Ingenieurwissenschaftlichen Fakultät

der Rheinischen Friedrich-Wilhelms-Universität Bonn

von

Felix Maximilian Bauer

aus

Bonn, Deutschland

Bonn 2025

Referentin:

Prof. Dr. Andrea Schnepf, Rheinische Friedrich-Wilhelms-Universität Bonn,
Deutschland

1. Korreferent:

Prof. Dr. Gabriel Schaaf, Rheinische Friedrich-Wilhelms-Universität Bonn,
Deutschland

2. Korreferent:

Prof. Dr. Guillaume Lobet, Université catholique de Louvain, Belgien

Tag der mündlichen Prüfung: 16.12.2024

Angefertigt mit Genehmigung der Agrar-, Ernährungs- und Ingenieurwis-
senschaftlichen Fakultät der Universität Bonn

Science is not finished until it's communicated.

SIR MARK WALPORT

Abstract

CLIMATE CHANGE and the depletion of essential resources like phosphorus are challenging agriculture by reducing water and fertilizer availability and ultimately threatening the security of the human food supply. Knowledge of how plants respond to changing environmental conditions is required to cope with these challenges. Plant growth information and corresponding environmental data are key to unraveling stress responses and revealing the underlying mechanisms. Understanding architectural and functional plant adaptations to stresses, such as water and nutrient limitation, is crucial to exploring new pathways to sustainable agriculture. It is vital to consider all organs, including the often-overlooked root system and surrounding soil, that are essential for water and nutrient uptake. Plant phenotyping and functional-structural plant modeling are key technologies for understanding plant responses to changing environments, making their continued development and application imperative. This doctoral project is dedicated to advancing the field of plant research by 1. developing a novel *in situ* phenotyping method for roots, 2. applying this method to assemble a comprehensive collection of in-field root and soil data, 3. investigating the architectural responses of *Zea mays* to phosphorus deficiency, 4. gaining a deeper understanding of the responses to stress by investigating the effects of phosphorus deficiency on the root system's conductance, and 5. placing the findings into an overall context.

First, a new method combining deep neural networks and automated feature extraction was developed and validated to analyze root images, reducing processing time by 98% while achieving high precision compared to manual annotation ($r=0.9$). Second, besides other technologies, this method was applied to assemble a comprehensive collection of in-field root and soil data over time in two minirhizotron facilities in distinct soil domains. The resulting open-access, time-series dataset includes dynamic crosshole ground-penetrating radar, minirhizotron camera measurements, and static soil sensor observations at a high temporal and spatial resolution over five years of *Zea mays* and *Triticum aestivum* experiments, including drought stress treatments and crop mixtures trials. Third, a combined approach of the developed phenotyping workflow and functional-structural plant

modeling was used to investigate the responses of *Zea mays* to varying phosphorus availability. Combining measured architectural plant parameters with root hydraulic properties enabled time-dependent simulations of plant growth and root system conductance under different phosphorus regimes, revealing that only plants with optimal phosphorus availability sustained a high root system conductance. In contrast, all other phosphorus levels led to significantly lower root system conductance under light and severe phosphorus deficiency. It was also shown that root system organization is critical for its function rather than mere total size. Finally, this thesis contributes to collaborative studies aiming to enhance phenotyping methods and further investigate *Zea mays* responses to environmental changes. We found that ground-penetrating radar could be employed as a root-sensing tool in the future. By linking aboveground crop data to the belowground dataset, we revealed that maize responses to water stress vary significantly with soil conditions. We combined the automated analysis method with functional-structural modeling to show that *Zea mays* domestication was driven by water availability, with seminal root number emerging as a critical adaptation trait, possibly providing key information for breeding drought-tolerant varieties. Lastly, we applied an *in silico* approach using a game engine that visualizes plant models in high-performance computing environments to generate virtual data for neural networks, enhancing their precision and informative power.

This work explores different methods, data, and models to understand plant responses to a changing environment across scales and provides new insights into the combined stress responses and development of *Zea mays*.

Zusammenfassung

DER KLIMAWANDEL und die Verknappung wichtiger Ressourcen, wie Phosphor, stellen die Landwirtschaft vor Herausforderungen, da sie die Verfügbarkeit von Wasser und Düngemitteln verringern und letztlich die Sicherheit der menschlichen Nahrungsmittelversorgung gefährden. Um diese Herausforderungen zu meistern, ist es notwendig, zu verstehen, wie Pflanzen auf sich ändernde Umweltbedingungen reagieren. Informationen über das Pflanzenwachstum und korrespondierende Umweltdaten sind entscheidend, um Stressreaktionen zu entschlüsseln und die zugrundeliegenden Mechanismen aufzudecken. Das Verständnis der strukturellen und funktionellen Anpassungen von Pflanzen an Stressfaktoren wie Wasser- und Nährstoffmangel ist entscheidend, um neue Wege hin zu einer nachhaltigeren Landwirtschaft zu finden. Dabei müssen alle Organe, einschließlich des Wurzelsystems, das für die Aufnahme von Wasser und Nährstoffen unerlässlich ist, berücksichtigt werden. Pflanzenphänotypisierung und funktionell-strukturelle Pflanzenmodellierung sind Schlüsseltechnologien für ein besseres Verständnis der Reaktionen von Pflanzen auf sich ändernde Umweltbedingungen, was die Fortentwicklung und Anwendung dieser Methoden unerlässlich macht. Dieses Promotionsprojekt widmet sich dem Fortschritt der Pflanzenwissenschaften durch 1. Entwicklung einer neuartigen *in situ* Phänotypisierungsmethode für Wurzeln, 2. Anwendung dieser Methode zur Zusammenstellung eines umfassenden Datensatzes von Wurzel- und Bodendaten, sowie 3. Identifizierung struktureller Veränderungen von *Zea mays* unter Phosphormangel, 4. Vertiefung des Verständnisses der Reaktionen auf Stress durch Untersuchung der Auswirkungen von Phosphormangel auf die Wurzelsystemleitfähigkeit, und 5. dem Einordnen der Ergebnisse dieser Arbeit in einen globaleren Kontext.

Erstens wurde eine neue Methode zur Analyse von Wurzelbildern entwickelt und validiert, die tiefe neuronale Netzwerke und automatisierte Merkmalextraktion kombiniert, welches die Bearbeitungszeit um 98% reduzierte und gleichzeitig eine hohe Präzision im Vergleich zur manuellen Annotation erreichte ($r=0,9$).

Zweitens wurde diese Methode zusammen mit anderen Technologien verwendet, um einen umfassende Datensatz von Wurzel- und Bodendaten über einen bestimmten Zeitraum in verschiedenen Bodenbereichen zu sammeln. Der resultierende Datensatz umfasst dynamische Crosshole-Bodenradarmessungen, Minirhizotron-Kameramessungen und statische Bodensensorbeobachtungen mit hoher zeitlicher und räumlicher Auflösung. Der resultierende Datensatz umfasst fünf Jahre *Zea mays*- und *Triticum aestivum*- Experimente, einschließlich Trockenstress- und Sortenmischungsversuchen. Drittens wurde ein kombinierter Ansatz des entwickelten Phänotypisierungs-Workflows und funktioneller-struktureller Pflanzenmodellierung verwendet, um die Reaktionen von *Zea mays* auf unterschiedliche Phosphorverfügbarkeiten zu untersuchen. Die Kombination von gemessenen architektonischen Pflanzenparametern mit hydraulischen Eigenschaften des Wurzelsystems, ermöglichte zeitabhängige Simulationen des Pflanzenwachstums und der Leitfähigkeit des Wurzelsystems unter verschiedenen Phosphorstufen und zeigte, dass nur Pflanzen mit optimaler Phosphorverfügbarkeit eine hohe Leitfähigkeit des Wurzelsystems aufrechterhielten. Im Gegensatz dazu, führten alle anderen Phosphormengen zu einem signifikanten Rückgang der Leitfähigkeit des Wurzelsystems bei leichtem sowie schwerem Phosphormangel. Zuletzt kombiniert diese Dissertation mehrere kollaborative Ansätze, um Phänotypisierungsmethoden zu verbessern und die Reaktionen von *Zea mays* auf Umweltveränderungen weiter zu untersuchen. Wir fanden heraus, dass das Bodenradar in Zukunft als Wurzelphänotypisierungsmethode im Feld eingesetzt werden könnte. Durch die Verknüpfung von oberirdischen Pflanzendaten mit dem unterirdischen Datensatz, konnten wir zeigen, dass die Reaktionen von Mais auf Wasserstress erheblich mit den Bodenbedingungen variieren. Eine Kombination der automatisierten Analysemethode mit funktionell-struktureller Modellierung zeigte zudem, dass die Domestikation von *Zea mays* abhängig von der Wasserverfügbarkeit war, wobei die Anzahl der seminalen Wurzeln als ein entscheidendes Anpassungsmerkmal identifiziert wurde. Diese Erkenntnisse liefern möglicherweise wichtige Informationen für die Züchtung dürreresistenter Sorten. Schließlich, wurde ein *in silico* Ansatz, der eine Computerspiel-Engine und Pflanzenmodelle kombiniert, entworfen, um virtuelle Daten für neuronale Netzwerke zu generieren und deren Präzision und Aussagekraft zu erhöhen.

Diese Arbeit kombiniert verschiedene Methoden, Daten und Modelle, um die Reaktionen von Pflanzen auf eine sich verändernde Umwelt auf verschiedenen Skalen zu erforschen und damit neue Einblicke in kombinierte Stressreaktionen und die Entwicklung von *Zea mays* zu gewinnen.

Preface

Welcome, dear reader!

The journey that has brought us to the point where you are reading this thesis began exactly 10 years ago. It all started with the simple idea of contributing to the most essential yet underexplored field for humanity - agriculture. Driven by this goal, I pursued a Bachelor's in Agriculture, followed by a Master's in Crop Science, and am now working towards a Ph.D., eager to learn everything that will bring me closer to achieving it.

As my journey continues, I invite you to join me in my quest to discover some of the elusive secrets of the verdant but partially buried kingdom of plants. Together, we will explore innovative methods to detect the hidden half of plants, excavate groundbreaking data treasures, and unleash powerful models to deepen our understanding of plant responses to a changing environment. All of this ties into the overarching goal: refining how we measure and understand plant structures and functions.

Now, as we finally embark on this journey, it is essential to acknowledge that while this thesis is primarily my work, it has been significantly shaped by the invaluable contributions of many others. Rather than keeping you in suspense, let us dive straight into the heart of the thesis. The acknowledgments for all who have supported this journey will be reserved for the end of this work, where their contributions can be properly recognized and sincerely appreciated.

With that in mind, let us jump in and start this adventure together!

Jülich
30.08.2024

Felix Maximilian Bauer

List of Publications

AT THE TIME of finalizing the dissertation for this doctoral project, parts of this work have been published in or submitted to scientific journals and contributed to scientific meetings as specified below. Chapters 2 - 4 are based on the publications numbered 1 - 3, respectively. Chapter 5 synthesizes information from the publications numbered 4 - 9. Appendices A, B, and C are supplementary information to Chapters 2, 4, and 5. Appendices D - H are based on the publications numbered 10 - 14, respectively.

Core Publications

- 1. Felix Maximilian Bauer**, Lena Lärm, Shehan Morandage, Guillaume Lobet, Jan Vanderborght, Harry Vereecken, Andrea Schnepf (2022). Development and validation of a deep learning based automated minirhizotron image analysis pipeline. *Plant Phenomics*, 2022. <https://doi.org/10.34133/2022/9758532>
- Lena Lärm*, **Felix Maximilian Bauer***, Normen Hermes, Jan van der Kruk, Harry Vereecken, Jan Vanderborght, Thuy Huu Nguyen, Gina Lopez, Sabine Julia Seidel, Frank Ewert, Andrea Schnepf and Anja Klotzsche (2023): Multi-year belowground data of minirhizotron facilities in Selhausen. *Scientific Data* 10, 672. <https://doi.org/10.1038/s41597-023-02570-9>
(*contributed equally to this publication)
- 3. Felix Maximilian Bauer**, Dirk Norbert Baker, Mona Giraud, Juan Carlos Baca Cabrera, Jan Vanderborght, Guillaume Lobet, Andrea Schnepf (2024). Root system architecture reorganization under decreasing soil phosphorus lowers root system conductance of *Zea mays*. *Submitted to Annals of Botany*.

Contributing Publications

4. Lena Lärm, **Felix Maximilian Bauer**, Jan van der Kruk, Jan Vanderborght, Shehan Morandage, Harry Vereecken, Andrea Schnepf, Anja Klotzsche (2024). Linking horizontal crosshole GPR variability with root image information for maize crops. *Vadose Zone Journal*, 23, e20293. <https://doi.org/10.1002/vzj2.20293>.
5. Peng Yu, Chunhui Li, Meng Li, Xiaoming He, Danning Wang, Hongjie Li, Caroline Marcon, Yu Li, Sergio Perez-Limón, Xinpeng Chen, Manuel Delgado-Baquerizo, Robert Koller, Ralf Metzner, Dagmar van Dusschoten, Daniel Pflugfelder, Ljudmilla Borisjuk, Iaroslav Plutenko, Audrey Mahon, Marcio F.R. Resende Jr., Silvio Salvi, Asegidew Akale, Mohammed Abdalla, Mutez Ali Ahmed, **Felix Maximilian Bauer**, Andrea Schnepf, Guillaume Lobet, Adrien Heymans, Kiran Suresh, Lukas Schreiber, Chloe M. McLaughlin, Chunjian Li, Manfred Mayer, Chris-Carolin Schön, Vivian Bernau, Nicolaus von Wirén, Ruairidh J. H. Sawers, Tianyu Wang, Frank Hochholdinger. Seedling root system adaptation to water availability during maize domestication and global expansion (2024). *Nature Genetics* 56, 1245–1256. <https://doi.org/10.1038/s41588-024-01761-3>.
6. Thuy Huu Nguyen, Thomas Gaiser, Jan Vanderborght, Andrea Schnepf, **Felix Maximilian Bauer**, Anja Klotzsche, Lena Lärm, Hubert Hüging, Frank Ewert (2024). Responses of field-grown maize to different soil types, water regimes, and contrasting vapor pressure deficit. *Biogeoscience*. <https://doi.org/10.5194/egusphere-2023-2967>.
7. Thuy Huu Nguyen, Gina Lopez, Sabine J. Seidel, Lena Lärm, **Felix Maximilian Bauer**, Anja Klotzsche, Andrea Schnepf, Thomas Gaiser, Hubert Hüging, Frank Ewert (2024). Multi-year aboveground data of minirhizotron facilities in Selhausen. *Sci. Data* 11, 674. <https://doi.org/10.1038/s41597-024-03535-2>.
8. Dirk Norbert Baker, **Felix Maximilian Bauer**, Mona Giraud, Andrea Schnepf, Jens Henrik Göbbert, Hanno Scharr, Ebba Pora Hvannberg, Morris Riedel (2024). A scalable pipeline to create synthetic datasets from functional–structural plant models for deep learning. *in silico Plants*, Volume 6, Issue 1, diad022. <https://doi.org/10.1093/insilicoplants/diad022>.
9. Dirk Norbert Baker, **Felix Maximilian Bauer**, Andrea Schnepf, Hanno Scharr, Morris Riedel, Jens Henrik Göbbert, Ebba Pora Hvannberg (2024). Adapting agricultural virtual environments in game Engines to improve HPC accessibility. *Communications in Computer and Information Science*. <https://doi.org/10.34734/FZJ-2024-03386>.

Proceedings

10. **Felix Maximilian Bauer**, Guillaume Lobet, Dirk Norbert Baker, Anna Galisnki, Zamiga Kahlilova, Lisa Zander, Peng Yu, Gabriel Schaaf, Andrea Schnepf. *In silico* investigation on phosphorus efficiency of *Zea mays*: An experimental whole plant model parametrization approach. Poster at *10th International Conference on Functional-Structural Plant Models (FSPM2023)*. <https://doi.org/10.34734/FZJ-2023-04032>.
11. **Felix Maximilian Bauer**, Mona Giraud, Dirk Norbert Baker, Guillaume Lobet, Andrea Schnepf. Modelling architectural and functional response of *Zea mays* to phosphorus deficiency based on experimental data. Presentation at *Plant Biology*, Savannah, GA, USA, 5 Aug 2023 - 9 Aug 2023. <https://juser.fz-juelich.de/record/1017292>.
12. **Felix Maximilian Bauer**, Lena Lärm, Normen Hermes, Harry Vereecken, Jan Vanderborght, Andrea Schnepf, Anja Klotzsche. The selhausen minirhizotron facilities: A unique set-up to investigate subsoil processes within the soil-plant continuum. Poster at *TERENO-OZCAR Conference 2023*. <https://doi.org/10.34734/FZJ-2023-04033>.
13. **Felix Maximilian Bauer**, Lena Lärm, Normen Hermes, Harry Vereecken, Jan Vanderborght, Jan van der Kruk, Thuy Huu Nguyen, Gina Lopez, Sabine Julia Seidel, Frank Ewert, Anja Klotzsche, Andrea Schnepf. Unrevealing subsoil processes in the selhausen minirhizotron facilities: Comprehensive insights into the soil-plant continuum with a new unique dataset. Poster at *AGU Fall Meeting, AGU23*, San Francisco, USA, 11 Dec 2023 - 15 Dec 2023. <https://juser.fz-juelich.de/record/1020308>.
14. **Felix Maximilian Bauer**, Mona Giraud, Dirk Norbert Baker, Guillaume Lobet, Andrea Schnepf. Functional-structural plant modelling based on experimental data reveals that soil phosphorus status influences root system conductance. Presentation at *International Society of Root Research 12th International Symposium (ISRR 2024)*, Leipzig, Germany, 2 Jun 2024 - 7 Jun 2024.

Note about the thesis structure

This thesis brings together both published and unpublished work. So, to those brave enough to read the entire document, I apologize in advance for any déjà vu moments — you have been warned!

Table of Contents

Abstract	v
Zusammenfassung	vii
Preface	ix
List of Publications	xi
List of Figures	xxiii
List of Tables	xxvi
Abbreviations	xxvii
1 Introduction	3
1-1 Changing environmental conditions and the implications for <i>Zea mays</i>	6
1-2 Importance and overview of (belowground) phenotyping	9
1-3 Introduction to functional-structural plant modeling	11
1-4 From phenotyping to model parameter estimation	14
1-5 Aims and Objectives	17
1-6 Outline of the thesis	18
2 Development and validation of a deep learning based automated minirhizotron image analysis pipeline	23
2-1 Introduction	25
2-2 Materials and Methods	28
2-2-1 Experimental test site	28
2-2-2 Data acquisition	28

2-2-3	Software tools	29
	Segmentation	29
	Feature extraction	30
2-2-4	Analysis pipeline	30
	Pre-processing	30
	Training	31
	Segmentation	32
	Converting	32
	Feature extraction	32
	Root analysis	33
2-2-5	Statistics, data processing and visualization	34
2-3	Results	35
2-3-1	Neural Network model validation	35
2-3-2	Comparison of automated and manual annotation	35
2-3-3	Time evaluation	39
2-4	Discussion	39
2-4-1	Availability and feasibility	39
2-4-2	Accuracy and comparability	40
2-4-3	Speed and efficiency	42
2-4-4	Limitations and further improvement	42
2-5	Conclusion	42
3	Multi-year belowground data of minirhizotron facilities in Selhausen	47
3-1	Background & Summary	48
3-2	Methods	51
3-2-1	Minirhizotron facilities	51
3-2-2	Study design	54
3-2-3	Ground-penetrating radar data	56
	Crosshole GPR data acquisition at the MR facilities	56
	Ground-penetrating radar data processing	58
3-2-4	Root images	60
	Root image acquisition at the minirhizotron facilities	60
	Root image data processing	60
3-2-5	Soil coring in the extra field	63
3-2-6	Soil sensor data	63
3-2-7	Soil water content using a mobile frequency domain reflectometry device	64
3-2-8	Soil sampling	64
3-3	Data Records	64
3-4	Technical Validation	66

3-4-1	Ground-penetrating radar data	66
3-4-2	Root Images	66
3-4-3	Soil sensor data	67
3-5	Usage Notes	67
3-5-1	Soil sensor data	67
3-5-2	Dielectric permittivity to soil water content	68
3-5-3	Soil hydraulic parameters	68
3-5-4	Updates	69
3-5-5	Above-ground data	69
3-5-6	Code availability	69
4	Root system architecture reorganization under decreasing soil phosphorus lowers root system conductance of <i>Zea mays</i>	73
4-1	Introduction	75
4-2	Materials and Methods	78
4-2-1	Experimental set-up	78
4-2-2	Image processing	79
4-2-3	CPlantBox parameter extraction	80
4-2-4	K_{rs} calculation	82
4-2-5	Statistical analysis	84
4-2-6	Data and code availability	84
4-3	Results	85
4-3-1	Plant structural responses to soil P level	85
4-3-2	Root system hydraulics	90
4-4	Discussion	91
4-4-1	P levels strongly influence axial root radius and crown root elongation	91
4-4-2	K_{rs} varies between fully fertilized and deficient plants, but not among those with severe to mild P deficiency	92
5	General Discussion	97
5-1	Towards new standards and methods for <i>in situ</i> root phenotyping	100
5-2	Combining multiyear above- and belowground data to investigate the soil-plant-atmosphere continuum comprehensively	102
5-3	Data-to-model pipelines combine <i>in situ</i> and <i>in silico</i> approaches to gain new insights into plant growth and hydraulics	104
5-4	<i>Zea mays</i> responses to environmental conditions: The case of phosphorus	109
6	Conclusions and Outlook	115
6-1	Conclusions	115
6-2	Outlook	117

Appendix A: Supplementary Materials to Chapter 2	119
Appendix B: Supplementary Materials to Chapter 4	125
Appendix C: Supplementary Materials to Chapter 5	131
C-1 Linking horizontal crosshole GPR variability with root image information for maize crops	133
C-2 Multi-year aboveground data of minirhizotron facilities in Selhausen . .	135
C-3 Responses of field-grown maize to different soil types, water regimes, and contrasting vapor pressure deficit	135
C-4 Seedling root system adaptation to water availability during maize domestication and global expansion	138
C-5 A scalable pipeline to create synthetic datasets from functional-structural plant models for deep learning.	143
C-6 Adapting Agricultural Virtual Environments in Game Engines to Improve HPC Accessibility	144
Appendix D: <i>In silico</i> investigation on phosphorus efficiency of <i>Zea mays</i>: An experimental whole plant model parametrization approach.	147
D-1 Introduction	148
D-2 Materials and Methods	148
D-3 Results and Discussion	149
D-4 Conclusion	149
Appendix E: Modeling architectural and functional response of <i>Zea mays</i> to phosphorus deficiency based on experimental data.	151
Appendix F: The selhausen minirhizotron facilities: A unique set-up to investigate subsoil processes within the soil-plant continuum.	153
Appendix G: Unrevealing subsoil processes in the selhausen minirhizotron facilities: Comprehensive insights into the soil-plant continuum with a new unique dataset.	155
Appendix H: Functional-structural plant modelling based on experimental data reveals that soil phosphorus status influences root system conductance.	157
H-1 Background	158
H-2 Objective	158
H-3 Material and Methods	158
H-4 Results and Discussion	158
Acknowledgements	159
Bibliography	161

List of Figures

1-1	The UN Sustainable Development Goals "2: Zero Hunger", "3: Good Health and Well-Being", "12: Responsible Consumption And Production", "13: Climate Action" and "15: Life on Land" are directly depending on the successful implementation of sustainable agriculture all around the globe (UN, 2023).	4
1-2	<i>Zea mays</i> production around the globe in 2022, according to FAOSTAT (2024b). Units are in tonnes (t).	5
1-3	<i>Zea mays</i> : a) shoot of a mature plant b) embryonic primary and seminal roots and postembryonic lateral and crown roots are already visible in 14-day-old wild type maize seedlings. c) Aboveground shoot borne brace roots of a 6-week-old plant (panel b and c are adapted with permission from Hochholdinger (2009)).	6
1-4	Computational plant modeling can be conducted on different scales, from molecular scale to field scale, depending on information density and desired information output.	12
1-5	Schematic procedure to design an analysis workflow to obtain FSPM parameter from phenotyping (data2model).	16
2-1	Schematic overview of the workflow of the automated analysis pipeline starting with image acquisition in the minirhizotron facility.	31
2-2	Example for one image processed by the automated root analysis pipeline. (a) The roots are "detected" by RootPainter according to the previous trained model. (b) The segmented image is exported and (c) converted to binary. (d) The last step is the skeletonization and feature extraction with RhizoVision Explorer.	33

2-3	Correlation of automated and manual analyzed root length, obtained from 2017. Each measurement date is considered separately for R_{UT} and R_{LT} . The color represents the density.	36
2-4	Comparison RLD of the data obtained from images originating from two minirhizotrons in the growing season 2015/16 and 2017, separated by plots grown with different treatments. The images were analyzed by hand (blue: manual) and by the automated analysis pipeline (red: automated). 2015/16: (a) R_{UT} manual, (b) R_{UT} automated, (c) R_{LT} manual,(d) R_{LT} automated; 2017: (e) R_{UT} manual, (f) R_{UT} automated, (g) R_{LT} manual,(h) R_{LT} automated;	37
2-5	Time requirements to run the automated analysis pipeline for a sample of 25,000 images. Left: All sub-processes together. Right: share of the neural network training, which is only required when no suitable model is available.	39
3-1	Overview of the location of the minirhizotron(MR)-facilities a) Map of the apparent electrical conductivity (ECa in [mS/m]) measured with the electromagnetic induction (EMI) (vertical dipoles, 9.7 cm depth of investigation, 135 cm coil distance) of the Selhausen test site. Provided by Brogi et al. (2019). b) Aerial photograph of the Selhausen test site and the MR-facilities. Both maps are given in WGS 1984 UTM Zone 32N [m]. For a) and b) the location of the MR-facilities is given by the blues rectangles, the upper terrace facility (R_{UT}) and the lower terrace facility (R_{LT}), the location of the access trench is indicated with a grey rectangle. c-d) Photos of the soil profiles of the loamy soil at the R_{LT} (c) and of stony soil at the R_{UT} (d).	52
3-2	Overview of the Minirhizotron (MR)-facilities. a) Schematic setup of the MR-facilities indicating that at each of the plots a different agricultural treatment was applied for the different growing seasons. The direction of the crop rows is perpendicular to the direction of the rhizotubes (red arrow). The measurements are carried out from the access trench. b) View within the access trench. c) Overview of one exemplary plot within the MR-facilities with the horizontal crosshole GPR ZOP measurement set up. Transmitter and receiver antennae are labeled Tx and Rx, respectively. Root image measurement are acquired using camera system attached to an index handle. d) Sensor location for one exemplary plot.	53
3-3	Overview of the experimental timeline including cultivars and management actions, such as sowing, harvest, pesticide applications and irrigation.	55
3-4	GPR processing steps	59
3-5	Root image processing steps	62
3-6	Folder structure of the repositories.	65

3-7	Data availability for the measurement seasons 2016 - 2021.	65
4-1	Workflow from experiment to CPlantBox model parameterization.	82
4-2	Principal component analysis (PCA) to identify the contribution of the plant parameters to the response of <i>Zea mays</i> to P deficiency. The big symbols corresponds to the centroids for the different P treatments.	85
4-3	Response of axial roots radii (A), crown root elongation (B) and leaf elongation rate (C) to different soil P availability levels.	87
4-4	Simulated plant structure with CPlantBox for all P levels. The given subtypes correspond to the denomination of the root types.	89
4-5	A: K_{rs} calculated for each P level with 100 simulation runs (shaded areas show the standard deviation to the mean); B: Comparison of different studies investigating K_{rs} of <i>Zea mays</i> with our results (blue).	90
5-1	Connections between Chapters 2-4 and the studies presented in this chapter. The arrows show the connection, which is either driven by data exchange (yellow), methodological transfer (blue), or by the use of similar model approaches (grey).	99
5-2	A multi-step structural-functional modeling pipeline to estimate K_{rs} and SUF. Each root system was traced with Root System Analyzer. An RSML file was exported from RSA and migrated to SmartRoot to manually label seminal roots. The parameter set was used to generate five realizations of virtual root systems with the stochastic CPlantBox model. The anatomical traits were referred to in the published articles and created with the GRANAR model. The radial hydraulic conductivity and axial hydraulic conductance (k_r and K_x) of these root anatomies were estimated using the MECHA model. From the CPlantBox root system architectures and their respective root hydraulic conductance, K_{rs} and SUF were determined with the model MARSHAL for each virtual root system (figure adapted from Yu et al. (2024)).	108
S1.1	3D spatio-temporal distribution of RLD measured in all tubes at one minirhizotron. Distances between tubes are not to scale. 1-8 represents the time steps.	120
S1.2	Comparison of root arrival curves of the data obtained from images originating from two minirhizotrons in the growing season 2017. The images were analyzed by hand (left: manual) and by the automated analysis pipeline (right: automated). 2017: a) R_{UT} manual, b) R_{UT} automated, c) R_{LT} manual, d) R_{LT} automated.	121
S1.3	Manual vs. automated analysis. The automated analysis misses a small part of the root and underestimates the total root length slightly.	121
S1.4	Root senescence visible from early to late measurement dates in the growing season 2015/16 and the corresponding segmentation and skeletonization.	122

S2.1 Schematic overview of the different organ parameters required for root and shoot calibration with CPlantBox.	126
S2.2 A: Axial root radii, B: Initial crown root elongation rate, C: Initial elongation rate of the leaves. D: Root fraction for different soil P availability levels ($p < 0.05$)	126
S2.3 Total volume [cm^3] of simulated root systems with all parameters as measured and with all parameters set as mean and only identified response parameters, elongation of crown roots and axial root radii, set as function of P level in soil.	127
S2.4 Biomass (dry mass) [g] of shoot, root and whole plant depending on soil P level.	127
S2.5 K_{rs} for 7, 14, 21 and 28 DAS depending on soil P concentration, depending on the mean of 100 simulations. The error-bars display the standard deviation.	128
S3.1 Exemplary comparison of the permittivity high-resolution root image dataset measured on August 5, 2020, and the respective root volume fraction (RVF). The different plots represent the different depths of 0.2–0.8 m, (a)–(d), respectively, for Plot 2 at R_{UT} . The solid blue line indicates the permittivity. The green bars indicate the RVF along the rhizotubes. The black solid line indicates the smoothed RVF along the rhizotube over five positions. The dashed black line represents the mean RVF along the rhizotubes (adapted from Lärm et al. (2024)).	134
S3.2 Overview of (a) above-ground measurement set-up in one exemplary plot (here for maize) within the minirhizotron facility, from the minirhizotron access trench: canopy temperature sensor, sampling area and leaf measurements, sap flow sensor installation with data logger, canopy chamber with LI-6400XT, and soil respiration chambers) (b) leaf gas exchange measurement with LI-6400XT machines (c) sap flow measurements with the Dynamax sensors, and (d) canopy chamber measurements for winter wheat (left) and maize (right). (adapted from Nguyen et al. (2024b)).	136
S3.3 Geographical variability of SRN in traditional varieties of maize. SRN was determined in globally collected traditional varieties of indicated geographical origin. Domestication and expansion times for maize populations are indicated accordingly. (Figure is adapted from Yu et al. (2024)).	139

S3.4	a) Comparison of seminal root numbers in maize lines originating from different climate groups according to the Köppen-Geiger climate classification maps. Significant differences were tested by one-way PERMANOVA with post-hoc test ($p < 0.05$); b) SRN decreases along a latitudinal gradient from south to north in Mexico. c) MAGIC founder allele effects in a 20 Mb window around <i>rtcs</i> ; d) Correlation between SRN and the proportion of Northern Flint sources in the US Ames panel; e) SUF of seminal roots and lateral roots as a function of SRN. For each SRN, the average proportion of water uptake per root type is expressed as a ratio relative to overall water uptake; f) SRN is negatively correlated with rooting depth of the primary root and lateral root density in different maize traditional variety accessions; g) Seminal root variation affects K_{rs} ; h) Comparison of drought tolerance between WT and plants of the two <i>ZmHb77</i> CRISPR-knockout lines after drought conditions and re-watering; i) Model of a potential function of <i>ZmHb77</i> on the formation of seminal roots and lateral roots in contribution to maize seedling drought tolerance (figures are adapted from Yu et al. (2024)).	142
S3.5	Comparison of parameter extraction pipeline between synthetic and real-world data. Real-world data, 23 plant images at this growth stage and angle, were acquired in controlled rhizotron experiments. Bottom: Analyzed skeletons of shoot organs, starting with the pseudo-stem. Right: Comparison of blade lengths in mm, compared across samples sorted by longest first. The error bars indicate the standard deviation on each axis (figure adapted from Baker et al. (2023)).	144
S3.6	Overview of technical components and data flows. The illustrated assignment to specific nodes is a performance recommendation, though individual components can share resources. A linked line indicates concurrent coupling (figure adapted from Baker et al. (2024a)).	145
S4.1	Workflow from 2D- images of shoot and roots to FSPM parameterization: 1) image acquisition, 2) segmentation, 3) feature detection and parameter extraction, 4) assemble parameter set, 5) plant structure from parameter.	150

List of Tables

2-1	Overview of the camera-systems and experiment timeline of minirhizotron images acquisition	29
2-2	Overview of the statistical comparison of automated and manual annotation. ΔRL is the difference between the mean total root length (mm) obtained from automated and manual analysis methods, and a Welsch two sample t-test shows whether differences are significant (* = $p < 0.01$).	38
3-1	Detailed overview of the GPR data acquired during growing season 2016, 2017, 2018, 2020 and 2021.	57
3-2	Overview of the camera-systems and experiment timeline of minirhizotron images acquisition	60
3-3	Detailed overview of the images taken at the growing season 2016, 2017, 2018, 2020 and 2021.	61
3-4	Overview of the repository content and data labelling. The labels always contain the facility name (R_{UT} or R_{LT}) and the year the data have been obtained. For the root images, each image is also labeled according to exact date (year (YYYY), month (MM), day (DD)), tube and position it was taken.	66
4-1	Overview of organ parameters (and their units) that are used to calibrate models with CPlantBox, as used for this study (day: d; integer:int), adapted from Schnepf et al. (2018), Zhou et al. (2020) and Giraud et al. (2023)	81
4-2	Overview of shoot organ specific architectural CPlantBox parameters, as described in Table 4-1, for the distinguished P regimes.	87

4-3	Overview of initial root system architectural parameters for the distinguished P regimes. These parameter describe the initiation time, maximal count and appearance probability of the different lateral root types, the seed position and simulation time.	88
4-4	Overview of root organ specific architectural CPlantBox parameters for the distinguished P regimes and the parameterset (general) for simulation to evaluate the root system response parameter.	88
S1.1	Detailed overview of the images taken at the growing season 2015/16 and 2017	123
S1.2	Comparison of the automated analysis pipeline and the manual annotation of the total root length obtained in the growing season 2017 with a linear regression. The confidence interval (95%) of the regression coefficient (ordinary least products) are listed in parenthesis. The bias is fixed if the 95% CI of the intercept do not include 0 and the bias is proportional if the 95% CI of the slope do not include 1.	124
S2.1	Overview of the hydraulic properties (k_r and K_x) used to compute dynamic root system conductance, based on the simulated root system architecture.	129
S2.2	Overview of statistical results for axial root radii, crown root elongation and leaf elongation for the P levels P0-P3. A Shapiro-Wilk Normality Test and Levene's Test for Equality of Variances were performed, followed by an ANOVA ($n = 5 - 12$).	129

Abbreviations

ANOVA	Analysis of variance
C	Carbon
CAL	Calcium-acetate-lactat
CO₂	Carbon dioxide
CNN	Convolutional neural network
CT	Computer tomography
CUDA	Compute unified device architecture
CRIM	Complex refractive index model
cv	Cultivar
DAS	Days after sowing
DM	Dry matter
DOI	Digital object identifier
EF	Extra field
EIT	Electrical impedance tomography
EMI	Electromagnetic induction
ERT	Electrical resistivity tomography
FB	First break
FDR	Frequency domain reflectometry

FSPM	Functional-structural plant model
GPR	Ground penetrating radar
GPU	Graphics processing unit
GUI	Graphical user interface
H₂O	Pure water
HPC	High performance computing
INRES	Institute of Crop Science and Resource Conservation
LAI	Leaf area index
K	Potassium
k_r	Radial hydraulic conductivity
K_r	Radial hydraulic conductance
K_{rs}	Root system conductance
k_x	Axial hydraulic conductivity
K_x	Axial hydraulic conductance
MAGIC	Multi-parent Advanced Generation InterCross
MR	Minirhizotron
MRI	Magnetic resonance imaging
N	Nitrogen
NO₃⁻	Nitrate
P	Phosphor
P₂O₅	Phosphate
PCA	Principal component analysis
PDR	Probability density function
PET	Positron emission tomography
PWP	Permanent wilting point
QTL	Quantitative trait locus
RGB	Red, Green, Blue
RLD	Root length density

R_{LT}	Lower Terrace rhizotron facility
RMSE	Root mean square error
RSML	Root system marker language
R_{UT}	Upper Terrace rhizotron facility
RVF	Root volume fraction
R_x	Receiver antennae
SD	Standard deviation
sEIT	Spectral electrical impedance tomography
SHP	Soil hydraulic properties
SRN	Seminal root number
SUF	Standard uptake fraction
SWC	Soil water content
SWP	Soil water potential
SWR	Soil water retention
TDR	Time domain reflectometry
TERENO	Terrestrial environmental observatories
T_x	Transmitter antennae
UAV	Unmanned aerial vehicle
UN	United Nations
US	United States of America
UTC	Universal time coordinated
VSI	Vienna Scientific Instruments GmbH
WARR	Wide-angle reflection and refraction
ZOP	Zero offset profile

*Agriculture is the most healthful, most useful
and most noble employment of man.*

GEORGE WASHINGTON

◀ ◊ ▶

In the following chapter, we will dive into the
topic, briefly introduce the thesis and formulate
its different objectives.

Chapter 1

Introduction

PLANTS ARE OF FUNDAMENTAL IMPORTANCE for life on earth, as they are the foundation of most ecosystems and the key producers in the food chain. They are not just passive elements of the environment; they actively contribute to regulating atmospheric gases and mitigating climate change by binding carbon dioxide and releasing oxygen (Crawley, 2009). Humans and plants have a complex relationship that dates far back into history. This heritage is evident today. In our modern society, plants provide food, fiber, medicine, energy, and living space for people and animals worldwide. The domestication of plants through agriculture allowed human civilization to evolve. We have domesticated plants to suit our needs, leading to a cultural shift from hunter-gatherer societies to agriculture-based societies (Schaal, 2019). Although the domestication of crops, such as wheat, started approximately 10,500 years ago, the most significant progress in agriculture has been achieved within the last century (Tanno and Willcox, 2006). With the beginning of the "Green Revolution" and the development of advanced technologies in the second half of the 20th century, agricultural production tripled, and the use of natural resources increased dramatically. However, agriculture now faces its biggest challenges.

The human population is still growing rapidly. By 2050, the world population is expected to reach more than 9 billion people. Ensuring food security is key since hunger and malnutrition persist and approximately 800 million people are undernourished (UN, 2023). To cope with these challenges, agricultural efficiency needs to be increased by approximately 60% (Alexandratos and Bruinsma, 2012). Modern research must, therefore, address these topics with the highest priority to increase and promote sustainable plant production while minimizing the ecological footprint of agriculture. However, climate change and associated altered environmental conditions, such as decreased water availability or the shortage of nutrients, complicate the matter. In order to meet the UN Sustainable Development Goals, especially: "Zero Hunger", "Good Health and Well-Being", "Responsible Consumption And Production", "Climate Action" and "Life on Land"

(Figure 1-1), we have to increase our understanding of environmental change and the resulting crop responses (UN, 2023). This includes a detailed understanding of underlying processes at different scales and the interaction of various key components, taking into account the effects of environmental conditions and modern agricultural practices.



Figure 1-1: The UN Sustainable Development Goals "2: Zero Hunger", "3: Good Health and Well-Being", "12: Responsible Consumption And Production", "13: Climate Action" and "15: Life on Land" are directly depending on the successful implementation of sustainable agriculture all around the globe (UN, 2023).

Maize (*Zea mays*), rice (*Oryza sativa*), and wheat (*Triticum aestivum*) account for more than half of the world's food production and human caloric intake. Among these three crops, maize is the front-runner in terms of yield produced and is, therefore, a crucial cornerstone for human nutrition. In 2022, all around the globe, 1.16 billion tons of maize were produced on 203 million ha of land area, which is an increase of more than 400 % over the last 60 years. In the same period, the land area used for cultivation only doubled, indicating an increase in maize production efficiency of approximately 200% (FAOSTAT, 2024b). Maize is grown all over the world; however, North and South America together account for almost half of the world's production (49.6%), followed by Asia (26.9%), Europe (8.8%) and Africa (8%) (Figure 1-2). The US and China together produce more than half of the total maize yield (626 mio. t).

Currently, the annual production increase in *Zea mays* cropping is 1.6%. However, to meet the demands driven by population growth, dietary shifts, and increased biofuel consumption, annual maize production needs to increase faster. Ray et al. (2013) predicted a required annual increase of approximately 2.4% per year in maize yields to meet the goal of doubling agricultural production in 2050. To achieve this, we have to understand how maize is cropped most efficiently and grasp how plants respond to changing environmental conditions. To do this, we have to extend our limited knowledge about the architectural and functional adaptations taking place in *Zea mays* exposed to extreme conditions, such as drought or nutrient deficiency, and gain comprehension of the underlying mechanism. These new insights hopefully increase our understanding of processes and are therefore essential to enhance breeding for new, more efficient, and less resource-demanding cultivars and additionally improve cropping management. To fully understand the responses of *Zea mays*, we must first understand the architecture of the plant.

Zea mays is a monocotyl plant, belonging to the family of *Poaceae*. It is a tall stout grass (1.2-4m height), producing a cereal grain (corn). The shoot of *Zea mays* consists mainly of the leaves, which are attached to a pseudo-stem, often

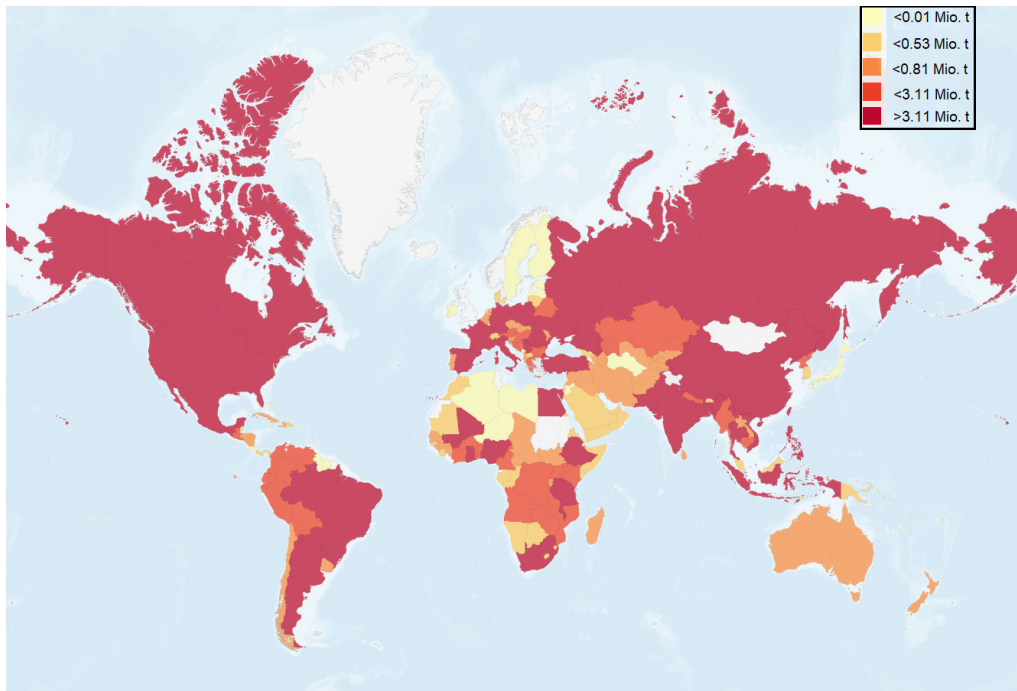


Figure 1-2: *Zea mays* production around the globe in 2022, according to FAOSTAT (2024b). Units are in tonnes (t).

also referred to as a stalk. After germination maize develops a single cotyledon, followed by the actual leaves. The leaves arise from nodes, alternately on opposite sides on the stalk. At the flowering stage, the tassel, the inflorescence of the male flower, develops at the top of the stem. The female inflorescence initially develops as a silk, appearing as a bundle of tubular hairs, each connected to a future kernel. Later, the whole female inflorescence turns into an ear, enveloped by multiple husks (Solaimalai et al., 2020). In modern varieties, grains and the corncob are mostly yellow. However, traditional varieties may have orange, red, brown, blue, purple, or black colors (Yu et al., 2024). The shoot structure is shown in Figure 1-3a.

The root system of a plant is crucial to access water and nutrients that are stored in the soil. The capability of the plant to take up these precious resources mainly depends on the suitability of the root system for given soil conditions. The morphological characteristics of the different root types together form the root system architecture (Lynch, 2007). The architecture of the root system of *Zea mays* is determined by different embryonic and postembryonic root types. Embryonic roots are formed early after germination, and postembryonic roots are formed later at different stages of development. While embryonic preformed roots dominate the early root system of the seedling, the adult rootstock is determined by postembryonic roots. The embryonic root system consists of a primary root, which is the first root emerging at germination, followed by the seminal roots. Both root types can have postembryonic lateral roots of different orders. Later, the adventitious roots develop, starting with the crown roots, which are developed at the shoot

nodes but are still located in the soil. A maize plant can have several crowns. Since they originate from the shoot, the crown roots are also called shoot-born roots (Figure 1-3b). A later type of shoot-born roots are the brace roots that are exclusively developed above-ground (Figure 1-3c). A maize plant typically develops several brace root nodes (Hochholdinger, 2009).

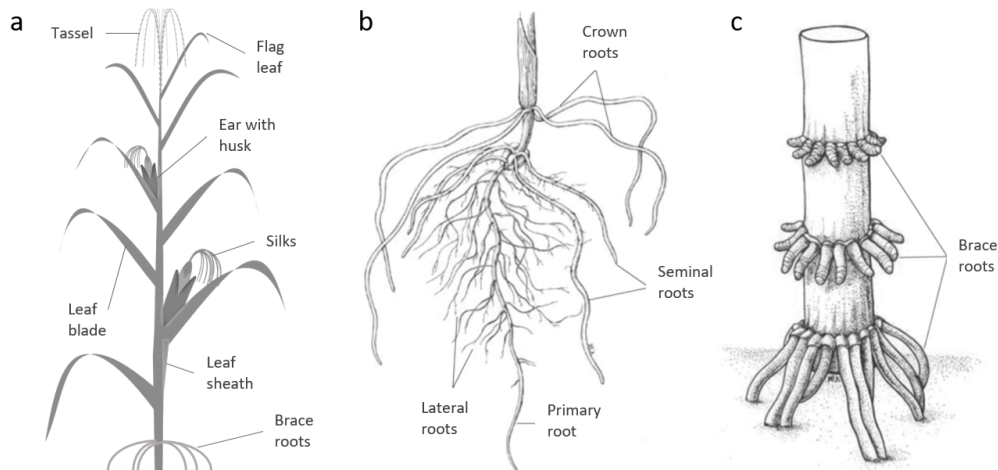


Figure 1-3: *Zea mays*: a) shoot of a mature plant b) embryonic primary and seminal roots and postembryonic lateral and crown roots are already visible in 14-day-old wild type maize seedlings. c) Aboveground shoot borne brace roots of a 6-week-old plant (panel b and c are adapted with permission from Hochholdinger (2009)).

1-1 Changing environmental conditions and the implications for *Zea mays*

For agriculture, the main problematic consequence of climate change is water availability. Agriculture is the main consumer of global freshwater ($900\text{--}1700 \times 10^9 \text{ m}^3 \text{ year}^{-1}$) (Chaturvedi et al., 2015). Climate change is expected to increase global evapotranspiration, because the hydrological cycle will get additionally disturbed due to elevated temperature. This reduces water availability, making water management a critical issue for sustainable agriculture. Additionally, the occurrence of drought, extreme weather conditions, and disturbances in rainfall patterns are a consequence of human-made climate change (Srivastav et al., 2021). With increasing latitudes, there will be increased precipitation in tropic regions, while already arid areas will have less precipitation. Consequently, regions that already have less water availability will even become drier and warmer. The Food and Agriculture Organization states that irrigation will have to increase around 5-20% within the next years to maintain crop production (FAO, 2011).

Additionally to the lack of water, the temperature increase affects soil health. Climate change has a negative impact on nutrient cycling and soil water content (Wagena and Easton, 2018). Changes in rainfall patterns and heat may change the

magnitude of nutrient, their transport, and consequently their plant availability (Boesch et al., 2001). Especially the macronutrient nitrogen (N) is prone to runoffs (Wang et al., 2015). A common practice in agriculture is to compensate for these losses with additional fertilization. However, approximately 14% of the total greenhouse gas emission of agriculture originates from this inorganic fertilization management, which is an increase of 45% since 2002 (FAO, 2015). Additionally to nutrient runoffs, the exploitation of finite natural resources poses new challenges to agriculture. The availability of phosphorus (P), which is a finite resource mined from rock phosphate, will decrease soon (Cordell et al., 2009). Already in 2030, it is expected that the mining costs will increase dramatically due to reduced mining efficiency, and consequently, the affordability and availability will decline soon (Reijnders, 2014). In the past, P fertilization has been a comparatively small financial investment for crop production in industry nations, which resulted in an excessive fertilization history in North America and Europe. However, excessive N and P fertilizer use significantly impacts the environment by affecting open water bodies (Randall, 2003). Besides N, P is the most important macronutrient for crop production. Especially P is limiting maize yields in approximately 30 % of all cultivated maize area (Heuer et al., 2017).

The deficiency of water and important nutrients triggers architectural responses in *Zea mays*. These responses affect both the shoot and the root system (Marschner, 2011). The inhibition of shoot growth in maize caused by water and nutrient limitation is of direct interest to agriculture, as the shoot is the relevant harvesting organ. However, since the root system is responsible for water and nutrient uptake, the effects caused by its underdevelopment are of indirect but major importance for crop production. Changes in plant architecture often imply functional changes, e.g. in water and nutrient uptake capacity or photosynthetic ability.

Limitation of water and essential nutrients, such as N and P, inhibit plant growth and ultimately lead to a reduction in yield. The responses of maize architecture to alternating effects of multiple deficiencies at once are complex and our knowledge is still very limited. However, the architectural reactions to water, N, or P limitation considered individually are already well known.

In the case of water stress, the maize plant reduces shoot size by limiting height and leaf area, the tassel growth is reduced as well, and the leaf angle is steeper (Ribaut et al., 2009). The stomata may close partially or fully to reduce water loss through transpiration. The root system often responds under water stress with an increased rooting depth and density, an enhanced lateral root formation, and root angle changes, generally leading to a carbon re-allocation from shoot to root system (Hochholdinger, 2009). Increased root diameter has also shown to be a drought resilience trait in *Zea mays* since soil penetration resistance triggers thicker roots (Lin et al., 2016). Larger root cortical cell size can improve drought tolerance by reducing metabolic costs (Chimungu et al., 2014) and reduced lateral branching under water can lead to a carbon allocation in favor of axial root (all roots not being lateral roots) diameter (Zhan et al., 2015). The reduction of crown root numbers was also reported as a beneficial response to drought (Gao and Lynch, 2016). Furthermore, cultivar-specific adaptation, through domestication and

target breeding, changed the root system to be beneficial under drought. Insights from recent studies identified seminal root number, primary elongation rate, and lateral distance on the primary root as major morphological traits contributing to drought resistance (see Chapter 5-3, Appendix C-4, and Yu et al. (2024)).

N limitation generally results in reduced shoot growth due to limited resources for synthesizing proteins and chlorophyll, resulting in significant reductions in shoot dry matter and overall biomass. Leaf area is heavily reduced (Binder et al., 2000, Pandey et al., 2000). N deficient plants often exhibit chlorosis, seen by a yellowing of the leaves (Khamis et al., 1990). Maize reallocates N from older leaves to younger leaves, resulting in a delayed senescence (Riedell, 2010). Similar to the response to drought, maize promotes primary root elongation, increasing the root-to-shoot ratio under N limitations to enhance nutrient acquisition from a larger soil volume (Gao et al., 2014). Generally, the total root system length increases under N deficiency, mainly driven by enhanced individual axial root elongation, but reduction in axial root number and general promoted lateral root growth (Chun et al., 2005). Furthermore, maize root growth angles become steeper under low N conditions (Trachsel et al., 2013). It is not surprising that water and N limitations trigger the same root system responses since plant available N is mainly transported as NO_3^- with the water. Therefore, the root system of a hypothetical ideotype would have similar attributes in most maize cropping environments. Lynch (2013) hypothesizes that a potential ideotype should have a large diameter primary root with few but long lateral roots, many seminal roots with a shallow growth angle, small diameter, and many lateral roots or alternatively a medium number of seminal roots with a steep growth angle, large diameter, and few lateral roots in combination with an abundant lateral branching of the initial crown roots, an intermediate number of crown roots with steep growth angles and few but long lateral roots, a whorl of supporting roots with high occupancy, which have a growth angle somewhat flatter than the growth angle for crown roots, with few but long lateral roots.

Regarding P limitation, maize responses, similar to water and N deficiency, with a general reduction in shoot biomass (Wen et al., 2017). P deficiency also affects leaf morphology, resulting in reduced leaf area and red chlorosis due to reduced leaf area index and decreased chlorophyll content. This lowers the photosynthetic capacity of the shoot (Zhang et al., 2018). The allocation of the remaining carbon is shifted from shoot to root, resulting in an increased root to shoot ratio, which is supposed to enhance P uptake (Lynch et al., 2005). However, the underlying changes in root system morphology are contrary to the responses under water and N limitation. Inhibitions of primary root growth, shallower axial root angle, and various changes in lateral root growth, such as the reduction of lateral root growth in the field, but also an increase in lateral branching in plants with few axial roots are known responses to P deficiency (Borch et al., 1999, Marschner, 2011, Zhu and Lynch, 2004). Also, contrary to water and N limitation, an increase in crown root number (Sun et al., 2018), and reduced axial root radii (Sheng et al., 2012, Zhang et al., 2012) has been reported to be beneficial under P deficiency.

Additionally to N and P, potassium (K) is a crucial macronutrient for crop production. However, in maize cropping, N and P deficiencies are more critical in maize production due to their direct roles in essential plant processes and typically result in more immediate and noticeable reductions in growth compared to K deficiency (Essel et al., 2020).

Although important changes in plant architecture under drought conditions and macronutrient limitations are known for each deficiency separately, the interplay between several deficiencies is often poorly understood. The effects of P deficiency and water deficiency on whole plant architecture are rarely investigated together; however, P deficiency frequently occurs in parts of the world where water is also limiting, such as regions in Africa and Australia. We must investigate these combined stresses' reciprocal effects on plant development to close this knowledge gap. Since combined effects complicate the investigations, we require modern, non-invasive phenotyping methods to obtain and analyze reliable plant data and apply sophisticated models to expand our ability to understand the relationships between processes.

1-2 Importance and overview of (belowground) phenotyping

The term "phenotype" was first used over 100 years ago by the botanist Wilhelm Johannsen to describe a wide range of characteristics in plants, microbes, fungi, and animals (Johannsen, 1911). In the 1960s, the term "phenotyping" was introduced, which refers to a quantitative analysis of the characteristics of an organism. Phenotyping can be considered the counterpart to genotyping, which analyzes the organism's genetic code to identify specific genetic variations. Plant phenotyping is the comprehensive detection, recording, and analysis of observable plant traits related to growth, development, and stress responses. This research domain aims to understand the genetic, environmental, and management factors that influence plant performance. Phenotyping measures a wide range of plant characteristics, including morphological parameters defining the plant's architecture, physiological parameters defining the plant's function, biochemistry, and growth dynamics. Phenotypic measurements can be taken at all stages of plant development and are a valuable resource for plant scientists to understand plant-environment interactions. In recent decades, phenotyping has become the most important tool for characterizing various plant processes, functions and structures, primarily through the non-invasive optical analyses of plant traits using, e.g., images. However, in contrast to genotyping, phenotyping is still considered a bottleneck in plant science, as the collection and analysis of observable traits is slow and labor-intensive.

With the increasing development of non-invasive technologies in the 2010s, a new era of plant phenotyping has started. The capacity and throughput of sensor-, automation- and computer-based tools grew, as did their availability, affordability, robustness, and scalability, making modern phenotyping methods interesting

beyond the borders of science, e.g., for commercial breeding (Watt et al., 2020). Together with the tremendous progress in data analysis through the integration of artificial intelligence, driven in particular by deep neural networks, phenotyping methods are developing fast. There is an incredible number of different methods for phenotyping plants, varying from molecular to field scale.

The current gold standard of shoot architecture phenotyping is RGB-, multi-, and hyper-spectral sensors, potentially combined with thermal measurement or a laser scanner, to generate optical representations of the canopy in 2-D, 3-D, or, if measured over time, 4-D (Paulus, 2019). From the resulting digital plant copies, structural traits can be derived. To obtain more functional implications about photosynthesis, fluorescence measurements can be conducted (Li et al., 2014). A new method to phenotype insect-plant interactions is acoustic phenotyping (Branding et al., 2023).

Measuring the hidden half of the plant is as important as measuring the above-ground part, but challenging since the root system is mostly covered by soil. Therefore, root phenotyping methods were developed comparatively late, and fewer phenotyping platforms are available (Atkinson et al., 2000). Currently, the International Plant Phenotyping Network (IPPN) lists 111 operating phenotyping facilities, each measuring a huge variety of different traits. Only 25 of them include root properties. However, in recent years, root phenotyping became more of a focus and was developed further, and a suit of measurement tools was developed (Atkinson et al., 2019). Root phenotyping is mainly divided into invasive and non-invasive methods. Invasive methods, such as soil coring, excavation, and trenches, are often used in the field to get an overview of the heterogeneity present in the experiment. Non-invasive methods are preferred to observe root development over time with less to no disturbance. Possibilities of non-invasive root observations are on a wide range, from simple, transparent windows for visual growth control to the use of rhizotrons, magnetic resonance imaging (MRI), computer tomography (CT), and positron emission tomography (PET) scans (Yang et al., 2020). Recently also, electromagnetic measurement methods, such as electrical resistance tomography, electromagnetic inductance, and Ground Penetrating Radar (GPR), have been applied to measure roots (Atkinson et al., 2019, Klotzsche et al., 2019, Lärm et al., 2024, Michels et al., 2024).

For both root and shoot, the progress in optical phenotyping led to a significant increase in data quantity. In the late 2010s, the development of neural networks for image analysis accelerated the progress in phenotypic data analysis (Pound et al., 2017). *In situ* root phenotyping in particular benefits from these new analysis methods (Smith et al., 2020a). Starting with leaf and shoot segmentation, convolutional neural networks (CNNs) were used to separate the targeted organ from the background automatically. Followed by subsequent feature extraction, such as area measurement, length, radius, convex hull, or perimeter, architectural parameters are derived easily (Ubbens and Stavness, 2017, Wang and Su, 2022). CNNs are now also frequently used for 2D root system segmentation tasks (Bauer et al., 2022, Smith et al., 2020a, 2022). However, feature extraction from the segmented root system still requires some effort and additional processing after

segmentation. Therefore, tools capable of performing this task must be combined or integrated into neural network-based analysis workflows to facilitate the process. CNNs are also applied to 3D data, such as MRI scans. However, they currently only have an assisting function since full automation is not yet feasible, and manual labor is still required to extract architectural root system traits (Selzner et al., 2023).

For the shoot, we are in the process of closing the gap to genotyping and eliminating the "phenotypic bottleneck" by using high-throughput phenotyping technologies, automated imaging systems, and neural network-based data analysis (Minervini et al., 2015, Song et al., 2021). In root system phenotyping, advances in non-invasive imaging techniques such as CT, MRI, and PET, combined with sophisticated neural network-driven software for root system analysis, are also helping to overcome the phenotypic bottleneck. However, especially with multi-dimensional data, faster and more accurate processing is required (Bauer et al., 2022, Selzner et al., 2023).

Phenotyping is crucial for further progress in plant science, as it provides essential insights into how genetic variations manifest in architectural and physiological traits, enabling effective breeding programs to improve crop yields and ultimately providing a deeper understanding of plant responses to environmental changes. Phenotyping data is also the foundation for computational plant modeling.

1-3 Introduction to functional-structural plant modeling

Functional-structural plant modeling (FSPM) is an approach that combines the architecture (structure) of a plant with its physiology (function) to create a comprehensive computational model to simulate growth and development. These models are of great value for plant sciences as they can predict how plants will respond to different environmental conditions and understand processes in detail (Dejong et al., 2011). In FSPMs, the plant architecture is usually represented as connected plant segments distributed in the 3D below- or above-ground space or both domains together. FSPMs can deal with the spatial distribution of environmental conditions. FSPMs are available on different scales (Figure 1-4). Typically, they are based on up-scaling, usually from organ to plant, but also from tissue to organ or from single plant to crop stand. To cope with complex environmental conditions, FSPMs can be coupled with other models, e.g., soil or crop models, and used together to solve more complex scenarios, ensuring that appropriate computational methods are used (Godin and Sinoquet, 2005).

The origins of FSPMs date back to the late 20th century, when advances in computer technology made simple, descriptive models of plant growth possible for the first time. The first models focused primarily on geometric representations of plant architecture, usually looking at either the shoot or the roots individually (Vos et al., 2009). A major step forward was the development of L-systems, where the basic idea is to define complex objects by gradually replacing parts

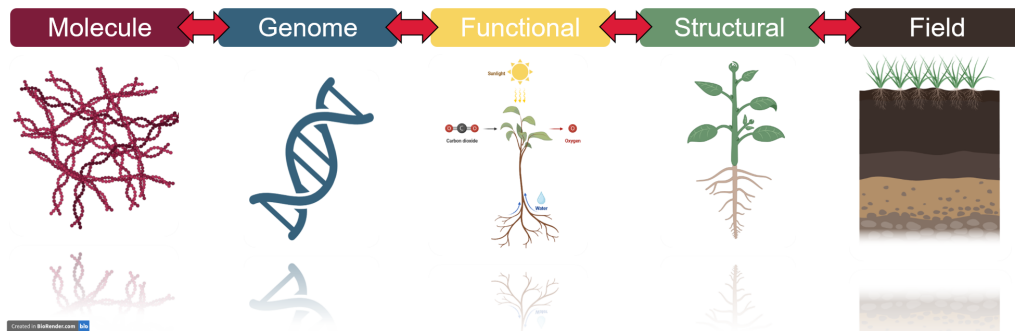


Figure 1-4: Computational plant modeling can be conducted on different scales, from molecular scale to field scale, depending on information density and desired information output.

of geometrical objects with a series of letters defined by rewriting rules, to simulate plant morphology. (Lindenmayer, 1968, Prusinkiewicz and Lindenmayer, 1990). On top of the structure, integrating process-based plant functions, such as carbon allocation or N distribution, facilitated the representation of basic physiology (Fourcaud et al., 2008). With further advances in computing methods, computational power, and the increased process-based understanding of plant physiology, FSPMs became more sophisticated and incorporated functional aspects, such as photosynthesis, transpiration, and nutrient uptake (Cieslak et al., 2011). For a long time, the root system architecture and functionality were still the missing puzzle part of FSPMs, however, due to the recent development of functional-structural root system models, this gap could be closed (Javaux et al., 2008, Postma et al., 2017, Schnepf et al., 2018). With the integration of the shoot and root system into a single FSPM, as it is done in CPlantBox by Giraud et al. (2023), scientists can now use FSPMs that simulate plant functions at the scale of a single (sub)organ up to the entire plant and crop stand.

FSPMs have a wide range of applications in plant sciences. They are used to enhance our understanding of plant-environment interactions, e.g. to improve breeding strategies or crop management. An exemplary application of FSPMs is to predict the effects of different root system architectures on the impact of water stress and, hence, plant performance and to assess the potential benefits of genetic modification (Vos et al., 2007). Another use case is the prediction of nutrient uptake by different cultivars at different soil conditions or under different nutrient supply levels (De Bauw et al., 2020). FSPMs are used at different agriculture management scales, such as lab, greenhouse, or for field applications (Vos et al., 2009).

The possible applications of FSPMs are as diverse as the technological advances and the research questions we want to address. In general, these models provide a powerful decision-making tool, allowing researchers to test different scenarios and develop strategies that have the potential to maximize productivity and sustainability. However, as with any model, an FSPM is only as good at answering a real-world question as the parameterization on which it is based.

Phenotyping data is required to parameterize an FSPM. Parameterization of an FSPM can be achieved by direct measurements of the shoot and root traits, such as e.g., leaf area, stem or root diameter, and length, which are obtained using high-throughput phenotyping platforms. However, since most FSPMs also include dynamic growth, we also require information on the trait's development over time.

We can use high-throughput phenotyping platforms to study how plants change over time. Modern imaging techniques like 3D laser scanning and MRI show us how the shoot is developing, while rhizotrons, MRI, or PET scans show us how the root system is developing (see Chapter 1-2). By combining these data sources and the shoot and root information, we can quantify that the FSPMs accurately reflect the architectures of plants in the real world. However, while phenotyping provides valuable data on many aspects of architectural plant traits, functional parameters are sometimes complex to measure, especially if development over time is regarded (Fiorani and Schurr, 2013). Especially critical key components of the plants, such as the time-dependent variations in hydraulic architecture, which has crucial implications for plant water uptake, are hard to phenotype, and consequently, it is a complex challenge to precisely investigate water uptake capacity based on mechanistic functions (Heymans et al., 2020, Meunier et al., 2018). FSPMs can help address this challenge by incorporating theoretical and empirical data to simulate these observable processes, providing insights into how plants regulate water transport, maintain structural integrity, and adapt to environmental changes. However, the required empirical data still needs to be obtained, and therefore, workflows and pipelines must be developed, validated, and applied to provide the data to the FSPM.

Besides the persisting challenge in complex functional data collection, the processing, analysis, and integration of data originating from high-throughput phenotyping methods for model parameterization is still challenging (Fiorani and Schurr, 2013).

Automation in data measurement and analysis is inevitable due to the vast amount of data produced by cutting-edge phenotyping methods (Pound et al., 2017, Watt et al., 2020). However, processing pipelines for complex data structures are still a bottleneck, especially when it comes to model parameterization, as FSPMs require highly precise data. This is because when model inputs already contain high uncertainties, validating the model becomes too complex (Bauer et al., 2024, Wang et al., 2020). Ensuring data quality and consistency is essential, as inaccuracies can cause faulty model predictions.

The pooling of different types of data, including measurements of the shoot and root system, requires advanced methods and robust analysis pipelines. Considering the dynamic nature of plant growth, we require continuous data collection over time, which is further complicating the parameterization process. In order to apply FSPMs to complex questions and unleash their full potential, overcoming the challenge of precise parameterization is key.

1-4 From phenotyping to model parameter estimation

In order to develop feasible analysis methods, tools, and combined pipelines to extract FSPM model parameters from phenotypic data, we have to understand which components of plant architecture are relevant for FSPM parameterization. This highly depends on the FSPM framework used. One of the most complex scenarios is the parameterization of a whole plant functional-structural model.

CPlantBox (Giraud et al., 2023) offers the possibility to generate full plant structures at the vegetative growth stage as a single topological network of organs based on structural parameterization. In most FSPMs, simulated plant architecture is composed of nodes with defined coordinates. The nodes have properties, such as type, radius, or hydraulic properties. Together the nodes form a connected network. To parameterize the plant structure, single organ attributes are required from measured data. These attributes depend on the organ. However, since all organs contribute to the node-network, length information, such as the maximal leaf or root length, width information, such as root and stem radii or leaf width, a branching information, such as lateral root emergence distance and delay or time delay between leaves and growth information, such as elongation rate of root, stem, and leaves, are the basic requirements for the structural whole plant parameterization. Additionally to this single organ information, data on general plant architecture are required, such as the amount of seminal or shoot-born roots and root crowns, their emergence delay, and the leaf shape type.

The data analysis methods and tools to extract these data highly depend on the data structure of the available phenotypic data. Obtaining whole plants, or at least undisturbed and connected whole root systems or shoot images or scans, is the convenient way to obtain reliable FSPM parameters.

Regarding 2D or 3D measurements, we can consider the depicted plant as a connected network, similar to the one FSPMs are often realizing. The end of each organ is the tip of a network branch, and root and leaf exit points are nodes at which the network branches out. Ideally, time information on node or tip creation and node and tip organ affiliation are also recorded. If all network data are assembled, only the length and diameter between the nodes and tips of the network have to be measured. If the node creation time information can be accessed as well, growth rates and potentially also the maximal length or area of each organ can be derived directly from the network structure. For the root system, the network analogy has already been often described, and even a data format describing the root system as a network structure by saving node and tip coordinates and assigning them functions, such as creation time and radii, is available (**R**oot **S**ystem **M**arker **L**anguage, Lobet et al. (2015)). For the shoot, the network analogy works as well as for the root system and has been implemented, e.g., through Multiscale Tree Graph (Godin and Caraglio, 1998). However, until today, it has not been used in FSPMs frequently. The drawback of this method is that the automation of the process of extracting the nodes-network and the parameters from it, is not yet far progressed.

Regarding optical phenotyping data, the first step is always a segmentation of all available plant organs, so we can distinguish which part of the image is part of the plant and contributing to the node-network (Pound et al., 2017). While there are already automated workflows for 2D data, optical 3D data require a high amount of manual interaction (Selzner et al., 2023). Once having the segmented 2D or 3D of a plant or the root system and shoot organs separately, a variety of software tools exist to extract the required parameter. The range of tools goes from highly flexible programming packages allowing full automation but are complex to use, such as PlantCV (Gehan et al., 2017), over semi-automated GUI-based tracking software, such as SmartRoot (Lobet et al., 2011) or RootSystemAnalyzer (Leitner et al., 2013b) to mostly manual drawing and tracing solutions, such as VRoot (Baker et al., 2024b). The mutual advantage of this procedure is that the extracted parameters are directly usable for FSPM parameterization. However, it is often the case that we do not have data from completely measured plants but only from fragments of organs, such as broken root systems, as measured in a minirhizotron or leaf area data obtained from UAVs.

Additional methods, having the capability to estimate model input parameters based on these unconnected or fragmented plant organ architecture measurements, are therefore required. These kinds of data can be used to obtain aggregate data, such as leaf area index (LAI) or root length density (RLD). Inverse model parameter estimation from aggregated parameters is a promising method. E.g., Morandage et al. (2021) developed a method that takes RLD data that are derivable from, e.g., soil coring or minirhizotrons images, as input for a Bayesian inference with Markov chain Monte Carlo algorithm to estimate architectural root model input parameters. Further development of this approach would significantly help to identify parameters from aggregated data.

On top of the structural parameters that are crucial to simulate the architecture of a plant, further parameters for the functional aspects of the plants are required. In order to obtain these data, phenotyping of anatomical features, such as xylem and phloem vessel size and count, may help to compute the hydraulic properties. Tools to analyze the anatomical structure of the measured organ, such as ROXAS for shoots (von Arx and Carrer, 2014) or GRANAR for roots (Heymans et al., 2020), help gather this information. In conjunction with the hydraulic simulator MECHA, these data provide insights into plant hydraulic properties that are required to parameterize an FSPM so that functional simulations, such as water and solute transport within the plant, are enabled (Couvreur et al., 2018). However, gathering all information from a single experimental set-up or even the same plant is often not feasible, although it would be desirable. Therefore, complex FSPM parameterization problems often combine data originating from different sources and methods.

The methodological examples described above demonstrate that methods, tools, and pipelines used to obtain model parameters are as diverse as the phenotyping methods used to obtain the underlying data. However, the procedure to design an analysis workflow stays the same for every method. Therefore, the following step-by-step workflow was created to standardize the development of a data-to-model

workflow, as shown in Figure 1-5. Step 1 is the identification of the desired parameter(s). The second step is the choice of the method and technique to phenotype the desired corresponding traits. If the phenotyping was already performed before the target parameters were defined and the dataset already exists, step 3 is especially important. In the third step, the data structure has to be defined, which is the preparation for the following steps. Step 4, the pre-processing, is optional and highly depends on the available data format and structure. Step 5 is the core part of the analysis, where we have to choose the right tools for our (pre-processed) data. The last step, the post-processing, is also optional and mainly serves as a verification that the previous steps were successful. Sticking to these 6 steps facilitates the data-to-model workflow for FSPM parameterization.

Once we have a well-parameterized FSPM, it can answer different scientific questions regarding plant development and responses under various environmental conditions. In the past, FSPMs have been used to quantify how resource allocation is affected by plant architecture (Godin and Sinoquet, 2005), how light distribution within a canopy affects photosynthesis plant growth (Vos et al., 2009), how environmental stresses, such as drought or high temperature, impact plant architecture and function (Chenu et al., 2008), how breeding strategies can be optimized for specific environments (Boote et al., 2021), how nutrient availability influence root growth patterns and overall plant development (Postma and Lynch, 2011), or how genotypes are affecting the root system conductance (Yu et al., 2024).

FSPMs' application cases are versatile and mainly limited by model implementation and data quantity and quality. Therefore, developing comprehensive FSPM toolboxes, such as CPlantBox, is crucial. These toolboxes should combine different structures and processes across various scales to cover as much of the reality as possible. Measuring, analyzing, and structuring the underlying data correctly is key for accurate model predictions.

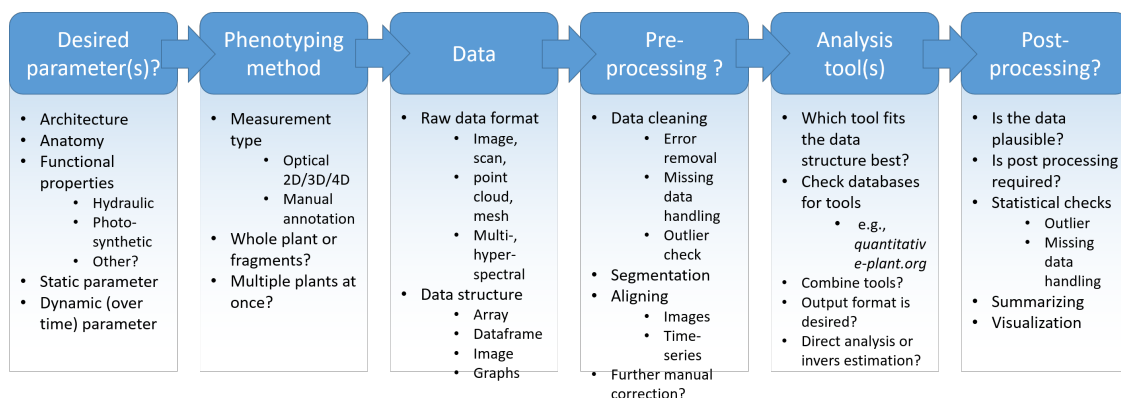


Figure 1-5: Schematic procedure to design an analysis workflow to obtain FSPM parameter from phenotyping (data2model).

1-5 Aims and Objectives

This work focuses on developing and validating a new phenotyping method to increase our ability to non-invasively collect and analyze *in situ* root development information over time and at different scales. Furthermore, this work aims to collect a unique and comprehensive belowground dataset, including all agronomic aspects over a longer time period that are required to enable further ground-breaking research on plant responses to changing environments. Ultimately, this work combines phenotyping with FSPMs to understand the consequences of combined environmental stresses, in particular, how the absence of the crucial macronutrient phosphorus is affecting the capacity for water uptake of *Zea mays*. Additionally, this work contributed to several collaborative studies with the methods, data, and models presented in Chapters 2-4. These studies focus on new phenotyping methods, such as GPR, the creation of comprehensive aboveground datasets complimenting the subsoil dataset presented in this work, the domestication and adaptation of maize to water availability over time, and *in silico* methods to increase our phenotyping and modeling capacities by using high-performance computing (HPC) and computer game engines combined with virtual worlds.

The overall objective of this work is to improve the structural and functional quantification of plants with a special focus on their root systems.

In detail, this work is focused on the following main research objectives:

1. Develop, implement, and validate an automated minirhizotron image analysis method, enabling a faster and objective analysis of minirhizotron data to decrease resource demand for the analysis process and increase data quantity and quality.
2. Collect and provide a comprehensive subsoil minirhizotron data set for a wide range of scientific domains and applications.
3. Investigate the architectural responses to phosphorus deficiency in *Zea mays* by using phenotyping and modeling methods
4. Quantify the effect of phosphorus-related changes in plant architecture and physiology on water uptake capacity, by parameterizing a functional-structural plant model of *Zea mays* with CPlantBox, based on the previously obtained plant-scale phenotyping data.
5. Transfer the phenotyping and model pipelines previously developed to other application cases with a focus on investigating the response of *Zea mays* to changing environmental conditions. Apply the methods, data, and models used to approach the above objectives to further develop and test new *in situ* and *in silico* methods at different scales to phenotype *Zea mays*, analyze data and predict the architectural and functional responses to environmental conditions. In particular, evaluate GPR as a method, generate an aboveground dataset corresponding to the belowground dataset, evaluate the root response of maize under dry and wet field conditions in different

soils, provide a method and model that assist in unraveling the *Zea mays* domestication history, and generate data to further develop new phenotyping methods built on immersive technologies.

1-6 Outline of the thesis

This thesis is composed of six chapters and eight appendices:

Chapter 1 is the introduction chapter. It provides an overview of changing environmental conditions and the implication for *Zea mays*, the importance of phenotyping, functional-structural plant modeling, and how to combine these two disciplines to enable deeper insight into plant responses. It further introduces the aims and objectives and provides a brief outline of the content of this work.

Chapter 2 introduces a newly developed and validated minirhizotron image analysis pipeline, based on deep neural network segmentation of roots and the subsequent automated feature extraction. The presented method increases minirhizotron image analysis by approximately 99% and increases objectivity and metrics quantity and quality. The data produced in this study are, amongst other data, presented in detail in Chapter 3.

Chapter 3 focuses on a holistic and comprehensive sub-soil data set acquired at two minirhizotron facilities in Selhausen, Germany. The data acquisition and processing includes data collected for the years 2015 - 2021 for *Triticum aestivum* and *Zea mays* grown on two different soil types. The measurement methods presented include minirhizotron root images, time-lapse horizontal crosshole GPR, soil sensors recording soil water content, soil water potential, and soil temperature, measured with Time-Domain-Reflectometers, tensiometer and MPS-2 sensors, respectively.

Chapter 4 investigates the response of *Zea mays* to decreasing soil phosphorus availability. Architectural changes to phosphorus limitation are obtained by phenotyping and used for functional-structural plant modeling to enable deeper insights into the impacts of combined stresses. Changes in plant hydraulics are investigated using a CPlantBox model, leading to new insights into the implications of phosphorus deficiency on the conductivity of the root system.

Chapter 5 discusses the results made in Chapters 2-4 and sets them in a global context. Additionally, this chapter combines the published results of six studies to which the work in this dissertation has made significant contributions.

Chapter 6 summarizes the key results of the doctoral project and presents general conclusions. Recommendations for future work and research topics are provided as an outlook.

Appendix A contains supplementary information to Chapter 2.

Appendix B contains supplementary information to Chapter 4.

Appendix C includes a comprehensive overview of all published studies to which this work has made significant contributions and supplementary information pertinent to Chapter 5.

Appendices D-H contain conference proceedings about methods, data, and results developed during the studies presented in Chapters 2-4 and published on the way to finish the here presented doctoral project.

*A baby learns to crawl, walk and then run. We
are in the crawling stage when it comes to
applying machine learning.*

DAVE WATERS

« ◊ »

The following chapter presents a new high-throughput image analysis pipeline for root phenotyping that significantly reduces processing time and achieves high accuracy through the use of deep neural networks and automated feature extraction.

Development and validation of a deep learning based automated minirhizotron image analysis pipeline

Abstract

ROOT SYSTEMS of crops play a significant role in agro-ecosystems. The root system is essential for water and nutrient uptake, plant stability, symbiosis with microbes and a good soil structure. Minirhizotrons have shown to be effective to non-invasively investigate the root system. Root traits, like root length, can therefore be obtained throughout the crop growing season. Analyzing datasets from minirhizotrons using common manual annotation methods, with conventional software tools, are time consuming and labor intensive. Therefore, an objective method for high-throughput image analysis that provides data for field root-phenotyping is necessary. In this study we developed a pipeline combining state-of-the-art software tools, using deep neural networks and automated feature extraction. This pipeline consists of two major components and was applied to large root image datasets from minirhizotrons. First, a segmentation by a neural network model, trained with a small image sample is performed. Training and segmentation are done using RootPainter. Then, an automated feature extraction from the segments is carried out by RhizoVision Explorer. To validate the results of our automated analysis pipeline, a comparison of root length between manually annotated and automatically processed data was realized with more than 36,500 images. Mainly the results show a high correlation ($r=0.9$) between manually and automatically determined root lengths. With respect to the processing time, our new pipeline outperforms manual annotation by 98.1

- 99.6 %. Our pipeline, combining state-of-the-art software tools, significantly reduces the processing time for minirhizotron images. Thus, image analysis is no longer the bottle-neck in high-throughput phenotyping approaches.

Adapted from: **Felix Maximilian Bauer**, Lena Lärm, Shehan Morandage, Guillaume Lobet, Jan Vanderborght, Harry Vereecken, Andrea Schnepf (2022): Development and validation of a deep learning based automated minirhizotron image analysis pipeline. *Plant Phenomics*, 2022, <https://doi.org/10.34133/2022/9758532>

2-1 Introduction

ROOTS ARE AN ESSENTIAL COMPONENT of the global biosphere. They are mainly responsible for the acquisition of the resources water and nutrients for the entire plant. In most ecosystems, these resources are the limiting factors for growth of plant organs and yield (Atkinson et al., 2000). Water and nutrient uptake are directly linked to the parameters defining the root system, like length, diameter or branching. Therefore, collecting information about the root system becomes increasingly significant. In order, to improve water and nutrient uptake of plants for specific soil and climatic conditions, it is essential to obtain information about the root system architecture of plant species that have been shown to be beneficial for the given conditions (Lynch, 2007). For plant breeding, this will help to develop new genotypes, which are able to cope better with, e.g., drought stress and are more efficient in nutrient uptake (Lynch, 2013). This will not only help to increase the cultivated area for certain species, it might also lead to higher yields. This especially applies to locations with less suitable environments for highly productive agriculture. The negative impact on the soil should be minimized at the same time (Bianco and Kepinski, 2018).

The direct observation of roots is difficult, because the root system is surrounded by soil, making it challenging to visually measure the roots. To avoid that measurements heavily disturb the plant and its environment, permanent installed equipment, like rhizotubes, or the construction of a minirhizotron, are crucial (Atkinson et al., 2019). Minirhizotrons are useful tools to collect data about the root system without disturbing the environment of the roots or the plant itself. Moreover, they allow root observations over the whole vegetation period at a high temporal resolution and the comparison of different vegetation periods and crop types. Transparent rhizotubes, installed below ground, function as a window in the soil. Guided scanners and camera-systems provide high resolution images of the roots and the surrounding soil. Consequently, the non-invasive root measurements can be repeated multiple times during the growing period under *in situ* conditions. However, large minirhizotron facilities include tubes in different depth-levels. Measurements in several depths and time lapse observations result in big datasets that often consist out of 10,000 images and more (Cai et al., 2016a). Images provided by minirhizotrons strongly differ from, e.g., root scans gained from excavated and washed roots (Zeng et al., 2010). Various soil conditions around the tubes in different depths lead to a wide range of heterogeneous images with different characteristics. Beside the actual roots, soil structures and disturbing fragments, including small animals, are depicted. Different soil conditions in various depths and at varying locations lead to varying color and light conditions and therefore make the automated processing of minirhizotron-images a challenging task (Vamerli et al., 2011).

To analyze roots mainly two steps are needed, the segmentation of root objects and the object quantification (Leitner et al., 2013b). Due to the heterogeneity within minirhizotron images, the segmentation is very complicated. Different analysis approaches emerged, represented by a numerous collection of software

tools, designed to extract the information about the root system (Lobet et al., 2013). These tools work manually, or in a (semi-)automated way. Manual annotation tools for minirhizotron images, like WinRhizoTRON (Regent Instruments Incl.), or RhizoTrak (Möller et al., 2019) rely on the human interaction with each individual image taken, to track each root by hand. It requires the user to follow every root depicted in the image by hand and mark start, branch and endpoints. Semi-automated and automated approaches with software-tools exist to facilitate and speed-up the post-processing of the images (Vameralli et al., 2011). Filter algorithms used to increase the contrast between root and background and to find root structures by typical geometrical shapes, were proposed by several authors (Dowdy et al., 1998, Murphy and Smucker, 1995, Zeng et al., 2010). Semi-automated software like RootSnap! (CID Bioscience) and Rootfly (Zeng et al., 2008) require a manual annotation, but also provide root suggestions by a filter created on an initial dataset. Consequently, most of these programs are strictly limited to certain type of images, like high-contrast root scans (Yasrab et al., 2019). Eventually, this has the consequence that the annotation of the roots in most minirhizotron images needs to be done almost exclusively manually. Depending on the number of images taken and the number and length of roots, the manual and semi-automated analysis can take weeks to years. Previous studies found that the estimated amount of minirhizotron images, annotated with an annotation software, was between 17 and 38 images h^{-1} (Ingram and Leers, 2001). Adapted to the working routine with Rootfly, it takes 1-1.5 h annotation time for an image area of 100 cm^2 depicted soil (Smith et al., 2022). Further, the results underlie the subjectivity of the annotator, because annotations are done according to personal experiences and knowledge of the annotator.

Deep learning has developed to the Gold Standard of machine learning methods within the recent years. Deep neural networks are able to learn from big datasets and provide outstanding results on complex cognitive challenges, even beating human performance in some application fields (Alzubaidi et al., 2021). Convolutional Neural Networks (CNN), a subclass of deep learning models, have been created to deal with data in the shape of multiple arrays and are therefore suitable for high-dimensional data like images (LeCun et al., 2015). They have the potential to perform a decent automated detection of regions of interests within a heterogeneous and noisy dataset (Janiesch et al., 2021). Transferred to the analysis of minirhizotron images, CNNs should have the capability to precisely identify and segment roots in images where the roots cannot be segmented sufficiently by, e.g., explicitly programmed thresholds or filter algorithms. CNNs were already used successfully to localize plant organs, including roots (Kamilaris and Prenafeta-Boldú, 2018, Keller et al., 2018, Pound et al., 2017, Santos et al., 2020). However, the use of CNNs has mainly been proven on data originating from controlled environment, like lab experiments (Yasrab et al., 2019). Furthermore, they are often limited to the use of one or a few fixed pre-trained neural network models (Narisetti et al., 2021), or they are not easily usable for non IT-professionals (Shen et al., 2020). The main reason for this is the required knowledge and competences in machine learning and programming needed to create a CNN-based system. Especially the data partition between training and

validation, the process of annotation and the setup of network architecture make the use of CNNs complicated (Smith, 2018). Although the use of CNNs is promising for root segmentation and first approaches to use CNNs to segment roots have been successfully accomplished with, e.g., the SegRoot networks, it is not subject of many published studies and not yet widely used as phenotyping tool for root traits (Wang et al., 2019). To make the advantages of CNNs widely utilizable, a software, combining the annotation, training and segmentation process with CNN together in an interface easy to handle, is the key for general use of neural networks for automated root segmentation. The recently published software tool RootPainter is one of the most promising approaches for this task (Smith et al., 2022).

However, fast and reliable segmentation is only the first step of root analysis. For the root quantification another tool is required to obtain morphological and topological features from segmented images. For this task conventional automated root analysis tools, like WinRhizo (Regent Instruments Incl.) and IJ_Rhizo (Pierret et al., 2013) can be used. Recent progress in the development of root-system feature extraction from high-contrast images or scans have resulted in new software tool with the ability of extracting multiple features with a high precision. On the front line of current developments is the new software RhizoVision Explorer, providing the functions to accurately skeletonize a high-contrast segmented image, to correct the skeleton and deriving several features from it (Seethepalli et al., 2021).

The aim of our study is to develop a generally applicable, automated analysis pipeline, based on state-of-the-art technologies and software to extract root traits from minirhizotron images. This includes data annotation for neural network training, segmentation and feature extraction. The automated analysis pipeline has to meet the requirements in *i*) availability and feasibility, *ii*) accuracy and comparability, *iii*) speed and efficiency. It was an important requirement to us that this workflow should be feasible for root scientists, who only have basic knowledge in programming or computer science. This workflow should make fast root phenotyping easily accessible for newcomers in root science and lower the time and effort needed to get into the topic. Therefore, it relies on already published software. This workflow further should underline the practicability of deep learning phenotyping tools for the scientific root analysis routine. All software required to use this automated root image analysis pipeline are freely available and easy to operate. Another key advantage of our study is the scope of data used for validation and comparison and the concomitant claim to a general validity of this pipeline. To test and validate the automated analysis pipeline, datasets obtained from several years and two minirhizotron facilities were processed and compared to previously manual annotated data (Cai et al., 2018a,b, 2016a, Morandage et al., 2021). Previous studies evaluating the results of a CNN-automated image analysis for root images originating from (mini)rhizotrons used between 40 - 857 images (Narisetti et al., 2021, Smith et al., 2022, Wang et al., 2019). In our test we evaluated the results of more than 107,000 images of which we used more than 36,500 for a direct one-to-one comparison of manual human annotation to our automated analysis pipeline. The images represent different *in situ* conditions. In this pa-

per we will present the detailed procedure on operating the automated analysis pipeline and compare its performance to a previously done manual annotation for a decent evaluation.

2-2 Materials and Methods

2-2-1 Experimental test site

The data used for the automated analysis pipeline were collected at the two minirhizotron facilities at the Selhausen test site of the Forschungszentrum Jülich GmbH (50°52'07.8"N, 6°26'59.7"E), Germany (Bogena et al., 2018, Weihermüller et al., 2007). The field, in which the minirhizotron facilities are located, has a slight incline with a slope of under 4°. The two minirhizotron-facilities are approximately 150 m apart. The minirhizotron facility located at the top of the field is hereafter referred to as R_{UT} (rhizotron upper terrace) and the minirhizotron at the lower part of the field as R_{LT} (rhizotron lower terrace). The thickness of the soil layer with silty loam texture varies strongly along the field-slope. While it is not present at the top, its thickness at the bottom is up to 3 m. At R_{UT} the gravel content is 60 % while at R_{LT} it is only 4 %. Both facility contain 54 horizontally installed, transparent tubes with each a length of 7 m and an outer diameter of 6.4 cm. The tubes are separated into three plots with each three vertical, slightly shifted (10 cm) rows of six tubes, where three different treatments can be studied. The tubes in each row are installed in -10 cm, -20 cm, -40 cm, -60 cm, -80 cm and -120 cm depth. Past treatments include different irrigation patterns (sheltered, rainfed, irrigated), different sowing densities and dates (later sowing in sheltered plot), or cultivar mixtures (two single cultivar treatments and one mixture). The two minirhizotron facilities were installed in 2012 (R_{UT}) and 2014 (R_{LT}), respectively. Further construction details are explained in (Cai et al., 2016a).

2-2-2 Data acquisition

Two different camera systems manufactured by Bartz (Bartz Technology Corporation) and VSI (Vienna Scientific Instruments GmbH) were used to capture the root images in the minirhizotrons. Both camera-systems are designed to be used manually. A regular measurement produces 40 images per tube. 20 images are taken 80° clockwise and 20 images 80° counter-clockwise from the tubes top point (Cai et al., 2018b, 2016a, Klotzsche et al., 2019, Morandage, 2020). In this study, the collected images of three crop growing seasons from 2015/16 and 2017 were taken into account. Depending on the year and measurement date either the Bartz- or the VSI-system was used. The crops cultivated at the test site and used for this study were *Triticum aestivum* cv. Ambello in 2015/16 (winter wheat) and in 2017 *Zea mays* cv. Zoey. Table 2-1 gives an overview on camera system used, the resolution of the images, measurement years, measured time period and cultivars observed. Depending on crop growing season, the total amount of

measurement dates varied between 21 and 38. The amount of images, taken at one measurement date, varied according to the amount of tubes measured at this measurement date (Table S1.1). This was depending on the state of vegetation evaluated in field.

Table 2-1: Overview of the camera-systems and experiment timeline of minirhizotron images acquisition

camera system	Bartz	VSI
original resolution (px)	754 x 510	3280 x 2464
converted resolution (px)	1508 x 1020	2060 x 2060
real size (mm)	16.5 x 23.5	20 x 20
growing season	2015/16 & 2017	2017
culture	2015/16: <i>Triticum aestivum</i> cv. Ambello 2017: <i>Zea mays</i> cv. Zoey	<i>Zea mays</i> cv. Zoey
time period (dd/mm/yy)	16/11/15 - 23/06/16 23/06/17 - 12/09/17	08/06/17 - 22/06/17

Over the past years, the root images collected in the minirhizotron facilities in Selhausen were analyzed manually, using Rootfly as a semi-automated tracking tool for the root length and root counts (Cai et al., 2018a,b, 2016a, Morandage, 2020, Zeng et al., 2008). In this study the images of the years 2015/16 and 2017 were analyzed. The manual annotation of 2015/16 and 2017 has been already published in (Cai et al., 2018b, Morandage et al., 2021). Further a sub-sample of the root images was manually annotated by two persons separately in Rootfly. 1,760 images were used for the comparison between both annotators, and the annotators and the results of the automated analysis pipeline, to test if there are differences in terms of human subjectivity .

2-2-3 Software tools

Our proposed automated minirhizotron image analysis pipeline is based on two software tools for the segmentation (Smith et al., 2022) and the automated feature extraction (Seethepalli and York, 2020). Furthermore, scripts to convert the segmented images and analyze the outcome are available. For an easy accessibility all scripts are available together within the GUI of the executable RootAnalysisAssistance (Supplementary Material). The conversion of the segmented images is also possible within RootPainter.

Segmentation

RootPainter, a software tool for the deep learning segmentation of biological images with an included annotation function provides an interactive training method within a GUI, using a U-net based CNN. U-net was developed to train with less images for a more precise segmentation and is therefore suitable when it comes to images where the manual annotation is especially time and labor consuming (Ronneberger et al., 2015, Smith et al., 2022). RootPainter was developed to

make training-data creation, annotation and network-training accessible for ordinary users. It provides a dataset creation function, which allows an easy selection of training images and cropping them in multiple tiles and to a suitable size for the interactive training. The training mode provides an interactive graphical platform to manually annotate a small part of the dataset and create a neural network model. Further, a mode to segment whole image directories at once is provided. For training and segmentation a Graphics Processing Unit (GPU) is required (Smith et al., 2022). However, a full minirhizotron image analysis is based on two main components, the segmentation and the root trait extraction. Although RootPainter provides an inbuilt function for basic root trait extraction based on the previous segmented images, it does not provide, e.g., a skeleton correction function and a comprehensive feature extraction including multiple root traits. For our pipeline the feature extraction part should provide multiple morphological and architectural root features with a high accuracy. Furthermore, the possibility of a systematic correction function should be implied. Therefore a platform fulfilling these requirements was used for feature extraction.

Feature extraction

RhizoVision Explorer represents the current state-of-the-art technology with a sophisticated automated root traits extraction from segmented root images, by combining the abilities of several existing root image analysis platforms. This includes skeletonization of the segments, filter, filling, smoothing and pruning functions (Seethepalli et al., 2021, Seethepalli and York, 2020). However, like most programs for automated root system analysis it is built for the use with binary images or high contrast scans and therefore not suitable for minirhizotron images. The capability of RhizoVision Explorer are nevertheless useful when applied to already segmented minirhizotron images.

2-2-4 Analysis pipeline

The starting point for the automated analysis pipeline is a directory containing the raw images captured at the minirhizotron facility. The pipeline was run on a GPU-server with 4 Nvidia GeForce RTX 2080 Ti (NVIDIA Corporation). As client, a computer with an Intel i5-8265U processor and 24GB RAM, operated on Windows 10, was used. However, it is also possible to run the pipeline on one machine, if there is a GPU with CUDA available, or to use the Google Colaboratory (Google Colab). An overview of all following steps is explained in Figure 2-1.

Pre-processing

The first step of the pipeline is the pre-processing of the images. Depending on the image acquisition system either an up- or down-scaling and a distortion correction is performed (supplementary data). In the same step a labeling, sorting and registration of the images is done automatically. If the images are already ready to use, this step can be omitted.

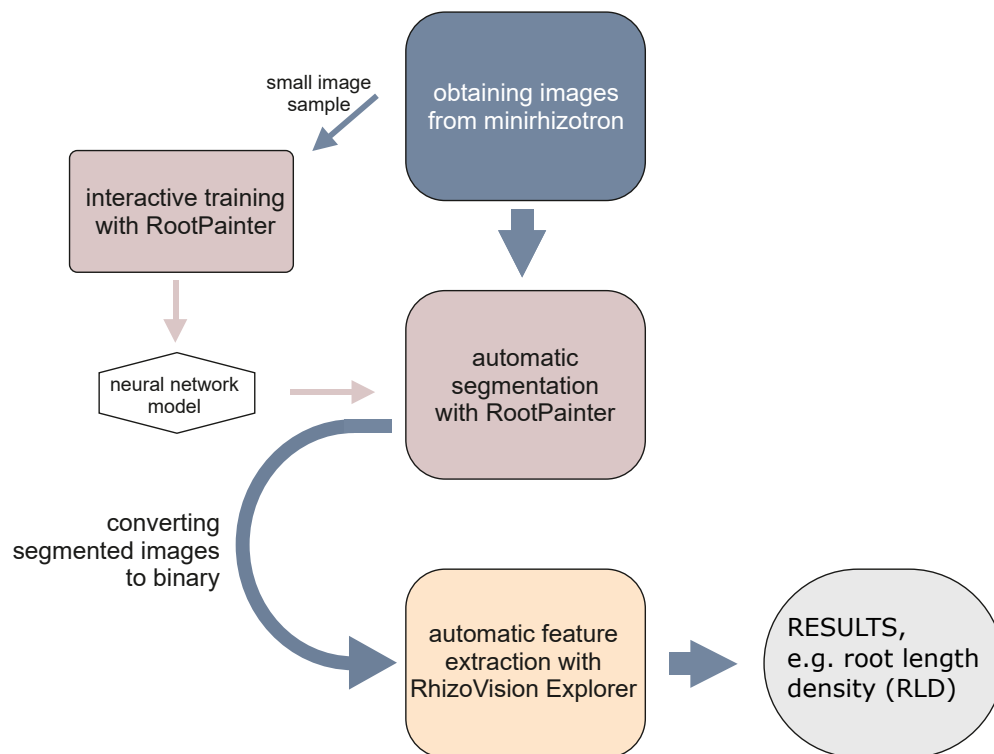


Figure 2-1: Schematic overview of the workflow of the automated analysis pipeline starting with image acquisition in the minirhizotron facility.

Training

This step is only needed if no suitable neural network model exists for the targeted dataset. The process, to train a model for root segmentation starts with the creation of a training dataset and subsequently a new project in RootPainter. We highly recommend to balance the training data according to the factors influencing image visually, in order to maximise the heterogeneity in the training data. Images with different quantities of roots and various root types at different locations should be included. In our case the training dataset for one model contains a balanced amount of images from two different minirhizotron facilities, respectively soil types, depths, tubes and dates. We used only a small amount of images from all available images. For each camera system a separate model was trained, because the images of the two cameras differ significantly. The annotation can be done in the GUI. The roots are annotated as "foreground", soil and other not root-belonging fragments as "background". After the training is started, RootPainter automatically creates neural network models, depending on the annotation done previously. The progress can be seen in real time, because RootPainter provides previews of the segmentation done by the actual model. These proposals can be corrected and supplemented by the user. The training procedure used in this study is the "corrective training". It is intended for large datasets and therefore suitable for the minirhizotron image data. Essentially this training approach starts with

annotating a few images in detail and then continue with correcting only the false-positive and false-negative suggestions of the current model. After finishing the interactive annotation the training is completed automatically. Further details and instructions are explained in (Smith et al., 2022).

Segmentation

The fully-automated segmentation is done with the best model previously trained with a small selection of images from the corresponding measurements. To perform the fully-automatic segmentation, all images have to be located in one directory. The segmentation process itself is started from the RootPainter main menu. For each minirhizotron image stored in the directory, one segmented image will be created (Figure 2-2a, Figure 2-2b).

Converting

To import the segmented images into RhizoVision Explorer in the next step, it is essential to convert the images to binary, otherwise the images are not loaded properly (Figure 2-2c). This step is performed by a conversion-script, which converts the mono-colored segmented images to black and white images and reduces the images information to binary by only giving information for either black or white pixels. The conversion-script is available as python script or within the *RootAnalysisAssistance*-GUI. It is possible to either browse the image-folders to convert manually, or to process the conversion of a certain image directory in a batch mode. This option is suitable for fast processing a large amount of segmented images. The conversion option is also available within the RootPainter-GUI.

Feature extraction

The final step is the feature extraction, performed by RhizoVision Explorer. This is also done in batch mode. The threshold of the non-root filter, hole filling, edge smoothing and pruning was chosen in a standardized way and uniform for each parameter, depending on the resolution of the image. For the images resulting from the Bartz-system the threshold is 13 px and for the VSI-system 20 px. This results in filtering parts smaller than 0.2 mm^2 and filling holes bigger than 0.2 mm^2 . To minimize the influence of segmentation mistakes at the border between root and soil and thus reduce the false detection of non-existent laterals, the minimum size for a lateral root to be detected as a branching root is the parent roots radius multiplied with 0.2 mm. The architectural and morphological information are exported as CSV and the processed segmented images with the calculated skeleton is saved as PNG (Figure 2-2.d). The feature extraction is started from the RhizoVision Explorer GUI. Further details and background information are explained in (Seethepalli et al., 2021).

Root analysis

As last step in addition to the feature extraction, the two-dimensional root length density (RLD) is calculated from the total root length and the window size of the image in the unit of cm cm^{-2} . Furthermore, the number of root tips and branch points, the total root length, the branching frequency, the network and surface area, the diameter (average, median and maximal), the perimeter and the volume can be extracted from the RhizoVision Explorer output CSV and applied to spatio-temporal analysis of the root system (Figure S1.1 and supplementary data).

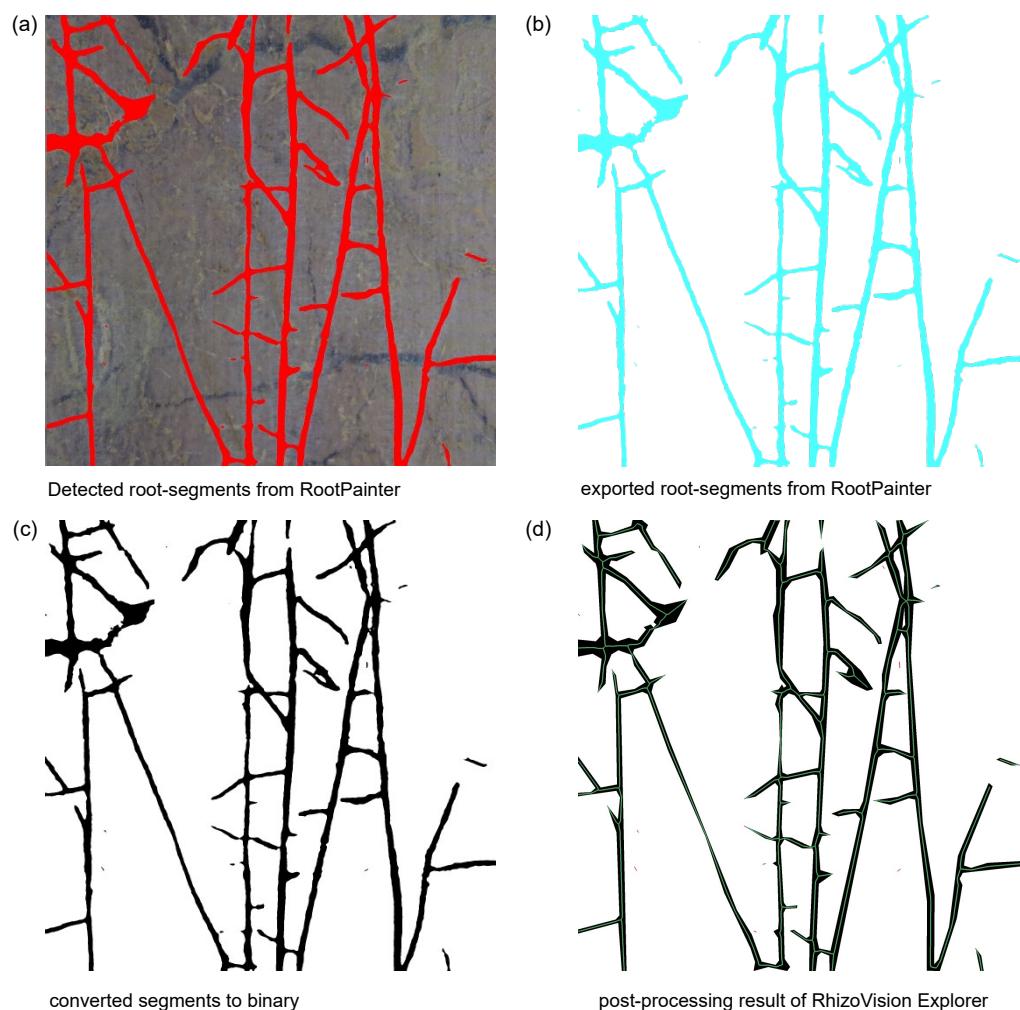


Figure 2-2: Example for one image processed by the automated root analysis pipeline. (a) The roots are "detected" by RootPainter according to the previous trained model. (b) The segmented image is exported and (c) converted to binary. (d) The last step is the skeletonization and feature extraction with RhizoVision Explorer.

2-2-5 Statistics, data processing and visualization

Python 3.8 with *Pandas 1.0.5*, *Numpy 1.18.5*, *Matplotlib 3.2.2*, *Pillow 8.2.0* and *SciPy 1.5.0* have been used for statistics, data processing and visualization.

The F_1 -score (eqn. 1) is a measure commonly used to evaluate neural network models (Smith et al., 2022). The F_1 combines precision and recall and has been designed to work on imbalanced data. Precision evaluates the percentage of all correct positive predictions and recall indicates how many positive of all positives the model found. F_1 values are bounded between 0 and 1, the highest value is indicating perfect precision and recall.

$$F_1 = 2 * \frac{precision * recall}{precision + recall} \quad (2-1)$$

$$precision = \frac{T_P}{T_P + F_P} \quad (2-2)$$

$$recall = \frac{T_P}{T_P + F_N} \quad (2-3)$$

where T_P are the *true positive*, F_P the *false positive* and F_N are the *false negative* pixels. The F_1 -score was calculated during the interactive training. True positive pixels are correct recognized pixels, where roots are correctly classified as roots. False positive pixels are pixels classified as root, not including a part of a root and false negative pixels are pixels including parts of a root, but are classified as background.

The outcome of the automated root annotation was compared to the manual annotation by means of the pearson correlation coefficient, both on the data set as a whole as well as on individual measurement dates for the seasons 2017. For the same season we calculated the mean of the total root length per image for each measurement date and used a Welch two-sample t-test to assess whether the differences between automated analysis and manual annotation of the total root length (ΔRL) were statistically significant. Furthermore the normalized root mean squared error (NRMSE) was calculated according to eqn. (4).

$$NRMSE = \frac{\sqrt{\frac{\sum_{i=1}^n (y_i - \hat{y})^2}{n}}}{y_{max} - y_{min}} \quad (2-4)$$

where $n = sample\ size$, y_i is the i^{th} observation of y and \hat{y} is the predicted y value.

Additionally a linear Model II regression (ordinary least products) was performed to test for fixed and proportional bias with the total root length of 2017 data. We choose this type of regression because the x -values might also be subject to errors (Delory et al., 2017, Ludbrook, 1997). For each measurement date and facility, a model was fitted and the 95% confidence interval (95% CI) of slope and intercept was calculated. We considered a fixed bias if the 95% CI of the intercept did not

include 0 and there was a proportional bias if the 95% CI of the slope did not include 1.0.

The manual per-image annotation with Rootfly of 2015/16 data is no longer available. However, the images and mean RLD values per tube are available and therefore were used for comparison. Based on this the RLD resulting from automated and manual analysis methods was calculated for every minirhizotron tube and measurement date (Figure S1.1) and compared as a proxy for a common root measurement parameter (Zuo et al., 2004). In this analysis, all growing periods 2015/16, and 2017 were included.

2-3 Results

2-3-1 Neural Network model validation

The F_1 for both neural network models trained for each camera-system is high. The F_1 for the Bartz-system is 0.78 and 0.81 for VSI-system model. After 60 epochs without any improvement the neural network training was stopped automatically.

2-3-2 Comparison of automated and manual annotation

Considering all images used for comparison, the overall correlation of total root length between manual annotation and automated analysis pipeline is very high with $r = 0.9$.

The correlation was performed with 16,599 images taken at R_{UT} and 21,082 images taken at R_{LT} . For the data obtained in the growing period 2017, the correlation is high to very high ($r = 0.77 - 0.94$) for every measurement date except the first measurement date at R_{LT} ($r = 0.57$) (Figure 2-3). Generally, the correlation shows an increasing trend towards later measurement dates (Table 2-2). ΔRL and NRMSE indicate low values for most measurements dates at both facilities. Regarding especially the ΔRL it can be seen, that the differences in mean between manual annotation and automated analysis pipeline in 2017 are very low -0.5 mm (R_{UT}), -0.77 mm (R_{LT}). However, the t-test indicates that there are no significant differences between the mean of total root length except for measurement date 4 at R_{UT} . The slope of the linear regression models is slightly under one in most cases and the intercept marginally higher than 0 for all measurement dates. Both fixed and proportional bias were detected within almost every measurement date (Table S1.2).

Regarding the RLD values from 2015/16, one specific difference between manual and automated analysis is visible. Until the 14th measurement date the RLD is continuously increasing and then stagnating in the 2015/16 data resulting from manual annotation. The RLD from the automated analysis follows the same trend but decreases from 14th measurement date continuously. Beyond this, the

RLD curves of both methods are very consistent (Figure 2-4). In 2017 datasets, only negligible differences between manual and automated analysis method are recognizable, except for the first measurement date at R_{LT} (Figure 2-4f, Figure S1.2b) and first two dates and a small peak at the fourth measurement at R_{UT} (Figure 2-4h).

The comparison between two human annotators and each annotator and the automated analysis pipeline separately shows that the correlation between the person 1 and the pipeline is $r = 0.92$ and the correlation between person 2 and the pipeline is $r = 0.79$. The correlation between both persons is the lowest ($r = 0.73$).

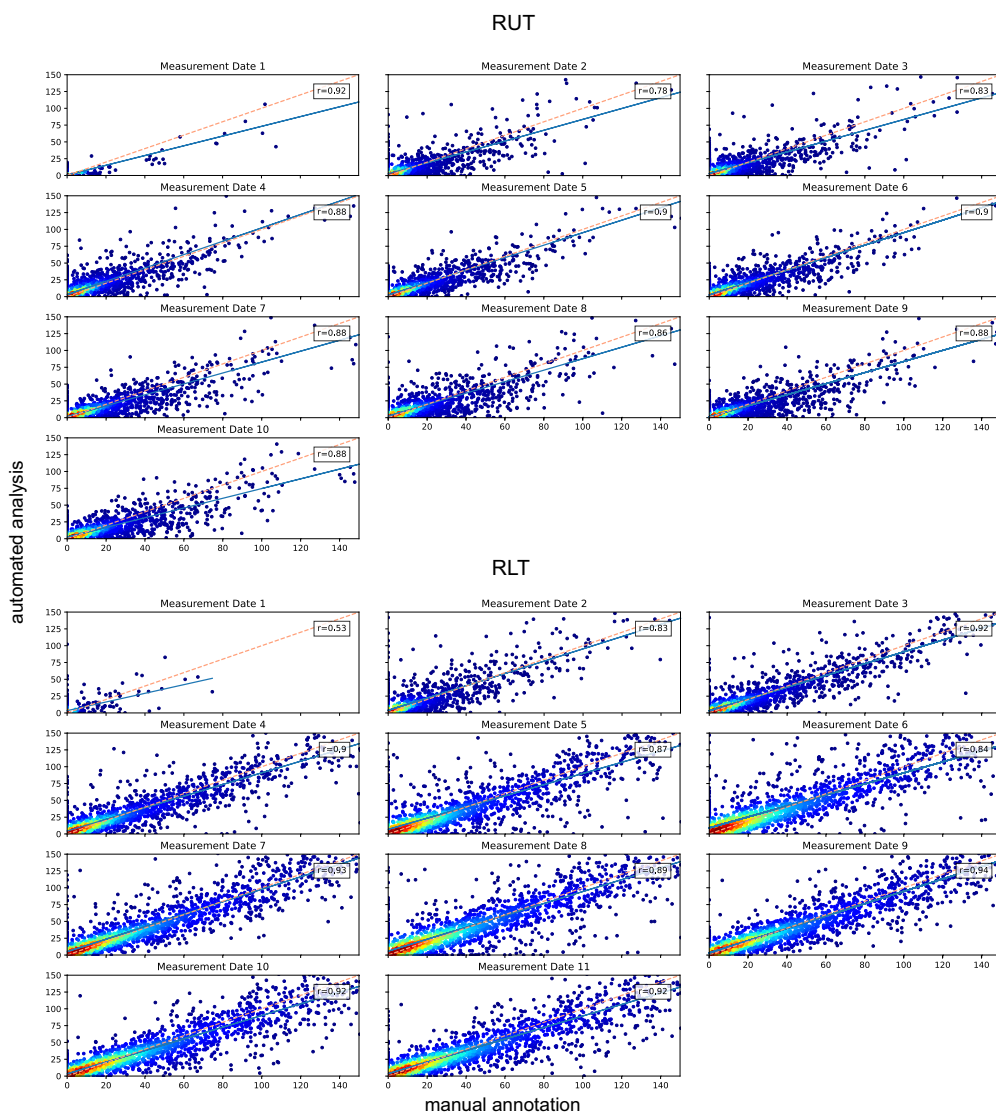


Figure 2-3: Correlation of automated and manual analyzed root length, obtained from 2017. Each measurement date is considered separately for R_{UT} and R_{LT} . The color represents the density.

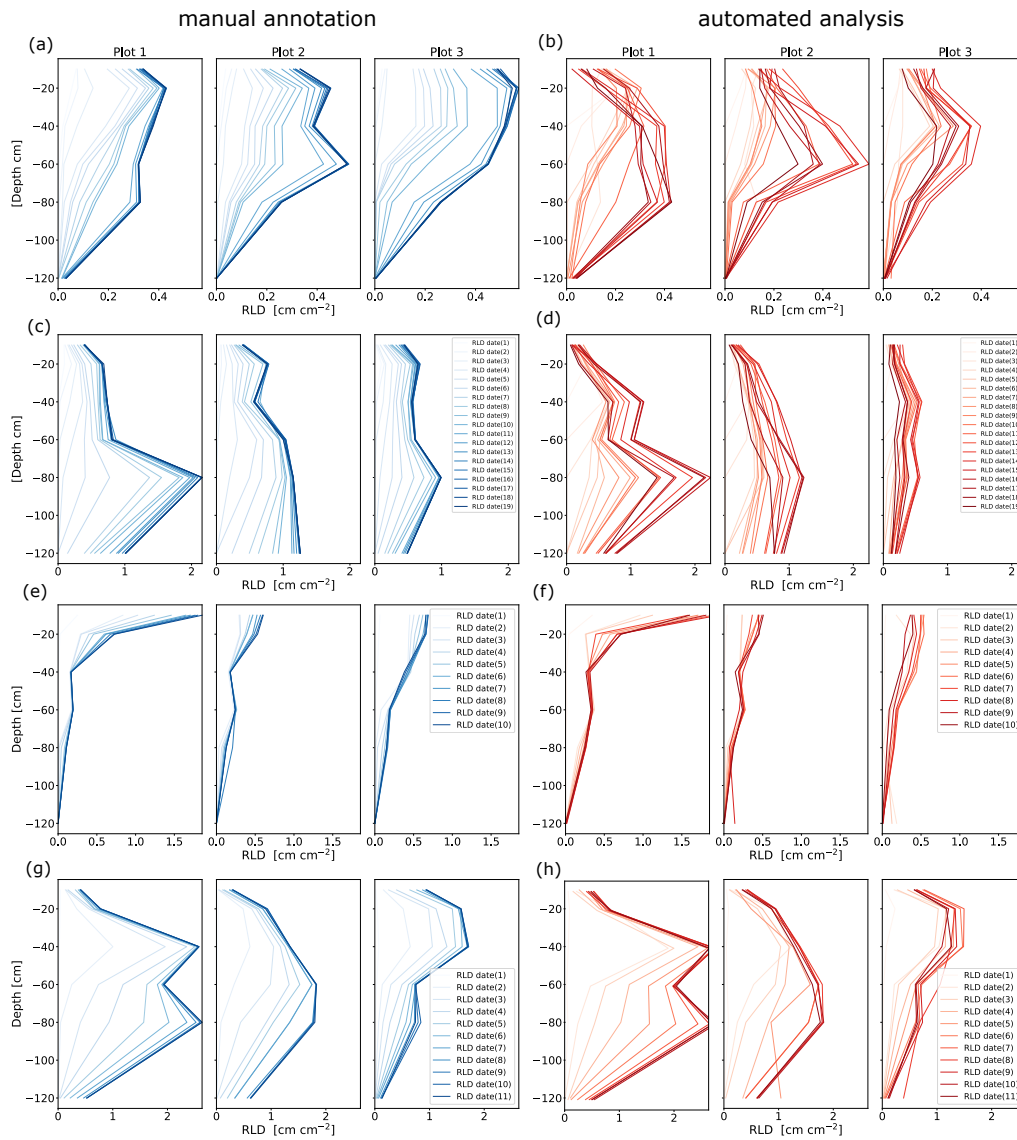


Figure 2-4: Comparison RLD of the data obtained from images originating from two minirhizotrons in the growing season 2015/16 and 2017, separated by plots grown with different treatments. The images were analyzed by hand (blue: manual) and by the automated analysis pipeline (red: automated). 2015/16: (a) R_{UT} manual, (b) R_{UT} automated, (c) R_{LT} manual, (d) R_{LT} automated; 2017: (e) R_{UT} manual, (f) R_{UT} automated, (g) R_{LT} manual, (h) R_{LT} automated;

Table 2-2: Overview of the statistical comparison of automated and manual annotation. ΔRL is the difference between the mean total root length (mm) obtained from automated and manual analysis methods, and a Welsch two sample t-test shows whether differences are significant (* = $p < 0.01$).

measurement date		2017	
		R _{UT}	R _{LT}
1	ΔRL	0.45	0.42
	<i>NRMSE</i>	0.071	0.077
	<i>r</i>	0.92	0.53
2	ΔRL	0.89	1.17
	<i>NRMSE</i>	0.071	0.053
	<i>r</i>	0.78	0.83
3	ΔRL	0.95	0.54
	<i>NRMSE</i>	0.057	0.052
	<i>r</i>	0.83	0.92
4	ΔRL	2.94*	0.65
	<i>NRMSE</i>	0.051	0.055
	<i>r</i>	0.88	0.9
5	ΔRL	1.36	0.92
	<i>NRMSE</i>	0.041	0.072
	<i>r</i>	0.9	0.87
6	ΔRL	1.35	1.7
	<i>NRMSE</i>	0.044	0.065
	<i>r</i>	0.9	0.84
7	ΔRL	-1.46	1.8
	<i>NRMSE</i>	0.046	0.058
	<i>r</i>	0.88	0.93
8	ΔRL	0.11	0.55
	<i>NRMSE</i>	0.045	0.073
	<i>r</i>	0.86	0.89
9	ΔRL	-1.41	-0.97
	<i>NRMSE</i>	0.039	0.057
	<i>r</i>	0.88	0.94
10	ΔRL	-2.44	-2.89
	<i>NRMSE</i>	0.039	0.047
	<i>r</i>	0.88	0.92
11	ΔRL		0.65
	<i>NRMSE</i>		0.065
	<i>r</i>		0.92

2-3-3 Time evaluation

The time required to train the neural network model mostly depends on the amount of images included in the training dataset. Approximately 65 % of the time needed is used for training of the deep neural network. The annotation takes 40 % of the time, based on a mean of 200 annotated images h^{-1} . The range it took to annotate one image was between 1 and 180 s per image, depending on the accuracy of the proposed segmentation. The time required for annotation decreases significantly with increasing training time. The mean time needed by the network for the training of a dataset of 1,500 images, was approximately 5h, excluding the real-time training during the annotation. This is approximately 25 % of the entire processing time. Segmentation took around 27 % of the total time. With 4 Nvidia GeForce RTX 2080 Ti GPUs and a batch size of 12 the segmentation took around 0.7 s per image. Converting the segmented to binary images and the final feature extraction took around 8 % of the time (Figure 2-5).

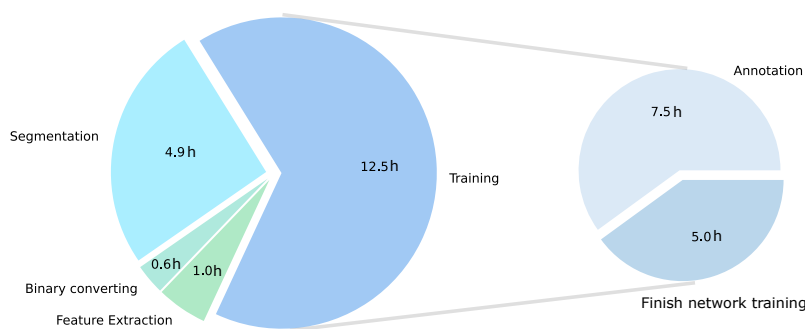


Figure 2-5: Time requirements to run the automated analysis pipeline for a sample of 25,000 images. Left: All sub-processes together. Right: share of the neural network training, which is only required when no suitable model is available.

2-4 Discussion

2-4-1 Availability and feasibility

The availability is the parameter for how easily accessible all components of the automated pipeline are for everyone. The feasibility defines how easy the proposed pipeline and with that the required software can be operated. The equipment needed to apply the new workflow requires a computer with a powerful GPU, or alternatively a basic computer, an additional server with powerful GPUs and a network-connection between both. Furthermore, the software packages of RootPainter and RhizoVision Explorer are needed and the conversion and analysis script are required. All this is open-source available (Seethepalli and York, 2020, Smith et al., 2022). All software can be found in the section "data availability".

The training of the model requires interaction with RootPainter, if the user wants to start the training of a new model or corrects a segmentation within the training process. This step is therefore not fully automated. All other components of the automated analysis pipeline are automated. The interactive mode of the training represents a major time saving compared to the conventional separation of the training step and the application step. Adaptations to the model can be done “on the fly” with little time investment, facilitating, e.g., the adaptation to new types of images. Once the model is trained, the human interaction needed to apply the pipeline is reduced to a few “clicks”. With a suitable model available, the user has to interact actively three times with the automated pipeline, (1.) to start the segmentation, (2.) to convert the segments to binary and (3.) to start the feature extraction. No deeper knowledge in computer science is needed, because all intermediate steps are available within a GUI. However, the first implementation of the RootPainter environment at the server part of the setup requires basic knowledge in server administration or support.

In contrast to manual or semi-automated operated root analysis programs, like different tools based on ImageJ, DART, GiA Roots, SmartRoot, EZ-Rhizo or Rootfly, the expenses in time, knowledge and experiences required to apply the automated workflow, are much lower. This is granted due to the very small interactions needed for the automated analysis pipeline (Armengaud et al., 2009, Bot et al., 2009, Galkovskyi et al., 2012, Lobet et al., 2011, Pierret et al., 2013, Zeng et al., 2008).

2-4-2 Accuracy and comparability

The accuracy evaluates the automated analysis pipeline in terms of reliability and exactness of the generated data. Comparability is given, if the results of the automated analysis pipeline can be compared to the outcome of previously evaluated data of the same kind, like the manual annotation performed with Rootfly. The most important characteristic of the automation of plant data analysis is the reliability of the generated datasets. Therefore, the accuracy of the observed root traits has to be as close to the ground truth as possible (Atkinson et al., 2019). In our study we used the manual annotation of the roots as comparison. The manual annotation was performed by different persons and over a long time period. Consequently, a certain subjectivity was included in this process.

Generally, the results for 2017 data analyzed automatically and manually are very close to each other, indicating a general great fit of the models used for images originating from 2017.

However, there is a fixed and proportional bias between automated analysis and manual annotation, showing a minor but systematic underestimation of total root length from the automated analysis (Table S1.2) that increases slightly to the later measurement dates, see also the negative ΔRL values in Table 2-2. This originates from the fact that the neural network model is only able to segment roots, if they are also visible by the human eye. Rarely, small parts of roots are covered by soil and this can only be compensated to a certain extend by training the neural

network and filling holes with RhizoVision Explorer (Figure S1.3). The more roots there are in the images, the more likely this segmentation mistake occur. Although this is a disadvantage of the automated analysis pipeline, its main purpose is to provide reliable and consistent data for a qualitative biological analysis. The known systematic bias in the method is well predictable in contrast to the bias originating from different annotators. Consequently, the data obtained from the automated analysis pipeline are more robust and reliable, which is in advantage for further biological conclusions drawn from the data.

The consistency of the automated analysis results becomes especially visible regarding the RLD plots plotted from 2015/16 and 2017 data (Figure 2-4). The decrease in 2015/16 RLD profiles that is not monitored in the manual annotation data, originated from the root senescence (Figure S1.4). The senescence could be better evaluated by the neural network than by the human annotator. In manual annotation the slight, gradual discoloration of the roots visually revealing the senescence is easy to miss. Furthermore, it is a complicated work step in Rootfly to eliminate already annotated roots at the right point in the timeline. Taking this into consideration, the results of the method comparison for 2015/16 and 2017 data shows impressive results, regarding accuracy and comparability of the automated analysis pipeline.

Regarding the biological conclusions that could be derived from the data, the differences between the methods are negligible, as we are working with minirhizotron data that cover a huge spatial and temporal resolution and are measured in heterogeneous conditions. Especially the consistent low ΔRL and NRMSE (Table 2-2), as well as the high conformity of the RLD profiles (Figure 2-4) indicate that the qualitative conclusions derived from data provided by the automated analysis pipeline are at least the same as from manual annotation. Considering the influence of the human subjectivity on manual annotation, the automated pipeline additionally provides objectivity that most likely cannot be reached, if more than one annotator does the manual annotation.

The manual annotation itself requires a certain level of expertise in root phenotyping. This expertise is gained with a lot of personal experiences (Vamerali et al., 2011, Zeng et al., 2008). Therefore, it can be hypothesized that there is also a significant influence of subjectivity in human annotation. Over the years, different persons annotated the root datasets. Hence, the impact of differences resulting from varying manual annotation strategies might influence the results more than the differences between manual and automated analysis. The direct comparison between two annotators showed a lower correlation between the persons annotating, than between the automated analysis pipeline and each human annotator. Consequently, we concluded that the human effect on manual annotation is higher than the impact of a mistake done by the automated workflow.

The automated analysis pipeline provides a level of objectivity, a human annotator cannot achieve. Therefore, it is highly probable that with the application of the automated pipeline associated minimization of the human influence will significantly improve objectivity and also accuracy of the minirhizotron image analysis.

2-4-3 Speed and efficiency

The speed is the pure amount of time the pipeline requires to analyze a certain amount of images. Efficiency is defined through the amount of time and labor needed to analyze a dataset in contrast to manual annotation. The time required to analyze root images by hand is enormous. The estimated time to analyze 100 cm² of depicted soil is 1 - 1.5 h (Smith et al., 2022). This is consistent with the results of other studies, needing approximately 1 h for annotating 17-38 images manually (Ingram and Leers, 2001). Intern evaluation reproduced the same results. To annotate 25,000 images, which is approximately the amount of images for a shorter growing season, the annotation time needed is 1,000 - 1,500 h. The time needed to process the same amount of images with the automated pipeline is approximately 19 h, including the training of the neural network. Without the training, the segmentation and feature extraction would only take around 6.5 h for all images. The resulting benefits in time saving are massive (Figure 2-5). Generally, only around 1.2 % - 1.9 % of the time needed for manual annotation is needed by the automated workflow to process the data, including the training. Excluding the entire training process, the automated workflow requires only 0.4 % - 0.65 % of the time needed to annotate the same amount of images manually with, e.g., Rootfly. Regarding the advantages of time saving, it further has to be taken into account that the time of interaction with the computer is decimated to almost zero, once the training is completed.

2-4-4 Limitations and further improvement

Although the current automated analysis pipeline does include time series in form of either root length density depth profiles at different time points or in form of root arrival curves, i.e., root length as a function of time at different depths, individual roots and their phenology are not followed from their birth to their death. This could be of high interest, for example, to root ecologists. To fully exploit minirhizotron data it would be a significant progress to add a single root tracking possibility, including root order and status. The implementation of these functions would improve the pipeline and enhance the use-cases for root ecologists.

2-5 Conclusion

We propose a new approach to analyze large amounts of 2D root image data. This became necessary with the big amount of data created in experimental field sites such as the minirhizotron facilities in Selhausen (Germany) as well as others (Svane et al., 2019, Ytting et al., 2014). The automated analysis pipeline illustrated in this study, is a suitable solution to easily and accurately analyze minirhizotron images in significantly less time. To the best of our knowledge, we are the first study testing a deep learning and automated feature extraction combining high-throughput minirhizotron image analysis pipeline to this extent. The biggest advantage of the automated workflow is the massive saving in time.

Precisely expressed, the required time is reduced by more than 98 % in contrast to manual annotation, while providing several root traits, including number of root tips, number of branch points, root length, branching frequency, network area, perimeter, volume, surface area and diameter on a spatio-temporal scale. The required root traits can be made available quickly which may speed up further analysis and applications of this type of data. In conclusion, the automated pipeline outperforms the manual annotation in time requirements and information density, while providing reliable data and feasibility for everyone. Tested with more than 107,000 minirhizotron images, including more than 36,500 images for detailed comparison, obtained from two growing seasons and different soil types, depths and cultures our results indicate a high general validity for the presented pipeline. Irregularities in the match of manual annotation and analysis pipeline can be essentially explained with rarely occurring missed segmentations of root fragments by the automated analysis pipeline, due to soil covered roots and mainly by the influence of human subjectivity in manual annotation. Balanced training datasets and consequent annotation of the training data are the key to good results. If these facts are considered, the here presented and evaluated pipeline has the potential to be the new standard method for reliable high-throughput root phenotyping of minirhizotron images.

Data is the new science. Big data holds the answers.

PAT GELSINGER

◀ ◊ ▶

In the following chapter, we will focus on the comprehensive dataset of root and soil data collected at minirhizotron facilities, explore the methods of data collection, and discover the potential of these data for understanding the soil-plant continuum.

Multi-year belowground data of minirhizotron facilities in Selhausen

Abstract

THE PRODUCTION OF CROPS secure the human food supply, but climate change is bringing new challenges. Dynamic plant growth and corresponding environmental data are required to uncover phenotypic crop responses to the changing environment. There are many datasets on above-ground organs of crops, but roots and the surrounding soil are rarely the subject of longer term studies. Here, we present what we believe to be the first comprehensive collection of root and soil data, obtained at two minirhizotron facilities located close together that have the same local climate but differ in soil type. Both facilities have 7m-long horizontal tubes at several depths that were used for crosshole ground-penetrating radar and minirhizotron camera systems. Soil sensors provide observations at a high temporal and spatial resolution. The ongoing measurements cover five years of maize and wheat trials, including drought stress treatments and crop mixtures. We make the processed data available for use in investigating the processes within the soil–plant continuum and the root images to develop and compare image analysis methods.

Adapted from: Lena Lärm^{*}, **Felix Maximilian Bauer^{*}**, Normen Hermes, Jan van der Kruk, Harry Vereecken, Jan Vanderborght, Thuy Huu Nguyen, Gina Lopez, Sabine Julia Seidel, Frank Ewert, Andrea Schnepf and Anja Klotzsche (2023): Multi-year belowground data of minirhizotron facilities in Selhausen. *Scientific Data* 10, 672. <https://doi.org/10.1038/s41597-023-02570-9>
(*contributed equally to this publication)

3-1 Background & Summary

AS A RESULT OF CLIMATE CHANGE, ensuring food security for the vastly growing human population is one of the major challenges of the 21st century. While climate change is exerting increasing pressure on the availability of natural resources such as water and soil nutrients, there is an increasing demand on food production. To ensure food security for the growing world population, agricultural production will have to increase by at least 60% by 2050 (Alexandratos and Bruinsma, 2012). The yield of agricultural crops therefore needs to be increased and yield stability under changing conditions must be preserved, if current consumption patterns are maintained. A comprehensive understanding of all processes within agro-ecosystems is crucial to identify the key parameters to maintain yield stability and increase yield. The main source of water and nutrients for plants is the rhizosphere and the surrounding soil. Key parameters for potential improvements in water and nutrient efficiency could be revealed through a comprehensive understanding of the soil–plant continuum and its processes. This includes parameters describing the root architecture, influencing processes such as root water, and nutrient uptake, which governs the yield (Lynch, 2007). Field phenotyping, especially incorporating below ground information is crucial for breeders to capitalize on developments in genetics, since information identified under controlled environment are often not accounting for "real-world" field conditions (Araus and Cairns, 2014). In-field observations also enable to investigate quantitative traits, particularly those related to root features that influence drought stress tolerance. Therefore, field phenotyping facilities including below ground information provide precious data for breeders (York, 2021). Additionally, knowledge about soil heterogeneity is crucial to understanding the distribution in soil water and nutrient content.

The data presented here include information about crop-relevant subsoil data – such as soil water content, soil water potential, soil temperature, and root development – on a high temporal-spatial resolution for multiple crop growing periods.

There are several techniques to observe roots non-destructive. The whole root system development can be observed with rhizotrons, equipped with a clear window on the side. Rhizotrons exist in various shapes for greenhouse and in-field observation (Silva and Beeson, 2011, Wasson et al., 2020). If installed above ground, these rhizoboxes allow for the sampling and imaging of root systems through easily accessible windows and apertures at the side (Rasmussen et al., 2020, Thorup-Kristensen et al., 2020). In the past, several in-field rhizotrons often took the form of covered underground cellars or walkways with transparent windows or side walls for observing root development. In order to avoid expensive construction and maintenance costs, transparent – minirhizotrons (MR) – were introduced, enabling the *in situ* observation of the root in a fixed position, but at several depths (Taylor et al., 1990). By installing transparent tubes with an inclination, they could be accessed from the surface. These rhizotubes were subsequently also used in rhizotron facilities, where they were installed horizon-

tally from the trench walls at different depths to ensure that root distributions and root development could be observed in a larger soil volume than only at the side walls (Van de Geijn et al., 1994). It is important that the installation of the rhizotubes is causing as little soil disturbance as possible. Especially in fine textured soil, less soil compaction around the tube, caused by the installation process, might alter the root growth (Johnson et al., 2001). These influences on the collected root data can be reduced to a negligible minimum when auger with the same diameter as the rhizotubes are used to drill holes for tube insertion, the soil is re-compacted according to previous bulk density measurements and a resting period is respected after tube installation (6-17 month) (Johnson et al., 2001, Joslin et al., 2006, Pritchard et al., 2008, Vamerali et al., 2012). The permanent installation and maintenance of MR at several depths has only been done on very rare occasions due to the high manufacturing effort involved (Svane et al., 2019, Van de Geijn et al., 1994). However, this kind of MR facility enables insights into processes within the soil–plant continuum at the plot scale, while offering high instrumentation for multifaceted observations at high spatial and temporal resolution.

One way to observe the root growth is imaging the roots and surrounding soil through the transparent rhizotubes with a special camera system. To analyze the resulting root images, various methods from root counting to single root analysis were performed with several manual or semi-automated software tools (Atkinson et al., 2000, Möller et al., 2019, Vamerali et al., 2012, Zeng et al., 2010). Depending on the targeted phenotypic traits and root image quality it is not always feasible to extract it manually from the images (Atkinson et al., 2019, Vamerali et al., 2012). In contrast to genotype analysis, which can be performed with various high-throughput methods, the phenotyping of corresponding plant architecture and anatomy is still a bottleneck (Minervini et al., 2015). Image analysis based on the convolutional neural network (CNN) is the most promising way to close this gap (Song et al., 2021). In particular, CNNs are used to automatically detect different plant organs by segmenting them from the background (Kamilaris and Prenafeta-Boldú, 2018). While this is already established for above-soil organs of plants, applying these techniques to extract information about the root system remains challenging, especially under field conditions (Ubbens and Stavness, 2017, Wang and Su, 2022). This is mainly due to the lack of availability of root image data, which are required to train a segmentation model, compared to shoot image data. Capturing shoot images is inexpensive and easy, while in-field root imaging is time- and labor-intensive (image acquisition time is 5-10 minutes on average per tube) (Atkinson et al., 2019, Yang et al., 2020).

In addition to the root information, soil sensors measure point information on soil water content, soil water potential and soil temperature. Moreover, the spatial soil water content per depth can be measured with a ground-penetrating radar (GPR) (Klotzsche et al., 2019, Yu et al., 2020) between two neighboring rhizotubes.

The two MR facilities (Cai et al., 2016b) in Selhausen, Germany, enable longer term studies of the soil–plant continuum on two different soils in the same climate. To investigate the different components of the soil–plant continuum, these

MR facilities offer unique conditions to record 4D subsoil information for multiple growing seasons under different field conditions and agronomic treatments. Detailed information about soil water content (SWC), soil water potential, and soil temperature was obtained at two locations within different soil types by the soil sensors mentioned above. Furthermore, morphological root information was obtained *in situ*, including relevant root system traits such as length, diameter, branching frequency, etc.. Root traits were acquired with cameras, taking images through horizontal transparent rhizotubes installed at several depths (Cai et al., 2016b, Morandage et al., 2021). Since all measures to avoid altered root growth due to tube installation were taken, the root parameters are expected to have at most negligible deviations in this respect.

The data collected in this study can be used to develop, calibrate, and validate models of the soil–plant continuum across different scales (Schnepf et al., 2022b) with regard to different root zone components such as soil processes, including flow processes (Landl et al., 2021, Vereecken et al., 2016), root development (Schnepf et al., 2022a), and biopores (Landl et al., 2019) as well as different model compilations such as single-plant and (Schnepf et al., 2022a) multi-plant modeling (Morandage et al., 2019) or soil water content and root water uptake modeling (Cai et al., 2017, 2018b). The data include agronomically relevant information for breeding water-efficient cultivars and for field management under various conditions, which can be directly used by, for example, agronomists and biologists. Furthermore, the root image data provided here can be used to train and benchmark neural networks, since deep learning-based technologies are a fast and continuously developing branch of plant and agronomic data analysis. The images presented in this paper, which correspond to the root data, are – to the best of our knowledge – the largest available MR image collection, covering several years, cultivars, and agronomic treatments. In this context, the advantage of this image collection is twofold. Firstly, we provide more than 160,000 MR images in one freely available and categorized dataset. Secondly, we simultaneously publish reference data that can be used for validation. On the one hand, this will help machine learning scientists to develop models, capturing more heterogeneity. On the other hand, soil and plant scientists will benefit directly from the analyzed data. The dataset was acquired for the years 2016, 2017, 2018, 2020, and 2021, and will be continued in the future. The dataset will thus be added to each year. Data for the years 2012–2015 are partly available, but are not included in this publication. The related above-ground data, including measurements on crop development, transpiration fluxes, and assimilation rates, will be published in a corresponding paper.

3-2 Methods

3-2-1 Minirhizotron facilities

The data for this publication were acquired at two MR facilities, allowing us to observe root growth through the rhizotubes and to measure 4D geophysical data. A detailed description of the construction of the MR facilities is provided in Cai et al. (2016b). Here, we provide a basic overview of the facilities and the data acquisition.

The MR facilities are situated within the TERENO (TERrestrial ENvironmental Observatories) Eifel/Lower Rhine observatory near Selhausen, Germany (50°52'N, 6°27'E) (see Figure 3-1a). The Selhausen test site was mentioned in various studies ranging from geophysical observations and soil physics to root and plant modeling (Bauer et al., 2011, Bogen et al., 2018, Brogi et al., 2019, Cai et al., 2017, Jadoon et al., 2012, Weihermüller et al., 2007). The weather station (SE_BDK_002) is located within the Selhausen test site. The recorded parameters are used to calculate the evapotranspiration with a temporal resolution of 10 min. The data are available in the TERENO Data Discovery Portal (<https://ddp.tereno.net/ddp/>). The soil at the two MR facilities was deposited by fluvio-glacial sediments of the river Rur catchment during the Pleistocene (Bogen et al., 2018, Cai et al., 2016b, Pütz et al., 2016). Different river sediments were deposited at each MR facility. The upper terrace sediments consist of gravely, partly stony, and silty sand, and it is here where the upper terrace MR facility (R_{UT}) is located. It is classified as Orthic Luvisol with a high stone content (>50 %) (Yu et al., 2020) according to the World Reference Base for Soil Resources (IUSS Working Group WRB, 2007). The soil at the lower terrace is classified as Cutanic Luvisol (Ruptic, Siltic) (Bauer et al., 2011), and it is here where the lower terrace MR facility (R_{LT}) is located. The soil organic content and total soil nitrogen (derived from 2020) were 1.14 % and 0.116 % (0–0.3 m), 0.66 % and 0.081 % (0.3–0.6 m), and 0.42 % and 0.059 % (0.6–1 m) in R_{LT} as well as 1.39 % and 0.128 % (0–0.3 m, with a stone weight of 45 %) in R_{UT} . The sand, silt, and clay contents are on average 16 %, 63 %, and 21 % (0–1 m, R_{UT}) and 32 %, 53 %, and 15 % (0–0.3 m, R_{UT}). The different soils cause a 4° morphology incline from R_{UT} towards R_{LT} (see Cai et al. (2016b)). Due to regular tilling and plowing, a 0.3-m-thick plow layer (Ap horizon) was present in the upper 0.3 m of the two MR facilities (see Figure 3-1b and 3-1c).

To compare different agronomic treatments under the same soil and atmospheric conditions, the two MR facilities were divided into three plots (Figure 3-2a). Within the individual plots, three horizontal rhizotubes were installed at each of six different depths between 0.1 m and 1.2 m, each with a length of 7 m. The rhizotubes were embedded at a distance of 0.75 m in the horizontal axis (Figure 3-2a). For each crop growing season, a crop row orientation perpendicular to the rhizotubes was chosen. To perform the measurements within the rhizotubes an access trench was built within the ground in front of the plots, from which the rhizotubes can be reached. At R_{UT} , the soil was excavated and refilled while installing the rhizotubes, which was due to the high stone content. A plastic

foil was installed down to 1.3 m depth to separate the plots. At R_{LT} , the soil is undisturbed since the installation was performed by drilling. The soil was precisely compacted layer by layer to the same bulk density as the undisturbed soil (see Cai et al. (2016b)). For R_{UT} , the differences in excess length is negligible, as they are less than < 0.02 m. In contrast, for R_{LT} , excess lengths are up to 0.10 m. This was taken into account during the processing of the data. Due to soil erosion and soil compaction after tillage and seedbed preparation, the depths of the rhizotubes vary between the individual measurement seasons. The individual rhizotube depths are provided in the repository “Additional_Information” (Lärm et al., 2023a).

In addition to the measurements (GPR and root images) that can be performed within the rhizotubes, various soil sensors are embedded within the soil (see Soil Sensor Data section). Above ground at R_{LT} , there is a monitoring system for spectral electrical impedance tomography (sEIT) (Weigand et al., 2022). A water reservoir is installed to provide rainwater for irrigation.

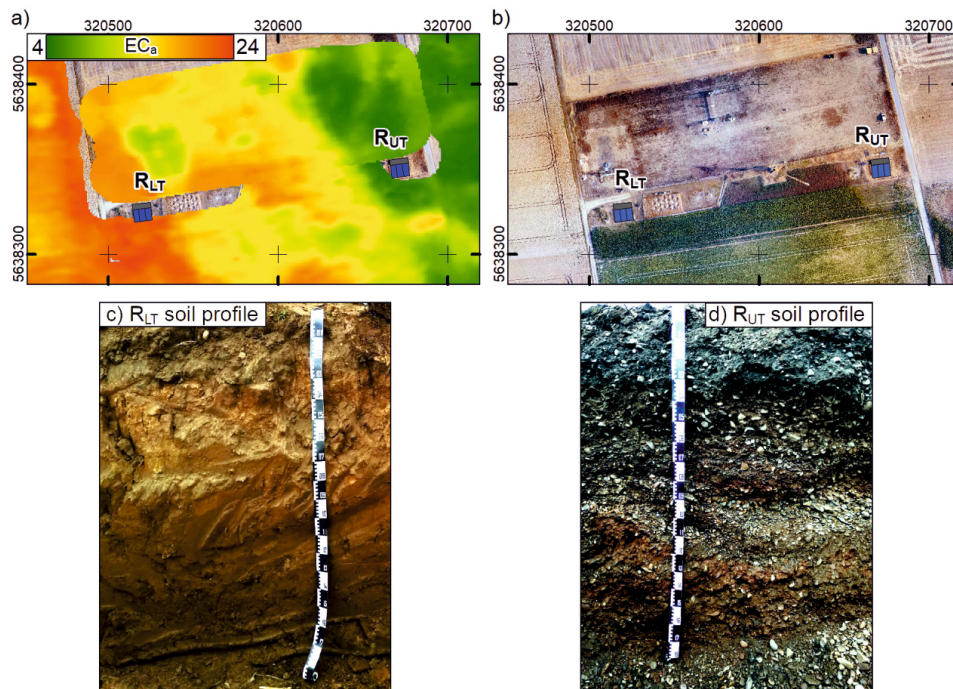


Figure 3-1: Overview of the location of the minirhizotron(MR)-facilities a) Map of the apparent electrical conductivity (EC_a in [mS/m]) measured with the electromagnetic induction (EMI) (vertical dipoles, 9.7 cm depth of investigation, 135 cm coil distance) of the Selhausen test site. Provided by Brogi et al. (2019). b) Aerial photograph of the Selhausen test site and the MR-facilities. Both maps are given in WGS 1984 UTM Zone 32N [m]. For a) and b) the location of the MR-facilities is given by the blues rectangles, the upper terrace facility (R_{UT}) and the lower terrace facility (R_{LT}), the location of the access trench is indicated with a grey rectangle. c-d) Photos of the soil profiles of the loamy soil at the R_{LT} (c) and of stony soil at the R_{UT} (d).

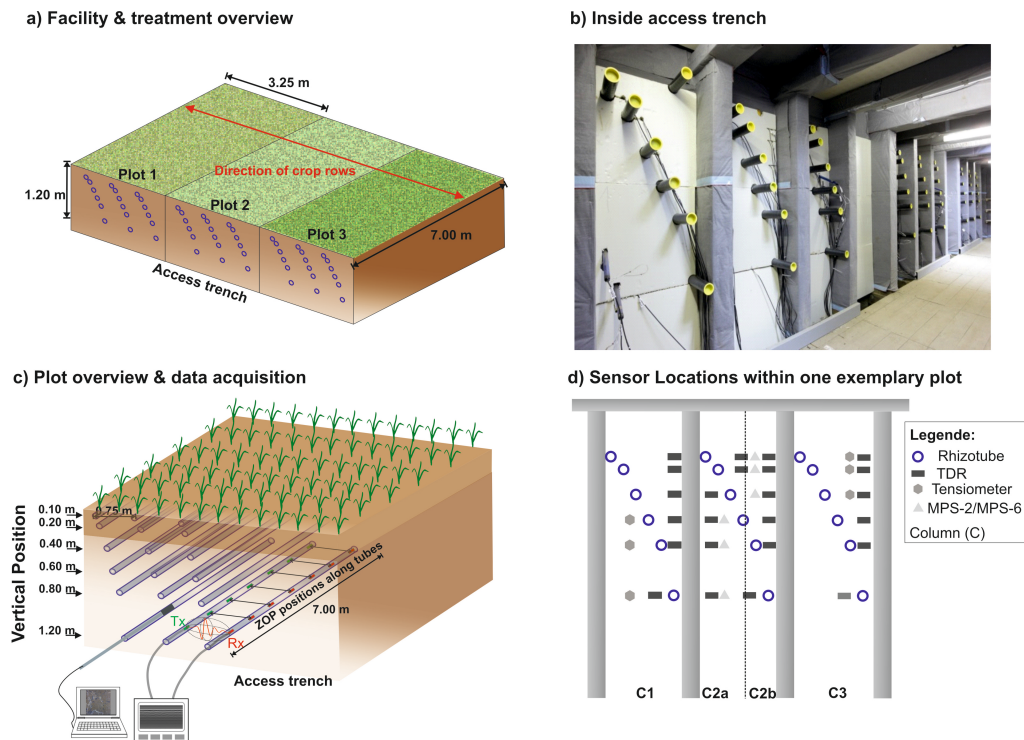


Figure 3-2: Overview of the Minirhizotron (MR)-facilities. a) Schematic setup of the MR-facilities indicating that at each of the plots a different agricultural treatment was applied for the different growing seasons. The direction of the crop rows is perpendicular to the direction of the rhizotubes (red arrow). The measurements are carried out from the access trench. b) View within the access trench. c) Overview of one exemplary plot within the MR-facilities with the horizontal crosshole GPR ZOP measurement set up. Transmitter and receiver antennae are labeled Tx and Rx, respectively. Root image measurement are acquired using camera system attached to an index handle. d) Sensor location for one exemplary plot.

3-2-2 Study design

The MR facilities allow an *in situ* investigation of the soil–plant continuum. To observe the impact of drought stress and planting density on different crops and the impact of crop mixtures on root development, various agronomic treatments were carried out for the different plots. This includes, depending on the growing season, surface water treatment (sheltered, natural/rainfed & irrigated), planting density, sowing date, and different crop cultivar mixtures. In this study, we present the data of multiple crop growing seasons between the years 2016 and 2021. An overview of the individual crop growing seasons and the agricultural treatments is provided in the repository “Additional_Information” (Lärm et al., 2023a).

During the 2016 crop growing season, the goal was to compare different drought stress levels for winter wheat (*Triticum aestivum*, cv. Ambello). A shelter was therefore installed on Plot 1 for both MR facilities. The shelter had a cover, which was removed when no precipitation was forecasted. Plot 2 was left under natural conditions and is also referred to as the rainfed plot. For Plot 3, irrigation pipes were installed and the soil was irrigated regularly. The individual irrigation values can be found in the “Additional_Information” (Lärm et al., 2023a). For crop growing seasons 2017 & 2018, *Zea mays* (cv. Zoey) was chosen and the shelter needed to be removed due to the height of the crop. This resulted in two rainfed plots (Plot 1 and Plot 2). As before, Plot 3 was irrigated. In 2018, the influence of the sowing date and the planting density was investigated on Plot 1 for R_{UT} and R_{LT}, respectively.

Since the 2020 crop growing season, the focus of research was on comparing the different crop root architectures of cultivars – purely sown and in a cultivar mixture with alternating rows. To explore the beneficial effects of mixing deep and shallow rooting cultivars, one cultivar chosen was always a deep rooting, while the other one was a shallow rooting cultivar. The surface water treatment was therefore uniform for all three plots. Irrigation was only applied to all crops under heavy drought conditions when the crops showed severe drought stress symptoms. For the 2020 crop growing season, two different *Zea mays* cultivars (cv. Sunshinos and cv. Stacey) were sown on Plot 1 and Plot 3, respectively. The cultivar mixture was sown on Plot 2. For the 2021 growing season, winter wheat (*Triticum aestivum*) with two different cultivars (cv. Milaneco and cv. Trebelir) was again sown on Plot 1 and Plot 3, respectively. The mixture was sown on Plot 2. In 2021, irrigation was not required since the winter wheat was sufficiently supplied by precipitation and the crops did not show any stress symptoms (Figure 3-3). In order to perform destructive measurements above and below ground in 2020 and 2021, a replication field (extra field (EF)) next to R_{LT} was sown. The EF had the same dimension and plot design as the MR facilities and was located on the west side of the facility (see Above-Ground Data section).

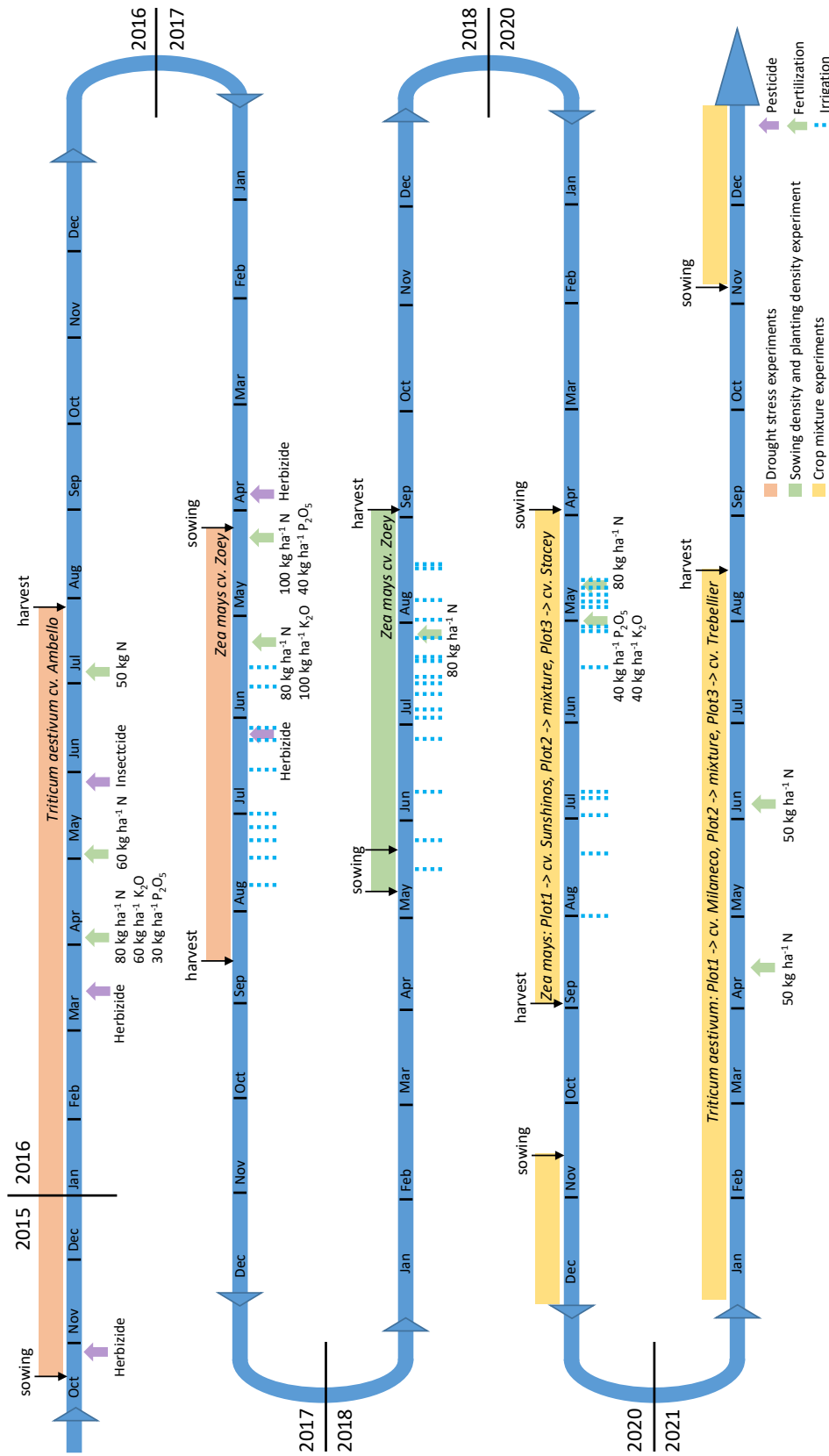


Figure 3-3: Overview of the experimental timeline including cultivars and management actions, such as sowing, harvest, pesticide applications and irrigation.

3-2-3 Ground-penetrating radar data

Crosshole GPR data acquisition at the MR facilities

The time-lapse GPR data were collected using a 200 MHz PulseEKKO borehole system manufactured by Sensors and Software (Canada). Crosshole zero-offset-profiling (ZOP) measurements were carried out, with the transmitter (Tx) and receiver antennae (Rx) located within neighboring rhizotubes. Both antennae were simultaneously pulled in parallel positions along the length of the rhizotubes, with a spacing of 0.05 m between the individual ZOP positions. An electromagnetic (EM) wave is emitted by Tx, which is sent through the soil and then recorded by Rx. Changes in soil and root properties between the rhizotubes affect the measured GPR traces and, therefore, information about the medium parameters can be obtained (more information can be found in Klotzsche et al. (2019)). Due to the different rhizotube lengths of both MR facilities, the length over which the ZOPs are collected is 6.70 m and 6.40 m, resulting in 115 and 109 traces for R_{UT} and R_{LT}, respectively.

For a time-zero calibration, wide-angle reflection and refraction (WARR) measurements are carried out within the access trench. Here, Rx antennae are moved over a distance of 6.0 m with a step size of 0.1 m, while the Tx antennae are fixed at the zero location. At least four calibration measurements per MR facility and measurement day were performed to capture daily variations of the time-zero (see GPR Data Processing section).

In contrast to the root images, which capture the soil in contact with the rhizotubes, the ZOP measurements investigate the soil between two rhizotubes. A 1D horizontal permittivity profile is thus obtained. For the measurement seasons 2016–2018, only one horizontal permittivity plane was measured per depth. For Plot 1 and Plot 2, this were the slices between column C1 and C2, and for Plot 3 between column C2 and column C3. In 2020, two main planes were measured per depth; occasionally only one plane was measured with the same configuration as for the previous measurement seasons. Table 3-1 indicates that the number of horizontal permittivity planes was measured per measurement date.

Table 3-1: Detailed overview of the GPR data acquired during growing season 2016, 2017, 2018, 2020 and 2021.

no	fac	2016		2017		2018		2020		2021	
		date	pl								
1	R _{UT}	03.02.2016	12	26.04.2017	15	25.04.2018	15	19.03.2020	12	-	-
	R _{LT}	03.02.2016	-	26.04.2017	14	25.04.2018	14	-	-	25.11.2020	29
2	R _{UT}	30.03.2016	15	03.05.2017	15	02.05.2018	15	12.05.2020	30	-	-
	R _{LT}	30.03.2016	10	03.05.2017	14	02.05.2018	14	-	-	02.12.2020	30
3	R _{UT}	08.04.2016	15	10.05.2017	14	09.05.2018	15	28.05.2020	30	-	-
	R _{LT}	08.04.2016	15	10.05.2017	14	09.05.2018	14	-	-	14.12.2020	29
4	R _{UT}	14.04.2016	15	17.05.2017	15	14.05.2018	15	03.06.2020	30	-	-
	R _{LT}	14.04.2016	15	17.05.2017	14	14.05.2018	14	-	-	14.01.2021	29
5	R _{UT}	20.04.2016	15	23.05.2017	15	24.05.2018	15	10.06.2020	30	-	-
	R _{LT}	20.04.2016	15	23.05.2017	11	24.05.2018	14	-	-	27.01.2021	29
6	R _{UT}	28.04.2016	15	31.05.2017	15	20.06.2018	15	17.06.2020	25	-	-
	R _{LT}	28.04.2016	15	31.05.2017	14	20.06.2018	14	-	-	10.02.2021	29
7	R _{UT}	04.05.2016	15	07.06.2017	15	27.06.2018	15	06.07.2020	29	04.03.2021	30
	R _{LT}	04.05.2016	15	07.06.2017	14	27.06.2018	14	-	-	-	-
8	R _{UT}	12.05.2016	15	14.06.2017	15	04.07.2018	15	15.07.2020	30	-	-
	R _{LT}	12.05.2016	15	14.06.2017	14	04.07.2018	14	-	-	09.03.2021	-
9	R _{UT}	19.05.2016	15	21.06.2017	15	09.07.2018	15	23.07.2020	5	11.03.2021	30
	R _{LT}	19.05.2016	15	21.06.2017	14	-	14	-	-	11.03.2021	-
10	R _{UT}	25.05.2016	15	05.07.2017	15	11.07.2018	15	27.07.2020	30	19.03.2021	24
	R _{LT}	25.05.2016	15	05.07.2017	14	11.07.2018	14	-	-	19.03.2021	-
11	R _{UT}	02.06.2016	15	12.07.2017	15	18.07.2018	15	05.08.2020	5	30.03.2021	15
	R _{LT}	02.06.2016	14	12.07.2017	14	18.07.2018	14	-	-	30.03.2021	29
12	R _{UT}	09.06.2016	15	19.07.2017	15	19.07.2018	15	-	-	15.04.2021	30
	R _{LT}	09.06.2016	15	19.07.2017	14	19.07.2018	14	-	-	15.04.2021	-
13	R _{UT}	13.06.2016	15	27.07.2017	15	20.07.2018	15	-	-	14.07.2021	30
	R _{LT}	13.06.2016	15	27.07.2017	14	20.07.2018	14	-	-	22.07.2021	-
14	R _{UT}	20.06.2016	15	02.08.2017	15	25.07.2018	15	-	-	28.07.2021	30
	R _{LT}	20.06.2016	14	02.08.2017	14	25.07.2018	14	-	-	28.07.2021	29
15	R _{UT}	27.06.2016	15	09.08.2017	15	01.08.2018	15	-	-	04.08.2021	30
	R _{LT}	27.06.2016	14	09.08.2017	14	01.08.2018	14	-	-	04.08.2021	28
16	R _{UT}	04.07.2016	15	14.08.2017	15	08.08.2018	15	-	-	18.08.2021	15
	R _{LT}	27.06.2016	15	09.08.2017	15	01.08.2018	15	-	-	04.08.2021	30
17	R _{UT}	20.07.2016	15	23.08.2017	15	15.08.2018	15	-	-	-	-
	R _{LT}	20.07.2016	15	23.08.2017	14	15.08.2018	14	-	-	25.08.2021	30
18	R _{UT}	27.07.2016	15	30.08.2017	15	22.08.2018	15	-	-	-	-
	R _{LT}	27.07.2016	15	30.08.2017	14	22.08.2018	14	-	-	31.08.2021	23
19	R _{UT}	01.08.2016	15	06.09.2017	15	05.09.2018	15	-	-	10.09.2021	30
	R _{LT}	01.08.2016	15	06.09.2017	14	05.09.2018	14	-	-	10.09.2021	19
20	R _{UT}	08.08.2016	15	13.09.2017	15	17.09.2018	15	-	-	29.09.2021	30
	R _{LT}	08.08.2016	15	13.09.2017	14	17.09.2018	14	-	-	-	-
21	R _{UT}	15.08.2016	15	20.09.2017	15	24.09.2018	15	-	-	03.11.2021	30
	R _{LT}	15.08.2016	15	20.09.2017	14	24.09.2018	14	-	-	03.11.2021	27
22	R _{UT}	-	-	27.09.2017	15	02.10.2018	15	-	-	-	-
	R _{LT}	-	-	27.09.2017	14	02.10.2018	14	-	-	-	-

Ground-penetrating radar data processing

From horizontal GPR crosshole ZOP measurements, we can derive the relative dielectric permittivity ε_r , which can be transformed into SWC using appropriate petrophysical relationships. All the required pre-processing steps are explained in detail by Klotzsche et al. (2019). Here, we highlight the most important aspects. Firstly, a dewow filter is applied, which reduces low-frequency noises on the GPR data. Secondly, a time-zero (T_0) correction of the ZOP data is performed and thirdly, the first breaks (FB) of the signals are estimated (Figure 3-4a).

Following this processing procedure, the EM wave travel times between the neighboring rhizotubes for each ZOP position are obtained. Since the horizontal spacing between the neighboring rhizotubes ($d_{\text{rhizotubes}}$) is known to be 0.75 m, the EM wave velocity v for each ZOP position can be calculated using the obtained travel times (t_{travel}), see Figure 3-4b. As suggested by Jol (2008), when considering low-loss and non-magnetic soils the EM velocity v can be transformed into the relative dielectric permittivity ε_r of the bulk material with

$$v = \frac{c}{\sqrt{\varepsilon_r}} \quad (3-1)$$

where c is the speed of light (~ 0.3 m/ns).

Because of the presence of the soil sensors and pertaining cables in the first 0.75 m away from the facility wall, GPR measurements were made between 1 and 7 m away from the facility wall. Close to the surface (depth of 0.1 m) the radar wave interferences of the critically refracted air wave and the direct wave (Klotzsche et al., 2019) occur. Therefore, these data were excluded. Additionally, at R_{LT} , an sEIT system is installed and the metal parts interfere with the GPR waves. Therefore, at a depth of 0.2 m, where the sEIT system is located, the data were also excluded.

GPR-derived permittivity can be transformed into the soil water content (SWC), which provides a parameter that is directly used in soil science. This is achieved by using different conversion formulas, which are based on empirical relationships and petrophysical, volumetric mixing models (see Huisman et al. (2003) and Steelman and Endres (2011)). In this data descriptor, we provide the permittivity values to ensure that the conversion can be chosen by the user of the data. In the past, we have used two conversions, the Topp's equation Topp et al. (1980) and the complex refractive index model (CRIM) (Steeleman and Endres, 2011) (see Klotzsche et al. (2019) and the Dielectric Permittivity to Soil Water Content section).

GPR data processing

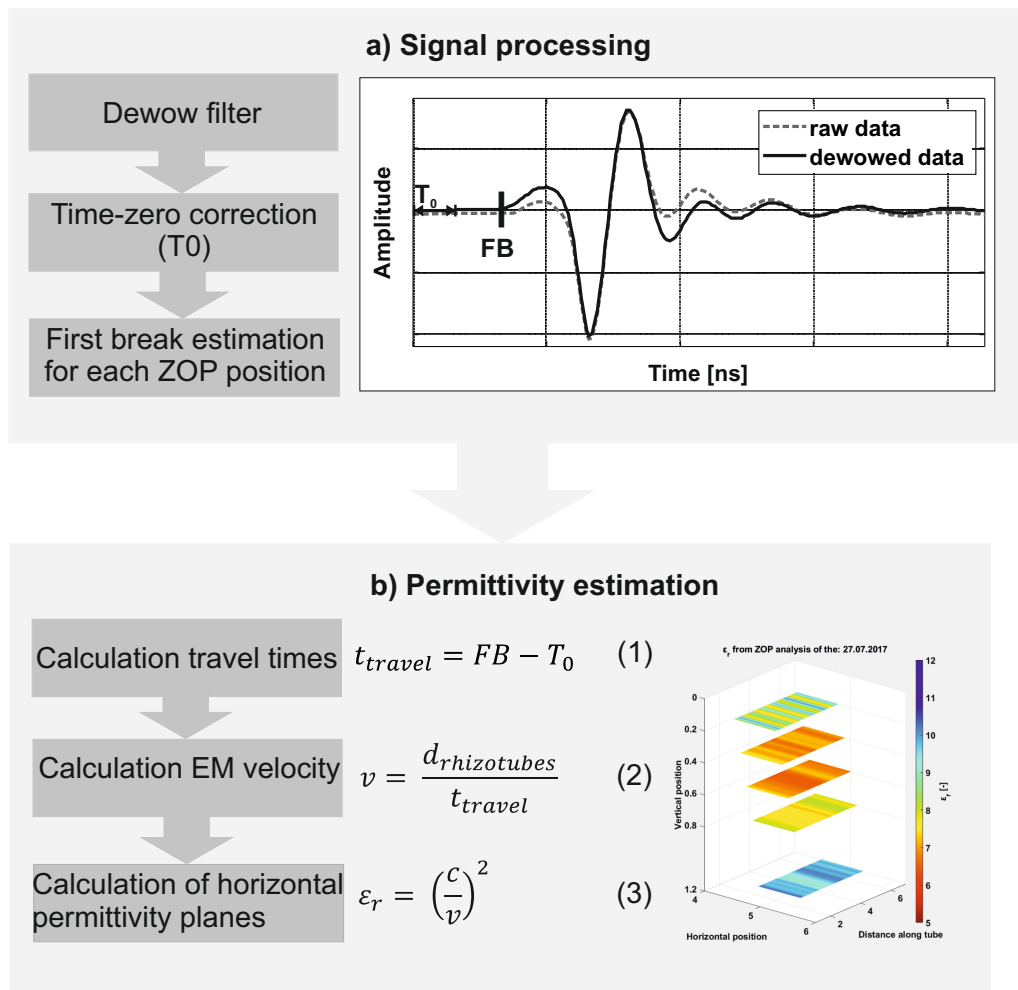


Figure 3-4: GPR processing steps

3-2-4 Root images

Root image acquisition at the minirhizotron facilities

Images of roots and the surrounding soil were captured through the transparent rhizotubes. The amount of images obtained varied depending on the vegetation and the progress of root development. To save resources, the depth of measurement was continuously increased at the beginning of each growing season as root depth increased. Meticulous care was taken not to omit any root depth at which roots were already present. A measurement produces always 40 images per tube. Half of the images were taken 80° clockwise and the other half were taken 80° counter-clockwise from the top point of the rhizotubes. Two different camera systems were used over time to take the images. The camera used in 2016, and for most measurements in 2017, was manufactured by Bartz (Bartz Technology Corporation). The camera used for some of the images taken in 2017 and for all images taken in 2018, 2020, and 2021 was produced by VSI (Vienna Scientific Instruments GmbH). The photographed area differs depending on the camera (Table 3-2). Table 3-3 provides a detailed overview of the images taken over the different growing seasons.

Table 3-2: Overview of the camera-systems and experiment timeline of minirhizotron images acquisition

camera system	Bartz	VSI
resolution (px)	1508 x 1020	2060 x 2060
real size (mm)	16.5 x 23.5	20 x 20
wavelength (nm)	400-780	400-780
growing season	2016 & 2017	2017 & 2018 & 2020 & 2021

Root image data processing

The post processing of the images was performed by an automated analysis pipeline including neural network segmentation and automated feature extraction following the analysis pipeline of Bauer et al. (2022). Neural network training and image segmentation were performed with the RootPainter (Smith et al., 2022) software. Firstly, the roots were segmented by a CNN. As part of the process, the roots are separated from the background and extracted as binary image data. A small subset of the root images is used as training data to train the CNN. The evaluation of the models was performed with the F1-score (>0.7 for each model used). More information on the models can be found in Bauer et al. (2022). The resulting neural network model was then used for the segmentation of the roots. The segmentation of the images was performed in a batch process. Secondly, the morphological features were extracted by the automated feature extraction program RhizoVision Explorer (Seethepalli et al., 2021). This includes multiple automated steps for thresholding obstacles and filling holes smaller than

Root image processing

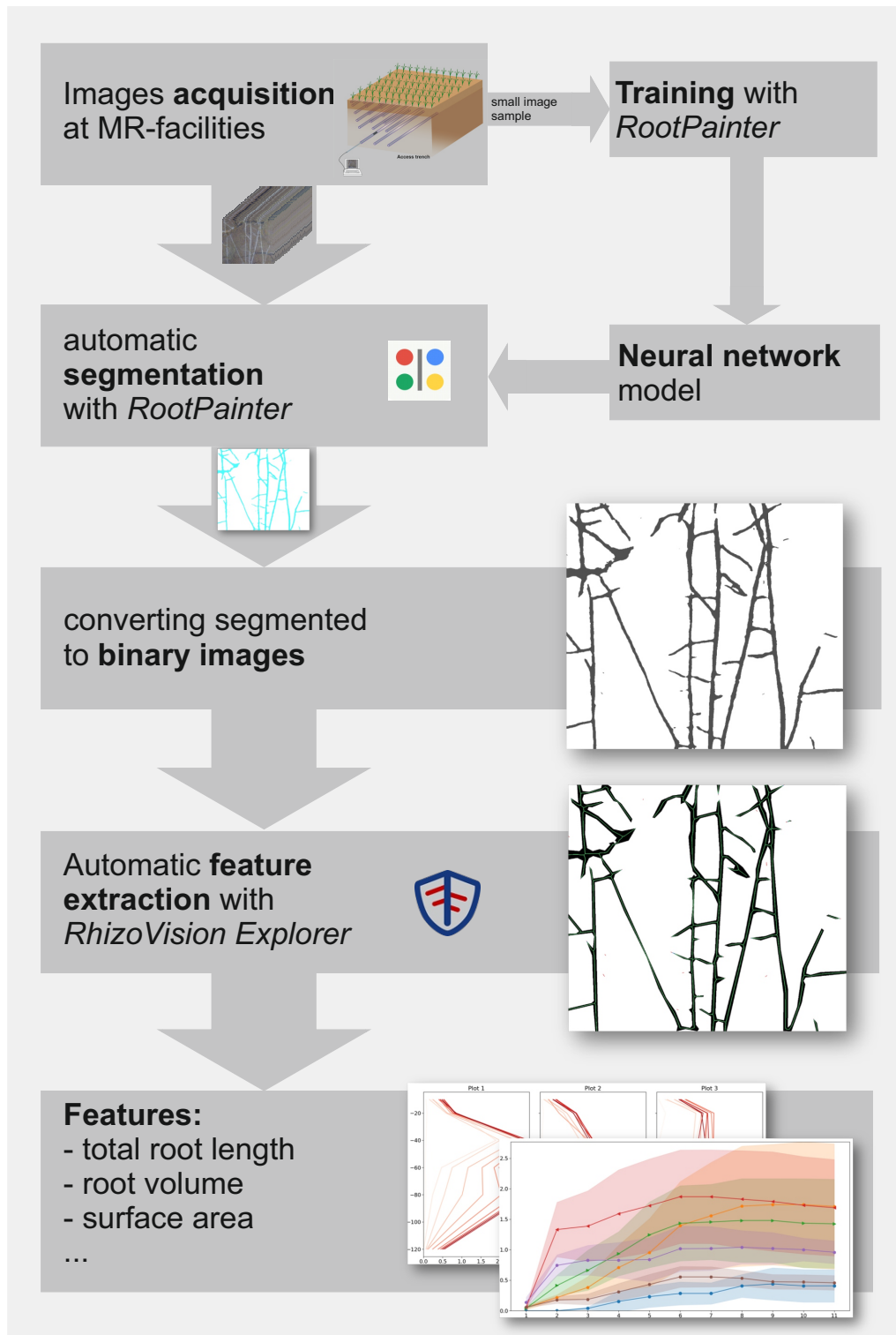


Figure 3-5: Root image processing steps

3-2-5 Soil coring in the extra field

Soil coring was performed in the EF (extra field established next to R_{LT}) dedicated to destructive belowground measurements in 2020 (maize) and 2021 (winter wheat). The soil next to R_{UT} is not homogeneous, which is why a representative replica was not feasible. The maize roots were extracted once on July 14, 2020 when the crops were in BBCH 65, whereas the winter wheat roots were extracted on June 16, 2021 when the crops were in BBCH 69. The soil was cored using a root auger with an inner diameter of 0.9 m and a length of 1.0 m, and the cores were drilled directly around the plant. The soil core was then divided into 0.1 m pieces and filled into plastic bags. For maize in 2020, four replicates were taken in Plot 1 and four replicates in Plot 3 of the EF (no core was taken in the cultivar mixture treatment – Plot 2). For winter wheat in 2021, one replicate was taken in Plot 1, one in Plot 3, and two in Plot 2 of the EF (one core for each variety in the cultivar mixture). The soil samples were then put into refrigerators and processed step by step. The samples were later soaked in tap water, washed, and passed through several sieves with mesh sizes of 1.00 mm, 0.83 mm, and 0.5 mm until the coarsest soil and residues were cleared. The roots were subsequently stored in tap water at 3°C until they were scanned with an EPSON scanner (HP Expression 1100XL). The roots of each sample were laid (preferably without overlaps) into an acrylic glass plate filled with tap water and were subsequently scanned. The images of the scanned roots were processed using a similar procedure as for the minirhizotron images, resulting in the total length estimation of the roots and the root length density (Han et al., 2021).

3-2-6 Soil sensor data

All plots within the two MR facilities have the same layout. Each plot contains three horizontal rhizotubes per depth but the soil sensors are distributed into four columns, with the middle section divided into two columns, column C2a and C2b (see Figure 3-2 c). For each column, there are four TDR-sensors installed for each of the six depths. For the tensiometers and the soil water potential and soil temperature sensors, one sensor is installed for each depth. The distribution over the four columns is shown in Figure 3-2 c.

To measure the soil water potential for dry soil conditions and to acquire the soil temperature, MPS-2 sensors manufactured by Decagon Devices, Inc., US are used. The soil water potential is measured in a range of -9 kPa to -100,000 kPa (pF 1.96 to pF 6.01) with a resolution of 0.1 kPa. The accuracy is of $\pm(25\%$ of reading +2 kPa) over the range of -9 to -100 kPa and proven to be higher for drier conditions until permanent wilting point (-1,500 kPa) under lab conditions and -4,500 kPa under field conditions by the manufacturer. The soil temperature is measured in a range of -40°C to 60°C with a resolution of 0.1°C. The soil water potential for wet soil conditions is measured using T4 pressure transducer tensiometers manufactured by UMS GmbH, Germany. The measurement range is -85 kPa to +100 kPa with an accuracy of ± 0.5 kPa. To acquire and record the soil sensor data, all sensors – with the exception of the TDR sensors – are connected to a

DataTaker DT85 manufactured by Omni Instruments Ltd, UK. The TDR sensors were manufactured by the institute's technicians and consist of three rods, with a length of 200 mm and a spacing of 26 mm. The TDR sensors are connected to institute-made multiplexers (50C81-SDM), providing a lower relative error ($>1\%$) than commercial system (Weihermüller et al., 2013). To acquire and record the data, the multiplexers are connected to a TDR100 Time-Domain Reflectometer manufactured by Campbell Scientific, Inc., US. Because of the high stone content at R_{LT} the relationship of SWC and dielectric permittivity measured by the TDR was calibrated in the lab (Cai et al., 2016b). For information on SWC calculation see Dielectric Permittivity to Soil Water Content section.

3-2-7 Soil water content using a mobile frequency domain reflectometry device

In addition to the soil sensors (see Soil Sensor Data section), the soil water content was measured using the mobile FDR device that employs the HH2 moisture sensor with the ThetaProbe ML3 (ecoTech Umwelt-Meßsysteme GmbH, Bonn, Germany). Due to the nature of the soil at R_{UT} , the soil moisture was only measured for the topsoil, while for the R_{LT} and EF, the soil water was measured at depths of 0 m, 0.30 m, 0.6 m, and 0.9 m. In total, the soil water was measured ten times in each plot of the R_{UT} , six times in each plot of the R_{LT} , and eleven times in each plot of the EF over the crop growing season. The sensor was always placed between crop rows.

3-2-8 Soil sampling

In September 2020, a new irrigation tank was installed at R_{LT} and undisturbed soil samples were taken from the trench for the new tank. The samples were taken from several depths and analyzed in the in-house soil physics lab. The soil hydraulic parameters were measured using the HYPROP (Meter, München, Germany) method (Schindler et al., 2010) and a WP4 Dewpoint Potentiometer (Decagon Devices, WA, USA). The saturated hydraulic conductivity was derived using the KSAT system (Meter, München, Germany). Soil texture was determined according to DIN ISO 11277 using the pipette method combined with wet sieving (Müller et al., 2009).

The soil hydraulic properties can be found in “Additional_Information” (Lärm et al., 2023a).

3-3 Data Records

All data were uploaded to Geonetwork in accordance with ISO 19115. The data were persistently stored and will be regularly updated (see Usage Notes). The data were subdivided according to the characteristics of the sensing method and data type. GPR data (Lärm et al., 2023b), root data (Lärm et al., 2023c) root

The data can be downloaded using the following links:

GPR data: <https://doi.org/10.34731/cg3t-nb88>,
 Root data: <https://doi.org/10.34731/7x05-2r96>,
 Root images: <https://doi.org/10.34731/5zwe-t974>,
 Soil sensor data: <https://doi.org/10.34731/ffsk-sy65>,
 Additional information: <https://doi.org/10.34731/st8e-4082>.

Table 3-4: Overview of the repository content and data labelling. The labels always contain the facility name (R_{UT} or R_{LT}) and the year the data have been obtained. For the root images, each image is also labeled according to exact date (year (YYYY), month (MM), day (DD)), tube and position it was taken.

repository	data label	size
GPR_Data	<i>FACILITY_YYYY_GPR_EPS.csv</i>	2.68 MB
Root_Data	<i>FACILITY_YYYY_ROOT_PARAMETER.csv</i>	21.6 MB
Root_Images	<i>FACILITY_YYYYMMDD_TUBE_WINDOW_MEASUREMENT_INITIALS.jpg</i>	199 GB
Soil_sensors_Data	<i>FACILITY_SENSOR_YYYY_ALL.csv</i>	103 MB
Additional_Information	experiment, irrigation and soil overview (CSV)	1 MB

Some root image data have been previously used and published. Root length data from 2016 were used by Nguyen et al. (2020). Root length data obtained from the images and the soil moisture values, measured by TDR and MPS-2 sensors on both facilities in 2016 and 2017 were used by Morandage et al. (2021). The root image data of R_{UT} from June 8, July 13, and September 12, 2017 were used by Nguyen et al. (2022b). However, the root lengths used in these three studies were obtained by a different method and are based on a manual single root annotation (Zeng et al., 2008). The root length data of R_{UT} and R_{LT} from 2017 were published by Bauer et al. (2022) to validate the analysis pipeline used to extract all root data. The GPR data and the mean soil water content values calculated from TDR sensors from 2016 and 2017 have already been partly used by Klotzsche et al. (2019).

3-4 Technical Validation

3-4-1 Ground-penetrating radar data

The GPR permittivities (Lärm et al., 2023b) were manually checked for plausibility and unreliable data were excluded. Implausible permittivity outliers were manually detected and removed.

3-4-2 Root Images

The root data (Lärm et al., 2023c) derived from the minirhizotron images (Lärm et al., 2023d) were automatically analyzed by the pipeline following Bauer et al. (2022) using deep neural networks and automated feature extraction (Seethepalli et al., 2021, Smith et al., 2022). Using this approach, part of the total root length

data has been representatively compared to a manual annotation of the images. Approximately 36,500 images were used for validation. The correlation of total root length values obtained from the same images by manual annotation and automated analysis is very high ($r=0.9$) (Bauer et al., 2022).

3-4-3 Soil sensor data

The data (Lärm et al., 2023e) of the different sensor types were filtered for the different measurement ranges listed in the Methods Soil Sensor Data section. To remove outliers, we applied a Hampel filter, which involves a sliding window being moved over the data. As a window size, we used 10 data points for each size of the element, which corresponds to 5 h for the tensiometers and MPS-2 to 10 h for the TDR sensors. For the element, we calculated the median and the standard deviation. If the element deviated more than one time the standard deviation, then the element is replaced by the median (Hampel, 1974). Additionally, the data from the different soil sensors were manually checked for plausibility and unreliable data were excluded. The TDR sensor data were filtered for errors in the TDR wave recordings and data for different dates and sensors were excluded.

3-5 Usage Notes

Figure 3-7 provides information on which periods of data are available for the different measurement seasons and the different measurement techniques. In 2019, no crops were sown on the MR facilities due to a project change. In 2020 and 2021, the datasets do not cover the whole growing period due to technical issues within the access trench and the measurement systems. Different measurement intervals were used for the different measurement techniques. For the root images and the GPR measurements, weekly measurements were performed when possible during the vegetation period. The interval was adjusted to a biweekly period for the root images when the root growth stagnated. The availability of the sensor data (TDR, Tensiometer & MPS-2) depends on the technical state of the measuring devices, and in 2020 and 2021 there were problems with the data recording system. The measurements should be recorded as continuous measurements with measuring intervals of 30 min for tensiometers and MPS-2 sensors and 1 hour for TDR sensors. All timestamps are UTC+1.

3-5-1 Soil sensor data

Due to the measurement interval and the sensitivity of the TDR permittivity time series results, we suggest applying a median filter or similar filters to the TDR dataset to smooth the data as well as to remove the outliers, as mentioned above.

3-5-2 Dielectric permittivity to soil water content

Using the geophysical measurement techniques mentioned in this study, we provide the dielectric permittivity of the soil. Point information is provided by the TDR measurements and spatial information along the rhizotubes is provided by the GPR measurements. The dielectric permittivity can be converted to the soil water content. In the past, literature using TDR and GPR data measured within the MR facilities have used the empirical Topp's equation (Topp et al., 1980) and the petrophysical relationships referred to as the complex refractive index model (CRIM) (see Huisman et al. (2003)). The Topp's equation is valid for sandy loam to clay and requires the bulk permittivity of the soil (ϵ_r) to derive the soil water content (SWC):

$$SWC = -5.3 \times 10^{-2} + 2.92 \times 10^{-2} \epsilon_r - 5.5 \times 10^{-4} \epsilon_r^2 + 4.3 \times 10^{-6} \epsilon_r^3. \quad (3-2)$$

For the petrophysical relationship CRIM, which considers the different dielectric components of the soil (air, soil matrix, and soil water), we obtain

$$SWC = \frac{\sqrt{\epsilon_r} - (1 - \phi)\sqrt{\epsilon_s} - \phi}{\sqrt{\epsilon_w} - 1}. \quad (3-3)$$

For the CRIM approach, additional parameters such as the porosity ϕ and the permittivity of the soil matrix ϵ_s , air ($\epsilon_a = 1$) and water ($\epsilon_w = 84$, at 10°C) are necessary. The permittivity of the soil matrix is 4.7 and 4.0 for R_{UT} and R_{LT}, respectively (Robinson et al., 2005). The porosity in the plow layer is considered to be 0.33 and 0.4 for R_{UT} and R_{LT}, respectively. For underlying subsoil, the porosity is considered to be 0.25 and 0.35, respectively (Weihermüller et al., 2007). In particular, for R_{UT}, we recommend using the CRIM relationship instead of the Topp's equation due to the high stone content.

3-5-3 Soil hydraulic parameters

To provide information on, for example, rhizosphere modeling, we provide an overview of the soil hydraulic parameters, which were derived for the MR facilities using different methods. In Cai et al. (2017), soil hydraulic parameters (SHP) for both MR facilities can be estimated. These were derived by inverse modeling using soil water content, potential measurements, and root observations of winter wheat. Yu et al. (2020) and Jadoon et al. (2012) estimated the SHP using hydrogeophysical inversion for R_{UT} and R_{LT}, respectively. The SHP for R_{LT} was derived by an inverse parameter estimation using a 1-dimensional CO₂ transport and carbon turnover model, with direct soil sampling and laboratory analysis by Bauer et al. (2011).

3-5-4 Updates

The data corresponding to this paper will be updated regularly on a yearly basis once the analysis is finalized. The updated data can be downloaded from these DOIs:

GPR data: <https://doi.org/10.34731/renq-an61>,
Root data: <https://doi.org/10.34731/jnhr-ke36>,
Root images: <https://doi.org/10.34731/jgd1-tq27>,
Soil sensor data: <https://doi.org/10.34731/rb0q-a208>,
Additional Information: <https://doi.org/10.34731/ke7b-a021>.

3-5-5 Above-ground data

The related above-ground data are managed by the Crop Science group of the Institute of Crop Science and Resource Conservation (INRES), University of Bonn, and will be available upon demand in a future data paper. These data have been partially published in Nguyen et al. (2020), Nguyen et al. (2022a), (2022b) (Nguyen et al., 2022b). The data measured within the EF were carried out by the project partner at INRES.

3-5-6 Code availability

Custom code was used to process the data. For the GPR Data we used MATLAB version: 9.13. 0 (R2022b) to run the codes. The root image processing and soil sensor data is run with Python 3.10.10. Processing codes for the roots images can be found in the Supporting Material for Bauer et al. (2022) at <https://doi.org/10.34731/pbn7-8g89>. The soil water content data measured with the FDR device was processed using R version 4.0.2.

The custom codes can not be made publicly accessible due to copyright issues, but are available upon request.

No phosphorus, no food—it's as simple as that.

VACLAV SMIL

◀ ◊ ▶

In the next chapter, we explore how varying soil phosphorus levels influence the development of *Zea mays*, using experiments and functional-structural plant modeling to uncover the critical connections between nutrient availability, root system architecture, and water uptake capacity.

Root system architecture reorganization under decreasing soil phosphorus lowers root system conductance of *Zea mays*

Abstract

THE GLOBAL SUPPLY of phosphorus is decreasing. At the same time, climate change reduces the availability of water in most regions of the world. Insights on how decreasing phosphorus availability influences plant architecture are crucial to understanding its influence on plant functional properties, such as the root system's water uptake capacity. In this study, we investigated the structural and functional responses of *Zea mays* to varying phosphorus fertilization levels focusing especially on the root system's conductance. A rhizotron experiment with soils ranging from severe phosphorus deficiency to sufficiency was conducted. We measured the architectural parameters of the whole plant and combined them with root hydraulic properties to simulate time-dependent root system conductance of growing plants under different phosphorus levels. We observed changes in the root system architecture, characterized by decreasing crown root elongation and reduced axial root radii with declining phosphorus availability. Modeling revealed that only plants with optimal phosphorus availability sustained a high root system conductance, while all other phosphorus levels led to a significantly lower root system conductance, both under light and severe phosphorus deficiency. We postulate that phosphorus deficiency decreases root system conductance, which

could mitigate drought conditions through a more conservative water use strategy, but ultimately reduces biomass and impairs root development and overall water uptake capacity. Our results also highlight that the organisation of the root system, rather than its overall size, is critical for estimating important root functions.

Adapted from: **Felix Maximilian Bauer**, Dirk Norbert Helmrich, Mona Giraud, Juan Carlos Baca Cabrera, Jan Vanderborcht, Guillaume Lobet, Andrea Schnepf (2024). Root system architecture reorganization under decreasing soil phosphorus lowers root system conductance of *Zea mays*. *Annals of Botany*. mcae198, <https://doi.org/10.1093/aob/mcae198>.

4-1 Introduction

THE EXPLOITATION of finite natural resources poses new challenges to agriculture. The supply of phosphorus (P), a vital nutrient derived from finite resources, will decrease (Marschner, 2011). The predicted time for "peak phosphorus", i.e., the time at which global P production reaches its maximum due to the depletion of reserves and declines again immediately afterwards, is estimated around the early to mid-21st century (Reijnders, 2014). Additionally, excessive use of P fertilizer significantly impacts the environment by contributing to eutrophication, which harms open water bodies and leads to aquatic plant and algae growth, impairing water quality for other organisms and limiting water use for drinking, recreation, and industry (Randall, 2003). Especially in lakes, rivers, estuaries, and coastal oceans over-enrichment with P is a widespread problem (Carpenter et al., 1998). Most of the P stored in water bodies originates from agricultural and urban activities. P fertilizers dissolve quickly, releasing P faster than plants can absorb it. P fertilizers, bound on loose soil particles, are highly prone to being lost by erosion. P that is not used by plants or object to runoff losses is immobilised in the soil and subsequently not available for plants anymore. For these reasons, a reduction of P fertilization is required (Hussain et al., 2021).

Concurrently with the impending shortage of P, climate change is anticipated to lead to a scarcity of water across various regions around the globe (Gosling and Arnell, 2013). In view of this future water shortage, it is, therefore, crucial to gain an advanced understanding of how the reduced availability of soil P affects the plant's architecture, specifically functional alterations related to the plant's capacity for water uptake through its root system (Fry et al., 2018).

Zea mays is one of the most important crops worldwide and crucial for human nutrition (Ranum et al., 2014). Maize is sensitive to P deficiency and it is known that canopy development is inhibited by P deficiency, leading to yield decline. The plant's architecture changes under soil P limitation. P deficiency is often associated with reduced growth and rigid appearance of shoots. Limited soil P availability also induces changes in root architecture. Studies report different morphological changes, such as the inhibitions of primary root growth, shallower axial root angle, or various changes in lateral root growth, such as the reduction of lateral root growth in the field, but also an increase in lateral branching in plants with few axial roots (zero order roots) (Borch et al., 1999, Marschner, 2011, Zhu and Lynch, 2004), often resulting in a higher root to shoot biomass ratio (Lynch et al., 2005). Furthermore, an increase in crown root number has been reported to be beneficial under P deficiency (Sun et al., 2018). A reduced root radius was described as a response of *Zea mays* to reduced soil P availability in soil (Sheng et al., 2012, Zhang et al., 2012). However, no direct functional relationships between root system responses to P availability and root system functions have yet been established. Additionally, under field conditions, most plant responses are measured in rather coarse metrics and do not provide direct response functions (Lopez et al., 2023). Although a variety of different plant responses were reported, it remains uncertain which parameters (non-aggregated,

directly measurable attributes, such as type-dependent root length and number) have a direct impact on aggregated structural and functional root system traits, such as total root system volume or plants water uptake capacity.

The root system architecture and anatomy are the main factors that are important for the plant's water uptake capacity (Steudle, 2001). Root plasticity refers to the ability of plant roots to alter their growth depending on environmental conditions. Root architecture refers to the spatial and temporal distribution of roots within the soil. The root system can be described as an assembly of cylindrical root segments, and the root architecture defines the shapes of the individual segments, such as their length, radius, and orientation, as well as how they are connected. Root anatomy relates to the internal structure of the root. Together, they govern the root hydraulic properties.

The root hydraulic properties determine the plant's capacity to channel water from the soil to the roots and then to the aboveground organs. The root system conductance (K_{rs}) is a property of the root system and defines the absorptive capacity of the entire root system. As it is an intrinsic property of the root system, it does not depend directly on the surrounding soil environment. Consequently, K_{rs} is not conditioned by the characteristics of the perirhizal zone, the region surrounding the roots where radial symmetric flow and hydraulic gradient are generated by root water uptake (Vanderborght et al., 2024). However, K_{rs} depends on the size and age of the root system. The variability in K_{rs} can be very high; e.g., in young maize (up to one month), the K_{rs} can vary from 7.00×10^{-5} to 2.37×10^{-2} $\text{cm}^2 \text{d}^{-1}$ (Baca Cabrera et al., 2024).

In order to relate K_{rs} to the size, age, and architecture of the root system, it is necessary to know the hydraulic properties of the individual root segments that make up the whole root system. The radial hydraulic conductivity (k_r) of a root segment is a measure of the root's ability to take up water from the soil into its vascular system. k_r represents the ratio of the water uptake by a root segment to the water potential difference and the outer surface of the root segment. The axial hydraulic conductance (K_x) relates to the efficiency of water transport along the length of the root's main axis (Steudle, 2001). It represents the ratio of the axial water flow in a segment (J_x) to the potential gradient along the segment. Both k_r and K_x are intrinsic properties of the roots. k_r is often treated as an intensive property, i.e., it does not depend on the size or radius of the root segment. However, this is debatable as k_r can decrease with increasing root radius and cortical thickness, increasing the transport distance and, hence, the resistance to flow. K_x is an extensive property since K_x increases with an increasing cross-sectional area of the xylem tissue. k_r and K_x depend on the properties of the root tissues (cortex, xylem, casparian band), and changes in these properties at the cellular and organ levels can impact the root's overall hydraulic function, which might alter the root system conductance. A change in K_{rs} affects the plant's ability to uptake water (Meunier et al., 2020). Since ageing root architecture development depend on environmental conditions, variations in K_{rs} depend indirectly on the soil environment (Baca Cabrera et al., 2024, Meunier et al., 2017). Many different environmental influences, such as drought

or salinity, lower K_{rs} (Aroca et al., 2011). P deficiency was also suggested as an influencing factor for lowering K_{rs} in different species (Li et al., 2009, Mu et al., 2006, Shangguan et al., 2005).

We know that anatomical changes in the roots of *Zea mays* under P deficiency reduce the root hydraulic conductivity in very young plants but it has also been shown that line-specific differences in the anatomical formation can strongly influence the K_{rs} changes caused by P deficiency (Fan et al., 2007, Rishmawi et al., 2023). In general, the relationship between soil P availability and key architectural root system parameters that drive changes in K_{rs} is not well understood. Moreover, *Zea mays* was rarely the object of studies investigating the influences of P deficiency on K_{rs} . Continuous data showing changes in conductance of the whole root system to soil P limitation over time are lacking but would be helpful to understand the influence of decreasing soil P on K_{rs} . However, with experimental setups, it is especially challenging to quantify solely the effects of soil P limitation on whole crop and canopy development and its consequences on relevant physiological processes, such as water uptake-related functions. Especially for k_r , experimental measurements require complex setups, such as root pressure probe (Frensch and Steudle, 1989), measuring water flow of pruned roots within a pressure chamber (Zwieniecki et al., 2002), or using the high-pressure flow meter device on whole root systems for root system conductance, as proposed by (Tyree et al., 1994). The necessity of measuring k_r at several locations, in case of its variation along the root axis or for various root types, makes its experimental evaluation more challenging. Inverse modeling is a newer, additional method to obtain k_r and k_x values (Couvreur et al., 2018).

Functional-structural plant models (FSPMs) are a suitable tool to help investigate and interpret the reaction of the plant to a changing environment, such as the absence of a crucial nutrient. They can bridge the gap between the sub-organ and whole plant level and thus simulate mechanistically emerging plant phenotypes caused by the interaction of processes at smaller scales, such as the effect of radial and axial water fluxes through root segments on the whole plant water uptake. Indeed, FSPMs are computational frameworks that simulate plant growth by integrating physiological functions with (3D) structural representations of plant organs. In the context of P, FSPMs have already been used to test hypotheses regarding changes in the root architecture of *Zea mays*, such as a bigger inter-lateral distance (Postma et al., 2014) and a higher amount of seminal roots regarding its advantages for P uptake (Perkins and Lynch, 2021).

Although it has already been shown that root architecture and shoot size adaptation are affected by soil P availability, transferring these findings directly to the sub-organ level is very complex without a more detailed experimental investigation of how architecture changes at a high spatio-temporal resolution. Previous studies had however a coarse temporal or spatial resolution or focused on specific organs (Sun et al., 2018). Moreover, it is also suggested that potential reactions to P deficiency can already occur in very early growth stages (Brunel-Muguet et al., 2014), whereas experimental studies focused on older plants (Pereira et al., 2020). To the best of our knowledge, there are currently no studies investigating the

whole plant's architectural response of *Zea mays* to different levels of phosphorus availability, including the influence of this response and its consequences for K_{rs} .

This work aims to understand which root and shoot architectural parameters are responding to four decreasing soil P levels from sufficient to severe deficient and how this will affect the plant's root system capacity for water uptake. Therefore, this study has two main objectives:

1. Identify experimentally which structural parameters of maize organs show the strongest responses to soil phosphorus availability.
2. Parameterize and use *Zea mays* FSPMs from experimental data to analyse how root system conductance in maize adapts to the different soil P availability levels.

4-2 Materials and Methods

4-2-1 Experimental set-up

Five *Zea mays* cv. B73 plants per treatment were grown in rhizotrons (60 cm × 30 cm × 2 cm) (Pfeifer et al., 2014) under four levels of soil P availability, thereafter called P0, P1, P2, and P3. The experiment was conducted in a greenhouse at the *Forschungszentrum Jülich GmbH*, Germany (50°54'36" N, 6°24'49" E) from May to June 2022.

As substrate, a P deficient luvisol soil from the "Dikopshof" long-time fertilization trial (Wesseling, Germany) was used (Schellberg and Hüging, 1997). The initial plant available P concentration in soil (P extracted according to the calcium-acetate-lactate (CAL method), (Schüller, 1969)) was 1.8 mg P per 100 g soil (P0). The soil was fully enriched by all other nutrients and sufficiently supplied with demineralized water, so P was the only limiting factor for plant growth. The substrate was additionally fertilized (45% P₂O₅, Triplesuperphosphate). The resulting soil P concentration was respectively 3.3 mg 100 g⁻¹ for P1, 4.6 mg 100 g⁻¹ for P2, and 7.7 mg 100 g⁻¹ for P3. Together with P0, these four different soil P levels represent the different P content classifications for agricultural soils, low B to D range, as proposed by VDLUFA (Verband deutscher landwirtschaftlicher Untersuchungs- und Forschungsanstalten) (Wiesler et al., 2018). In the context of agricultural applications, P0 is in the range of severe, P1 of strong (B) and P2 of mild (low C) P deficiency, while P3 is P sufficient (D).

Always two seeds were planted in the rhizotrons and directly after germination of the first seed, the other seed was removed. The soil in the rhizotrons was saturated with demineralized water before the experiment began and in the first two weeks, 75 ml H₂O d⁻¹ and the following two weeks 125 ml H₂O d⁻¹ were added from the top. To obtain a high temporal resolution, imaging was first performed daily and, after 3 weeks, every two days. The measurements were performed until 28 days after sowing (DAS).

To phenotype the roots, a daily image of the root system was performed with a "PhotoBox" equipped with a high-resolution camera (EOS 70D; 14mm APS-C, Canon Inc., Tokyo, Japan), where the rhizotron was always located at the same position, avoiding distortion and image-shift (Pfeifer et al., 2014). This allowed us to take high-resolution images of the whole growing root system. During the experiment, the rhizotrons are stored in boxes at 45° inclination, so the root system will grow towards and along the window of the rhizotron. The windows remained covered and heat-shielded between the measurements, so the roots grew in a dark and heat-isolated environment. To obtain information about the shoot architecture of the maize plant, we performed a high-resolution 2D-RGB measurement with a fixed position horizontally to the plant. The camera (X-S10, Fujifilm Holdings K.K, Tokyo, Japan) was equipped with a fixed focal length lens (35mm APS-C, Fujifilm Holdings K.K, Tokyo, Japan). To ensure a good image processing a uniform blue background was installed. During the measurement, the rhizotron was fixed at an angle of 45°, to provide a vertical positioning of the maize shoot. To ensure detailed and accurate data collection, the shoot imaging was conducted just prior to the imaging of the roots. At the end of the experiment, a destructive biomass measurement was performed.

4-2-2 Image processing

The data obtained from root and shoot are available as 2D RGB images (shoot: JPG, 2080x2080 px; root: JPG, 2268x4862 px). To facilitate the analysis of the images, a mostly automated image-processing pipeline was established, streamlining the CPlantBox model parameterization from the experimental data (Fig. 1). The first step of image analysis was the segmentation of the targeted organ.

The shoot image analysis pipeline started with the segmentation of the maize crop shoot. This was performed by a colour-threshold-filter algorithm written in Python based on the OpenCV wrapper PlantCV and the OpenCV library itself (Gehan et al., 2017). The blue background was removed using a colour-based filter and only the predominantly green-to-red coloured plants were still present after filtering. Then, a semi-automated detection with RootSystemAnalyser (Leitner et al., 2013b) was performed. The parameters used for CPlantBox were directly derived from RootSystemAnalyser. We used the procedure already successfully applied in Yu et al. (2024).

For the root system part, we adapted the method from Bauer et al. (2022) to segment the roots in the image with a deep neural network model trained with RootPainter (Smith et al., 2022). We trained the neural network to ignore small gaps in the root system. However, since some gaps remained we added a feature to RootPainter, allowing manually correcting segmentation errors and tracing the root by hand if needed. The RootPainter add-on allowed us to analyse time series by transferring the segmentation of an image to the next consecutive image in the time series and only adding the additional segmented roots to the previous segmentation. The segmentation results were complete 2D binary root systems. The next processing step was the automated root tracing. RootSystemAnalyser di-

rectly provided the input parameter usable for CPlantBox, by manually choosing axial roots and automatically detecting the laterals. Finally, an RSML file (Root System Marker Language) for every root system and time step was produced by RootSystemAnalyser (Lobet et al., 2015). The first root was always flagged as the primary root. To discriminate between crown roots and all other root types, the crown roots were manually flagged in the RSMLs with SmartRoot (Lobet et al., 2011).

4-2-3 CPlantBox parameter extraction

CPlantBox is a modeling platform that can simulate the morphology and 3D topology of the plant and, among other processes, plant and soil water fluxes (Giraud et al., 2023). To use the CPlantBox modeling framework, plant parameters obtained from real plants are required to create a structure as either a virtual copy of an existing plant or a stochastic variation of a plant, representing the parameterized cultivar, respectively line (Schnepf et al., 2018, Zhou et al., 2020).

In terms of plant topology, it is possible to reduce the whole plant architecture to a handful of key parameters that are the input to calibrate CPlantBox. A precise parameterization of every organ type (e.g., leaf, basal roots) of the shoot and root system is required. This includes plant age at organ emergence, maximal length and initial elongation rate of stem, leaf and every root type. Depending on the organ, initial growth angle, radius, tropism, and branching distance and -pattern have to be defined (Figure S2.1). These parameters were used as direct model input to simulate the plant structure. We furthermore have parameters that describe general root system traits, such as (first) initiation time, maximal count and appearance probability of different lateral root types and the seed position. We also have organ-specific parameters, which had to be measured and calculated for every organ sub-type. Regarding the shoot, this only applied to the leaf and stem. For the root system, specific parameter-ensembles were derived for every root type, respectively primary embryonic root (primary root), seminal roots, crown roots and lateral roots. For maize, there exist also two different types of lateral roots (Heymans et al., 2021). We sub-divided first order laterals into l-(long) laterals, which have branching roots and s-(short) laterals.

In a CPlantBox simulation, each parameter is determined using the average value (mean) and variability (standard deviation, sd) from all the data points provided for parameterizing that specific organ. A comprehensive list detailing the parameters, their abbreviations, and the units of measurement can be found in Table 4-1.

The static root model parameters were directly derived from the RSMLs (Table 4-3). For the initial elongation rate parameter (r) a curve fitting was performed according to eq. 4-1 (Schnepf et al., 2018). We assumed a maximal root length (l_{max}) of 139 cm from literature and fitted r only (Ordóñez et al., 2018, Qiao et al., 2019). General root system parameters, such as the amount and delay of seminal and crown roots, were evaluated manually from the rhizotrons. For leaves, we also considered negative exponential growth, according to eq. 4-1. Growth data

from leaves that had not yet reached the phase of declining daily elongation rate were not used for the computation of r .

$$l_{exp}(t) = l_{max}(1 - e^{-\frac{r}{l_{max}}t}) \quad (4-1)$$

where t (d) is the time, l_{max} (cm) is the maximal length and r ($cm d^{-1}$) is the initial elongation rate.

Table 4-1: Overview of organ parameters (and their units) that are used to calibrate models with CPlantBox, as used for this study (day: d; integer:int), adapted from Schnepf et al. (2018), Zhou et al. (2020) and Giraud et al. (2023)

root	abbriv.	unit	shoot	abbriv.	unit
planting depth	<i>depth</i>	cm	nodal growth implementation	<i>nodalGrowth</i>	int [0,1]
first emergence of seminal roots	<i>first_B</i>	d	time period between leaves	<i>delayLat</i>	d
time period between basal roots	<i>delay_B</i>	d	rotation of leaves around stem	<i>RotBeta</i>	int [0-1]
max. no. of basal roots	<i>max_B</i>	int	shape type of leaves	<i>shapeType</i>	int [0,1]
first occurrence of crown roots	<i>first_S</i>	d	petiole width	<i>Width_petiole</i>	cm
time period between shoot-born roots	<i>delay_S</i>	int	max. area of leaf geometry	<i>areaMax</i>	cm ²
per root crown no. of shoot-born roots	<i>n_S</i>	d	of the leaves	<i>leafGeometry</i>	array
distance between crowns along the shoot	<i>dz_S</i>	cm	length of petiole	<i>l_b</i>	cm
root radius	<i>a</i>	cm	stem radius	<i>a</i>	cm
insertion angle	<i>θ</i>	rad	insertion angle leaf	<i>θ</i>	rad
length of basal zone	<i>l_b</i>	cm	length of stem until the first leaf	<i>l_b</i>	cm
apical delay	<i>l_{delay}</i>	cm d ⁻¹	length of leaf blade	<i>l_a</i>	cm
initial elongation rate	<i>r</i>	cm d ⁻¹	init. elongation rate	<i>r</i>	cm d ⁻¹
max. root length	<i>l_{max}</i>	cm	max. length	<i>l_{max}</i>	cm
tropism type ¹	<i>type</i>	int [0-3]	tropism type ¹	<i>tropsimT</i>	int [0-5]
tropism strength	<i>N</i>	int	tropism strength	<i>tropsimN</i>	int
root successor type	<i>successor</i>	int	successor	<i>successor</i>	type,% ²
type of root elongation ³	<i>gf</i>	int [0,1]	type of elongation ³	<i>gf</i>	int [0,1]
root lifetime	<i>rlt</i>	d	lifetime	<i>rlt</i>	d
max. segment length	<i>dx</i>	cm	max. segment length	<i>dx</i>	cm

¹ plagio-, gravi-, exo-, chemo-, hydro-, antigravi-, or age-dependent-tropism

²probability of emergence

³ negative exponential or linear growth

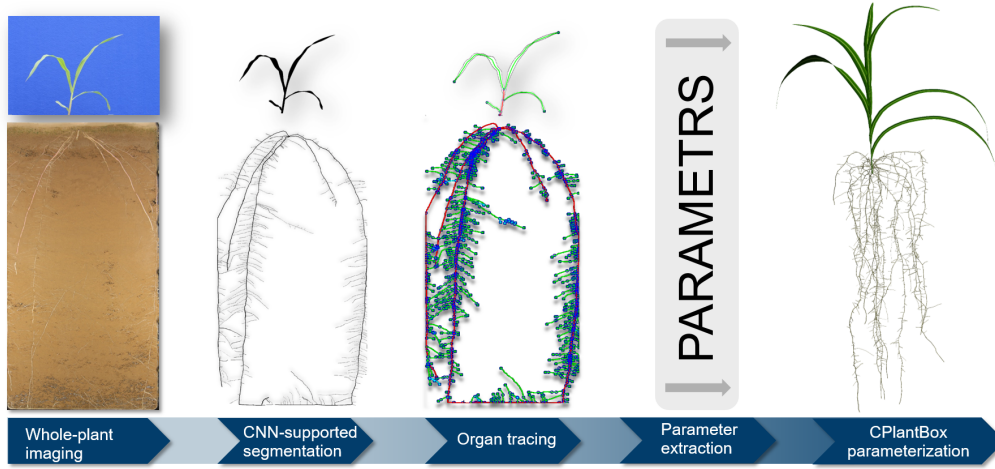


Figure 4-1: Workflow from experiment to CPlantBox model parameterization.

4-2-4 K_{rs} calculation

To calculate the root system conductance and assess the water uptake of the plant, information about k_r (d^{-1}) and K_x ($cm^3 d^{-1}$) is required (Meunier et al., 2018). The root hydraulic properties vary strongly among species, but also among genotypes of the same species (Rishmawi et al., 2023). However, most functional-structural simulations for maize rely on time dynamic hydraulic conductivity profile values from Doussan et al. (1998), a study conducted 25 years ago that only covers two root types, as highlighted in subsequent studies (Javaux et al., 2008, Meunier et al., 2020, Postma et al., 2017). Besides measuring the radial flow and root anatomy, hydraulic anatomy simulators integrated into new modeling software tools, can assist a more precise estimation of these values (Couvreur et al., 2018, Heymans et al., 2020, Passot et al., 2019). This enables new possibilities, such as the hydraulic atlas of *Zea mays* cv. B73 of Heymans et al. (2021). With these parameters, the hydraulic properties of the root system can be defined and the K_{rs} ($cm^2 d^{-1}$) can be calculated according to Couvreur et al. (2012),

$$K_{rs} = \frac{T_{act}}{\psi_{sr,eff} - \psi_{collar}} \quad (4-2)$$

where $\psi_{sr,eff}$ (cm) is the *effective* soil-root interface water potential felt by the roots, ψ_{collar} (cm) is the plant collar potential and T_{act} ($cm^3 d^{-1}$) is the actual plant transpiration rate and the net sum of the radial water flow rates (J_r , $cm^3 d^{-1}$) in the roots, respectively root segments that make up the root system, since no changes in plant water storage are taken into account. $\psi_{sr,eff}$ is obtained following the method of Couvreur et al. (2012):

$$\psi_{sr,eff} = SU F^T \cdot \psi_{sr} \quad (4-3)$$

where SUF (–) is the vector containing the standard uptake fraction, which is the ratio between the water uptake of each root segment and the total water uptake of the root system, and ψ_{sr} is the vector of soil water potentials at each root-soil interface. J_r is defined as:

$$J_r = K_r(\psi_{sr} - \psi_{xyl}) \quad (4-4)$$

$$K_r = 2\pi a_{organ} dl k_r \quad (4-5)$$

where K_r is the radial conductance ($cm^2 d^{-1}$) of a root segment with an infinitesimal length dl (cm). a_{organ} is the organ radius, and ψ_{xyl} is the xylem water potential (cm). As we assume steady-state water flow with no plant water storage variations, J_r is equal to the changes in axial water flow (J_x , $cm^3 d^{-1}$) along l , so we obtain:

$$J_r = \frac{\partial J_x}{\partial l} dl \quad (4-6)$$

$$J_x = K_x \frac{\partial \psi_{xyl}}{\partial l} \quad (4-7)$$

$$K_x = \frac{\pi a_{xyl}^4}{8\mu} \quad (4-8)$$

where a_{xyl} is the equivalent xylem radius, μ ($cm d^{-1} H_2O$) the dynamic water viscosity, assumed equal to that of pure water at $20^\circ C$. Note that we express water potentials in terms of water heads, as is common in models that simulate water flow in soils. Eq. 4-4 - 4-7 gives us a system of equations that are solved analytically using the method of Meunier et al. (2020), implemented in CPlantBox according to Giraud et al. (2023). The solution yields both J_r and ψ_{xyl} for a specific set of k_r and K_x .

We calculated the root hydraulic properties k_r and K_x from the values published in Heymans et al. (2021) for *Zea mays* cv. B73 (Table S2.1). We assumed that the k_r and K_x did not change between the different P treatments. We assume here that k_r and K_x does not depend on the root radius; however, the changes in radii between P treatments were considered when calculating radial conductance (eq. 4-5). Although it was shown that the aerenchyma structure can change under P deficiency (Fan et al., 2007), the inter-line specific differences in k_r and K_x are much higher in *Zea mays* than the reformation under P deficiency (Rishmawi et al., 2023). Furthermore, the aerenchyma reformation of *Zea mays* cv. B73 with a no-P treatment under lab conditions, is reported to be still very moderate (Fan et al., 2007). Finally, the few root hydraulic property data available for maize under P deficiency are hard to use for our model, since they only take a single root type (primary root) into account and are measured for very young plants grown in nutrient solution. The data from Heymans et al. (2021) are given as distance-dependent from the root tip distance and for every root type. The conversion from distance-dependent to age-dependent conductivity was done using eq. 4-9.

For a specific distance from the root base l (cm) the corresponding root segment age ($age(l_{exp}), d$) was calculated with

$$age(l_{exp}) = -\frac{l_{max}}{r} \ln\left(1 - \frac{l}{l_{max}}\right) \quad (4-9)$$

where r is the initial elongation rate, obtained from the experiments and eq. 4-1, l_{max} is the maximal root length and l is the current measured root length (from experimental data). In contrast to Doussan et al. (1998), we distinguished between primary root, seminal roots, crown roots, l-lateral roots and s-lateral roots. For the parameterization of the shoot organs we followed the simpler approach of Lobet et al. (2014), where it was assumed that the radial stem conductivity was 0 and the axial stem conductance ($cm^3 d^{-1}$) is also calculated according to the Hagen-Poiseuille law (eq.4-8).

We finally calculated the K_{rs} (eq.4-2) using the simulated plant architecture and the root hydraulic anatomy based on (Heymans et al., 2021).

4-2-5 Statistical analysis

All statistical analyses, besides a principal component analysis (PCA), were performed with Python 3.9.13. For significance testing of the experimentally measured parameter between P treatments, we applied a Shapiro-Wilk Normality Test and Levene's Test for Equality of Variances, followed by an ANOVA and Tukey post-hoc test with the "scikit" package (scikit-learn 1.4.2) (Pedregosa et al., 2011). The results of the statistical test are summarised in the Table S2.2. All parameters with significant differences ($p_{value} < 0.05$) were included in the PCA, namely axial root radii, leaf elongation and crown root elongation and we further added K_{rs} , dry matter, P to dry matter ratio and P measured in soil. We clustered for the different P treatments and included the five repetitions per treatment. For curve fitting of the initial elongation rate parameter (r) and maximal length (l_{max}), the "scipy" package was used (Virtanen et al., 2020). The PCA was performed with R 4.3.1 (R Core Team 2023) and the "FactoMineR" package (Le et al., 2008). For linear regression models of the identified response parameter, the "sklearn" package was used (Pedregosa et al., 2011). Plots were created with the "matplotlib" package (Hunter, 2007).

4-2-6 Data and code availability

All analysed data, code and model input files used for simulations and to plot the figure are publicly available and released in a GitHub repository <https://github.com/Plant-Root-Soil-Interactions-Modelling/CPlantBox/releases/tag/Publication2024> in the folder /experimental/pdef. The image data are available here: doi.org/10.5281/zenodo.11384890. We further transferred the simulation set-up to a docker container for easy access.

4-3 Results

4-3-1 Plant structural responses to soil P level

The influences of P deficiency on the architecture of young root systems appear complex. Although we observed a reorganisation in many different architectural root system traits, the clearest significant trends in root trait responses to P deficiency can be seen in the radius of axial roots and the elongation rate of crown roots (Figure S2.2A and Figure S2.2B). The radii of axial roots significantly increased with the amount of P fertilized. Only for the initial leaf elongation rate we found a significant architectural response of the shoot to soil P availability. The initial elongation rate was significantly higher for the highest P level (P3) compared to the two lowest P levels (P0-P1) (Figure S2.2C). Consequently, the maximal leaf area showed an increasing trend as well. Although stem length and diameter also increased slightly with higher P supply, the differences between the soil P levels were not significant. The destructively measured root mass fraction (root biomass/plant biomass) shows a decreasing trend with increasing soil P availability (Figure S2.2D). We performed a PCA, including the significant response parameters to P deficiency, which clearly demarcates clusters for each phosphorus treatment level, with minimal overlap between the confidence ellipses. This suggests a strong grouping effect in our data, reflective of the distinct phosphorus treatments applied (Figure 4-2). The PCA further revealed that axial root radii are closely associated with soil P content, while crown root elongation showed a notable correlation with the soil P to dry matter ratio (PB, $mg\ P\ g\ biomass^{-1}$). A similar positive correlation was observed between soil P and leaf elongation rate. Therefore, we considered crown root elongation rate and axial root radii as plastic response parameters for root system changes. Additionally, the leaf elongation rate was considered as shoot response to soil P availability.

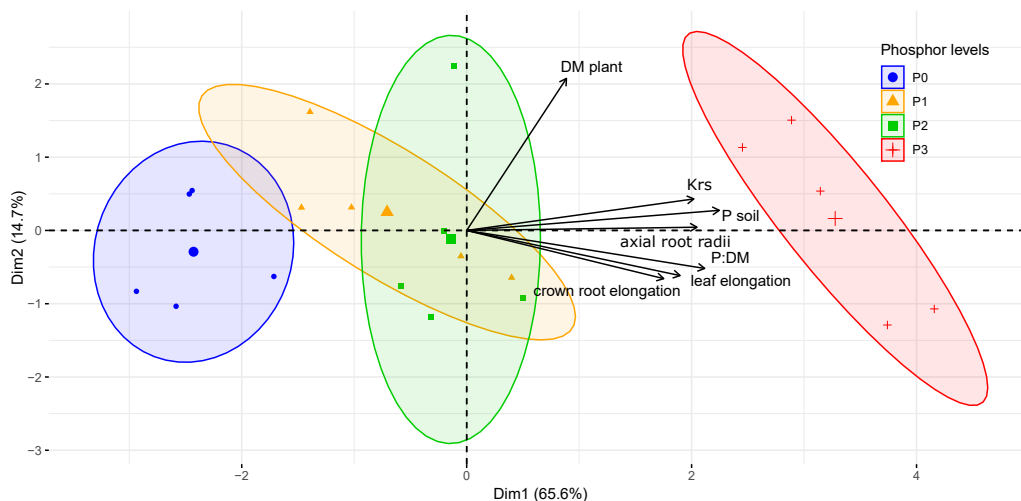


Figure 4-2: Principal component analysis (PCA) to identify the contribution of the plant parameters to the response of *Zea mays* to P deficiency. The big symbols corresponds to the centroids for the different P treatments.

For the radii of axial roots (a_{ax}) we found a direct linear relationship to P available in soil (Figure 4-3A) within the measured upper boundary (P_{max}) and lower boundary P_{min} ($mg\ hg\ soil\ (100\ g^{-1})$) of soil P, described as eq. 4-10.

$$a_{ax} = \alpha_{a_{ax}}P + a_{P_0}, \quad P_{min} < P < P_{max} \quad (4-10)$$

where parameter $\alpha_{a_{ax}}$ defines the increase in radii per unit of P in soil and a_{P_0} the intercept of the response that represents the radii at the theoretical situation of no available P in soil. We found that the crown root elongation rate a_{r_c} ($cm\ d^{-1}$) is a response to the ratio of P_{soil} to dry matter (DM, g) of the plant (eq. 4-11).

$$PB = \frac{P_{soil}}{DM_{plant}}, \quad (4-11)$$

$$r_c = \begin{cases} \alpha_{r_c}PB, & 0 < PB < PB_{max}, \\ \alpha_{r_c}PB_{max}, & PB \geq PB_{max} \end{cases}$$

where α_{r_c} is the increase in elongation per unit PB . PB_{max} describes the maximal PB we measured, which however aligns with several maximal crown root elongation rates, measured by other studies (Figure 4-3B).

The initial leaf elongation rate (r_l , $cm\ d^{-1}$) is a linear function of the P available in the soil and is described by eq. 4-12 (Figure 4-3C).

$$r_l = \alpha_{r_l}P + r_{P_0}, \quad P_{min} < P < P_{max} \quad (4-12)$$

where α_{r_l} ($cm\ d^{-1}$) is the increase in elongation per unit P, while r_{P_0} ($cm\ mg\ P\ d^{-1}\ hg\ soil$) is the intercept at the theoretical situation of no soil P. P_{min} and P_{max} ($mg\ hg\ soil$) describe the lower and upper boundaries of P for the r_l variations. Our observations revealed that the leaf area was maintained for plants with higher P supply and sharply decreased at the two lowest soil P levels (Table 4-2). The root volume increased linearly with the amount of available soil P (Figure S2.3).

For every soil P level, a complete CPlantBox parameter set was created for whole plant simulations (Figure 4-4). A full list of the parameters, including root system internalising parameters, as well as root and shoot specific parameters can be found in Tables 4-3, 4-4 and 4-2, respectively. We moreover created an FSMP, which simulates the dynamic growth of *Zea mays* cv. B73 under different soil P levels and modified only the identified key parameters (see section 4-4-1) according to the measured soil P levels. We compared the time-dependent simulated total root system volume and found no relevant absolute differences between the same treatments (Figure S2.3).

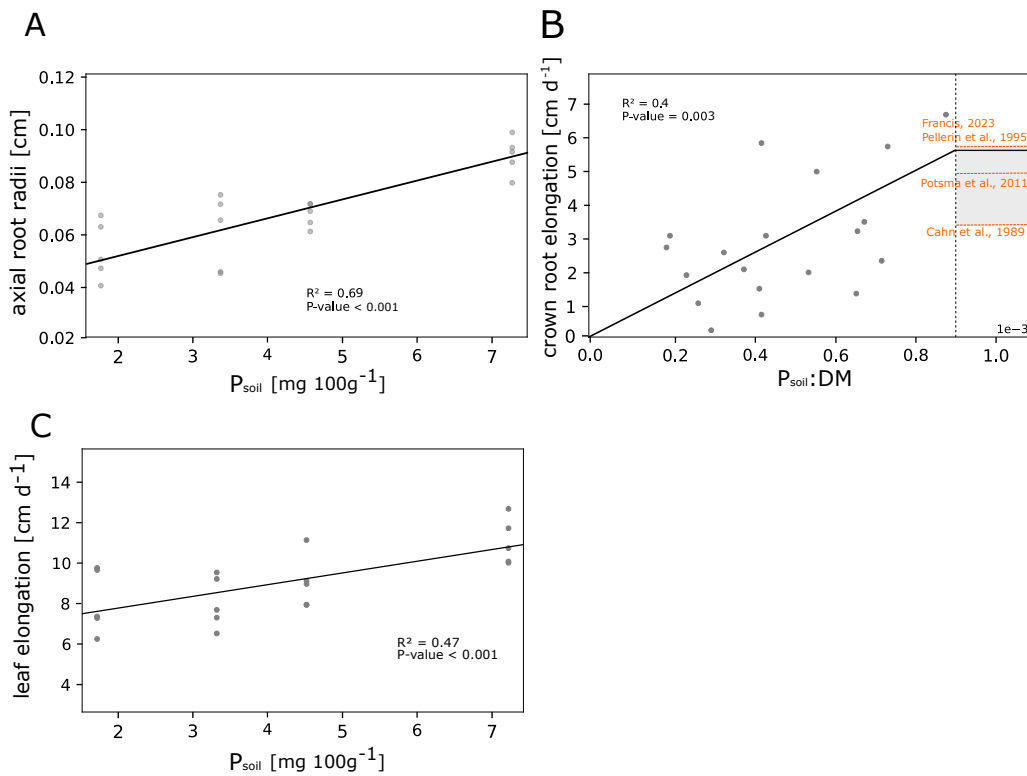


Figure 4-3: Response of axial roots radii (A), crown root elongation (B) and leaf elongation rate (C) to different soil P availability levels.

Table 4-2: Overview of shoot organ specific architectural CPlantBox parameters, as described in Table 4-1, for the distinguished P regimes.

params	P level	P0		P1		P2		P3	
	type	mean	sd	mean	sd	mean	sd	mean	sd
<i>a</i>	stem	0.187	0.01	0.16	0.02	0.166	0.014	0.130	0.0
<i>l_n</i>	stem	1.487	0.313	0.153	0.175	1.676	0.214	1.636	0.126
<i>r</i>	stem	0.759	0.876	0.915	1.034	1.0	0.772	1.129	0.66
	leaves	7.921	2.338	7.914	2.041	8.8	2.976	10.907	3.005
<i>l_b</i>	leaves	0.0	0.0	0.0	0.0	0.0	0.0	0.0	0.0
<i>l_{max}</i>	leaves	38.411	7.88	42.606	14.001	52.237	17.901	49.124	15.521
<i>θ</i>	leaves	0.705	0.306	0.773	0.055	0.794	0.403	0.739	0.262
<i>delay_{lat}</i>	leaves	3.0		3.0		3.0		3.0	
<i>RotBeta</i>	leaves	1.0		1.0		1.0		1.0	
<i>WidthBlade</i>	leaves	1.638		1.681		1.561		1.563	
<i>areaMax</i>	leaves	54.454		66.695		80.683		71.956	

Table 4-3: Overview of initial root system architectural parameters for the distinguished P regimes. These parameter describe the initiation time, maximal count and appearance probability of the different lateral root types, the seed position and simulation time.

root system parameter	P0	P1	P2	P3
$first_B$ [d]	3.6	3.6	3	4.0
$delay_B$ [d]	1.0	1.0	1.0	1.0
max_B [-]	3.5	3.5	3.5	3.5
$first_{SB}$ [d]	8.6	9.4	9.2	8.2
$delay_{SB}$ [d]	1.0	1.0	1.0	1.0
$delay_{RC}$ [d]	7.4	6.6	6.3	6.2
n_C [-]	3.0	3.6	3.4	3.0
$seedPos$ [x,y,z]	[0.0, 0.0, -3.0]			
$simulationTime$ [d]	28			
$successor\ probability$ on axial roots [l-lateral; s-lateral]	0.04; 0.96	0.05; 0.95	0.05; 0.95	0.05 ;0.95

Table 4-4: Overview of root organ specific architectural CPlantBox parameters for the distinguished P regimes and the parameterset (general) for simulation to evaluate the root system response parameter.

params	P level type	P0		P1		P2		P3		general	
		mean	sd	mean	sd	mean	sd	mean	sd	mean	sd
a	primary	0.054	0.012	0.064	0.017	0.067	0.01	0.091	0.01	0.069	0.003
	seminal	0.052	0.011	0.062	0.016	0.066	0.01	0.081	0.011	0.065	0.003
	crown	0.061	0.016	0.059	0.02	0.066	0.014	0.066	0.003	0.063	0.007
	l-lateral	0.025	0.011	0.024	0.009	0.025	0.008	0.03	0.007	0.026	0.002
	s-lateral	0.025	0.007	0.028	0.01	0.025	0.008	0.04	0.012	0.030	0.002
l_b	primary	0.8	0.899	1.879	2.385	3.183	2.236	3.777	5.681	2.410	2.033
	seminal	2.55	2.333	3.883	2.432	3.969	4.574	1.642	0.814	3.011	1.546
	crown	3.161	2.454	7.216	7.564	3.473	2.487	3.924	3.025	4.444	2.468
	l-lateral	2.27	2.433	1.732	1.441	2.854	2.349	1.779	1.392	2.159	0.564
l_{delay}	primary	0.212	0.153	0.481	0.597	2.63	0.284	1.743	1.331	1.267	0.527
	seminal	0.499	0.364	0.941	0.784	1.038	0.864	0.94	0.535	0.855	0.230
	crown	0.194	0.124	0.666	0.625	0.547	0.476	0.666	0.428	0.518	0.210
	l-lateral	0.327	0.294	0.618	0.444	0.341	0.305	0.442	0.309	0.432	0.071
r	primary	3.951	0.766	3.35	1.252	4.417	0.865	4.627	0.486	4.086	0.317
	seminal	3.28	1.955	2.149	1.417	2.912	0.644	3.239	1.698	2.895	0.567
	crown	2.981	2.693	2.556	2.902	2.29	2.146	4.886	2.583	3.178	0.319
	l-lateral	2.951	1.492	1.763	0.693	2.15	0.56	1.742	0.582	2.152	0.444
	s-lateral	2.555	2.479	5.078	4.814	5.292	4.982	5.97	5.168	4.724	1.263
l_{max}	l-lateral	5.549	3.821	4.756	2.513	6.736	3.546	4.794	2.392	5.459	0.721
	s-lateral	1.631	1.596	1.341	1.15	0.84	0.452	1.238	1.123	1.263	0.472
θ	l-lateral	1.194	0.375	1.262	0.309	1.344	0.324	1.413	0.324	1.303	0.029
	s-lateral	1.194	0.375	1.37	0.346	1.396	0.327	1.413	0.324	1.343	0.023
l_n	primary	0.466	0.0454	0.457	0.085	0.536	0.122	0.545	0.187	0.501	0.060
	seminal	0.847	0.327	0.519	0.116	0.767	0.202	0.773	0.234	0.727	0.087
	crown	0.847	0.327	0.628	0.244	0.811	0.419	0.754	0.124	0.760	0.125
	l-lateral	0.833	0.946	0.459	0.284	0.53	0.417	0.48	0.319	0.576	0.308



Figure 4-4: Simulated plant structure with CPlantBox for all P levels. The given subtypes correspond to the denomination of the root types.

4-3-2 Root system hydraulics

Based on the created FSPM we calculated K_{rs} . Our results indicate a close association of P in soil and K_{rs} (see Figure 4-2). The K_{rs} for a root system under high to mild P deficiency was significantly lower than for the root system with a high P supply. After 28 days, the simulated mean K_{rs} was between 0.014-0.016 cm^2d^{-1} for P0, P1 and P2, while P3 reached a mean K_{rs} of 0.021 cm^2d^{-1} at the same time point. The differentiation in K_{rs} between the treatments begins between 7 and 10 DAS (Figure S2.5). Figure 4-5 shows (A) the temporal evolution of K_{rs} according to our simulations and (B) in comparison with literature values.

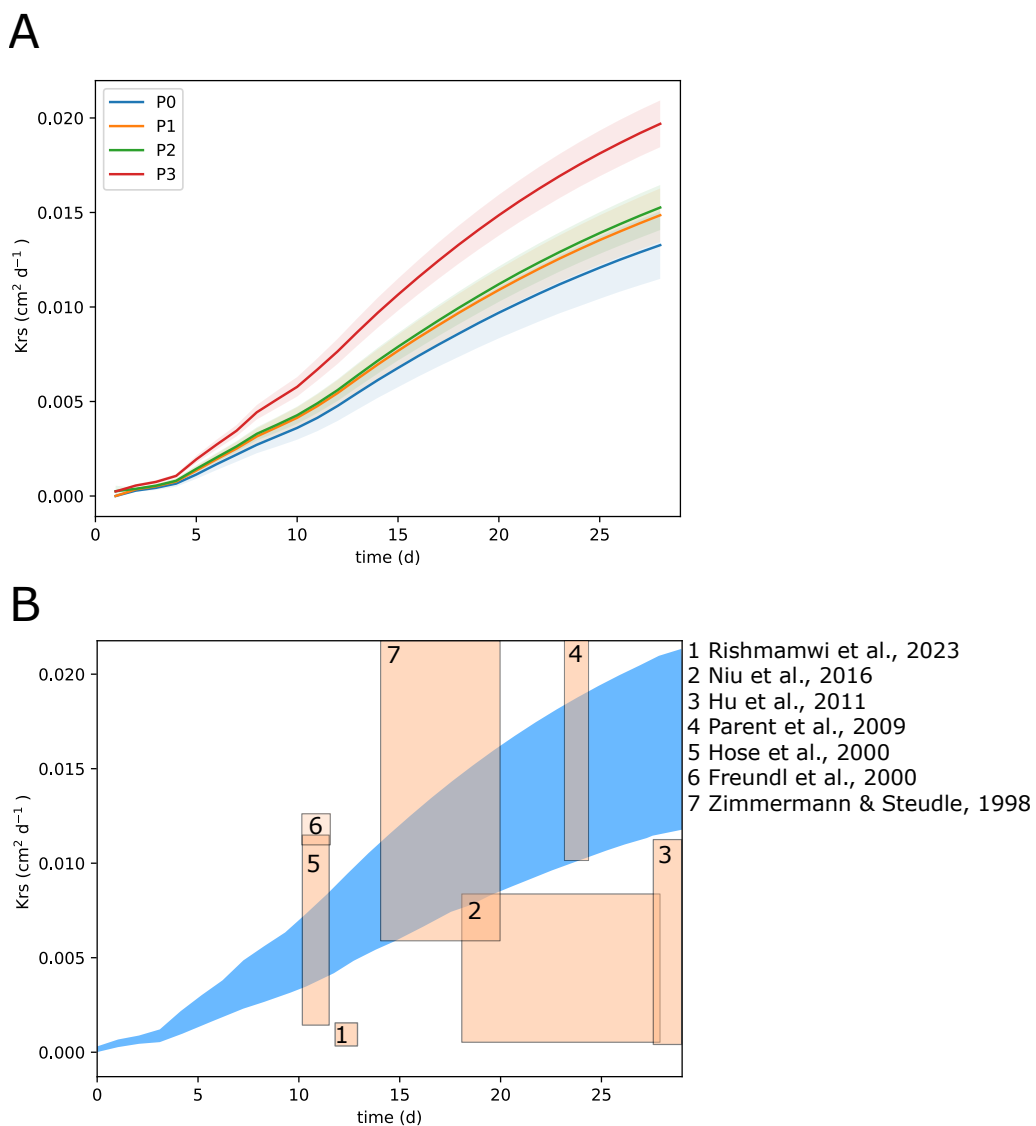


Figure 4-5: A: K_{rs} calculated for each P level with 100 simulation runs (shaded areas show the standard deviation to the mean); B: Comparison of different studies investigating K_{rs} of *Zea mays* with our results (blue).

4-4 Discussion

The here presented study focuses on two main points. First, we conducted a whole plant phenotyping experiment of *Zea mays* cv. B73 under various soil P availability conditions in rhizotrons to identify which architectural parameters of maize organs are responding most to variations in soil P availability. Second, we parameterized FSPMs based on the previously measured data to understand how root system conductance in maize adapts to the different soil P availability levels. With additional hydraulic property data (k_r, K_x) from Heymans et al. (2021), which was based on *Zea mays* cv. B73 anatomy, we could calculate the K_{rs} according to the different structures of the root systems. This allowed us to explore the water uptake capacities of each root system under static soil conditions.

4-4-1 P levels strongly influence axial root radius and crown root elongation

Having a close look at the architectural parameters of the plant, we could see that initial leaf elongation reacted to P deficiency. We observed clear differences in maximal leaf area depending on the P content in the soil, which originated from significant differences in the initial elongation rate of the leaf between high and low soil P levels, indicating that the P deficiency was already an important limitation in the initial growing phase of early leaves. Finally, a reduction of the maximal leaf area might have disadvantageous effects on water regulation and total photosynthesis. These results might be not surprising, as the P deficiency reaction of the plant is mainly linked to a rigid appearance of the shoot (Plénet et al., 2000). However, the quantitative empirical values presented here and the derived response functions are valuable additions, as, contrary to most studies, the functions are valid for soil P levels ranging from strongly limited to sufficient (Lopez et al., 2023).

The influences of soil P limitation on the root system were more complex to disentangle. Especially since there exist maize genotypes that are considered P efficient and P inefficient. B73 is considered an inefficient line and is thus suitable for investigation on the reaction to P deficiency, since possible reactions might be observed already under mild P stress (Kaeppler et al., 2000). When responding to environmental conditions, several phenes interact, so phenotypic effects are not always clear to observe in a single organ, although they become more clear from a holistic perspective, when all organs are evaluated together (Klein et al., 2020, York et al., 2013). We call this effect a plastic reorganization of the root system.

The reorganization effects are complex and our understanding of them is limited (Lynch, 2011). However, modeling approaches have already shown that an increasing amount of seminal roots might be beneficial for P uptake (Perkins and Lynch, 2021), although studies focusing on QTL identification of seminal root count and length report the opposite reaction of *Zea mays* cv. B73 under lab

conditions (Zhu et al., 2006). Our findings do not unequivocally support either of the divergent perspectives reported in the literature.

The reduced radii of axial roots as a response to P deficiency aligns with previous observations. We could show that there is a high linear relationship between plant-available soil P and axial root radii (Sheng et al., 2012, Zhang et al., 2012). Possibly the plant reduced carbon costs to invest it in other organs that might be beneficial for P uptake under soil P limitations or is shifting biomass allocation to more metabolically efficient root classes (Lynch, 2019, Lynch et al., 2005).

Regarding crown root development, we know that a higher number of crown roots is beneficial under P deficiency (Sun et al., 2018). However, past research has indicated that minimizing the amount of crown roots can substantially lower the metabolic expenses associated with root construction, allowing more metabolic energy to be allocated towards root extension (Gao and Lynch, 2016). Following the rhizoeconomic paradigm, this would suggest that an increased number of crown roots might already result in an initially reduced crown root elongation. Under conditions of nitrogen deficiency, it has been already observed that there is a decrease in the number of crown roots, which is accompanied by an increase in their elongation rate (Saengwilai et al., 2014). For plants under P deficiency, the response of crown root elongation is less well-defined. We found that crown root elongation in young plants is already an important response parameter for *Zea mays* under P deficiency and has a negative linear response to decreasing soil P availability in soil. As P leaching to deeper soil strata is limited, lower crown root elongation under limiting soil P conditions would support enhanced topsoil foraging, which is considered to be beneficial for a greater P uptake (Lynch, 2019). However, we could not detect a significantly higher number of crown roots in plants under soil P limitation. This may be attributed to the limitations of the rhizotron setup, which may impede the visibility of all crown roots. Alternatively, if crown root formation is indeed enhanced under P limitation, the effect may not be detectable until 28 DAS, necessitating a longer observation period for accurate quantification.

Overall, the observations in this study are not only meant to investigate shoot and root in terms of biological general validity but also to parameterize CPlantBox to obtain dynamic FSPMs under various soil P conditions and to obtain new findings from this model approach. To our knowledge, this is the first approach of a detailed whole plant 3D FSPM parameterization of *Zea mays*.

4-4-2 K_{rs} varies between fully fertilized and deficient plants, but not among those with severe to mild P deficiency

K_{rs} varies due to environmental conditions (Baca Cabrera et al., 2024, Freundl et al., 2000, Hose et al., 2000). It is known that K_{rs} is influenced by drought (Hu et al., 2011, Parent et al., 2009), osmotic stress (Niu et al., 2016), but also due to genotypic differences (Rishmawi et al., 2023). The K_{rs} values simulated with our *Zea mays* FSPM are in the same range as the ones given in these studies (7.00×10^{-5} - 2.37×10^{-2} $\text{cm}^2 \text{d}^{-1}$, see Figure 4-5B).

We found that when below a specific threshold, soil P limitations modulate the root system conductance, which might impact young plant vigour. Indeed, the *Zea mays* plants with the highest P supply had a significantly higher K_{rs} compared with the K_{rs} for the three lower soil P supply levels, indicating that, as soon as the plants suffer from P deficiency, the adjustment of the root architecture reduces their water uptake capability. Interestingly, the degree of severity of the P deficiency has no significant influence on K_{rs} . Changes in K_{rs} are not solely a consequence of architectural changes, but rather the result of a combination of altered root architectural traits under phosphorus deficiency and the corresponding adjustments in root functional properties that govern water uptake capacity. Especially soil P related changes in root radii and crown root length, due to faster elongation, (as shown by eq. 4-10 and eq. 4-11) influence the root's radial conductance, which significantly contributes to observed changes in K_{rs} . The reduction in axial root size alone causes a reduction in the radial conductance (as shown by eq. 4-5). In addition, shorter roots have a non-linear reduction in K_{rs} because the relation between root age, surface area and k_r and K_x is non-linear (Doussan et al., 1998, Meunier et al., 2017). The non-linear response of K_{rs} in plants with slower growing crown roots may be also attributed to the higher axial conductivity found in the proximal parts of crown roots compared to other root types. This, combined with the fact that crown roots are connected to the shoot's vascular system, enhances the propagation of xylem tension along crown roots, potentially providing benefits to faster growing crown roots than to slower growing ones (Ahmed et al., 2018).

A biological implication could be that plants under soil P limitation with lower K_{rs} decrease transpiration later than plants with high K_{rs} since they have lower water use and soil water would not be depleted so quickly, which is beneficial to mitigate potential drought stress. However, under sufficient water conditions, a high K_{rs} would be beneficial since the general capability of water uptake is higher. In rice, it has been demonstrated that at low soil P levels, the discrepancy in growth between well-watered and drought-stressed plants was insignificant compared to the difference observed in plants with sufficient soil P (De Bauw et al., 2020).

These are new insights, since studying K_{rs} experimentally on this high spatio-temporal scale is challenging, due to the complex architecture of root systems, their dynamic interactions with varying soil environments, and the technical difficulties associated with accurately measuring water flow through roots under different conditions (Heymans et al., 2020). With this approach, we also showed that computational modeling is overcoming these challenges and could be a tool for improving our understanding of the dynamic modulation of root water uptake mechanisms under soil P starvation since all other investigation methods only provide static information at a certain time point and of specific parts of the root system (Li et al., 2009, Mu et al., 2006, Shangguan et al., 2005, Yu et al., 2024).

Our results showed changes of the root system architecture under soil P limitations. Root volume increases linearly with soil P. We identified decreasing axial root radii and crown root elongation as key parameters for root systems and leaf elongation as the main shoot response to soil P limitation. We combined these

results into a functional-structural model to show that maximal potential water uptake capacity does not differ between plants with high and mild P deficiency plants but between fully P fertilized and P deficient plants. Both, root system anatomy and architecture are key to understanding root system function. Although root system architectural traits, such as volume, do increase linearly to soil P availability, the root system's capacity to take up water does not follow the same trend. That underscores that root system organization is critical for its function rather than mere total size. The main reasons for this phenomenon are the non-linear relationship of K_{rs} with root surface area, root length, and presumably volume (Baca Cabrera et al., 2024, Meunier et al., 2017), which is associated with the age dependence of k_r and k_x (Doussan et al., 1998).

To guarantee better generalizability, it would be important to validate whether these results are applicable in field conditions and across different maize varieties. Experimentally testing water uptake with two or more contrasting soil P concentrations would provide additional validation. Measuring or simulating actual transpiration and root water uptake would be another way to validate the findings on the influence of soil P limitation on water uptake capacity. Further research is required to investigate the effects on older plants. Furthermore, an evaluation of how the local intrinsic root hydraulic properties themselves might change under P deficiency and information on the internal P concentration within different plant organs under various soil P conditions would be a valuable addition to the results presented here. This study does not fully account for the complexity and heterogeneity of all soil conditions and cases of extreme P over- or under-supply in natural settings, which can significantly affect nutrient availability and plant growth. While the focus on P is critical, it is important to consider interactions with other nutrients and how they collectively impact plant growth and development. The impact of varying environmental conditions beyond controlled settings on P stress responses is not fully explored and it would be beneficial if further future studies include a range of genetic diversity within *Zea mays* to understand how different genotypes respond to P deficiency.

This is your last chance. After this, there is no turning back. [...] You stay in Wonderland and I show you how deep the rabbit hole goes.

MORPHEUS - MATRIX

« ◊ »

In the following chapter, we will finally connect the results presented in the previous chapters, place them in a broader context, and assess both the impact they have made and the potential influence they may have in the future.

Chapter 5

General Discussion

This chapter illustrates the contributions to the following studies:

Lena Lärm, **Felix Maximilian Bauer**, Jan van der Kruk, Jan Vanderborght, Shehan Morandage, Harry Vereecken, Andrea Schnepf, Anja Klotzsche (2024). Linking horizontal crosshole GPR variability with root image information for maize crops. *Vadose Zone Journal*, 23, e20293. <https://doi.org/10.1002/vzj2.20293>.

Thuy Huu Nguyen, Gina Lopez, Sabine J. Seidel, Lena Lärm, **Felix Maximilian Bauer**, Anja Klotzsche, Andrea Schnepf, Thomas Gaiser, Hubert Hüging, Frank Ewert (2024). Multi-year aboveground data of minirhizotron facilities in Selhausen. *Scientific Data* 11, 674. <https://doi.org/10.1038/s41597-024-03535-2>.

Thuy Huu Nguyen, Thomas Gaiser, Jan Vanderborght, Andrea Schnepf, **Felix Maximilian Bauer**, Anja Klotzsche, Lena Lärm, Hubert Hüging, Frank Ewert (2024). Responses of field-grown maize to different soil types, water regimes, and contrasting vapor pressure deficit. *Biogeoscience*. <https://doi.org/10.5194/egusphere-2023-2967>.

Peng Yu, Chunhui Li, Meng Li, Xiaoming He, Danning Wang, Hongjie Li, Caroline Marcon, Yu Li, Sergio Perez-Limón, Xinpeng Chen, Manuel Delgado-Baquerizo, Robert Koller, Ralf Metzner, Dagmar van Dusschoten, Daniel Pflugfelder, Ljudmilla Borisjuk, Iaroslav Plutenko, Audrey Mahon, Marcio F.R. Resende Jr., Silvio Salvi, Asegidew Akale, Mohammed Abdalla, Mutez Ali Ahmed, **Felix Maximilian Bauer**, Andrea Schnepf, Guillaume Lobet, Adrien Heymans, Kiran Suresh, Lukas Schreiber, Chloe M. McLaughlin, Chunjian Li, Manfred Mayer, Chris-Carolin Schön, Vivian Bernau, Nicolaus von Wirén, Ruairidh J. H. Sawers, Tianyu Wang, Frank Hochholdinger. Seedling root system adaptation to water availability during maize domestication and global expansion (2024). *Nature Genetics* 56, 1245–1256. <https://doi.org/10.1038/s41588-024-01761-3>.

Dirk Norbert Baker, **Felix Maximilian Bauer**, Mona Giraud, Andrea Schnepf, Jens Henrik Göbbert, Hanno Scharr, Ebba Pora Hvannberg, Morris Riedel (2024). A scalable pipeline to create synthetic datasets from functional–structural plant models for deep learning. *in silico Plants*, Volume 6, Issue 1, diad022. <https://doi.org/10.1093/insilicoplants/diad022>

Dirk Norbert Baker, **Felix Maximilian Bauer**, Andrea Schnepf, Hanno Scharr, Morris Riedel, Jens Henrik Göbbert, Ebba Pora Hvannberg (2024). Adapting agricultural virtual environments in game engines to improve HPC accessibility. *Communications in Computer and Information Science*. <https://doi.org/10.34734/FZJ-2024-03386>.

IN MY QUEST to unravel the complex interactions between maize and its environment, a new root phenotyping pipeline was developed, extensive datasets were gathered, and functional-structural plant models were developed and applied. As shown in Chapter 2 and 3, the advancements in automated minirhizotron image analysis and thereby generated belowground dataset provide us with a robust framework to further analyze and understand the dynamic responses of maize to changing conditions from greenhouse to field scale. Within this chapter, we will explore new possible technologies to monitor root presence in the field non-invasively, link aboveground data to our already presented belowground minirhizotron data, and provide an example of how to use both together to understand how field-grown maize responds to different soil types. Further, we investigate the possibilities of transferring our implemented phenotyping pipeline for data analysis and functional-structural plant model (FSPM) calibration and our model approach presented in Chapter 4 to other studies. Thereby, we explore the potential effects of domestication of *Zea mays* on root system architecture and model the functional implications of the adaptations. We will immerse ourselves in virtual worlds to tackle the bottleneck of data generation for neural network training with virtual data produced by a new approach. Finally, we shed light on the responses to P deficiency and the implications for future agriculture.

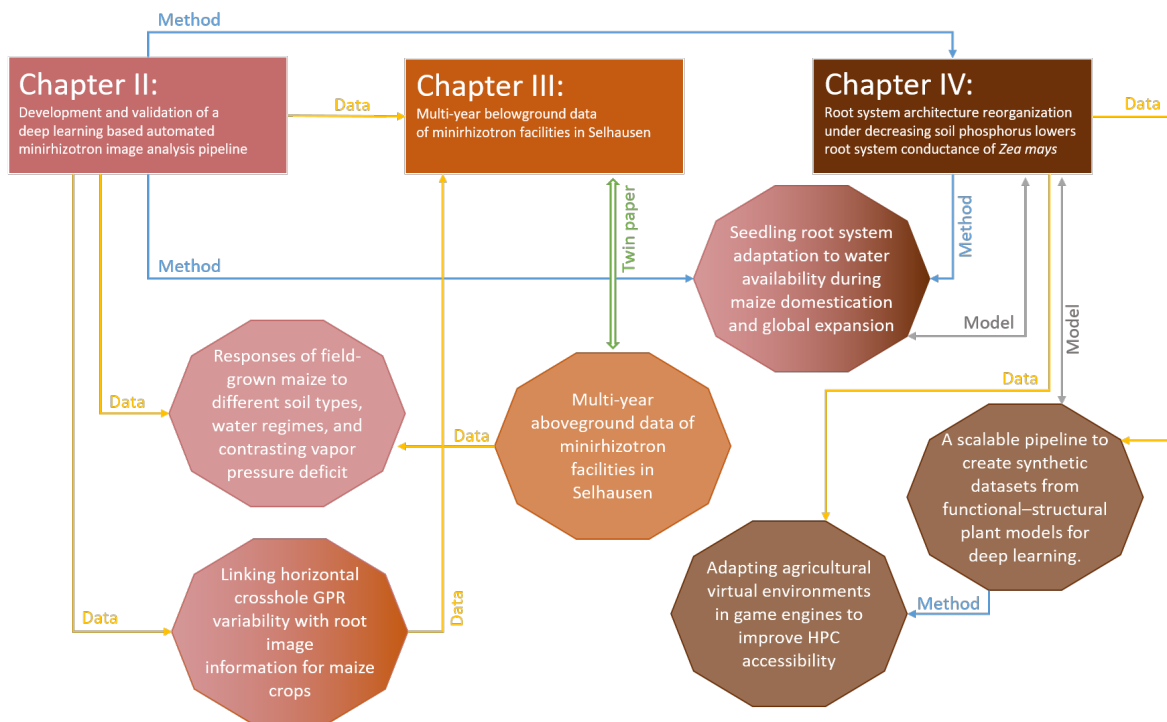


Figure 5-1: Connections between Chapters 2-4 and the studies presented in this chapter. The arrows show the connection, which is either driven by data exchange (yellow), methodological transfer (blue), or by the use of similar model approaches (grey).

The results of this work have contributed significantly to several studies by providing either methods, data, models, or a combination of these elements (as shown in Figure 5-1). This chapter illustrates the scientific use of the results of this work and sets it in the context of other studies. Extended information on all published studies to which this work has made significant contributions, as well as supplementary information relevant to this chapter, can be found in Appendix C.

5-1 Towards new standards and methods for *in situ* root phenotyping

The automated analysis pipeline illustrated in Chapter 2 is a suitable solution to easily and accurately analyze minirhizotron images in significantly less time by combining the automated segmentation tool RootPainter (Smith et al., 2022) with the automated feature extraction program RhizoVision Explorer (Seethepalli et al., 2021).

The highlight of this study, in addition to the development of the workflow presented, is the large-scale testing and validation. The pipeline was tested with more than 107,000 minirhizotron images, including more than 36,500 images for detailed comparison to manual annotation, obtained from two growing seasons and different soil types, depths, and cultures, resulting in an overall correlation of $r=0.9$. It was proved that the automated image analysis workflow is massively saving time, as the required time is reduced by more than 98 % in contrast to manual annotation while providing more root trait information. In conclusion, the automated pipeline outperforms manual annotation in terms of time requirements and information density while providing reliable data and feasibility for everyone. The presented and evaluated pipeline has already been the new standard method for reliable high-throughput root phenotyping of minirhizotron images, as highlighted by many studies individually (Balestrini et al., 2024, Banet et al., 2024, Berrigan et al., 2024, LaRue et al., 2022, Nair et al., 2023, Seethepalli et al., 2024, Smith et al., 2024, Solimani et al., 2023, Zhu et al., 2024). Weihs et al. (2024) states that the pipeline has removed the image analysis bottleneck to high-throughput phenotyping approaches by substantially reducing the processing time for minirhizotron imagery and outperforming traditional methods.

Generally, the development of neural network-based tools for root analysis has made significant progress in recent years, but the focus has often been on specific applications. RootNav 2.0 (Yasrab et al., 2019) and ChronoRoot (Gaggion et al., 2021) are also driven by a CNN but only suitable for young root systems on an artificial background. Other approaches using CNNs, such as SegRoot (Wang et al., 2019), faRia (Narisetti et al., 2021), and RootDetector (Peters et al., 2023), are often limited to the use of one or a few fixed pre-trained neural network models and, therefore, not easily usable for non-professionals or reach worse evaluation scores compared to the method presented here. Also, the majority of these tools do not permit direct annotation of training data without utilizing supplementary software. RootPainter (Smith et al., 2022), in contrast, offers the possibility of

creating individual models with interactive annotation. Although newer tools using CNNs for root segmentation and analysis are still being developed (Gillert et al., 2023, Huang et al., 2023), the hype towards CNN-based tools has started to decline. This might be because the current approaches, especially the here presented analysis pipeline, are already well-developed and tested. Currently, the focus shifts toward time-series analysis and other multi-dimensional data sources, such as MRI or CT, since automated data analysis is not far progressed for this kind of data (Selzner et al., 2023). RNNs (Recurrent Neural Networks) appear to be a promising approach to face this challenge since their architecture allows the input of temporal data (Weihs et al., 2024).

In the field of 2D minirhizotron image analysis, the method presented here represents the current gold standard. The presented models and datasets serve as benchmarks for other neural network-based root image analysis approaches (Banet et al., 2024, Khoroshevsky et al., 2024). Furthermore, our results were used to validate existing methods and justify using neural network-based tools in plant image analysis (Clark et al., 2024, Nair et al., 2023, Selzner et al., 2023, Smith et al., 2024, Zhu et al., 2024). Especially the way of using the Normalised RSME, as first shown in Bauer et al. (2022) (eq. 2-4), is now a standard in the root image analysis community to evaluate root data originating from neural network models (Banet et al., 2024, Khoroshevsky et al., 2024). Nevertheless, the pipeline's transferability to other application purposes, e.g., validating alternative root phenotyping methods, such as GPR (Ground Penetrating Radar), or applying it to whole connected root systems, remains to be explored (Bauer et al., 2022, Clark et al., 2024, Zhu et al., 2024).

Minirhizotron measurements are the method of choice for *in situ* root monitoring. However, it is not suitable for rapid, high-throughput screening or for use in precision agriculture. Finding additional ways, ideally with already existing methods, to complement our need for root measurement tools would be beneficial to increase spatial and temporal resolutions while minimizing measurement time.

GPR may help us to enhance the resolution and provide additional insights into the root system dynamics and their environmental responses. GPR is a geophysical method that uses electromagnetic wave propagation in the soil. From this, we can derive the relative dielectric permittivity (eq. 3-1) that can be directly linked to soil water content (SWC) with a high spatial resolution (Klotzsche et al., 2019). In the past, it has been shown that GPR can be used to detect coarse roots, such as tree roots applying a surface GPR (Guo et al., 2013). However, detecting finer root systems of important arable crops, such as *Zea mays*, using GPR is still challenging, and a ground-truth validation is required to approach this. The Selhausen minirhizotrons, presented in Chapters 2 and 3, are ideal experimental platforms to explore the capabilities to quantify root presence and development using GPR. Here, Klotzsche et al. (2019) already showed that the GPR signal and hence the SWC distribution, especially under dry soil conditions, is affected by maize root presence. However, it still remained elusive how the GPR-derived permittivity is linked to the presence of finer root systems.

The synthesis of camera and *in situ* horizontal crosshole GPR measurements between neighboring rhizotubes of minirhizotrons provides a comprehensive view into the plant-soil continuum, enabling the exact quantification of roots and linking them to GPR data. In Lärm et al. (2024), we aimed to non-invasively monitor the crops rooting zone by investigating the relationship between the root volume fraction and the GPR-derived permittivity in *Zea mays* crops in the corresponding measurement depths. To correlate the GPR data with the presence of roots, we applied the Chapter 2 presented analysis pipeline and used the resulting time-series data of root images for root volume fraction determination. We identified a clear, increasing trend during the vegetation period of the GPR data, correlating to a similar increase in root volume fraction during the same time period (Figure S3.1). We found that GPR-derived permittivity patterns show a consistent variability increase with higher root presence in soil, meaning that it can be used as a proxy for assessing root presence, which may improve data acquisition for agronomic studies and crop modeling and has future potential for using GPR for precision agriculture.

5-2 Combining multiyear above- and belowground data to investigate the soil-plant-atmosphere continuum comprehensively

The creation of the in Chapter 3 presented unique multi-year belowground data collection from the minirhizotron facilities in Selhausen would not have been feasible without the automated image analysis pipeline presented in Chapter 2.

The unique set-up of the Selhausen minirhizotron facilities, which are located close together in the same local climate but with different soil types, enables exceptional possibilities to measure the soil-plant continuum. The 7m-long horizontal tubes at several depths could be used for crosshole GPR and minirhizotron camera systems. Additionally, soil sensors (TDR, Tensiometer and MPS-2) provided observations at a high temporal and spatial resolution. The in Chapter 3 presented data cover five years of ongoing measurements of *Zea mays* and *Triticum aestivum* experiments, including validated root development data and dynamic and static soil moisture data, and the underlying soil permittivity values of drought stress and crop mixture trials. The open-access dataset was partly already used to develop, calibrate, and validate models of the soil-root continuum across different scales (Schnepf et al., 2022b) concerning different root zone components such as soil processes, including flow processes (Landl et al., 2021, Vereecken et al., 2016), root development (Schnepf et al., 2022a), biopore quantification (Landl et al., 2019), and different model compilations such as single-root system (Garré et al., 2012, Schnepf et al., 2022a) or multi-root system modeling (Morandage et al., 2019). Further application cases were soil water content and root water uptake modeling (Cai et al., 2017, 2018b). The data include relevant agronomic information for breeding water-efficient cultivars and for field management under various conditions, which is directly usable for agronomists. Evaluating the suit-

ability of GPR for root presence detection would not have been possible without this dataset (Lärm et al., 2024). This dataset provides a valuable opportunity to explore the significance of interannual variability in root growth patterns influenced by environmental factors such as soil moisture and temperature. We hope to increase our understanding of the complexity of root dynamics and their sensitivity to external conditions. We expect to enable holistic studies by gathering as much as possible of the environmental influences on crops.

However, this dataset is limited to the belowground part of the cropping zone. Therefore, only the root-soil continuum can be investigated fully with this information. To fully access the soil-plant-atmosphere continuum, above-ground crop and climate data are required. In Nguyen et al. (2024b) we present a comprehensive dataset from leaf to the canopy using several sensing techniques, including leaf chlorophyll, stomatal conductance and photosynthesis, canopy CO₂ exchange, sap flow, canopy temperature, and detailed plant growth traits, such as plant height, leaf area index, aboveground biomass, and yield measurements to complement the belowground dataset presented in this work (Figure S3.2). The aboveground data was collected under field conditions with different soil types, water treatments, and different wheat and maize varieties analog to the experimental set-up presented in Chapter 3. The final data collection also covers the same time period, location, and treatments. The data were made available for studying soil/water-plant relations and improving soil-plant-atmospheric continuum models, which are the backbone for the process understanding of crops and predictions for cropping systems. We made the data on the same platform and in the same standardized formats available (doi: <https://doi.org/10.34731/1a9s-ax66>).

Currently, the facilities in Selhausen stand as a unique and pioneering example, with only one comparable permanent set-up, the "RadiMax phenotyping facility" in Copenhagen, Denmark (Svane et al., 2019). However, due to the improved minirhizotron image data handling methods, new minirhizotron set-ups in new dimensions were recently constructed or are still under construction, such as the 3038 tube containing minirhizotron field at the University of Illinois at Urbana-Champaign (Champaign, IL, US) (Rajurkar et al., 2022), and the "HYDRAS" facilities at the ILVO (Merelbeke, Belgium) (Blanchy et al., 2024). These facilities, along with a few other smaller installations, use, in contrast to the Selhausen facilities, temporary and inclined installed minirhizotrons to address a range of agricultural research questions.

In the past, they were used to, e.g., evaluate key knowledge gaps regarding genetic and environmental effects on root system size and distribution in the field (Rajurkar et al., 2022), understand stress responses of root systems, such as temperature variations (Aidoo et al., 2018), water limitation (Cseresnyés et al., 2021), nutrient deficiency (Wacker et al., 2022), salinity (Shalhevet et al., 1995), investigate belowground carbon allocation and turnover (Chandrasoma et al., 2023), and identify genotypic cultivar differences (Svane et al., 2019). However, root senescence and decay have not yet been the focus of *in situ* root studies because the available analytical methods are not yet suitable for this purpose or only applicable to tiny selected datasets and not yet transferable (Gillert et al., 2023).

Another problem to overcome is the lack of data on senescencing and decaying roots. The data collection presented in Chapter 3 fills this gap since the below-ground dataset will include images and data of root senescence and decay as part of the ongoing data updates.

Although recent studies combined various soil, atmosphere, and plant measurements, such as soil CO₂ efflux, temperature, moisture content (Nair et al., 2023), waterlogging information (Qian et al., 2023), atmospheric and elevated CO₂ (Defrenne et al., 2021), photosynthetic active radiation, net photosynthesis rate, stomata conductance, stem water potential, and sap flow (Atta et al., 2022, Zhou et al., 2018) with minirhizotron root information, no study has ever published a dataset as comprehensive in measurement techniques, temporal- and spatial resolution, and experimental variety, as the one presented in this work. While minirhizotron images are published from time to time, such as in Xu et al. (2022), the scope and integration of the dataset in this study remain unparalleled. In conclusion, the combination of the above- and belowground dataset sets new standards while simultaneously emphasizing the importance of effectively using such detailed data to gain meaningful insights.

We made use of both here presented datasets (Chapter 3 and Nguyen et al. (2024b)) to investigate how *Zea mays* reacts to different soil types, water regimes, and contracting vapor pressure deficits (VPD). Precisely, we investigated the influences of the stony soil and the silty soil at the R_{UT} and R_{LT} minirhizotron facilities, different water regimes, namely irrigated and rainfed treatments on the root-to-shoot growth characteristics, and the hydraulic linkages between the soil and *Zea mays*. We used the data measured in the growing seasons of 2017 (low VPD) and 2018 (high VPD). In detail, we used the root growth data, analyzed with the method presented in Chapter 2, and soil moisture sensor data from the dataset in Chapter 3 and combined them with aboveground data from (Nguyen et al., 2024b). We found that the response of *Zea mays* to stress can be completely opposite depending on soil conditions. To cope with water deficit, *Zea mays* had a higher water uptake rate per unit root length and higher root segment conductance in the stony soil than in the silty soil, while at the same time, the crop reduced transpired water via reduced shoot size.

5-3 Data-to-model pipelines combine *in situ* and *in silico* approaches to gain new insights into plant growth and hydraulics

So far, we have mainly discussed data generation methods and plant behavior on the field scale. To fully understand the complex interactions between plants and their environment, we need to look at them in more detail in the context of critical environmental conditions, such as water and nutrient limitations. To understand plant reactions and the underlying mechanisms, we must look at the individual morphological characteristics of the plants and the genetic components that determine them. Exploring the complex architectural adaptations of the

root system and revealing the underlying functional and genetic drivers is crucial. Understanding the functional implications of the discovered plant responses is complex; however, it can be efficiently approached with modeling based on experimental data.

Recently, several studies have focused on plant reactions to environmental stresses, especially the root system responses to water or nutrient deficiency or changes in root system conductance (K_{rs}), as explained in detail in Chapter 4-1. Most of these studies are exclusively based on experimental observations, and FSPMs are rarely involved. Yet, these models can extend our research capabilities and provide insights into areas we cannot reach on an experimental scale alone. Almost all FSPMs have in common that they use an explicit simulated plant architecture. This requires parameterization with structural parameters. Obtaining these parameters is a complex task that requires precise phenotyping methods. By integrating the phenotyping method presented in Chapter 2 into a new workflow to extract single organ traits, we were able to create the first detailed structural whole plant model of *Zea mays* that includes all single organs, namely leaves, stem, primary root, seminal roots, crown roots and different types of lateral roots.

Building on such detailed FSPMs, it is possible to explore plant responses to environmental stresses. Among the group of FSPMs, functional-structural root models are particularly relevant for simulating responses to water or nutrient deficiency or changes in root system conductance. Well-known root models that are suitable to deal with these tasks and are still in use are SimRoot (Lynch et al., 1997) and its successor, OpenSimRoot (Postma et al., 2017), R-SWMS (Javaux et al., 2008), and SRI (Beudez et al., 2013). CPlantBox (Giraud et al., 2023, Schnepf et al., 2018, Zhou et al., 2020), the modeling framework used in this work, also provides these capabilities, with the additional option of coupling it with DuMu^x (Koch et al., 2021), which allows simulations of plant-rhizosphere-soil interactions. While SimRoot, OpenSimRoot, R-SWMS, and SRI only focus on the plant's root system, CPlantBox also offers the possibility of including shoot organs to simulate a complete 3D growing plant. As of today, CPlantBox is the only fully integrated model that simulates the dynamics of a variety of complete growing plants with a detailed description of each organ.

All named models are capable of modeling the root water uptake (Schnepf et al., 2023). Especially, R-SWMS was often applied in the context of water uptake simulations (Meunier et al., 2022), but was recently also used to predict pesticide uptake (Jorda et al., 2021). SimRoot was used in several cases to simulate ideotypes (Lynch, 2013), especially concerning nitrogen (N) (Saengwilai et al., 2021, 2014, Schneider et al., 2021) and phosphorus (P) uptake (Postma and Lynch, 2011) capabilities. Recent studies used OpenSimRoot to simulate the root system in order to provide insights into the dynamics of carbon partitioning (Punyasu et al., 2024), to identify beneficial root ideotype for low N conditions (Ajmera et al., 2022, Lynch et al., 2023, Schneider et al., 2021), and to understand how seminal root number (SRN), associated with domestication, improves N and P acquisition in maize seedlings (Perkins and Lynch, 2021). CPlantBox has been used to, e.g., investigate the P uptake strategies of *Oryza sativa* (De Bauw et al.,

2020), evaluate root development in stony soil (Morandage et al., 2021) and under mechanical and hydric stress at different soil compaction levels (de Moraes et al., 2019), discover how phloem anatomy restricts the root system architecture development (Zhou et al., 2023), model root elongation as a function of soil bulk density and matric potential (Seidel et al., 2022), simulate rhizodeposition patterns around growing and exuding root systems (Landl et al., 2021), model root water and nutrient uptake from dynamic soil (Mai et al., 2019), and as a benchmark for root water uptake modeling (Schnepf et al., 2023). CPlantBox was also used to calculate K_{rs} (Baca Cabrera et al., 2024, Selzner et al., 2023).

Generally, simulating K_{rs} with FSPMs is an emerging practice that is gaining increasing attention. In particular, *Zea mays* serves as a model plant for the development and validation of computational solutions for K_{rs} estimation. The initial straightforward methodologies were implemented a considerable period of time ago, as presented in the models of Doussan et al. (2006) and Javaux et al. (2008). Later, whole plant FSPMs, such as PlaNet, added the shoot hydraulic parameter by coarse approximations of leaf and stem conductance and taking the stomatal conductance as proxy for radial leaf conductivity (Lobet et al., 2014). Meunier et al. (2020) firstly developed a method to precisely estimate water flow in hydraulic architecture, based on a CPlantBox simulated root system architecture of maize (MAize Root System Hydraulic Architecture soLver (MARSHAL)). The same study also presents the first longer-term, time-dependent simulations of K_{rs} values for *Zea mays*, which have been compared to experimental values from the literature. However, all these studies use the simulated hydraulic parameters (k_r , K_x) of Doussan et al. (1998), which has, in contrast to the K_{rs} simulation presented in Chapter 4-3-2, several major drawbacks.

The spatial resolution of the Doussan et al. (1998) dataset is relatively coarse, with the values expressed in distance units relative to the root tips. Since no elongation rate is provided, the required conversion to time-dependent values has to be approximated. The most important difference to this work is that Doussan et al. (1998) provides k_r and K_x for two root types, namely axial roots and lateral roots. No separation between the hydraulic properties of primary, seminal roots, crown roots, and different types of lateral roots is made. It seems probable that simulations based on the parameters from Doussan et al. (1998) overestimate K_{rs} , particularly in seedlings and young plants. This is because primary and seminal roots contribute significantly to the total root system size at this stage of growth (Hochholdinger, 2009), and a mean value for axial roots, presumably heavily influenced by crown roots, is an inaccurate representation that produces biased results.

The in Chapter 4 presented maize FSPM is capable of estimating K_{rs} based on a comprehensive parameterized plant architecture and considers the hydraulic properties of primary, seminal roots, crown roots, long lateral roots, and short lateral roots individually. Compared to the studies mentioned above, this approach undoubtedly reduced the uncertainty and significantly increased information density for K_{rs} computation of *Zea mays*. Additionally, this work contributed a valuable and detailed dataset of architectural *Zea mays* parameters and a data-to-model

parameterization approach to obtain these data. However, a critical question that had to be assessed was whether this method could be successfully adapted to measurement setups that differ from those described in Chapter 4-2-1.

In Yu et al. (2024), we aimed to identify the genomic and geographical drivers for SRN formation. We, therefore, investigated the precise morphological influences and functional implications of the root system architecture of 218 representative traditional *Zea mays* cultivars on K_{rs} and standard uptake fraction (SUF). We did this with precise sub-organ phenotyping and functional-structural modeling. In a rhizobox set-up, we measured all varieties using the pipeline described in Chapter 4-2 to access root architectural and morphological traits. We found that SRN negatively correlates with primary root length and lateral root density along the primary root.

We then created one FSPM with CPlantBox for each cultivar, including statistical variation from several repetitions, for a 9-day-old seedling. Our simulation, which was performed in a simplified set-up used for the simulation procedure presented in Chapter 4-2-4 (Figure 5-2), showed that SRN affects seedling vigor by modulating K_{rs} . Since lateral roots mainly drive water uptake in young maize plants, we suggest that the reduction of SRN favors seedling establishment in water-limited conditions. Depending on our results, we concluded that variations in SRN may shape the size and branching of the entire root system, which in turn might determine the plant's water uptake capacity. By simulating the SUF, we could further demonstrate that lateral roots' relative contribution to total root water uptake decreases with increasing SRN. A soil-hydraulic modeling approach further showed that the point at which a small increase in transpiration provokes a large drop in leaf water potential at a given soil water potential (stress onset limit) occurred at a less negative leaf water potential in the traditional varieties with lower SRNs. This implies that plants with more seminal roots require higher flow rates at the same root length for water uptake and, therefore, a higher plant water potential to maintain transpiration than cultivars with a low SRN. Cultivars with low SRNs are, hence, more tolerant to drought conditions. With our simulations, we could provide evidence that root architecture changes, mainly driven by SRN variations, impact maize seedling's hydraulic properties.

The results of this study offer ground-breaking insights into root responses to changes in water availability and highlight the historical impact of domestication and adaptation on maize roots. Furthermore, this study underscores the potential of genetic advancement to assess climate resilience in future *Zea mays* generations and partly delivers the required knowledge to realize new breeding targets. Finally, the successful transfer of the method and model approach used in Chapter 4 to another research domain and application case proved that the results presented in this work are of significant importance and can help to address pressing issues in plant research, but also beyond.

The in this study presented comprehensive dataset of *Zea mays* architectural parameters was of significant interest to other studies in related fields, such as computer vision for plant phenotyping. As stated in Chapter 2, deep learning has expanded our ability to analyze new data and investigate structural plant

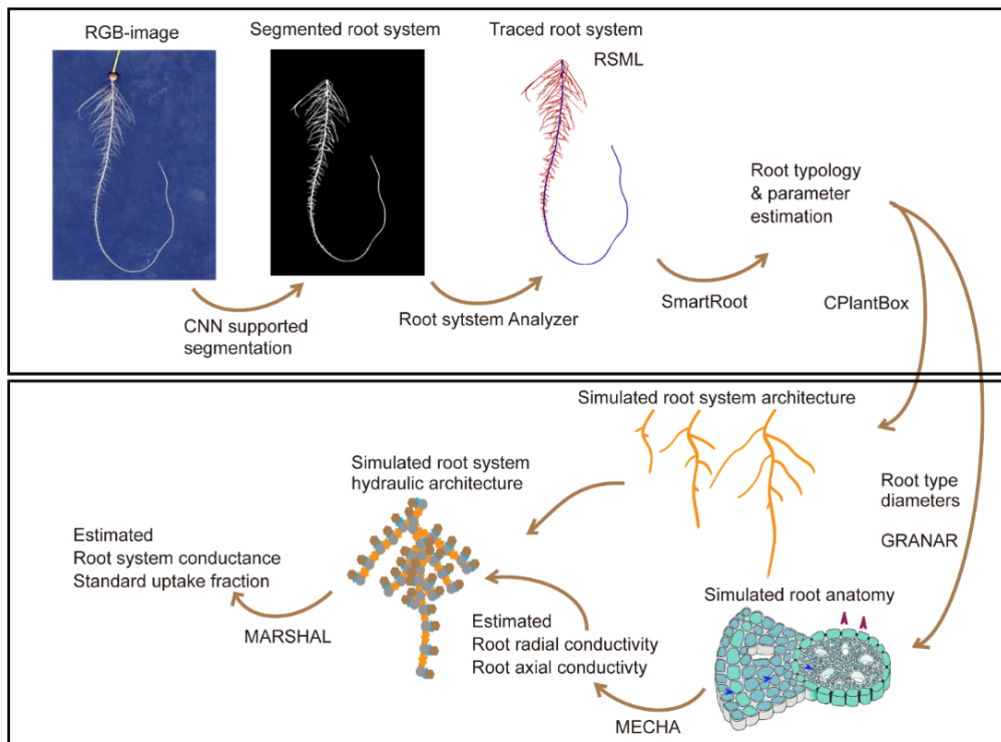


Figure 5-2: A multi-step structural-functional modeling pipeline to estimate K_{rs} and SUF. Each root system was traced with Root System Analyzer. An RSML file was exported from RSA and migrated to SmartRoot to manually label seminal roots. The parameter set was used to generate five realizations of virtual root systems with the stochastic CPlantBox model. The anatomical traits were referred to in the published articles and created with the GRANAR model. The radial hydraulic conductivity and axial hydraulic conductance (k_r and K_x) of these root anatomies were estimated using the MECHA model. From the CPlantBox root system architectures and their respective root hydraulic conductance, K_{rs} and SUF were determined with the model MARSHAL for each virtual root system (figure adapted from Yu et al. (2024)).

responses beyond the limits of our already implemented mechanistic approaches. Image analysis, in particular, has been significantly improved by this technique, and the quantity and quality of structural plant parameters obtained in a much shorter time is an enormous gain (Pound et al., 2017). The current bottleneck of deep neural networks is the amount of data required to train them (Bauer et al., 2022). In Baker et al. (2023), we followed a new approach to overcome this bottleneck. We built a coupling of an FSPM and a game engine to tackle the bottleneck of data generation for neural network training by producing virtual training data. Our newly developed method integrates a CPlantBox realized plant structure with a newly implemented shoot geometry into the game graphic engine "UnrealEngine" to generate synthetic images, including FSPM-provided ground-truth data, that can be directly used for user-defined neural network training.

To evaluate the reliability and precision of this method, we created a synthetic copy of the greenhouse set-up that was used in Chapter 4-2-1 and compared the results with the measured parameters. We aimed to measure the performance on an HPC cluster with a virtual drone flight, producing synthetic drone images of a virtual maize field based on the FSPM parameterization presented in Chapter 4-3-1. In a follow-up study (Baker et al., 2024a), we could furthermore implement the pipeline so that HPC resource use efficiency was accelerated, which helps with the development of more accurate and robust deep learning models. Most importantly, we presented the potential for large-scale use cases to benefit from these techniques. Generally, we found that our method is a promising and practical way to generate synthetic plant data for neural network training. The results of Baker et al. (2024a, 2023) demonstrated that the in this work presented models can be transferred to entirely new research areas beyond the realms of plant science.

In summary, this work provides a versatile method for obtaining plant parameters to parameterize a whole-plant FSPM framework, such as CPlantBox, and a comprehensive *Zea mays* dataset of plants with and without P limitation. The resulting method and data have been demonstrated to be transferable for different applications across different scales and scientific domains and have made a significant impact by contributing to several publications.

5-4 *Zea mays* responses to environmental conditions: The case of phosphorus

The role of P fertilization in agricultural systems is often neglected in regions of the world with highly industrialized agriculture, such as the EU, North America, or China, where soils typically contain abundant P reserves and P fertilizer is not (yet) a significant cost issue. Through a long history of excessive P fertilization, the anthropogenic release of reactive forms of P to land and oceans exceeded and still exceeds the safe operating range of our planet (Richardson et al., 2023). However, P is a resource derived from finite reserves. Some studies anticipate that global rock P will be available to meet the growing demand into the 22nd century (Helin and Weikard, 2019, Koppelaar and Weikard, 2013), while others predicted that all P resources should have been already depleted today (Reidinger, 1976). Whatever the exact time frame for P resources to end may be, the reality is that global P reserves are finite, and the depletion of accessible P sources is becoming an increasingly pressing concern. Although the depletion of P resources may not be the most acute issue, P production capacity from mining will decline in 10-20 years as production efficiency is reduced by increasing mining costs (Reijnders, 2014). Therefore, it can be reasonably deduced that the availability of P will inevitably decline soon.

For these ecological and economic reasons, we aim to reduce the P inputs into (agro-)ecosystems. Official fertilization recommendations from governmental and global institutions advise reducing the quantity of P fertilizer applied in agriculture (FAO, 2015, UN, 2023). For example, Germany has lowered the official

reference values for plant-available P in soil by about 30 % (Wiesler et al., 2018). Although, as a consequence, the use of P fertilizers has been reduced by 11 % worldwide in recent years and by as much as 54 % in Germany over the same period, it is interesting to note that crop yields are still increasing worldwide. Also, countries with a high degree of agricultural industrialization have not experienced any systematic loss of production (FAOSTAT, 2024a). This poses a central question: Is P scarcity a fundamental problem at all?

The short answer is: Probably yes! The long answer is complex and the results of this work will provide neither a comprehensive nor a fully satisfactory response to this question. However, it will shed light on some plant responses to reduced soil P availability that have remained obscure until now and help us to assess the consequences of reduced P availability for one of the most important and P sensible crops: *Zea mays*.

Reducing P fertilization has not been a major issue in industrialized regions because a long history of fertilization has enriched the P reserves in arable soils, and P is continuously supplied from these deposits for a number of years. To further understand why reducing P fertilization was an easy step for the farming industry to take without much thought, we first need to look at how P deficiency symptoms are assessed in the field. Since the harvest organs of the most relevant crops are located aboveground, the focus in the search for potential malnutrition symptoms lies on these parts of the plant. In maize, P deficiency is diagnosed by a rigid appearance of shoots, mainly characterized by reduced leaf area (Marschner, 2011). In severe cases of P deficiency, a reddish leaf discoloration is also visible. In this work (Chapter 4-3-1), we could show that in cases of reduced P in soil (4.6 mg P 100 g⁻¹ soil), the leaf area is maintained, and only in heavier cases of P deficiency (< 3.3 mg P 100 g⁻¹ soil) the leaf area started to reduce. While relevant changes in shoot growth were only observable in really low soil P conditions, the root system responded already to a milder P deficiency. The main responses were linearly decreasing axial root radius and initial elongation rates of crown roots with decreasing soil P, leading to a linear decrease in total root volume (Figure S2.3). While a reduction in root volume at reduced soil P levels is a known structural response of *Zea mays*, the specific morphological parameters driving this response were less well known. Sun et al. (2018) hypothesized that an increased amount of crown root might also be an adaptive response. However, since crown root emergence is staggered, the strong effects of this response would only become significant later in crop development and not in the early development stages (Lynch et al., 2005).

We gained groundbreaking insights by shifting the focus to root functionality. Interestingly, the K_{rs} responded non-linear to decreasing soil P and only the maize plants with an optimal soil P level maintained high K_{rs} , while in soil with any lower P level than optimal, K_{rs} decreased dramatically (>25 %). The K_{rs} values of plants exhibiting any degrees of soil P reduction are not statistically distinguishable from one another, which emphasizes a critical change in the functionality of the root system at any degree of P reduction in the soil (Figure 4-5). More precisely, any level of P deficiency reduces the plant's capacity to take up water.

In conclusion, while there are no notable alterations in shoot development when soil P is moderately depleted, the water uptake functionality of the root system is modified significantly (for a detailed explanation of the process, see Chapter 4-4-2). These results explain the generally accepted practice that soil P can be moderately reduced without losses since the harvested organ has no visible changes. However, this raises the question of when the root system's reduced water uptake capacity has a relevant impact on maize cultivation.

Plants under soil P limitation, with lower K_{rs} , decrease transpiration later than plants with high K_{rs} since a lower plant water potential is required to maintain water uptake (Ahmed et al., 2018, Yu et al., 2024). For the plant, this means that on the one hand, plants under P deficiency could potentially mitigate drought with a water-saving strategy because they have a higher drought stress resilience in beginning or mild drought conditions since a lower plant water potential is required to maintain uptake and the remaining soil water is depleted slower. On the other hand, higher K_{rs} could enhance drought recovery following severe drought conditions and would be generally beneficial under sufficient water conditions since the general capability of water uptake is higher.

Due to climate change, water availability decreases in most regions in the world (Gosling and Arnell, 2013). In the last years, less water is available in agricultural soils (Dorigo et al., 2017, Gruber et al., 2019). However, the reduction in water availability is predominantly observed during the pre-growing season and the initial growth stages of maize, while increasingly heavy precipitation events in the summertime have the effect of increasing water availability in the subsequent growth stages (Vargas Zeppetello et al., 2024). This accounts especially for the regions where maize is cultivated intensively (Proctor et al., 2022). It could be postulated that the effects of reduced water availability during the early growth stages were not prominent due to the simultaneous reduction in P input, as the root system's adaptation in K_{rs} to limited P availability may favor mitigation of the consequences of moderate drought conditions.

If applied to *Zea mays* growing strategies, this would mean that a reduced P intake might even be beneficial if mild drought conditions are present at the beginning of the growing season, as long as no severe P or water limitation is taking place. However, if it comes to maximizing yield and water is not limiting, a reduced soil P availability will lead to malnutrition symptoms and ultimately reduce yield. This is of particular concern in regions already facing water scarcity and in parts of the world where climate change is expected to intensify drought conditions.

In a world where soil P and water availability are becoming increasingly scarce, the stakes are high. We still need to learn more about the responses of maize and other crops to environmental stressors and their combined effects on plant development. Testing the hypothesis that a reduction in P input and the resulting root system's adaptation in K_{rs} may favor mitigation of the consequences of drought conditions in early growth state is only one of the topics we need to address towards sustainable agriculture and resource conservation. We must develop and refine models that accurately simulate root system responses to P deficiency, ideally based on mechanical processes. These models would be of major value

in predicting crop performance under limited nutrient conditions and may help to guide the development of P efficient cultivars and optimize fertilizer use. Due to soil reserves, a further reduction in P fertilization may be applicable in some regions for a few decades. Still, it is not a long-term solution, as this will result in the depletion of soil deposits and, consequently, in a global P scarcity. Since it is unlikely that plants will be able to grow effectively with minimal or no P intake, agriculture must consider alternative solutions to P depletion. Looking ahead, possible ways could be investigating the potential for P recycling from waste streams, developing crops that can utilize P more efficiently, or even engineering plants that can access P from currently unavailable sources in the soil.

Change is the end result of all true learning.

LEO BUSCAGLIA

<< ◊ >>

In the final chapter, we will tie it all together by summarizing the main findings, acknowledging the limitations and pointing to future directions.

Conclusions and Outlook

6-1 Conclusions

THE MAIN OBJECTIVES of this work were: 1.) to develop, implement and validate a new belowground phenotyping pipeline to increase our ability to non-invasively collect and analyze *in situ* root development information over time; 2.) to collect, archive and distribute a unique and comprehensive belowground dataset including important agronomic information over a longer time period for a wide range of scientific domains and applications; 3.) investigate the architectural responses to phosphorus (P) deficiency in *Zea mays* by; 4.) combining phenotyping and FSPMs to understand the consequences for water uptake capacity, giving important new insights in responses to environmental stresses; and 5.) transfer the phenotyping and modeling methods previously introduced to collaborators to jointly investigate the response of *Zea mays* to changing environmental conditions and to develop and test new *in situ* and *in silico* methods and to evaluate the transferability of the methods developed in this work. The common goal of these five main objectives, addressed in Chapters 2-5, is to explore plant responses to changing environmental conditions by integrating phenotyping and modeling across different scales.

Chapter 2 proposes a new approach to analyzing large amounts of 2D root image data. The automated analysis pipeline presented is a suitable solution to easily and accurately analyze minirhizotron images in significantly less time. The highlight of this study, in addition to the development of the workflow presented, is the large-scale testing and validation. The automated pipeline outperforms manual annotation in terms of time requirements and information density while providing reliable data and feasibility for everyone. Recent studies independently stated that the pipeline significantly contributed to removing the image analysis bottleneck to high-throughput phenotyping approaches by creating a new standard method.

The data analyzed with the pipeline presented in Chapter 2 provided the backbone for the dataset presented in Chapter 3, which features what may be the first comprehensive multi-year collection of root and soil data obtained in minirhizotron facilities. The dataset combines validated root development data and dynamic and static soil moisture data, including the underlying soil permittivity values of drought stress and crop mixture trials. All processed data is made open access available. The dataset can be used to, e.g., develop, calibrate, and validate models of the soil–plant continuum across different scales concerning different root zone components such as soil processes, including flow processes, root development, biopore quantification, or different model compilations such as single-plant or multi-plant modeling. Further potential application cases are soil water content and root water uptake modeling. The data include relevant agronomic information for breeding water-efficient cultivars, field management under various conditions, and training and benchmarking root analysis methods.

In Chapter 4, the scope and scale changed to elucidate the stress responses of individual *Zea mays* plants to P deficiency. By integrating the phenotyping method presented in Chapter 2 into a new workflow to extract single organ traits, we identified changes in the root system and shoot architecture under soil P limitation. Decreasing axial root radii and crown root elongation were identified as key parameters for the root system, and leaf elongation was the main shoot response to P deficiency. These data were successfully combined with precise root system hydraulic properties of the same *Zea mays* cultivar to enable dynamic plant growth simulations of root system conductance (K_{rs}). The modeling approach revealed that maximal potential water uptake capacity does not differ between plants with high and mild P deficiency plants but between fully P fertilized and P deficient plants. This provided new insights into the possible effects of combined water and P stresses. We postulate that under soil P limitation, plants with low K_{rs} would reduce transpiration later than plants with high K_{rs} because a lower plant water potential is required to maintain water uptake. As a result, soil water would not be depleted as quickly, which could be beneficial under drought conditions. However, a high K_{rs} would be beneficial under sufficient water conditions as the overall water uptake capacity is higher. Although root system architectural traits, such as volume, increase linearly to soil P availability, the root system's capacity to take up water, represented by the K_{rs} , does not follow the same trend. That underscores that root system organization is critical for its function rather than mere total size.

Finally, this work evaluates the transferability and usefulness of the methods, data, and models presented here by applying them in collaborative studies and placing them in the context of the current state of the art. By using the root data generated by the automated minirhizotron image analysis pipeline, we could evaluate GPR as a potential root phenotyping tool and explore the responses of *Zea mays* to different soil types, water availability, and contrasting vapor pressure deficits. In addition, the up-scaling of the parameterization and modeling workflow presented in Chapter 4 was used for a comprehensive screening of traditional maize varieties, ultimately leading to the identification of seminal roots number as the root system trait driving local adaptation in *Zea mays* domestication. Fi-

nally, we explored further possibilities to overcome the data bottleneck in neural network training for plant organ detection by combining a game engine, High Performance Computing, and the *Zea mays* model created in this work to virtually reproduce the greenhouse setup presented in Chapter 4 to generate virtual plant data with corresponding ground-truth.

The compilation of the different parts of this doctoral project has shown comprehensive and timely insight into phenotyping and functional-structural plant modeling applied to monitor and predict the responses of plants to changing environmental conditions across different scales.

6-2 Outlook

Building on the observations and conclusions, the following section should provide suggestions for further research.

Further improvements required for automated root image analysis

Although the pipeline to analyze minirhizotron images automatically is working fast, accurately, and mostly objectively with a high correlation to manual measurements, there are still occasional but systematic irregularities in the match of manual annotation and the results of the automated analysis pipeline. However, these mismatches can be explained by rarely occurring missed segmentation of root fragments by the automated analysis pipeline due to soil-covered roots. When this is considered, the systematic underestimation of the automated method is easy to correct. As in all neural networked-based analysis methods, balanced training datasets and consequent annotation of the training data are the keys to sufficient results. Although the time series analysis in the form of either root length density depth profiles at different time points or root arrival curves is supported in the workflow, individual roots and their phenology are not followed from birth to death. Implementing a function to track root senescence and decay into the existing method would be of high interest to researchers. Generally, it would be significant progress to add a single root tracking possibility, including root order and status. The implementation of these functions would improve the pipeline and enhance use cases.

Closing missing data gaps

The belowground dataset presented in this work is already very comprehensive. However, several scenarios are (yet) not covered, and it would be beneficial information in the future. Monitoring root senescence and decay would be especially interesting for future studies. Furthermore, increasing spatial and temporal measurement resolution would be helpful in covering more detailed insights into the plant soil continuum. Currently, the dataset only includes abiotic influences on crop development; however, adding biotic factors, such as microbial data, would

be a huge benefit. Additional GPR measurements, not only covering the planar spatio-temporal soil water content but also making measurements at different depths, would dramatically increase the soil water information density.

Up-scaling in modeling and validating hydraulic plant response to phosphorus deficiency across scales

Although the results shown in Chapter 4 provide valuable information on the interaction of P deficiency and K_{rs} at the level of the individual plant, it would be important to investigate the extent to which these effects are noticeable under field conditions. Furthermore, it would be important to test the robustness of the observed effects on cultivar variations. Further research is required to investigate the impact on older plants. An evaluation of how the local intrinsic root hydraulic properties themselves might change under P deficiency and information on the internal P concentration within different plant organs under various P soil conditions should be addressed in further studies. As in most modeling studies, this study does not fully account for the immense complexity and heterogeneity of all environmental conditions, such as soil conditions and cases of extreme P over- or under-supply in natural settings. Furthermore, it is important to consider interactions with other nutrients and how they collectively impact plant growth and development. Generally, we require extended knowledge of the impact of varying environmental conditions and combined stresses beyond controlled settings.

Appendix A: Supplementary Materials to Chapter 2

Supplementary Materials

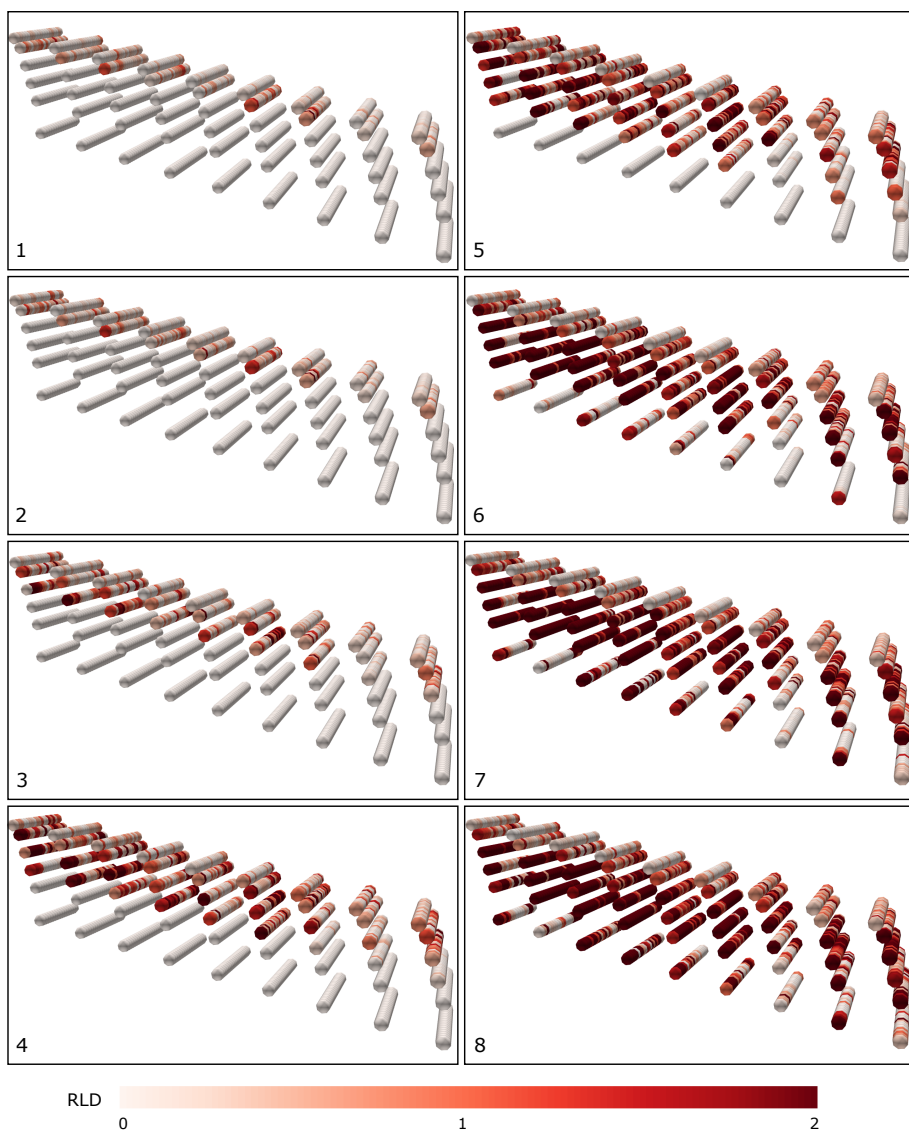


Figure S1.1: 3D spatio-temporal distribution of RLD measured in all tubes at one minirhizotron. Distances between tubes are not to scale. 1-8 represents the time steps.

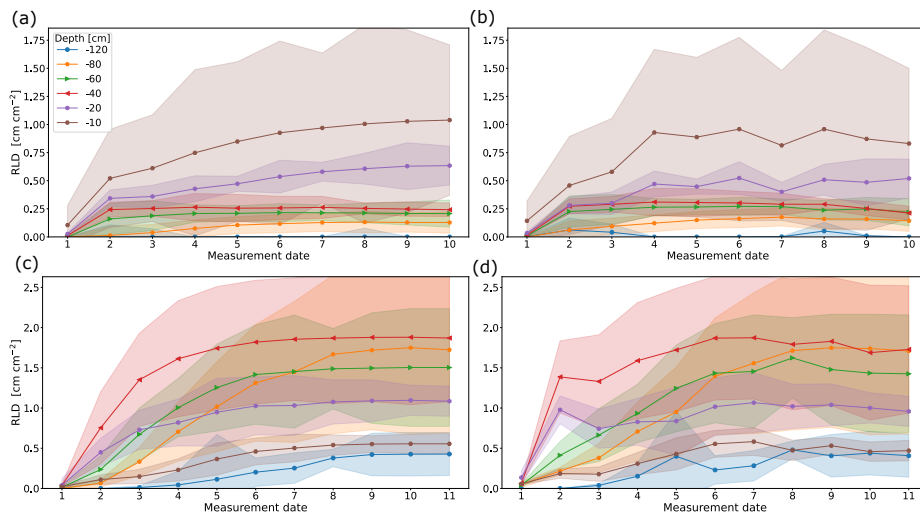


Figure S1.2: Comparison of root arrival curves of the data obtained from images originating from two minirhizotrons in the growing season 2017. The images were analyzed by hand (left: manual) and by the automated analysis pipeline (right: automated). 2017: a) R_{UT} manual, b) R_{UT} automated, c) R_{LT} manual, d) R_{LT} automated.

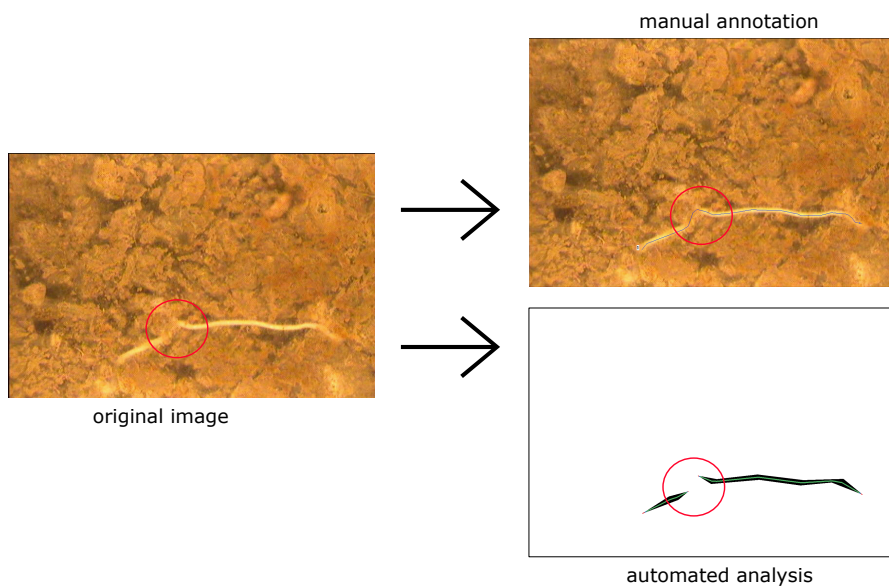


Figure S1.3: Manual vs. automated analysis. The automated analysis misses a small part of the root and underestimates the total root length slightly.

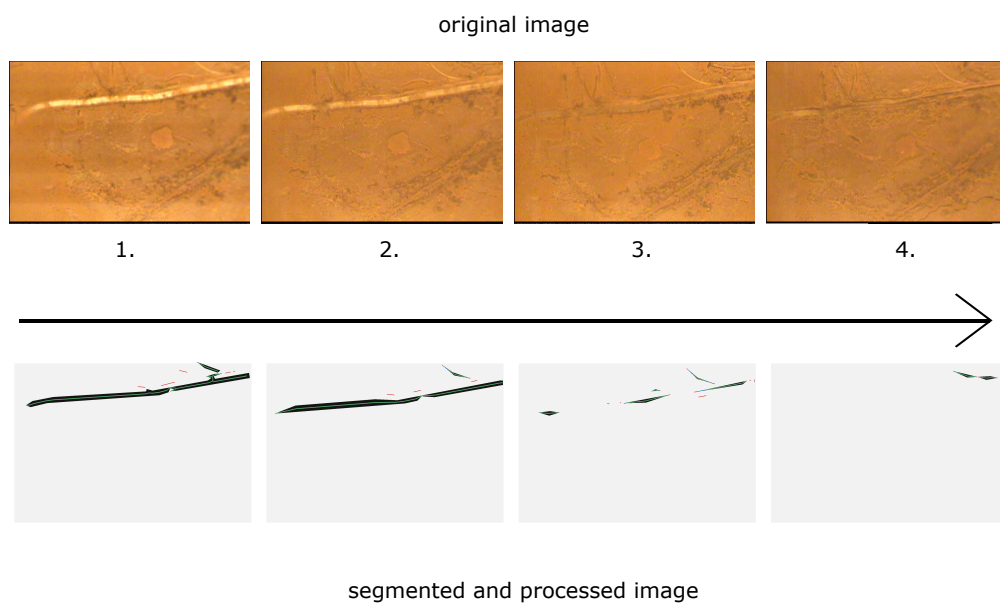


Figure S1.4: Root senescence visible from early to late measurement dates in the growing season 2015/16 and the corresponding segmentation and skeletonization.

Table S1.1: Detailed overview of the images taken at the growing season 2015/16 and 2017

measurement no.	2015/16			2017	
	facility	date	images	date	images
1	R _{UT}	16/11/15	720	08/06/17	480
	R _{LT}	16/11/15	720	08/06/17	584
2	R _{UT}	26/11/15	1,080	29/06/17	1,800
	R _{LT}	26/11/15	1,079	22/06/17	1,800
3	R _{UT}	17/12/15	1,800	06/07/17	1,800
	R _{LT}	17/12/15	1,439	29/06/17	2,160
4	R _{UT}	02/02/16	1,520	13/07/17	1,800
	R _{LT}	21/01/16	1,800	06/07/17	2,160
5	R _{UT}	12/02/16	1,800	20/07/17	1,800
	R _{LT}	12/02/16	1,800	13/07/17	2,160
6	R _{UT}	26/02/16	1,800	27/07/17	1,200
	R _{LT}	26/02/16	2,160	20/07/13	2,160
7	R _{UT}	14/03/16	1,800	02/08/17	1,840
	R _{LT}	14/03/16	2,160	27/07/17	1,430
8	R _{UT}	26/03/16	1,840	10/08/17	1,959
	R _{LT}	24/03/16	2,160	02/08/17	2,159
9	R _{UT}	07/04/16	2,160	23/08/17	2,120
	R _{LT}	07/04/16	2,160	10/08/17	2,160
10	R _{UT}	13/04/16	2,160	12/09/17	1,800
	R _{LT}	13/04/16	2,160	24/08/17	2,159
11	R _{UT}	29/04/16	2,160	-	-
	R _{LT}	29/04/16	2,160	12/09/17	2,150
12	R _{UT}	06/05/16	2,160	-	-
	R _{LT}	06/05/16	2,160	-	-
13	R _{UT}	13/05/16	2,160	-	-
	R _{LT}	13/05/16	2,160	-	-
14	R _{UT}	20/05/16	2,160	-	-
	R _{LT}	20/05/16	2,160	-	-
15	R _{UT}	27/05/16	2,160	-	-
	R _{LT}	27/05/16	2,159	-	-
16	R _{UT}	03/06/16	2,160	-	-
	R _{LT}	03/06/16	2,159	-	-
17	R _{UT}	09/06/16	2,160	-	-
	R _{LT}	09/06/16	2,160	-	-
18	R _{UT}	16/06/16	2,155	-	-
	R _{LT}	16/06/16	2,160	-	-
19	R _{UT}	23/06/16	2,149	-	-
	R _{LT}	23/06/16	2,156	-	-

Table S1.2: Comparison of the automated analysis pipeline and the manual annotation of the total root length obtained in the growing season 2017 with a linear regression. The confidence interval (95%) of the regression coefficient (ordinary least products) are listed in parenthesis. The bias is fixed if the 95% CI of the intercept do not include 0 and the bias is proportional if the 95% CI of the slope do not include 1.

measurement no.	facility	Intercept (95% CI)	Slope (95% CI)	Bias	
				Fixed	Proportional
1	R _{UT}	0.26 (0.08, 0.45)	0.73 (0.71, 0.74)	yes	yes
	R _{LT}	1.09 (0.83, 1.36)	0.7 (0.65, 0.75)	yes	yes
2	R _{UT}	2.8 (2.16, 3.44)	0.81 (0.78, 0.84)	yes	yes
	R _{LT}	3.5 (2.78, 4.23)	0.92 (0.89, 0.94)	yes	yes
3	R _{UT}	3.07 (2.46, 3.69)	0.8 (0.78, 0.83)	yes	yes
	R _{LT}	3.12 (2.45, 3.79)	0.88 (0.86, 0.89)	yes	yes
4	R _{UT}	2.99 (2.28, 3.7)	0.99 (0.97, 1.02)	yes	no
	R _{LT}	4.53 (3.63, 5.43)	0.86 (0.85, 0.88)	yes	yes
5	R _{UT}	2.35 (1.72, 2.97)	0.93 (0.91, 0.95)	yes	yes
	R _{LT}	6.68 (5.65, 8.07)	0.83 (0.81, 0.85)	yes	yes
6	R _{UT}	2.43 (1.75, 3.11)	0.93 (0.91, 0.95)	yes	yes
	R _{LT}	8.99 (7.51, 10.48)	0.82 (0.8, 0.84)	yes	yes
7	R _{UT}	1.55 (0.86, 2.24)	0.81 (0.79, 0.83)	yes	yes
	R _{LT}	4.99 (3.95, 6.03)	0.93 (0.91, 0.94)	yes	yes
8	R _{UT}	2.37 (1.61, 3.12)	0.85 (0.83, 0.88)	yes	yes
	R _{LT}	5.71 (4.38, 7.05)	0.89 (0.87, 0.91)	yes	yes
9	R _{UT}	1.18 (0.57, 1.79)	0.82 (0.81, 0.84)	yes	yes
	R _{LT}	3.0 (1.95, 4.05)	0.92 (0.9, 0.93)	yes	yes
10	R _{UT}	2.31 (1.65, 2.98)	0.72 (0.7, 0.74)	yes	yes
	R _{LT}	3.35 (2.2, 4.5)	0.87 (0.85, 0.88)	yes	yes
11	R _{UT}	-	-	-	-
	R _{LT}	3.61 (2.47, 4.75)	0.86 (0.84, 0.87)	yes	yes

Data Availability

- The supplementary data that support the findings of this study and help to operate the in this work introduced root image analysis pipeline, including an example, are open available. Furthermore, data and scripts to reproduce the RLD-profiles (Fig. 2-4) and RAC-curves (Fig. S1.2) are open to access with the same identifier: <https://doi.org/10.34731/pbn7-8g89>.
- RootPainter (Smith et al., 2022) is available at: <https://github.com/Abe404/rootPainter>
- RhizoVision Explorer (Seethepalli et al., 2021) is available at: <https://zenodo.org/record/4095629> and <https://github.com/rootphenomicslab/RhizoVisionExplorer>

Appendix B: Supplementary Materials to Chapter 4

Supplementary Materials

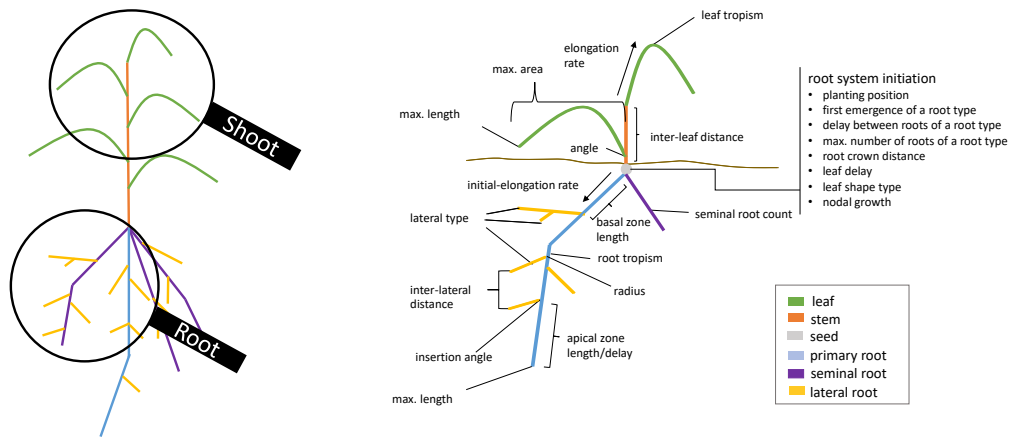


Figure S2.1: Schematic overview of the different organ parameters required for root and shoot calibration with CPlantBox.

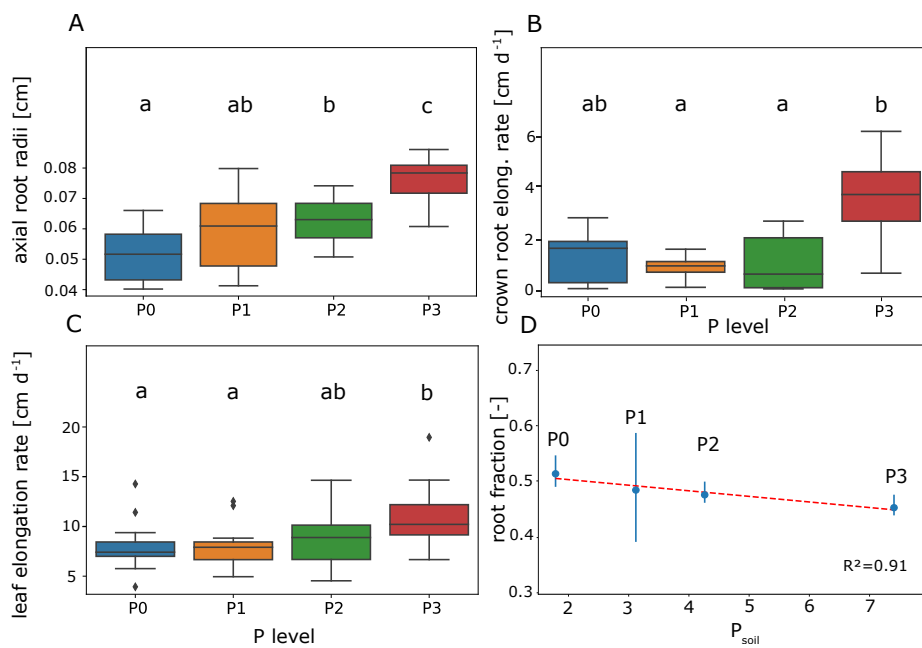


Figure S2.2: A: Axial root radii, B: Initial crown root elongation rate, C: Initial elongation rate of the leaves. D: Root fraction for different soil P availability levels ($p < 0.05$)

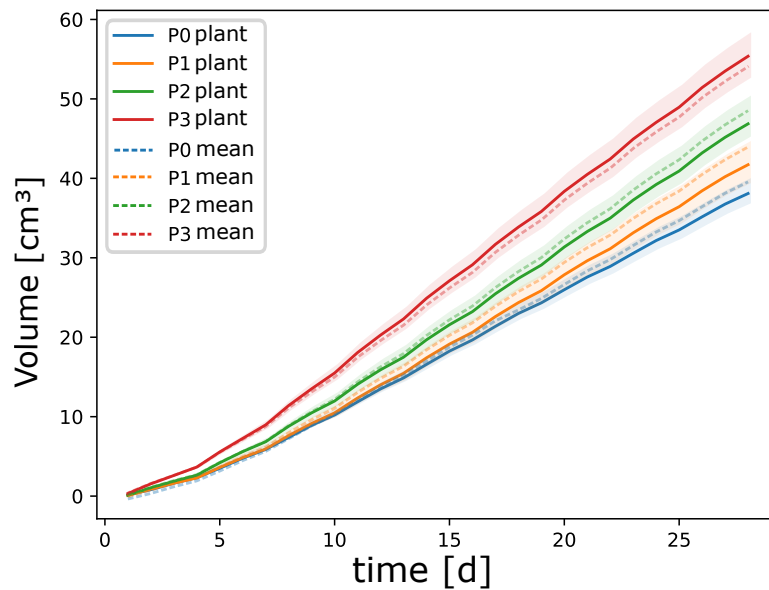


Figure S2.3: Total volume [cm^3] of simulated root systems with all parameters as measured and with all parameters set as mean and only identified response parameters, elongation of crown roots and axial root radii, set as function of P level in soil.

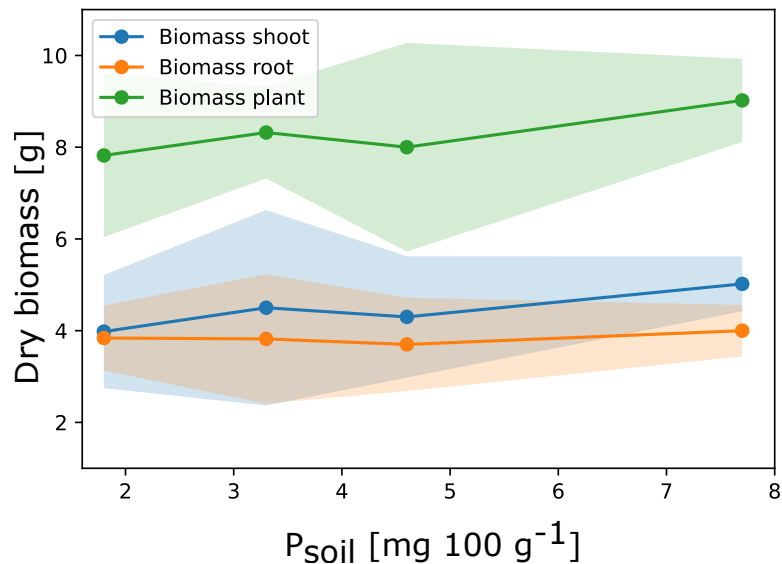


Figure S2.4: Biomass (dry mass) [g] of shoot, root and whole plant depending on soil P level.

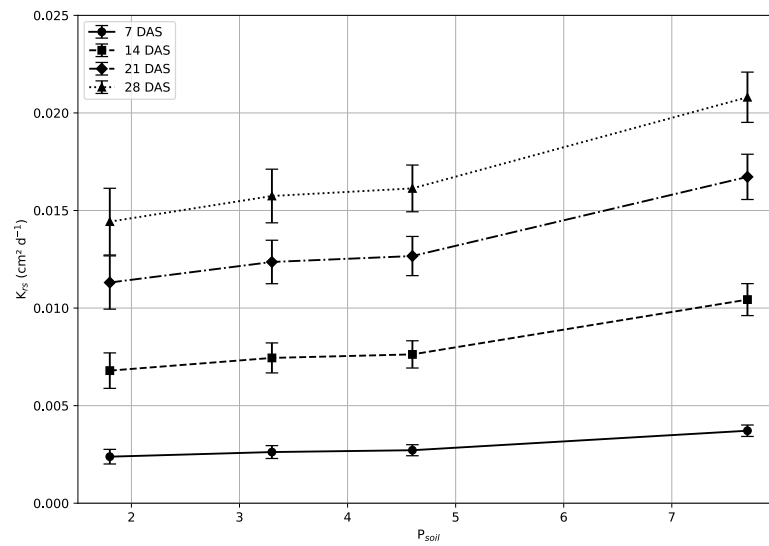


Figure S2.5: K_{rs} for 7, 14, 21 and 28 DAS depending on soil P concentration, depending on the mean of 100 simulations. The error-bars display the standard deviation.

Table S2.1: Overview of the hydraulic properties (k_r and K_x) used to compute dynamic root system conductance, based on the simulated root system architecture.

Primary			Seminal roots			Crown roots			Long laterals			Short laterals		
age	kr	Kx	age	kr	Kx	age	kr	Kx	age	kr	Kx	age	kr	Kx
0.11	1.06E-04	0.0014	0.13	1.13E-04	0.001	0.11	1.34E-04	0.0061	0.24	1.18E-04	4.48E-05	0.3	1.29E-04	1.49E-05
0.16	1.06E-04	0.0014	0.19	1.13E-04	0.0011	0.16	1.34E-04	0.0061	0.38	1.18E-04	4.63E-05	0.53	1.30E-04	1.60E-05
0.22	1.06E-04	0.0015	0.26	1.13E-04	0.0011	0.22	1.34E-04	0.0061	0.51	1.18E-04	3.62E-05	0.92	1.29E-04	1.58E-05
0.27	1.06E-04	0.0015	0.32	1.13E-04	0.0011	0.27	1.34E-04	0.006	0.66	1.18E-04	4.87E-05	>2.83	1.30E-04	1.58E-05
0.32	1.06E-04	0.0014	0.39	1.13E-04	0.0011	0.32	1.35E-04	0.0063	0.82	1.18E-04	3.97E-05			
0.38	1.06E-04	0.0015	0.45	1.13E-04	0.0011	0.38	1.34E-04	0.0059	0.98	1.18E-04	4.29E-05			
0.43	1.06E-04	0.0014	0.52	1.14E-04	0.001	0.43	1.35E-04	0.006	1.16	1.18E-04	4.66E-05			
0.65	1.06E-04	0.0015	0.78	1.22E-04	0.001	0.65	1.35E-04	0.0058	2.02	1.18E-04	4.22E-05			
0.87	1.06E-04	0.0014	1.05	1.22E-04	0.001	0.87	1.41E-04	0.0058	3.35	1.18E-04	3.86E-05			
1.09	1.06E-04	0.0015	1.31	1.23E-04	0.001	1.09	1.41E-04	0.0067	>6.28	3.75E-05	4.21E-05			
1.54	1.14E-04	0.0013	1.58	1.23E-04	0.0009	1.31	1.42E-04	0.0074						
1.77	1.14E-04	0.0014	1.85	1.23E-04	0.0009	1.54	1.43E-04	0.007						
2	4.00E-05	0.0013	2.12	1.23E-04	0.0008	1.77	1.47E-04	0.0064						
2.23	3.99E-05	0.002	2.4	1.24E-04	0.0008	1.99	1.48E-04	0.0068						
2.69	3.99E-05	0.1614	2.67	1.23E-04	0.0009	2.22	1.48E-04	0.0069						
2.93	4.00E-05	0.1633	2.95	4.22E-05	0.0008	2.69	1.44E-04	1.4277						
3.17	3.68E-05	0.1718	3.23	4.23E-05	0.0008	2.92	5.28E-05	1.5169						
3.41	3.68E-05	0.1736	3.52	4.24E-05	0.0009	3.16	5.28E-05	1.6072						
4.63	3.89E-05	0.1618	3.8	4.25E-05	0.0009	3.4	5.31E-05	1.6917						
7.25	4.10E-05	0.2438	4.09	4.26E-05	0.0009	4.63	5.08E-05	2.3449						
>10.12	4.29E-05	0.3336	5.57	3.93E-05	0.1122	7.24	5.24E-05	4.0946						
			8.71	4.16E-05	0.1015	>10.11	5.67E-05	6.6086						
			>12.16	4.31E-05	0.1505									

Table S2.2: Overview of statistical results for axial root radii, crown root elongation and leaf elongation for the P levels P0-P3. A Shapiro-Wilk Normality Test and Levene's Test for Equality of Variances were performed, followed by an ANOVA ($n = 5 - 12$).

		axial root radii				crown root elongation				leaf elongation			
		P0	P1	P2	P3	P0	P1	P2	P3	P0	P1	P2	P3
Shapiro-Wilk	F	0.89	0.68	0.6	0.48	0.93	0.98	0.83	0.98	0.89	0.9	0.95	0.92
Normality Test	p	>0.05	>0.05	>0.05	>0.05	>0.05	>0.05	>0.05	>0.05	>0.05	>0.05	>0.05	>0.05
Levene's Test for	F	1.09				2.45				1.07			
Equality of Variances	p	>0.05				>0.05				>0.05			
ANOVA	F	10.21				4.73				4.04			
	p	<0.001				0.01				0.01			

Appendix C: Supplementary Materials to Chapter 5

This appendix contains information on all published studies to which this work has made significant contributions, namely:

Lena Lärm, **Felix Maximilian Bauer**, Jan van der Kruk, Jan Vanderborght, Shehan Morandage, Harry Vereecken, Andrea Schnepf, Anja Klotzsche (2024). Linking horizontal crosshole GPR variability with root image information for maize crops. *Vadose Zone Journal*, 23, e20293. <https://doi.org/10.1002/vzj2.20293>.

Thuy Huu Nguyen, Gina Lopez, Sabine J. Seidel, Lena Lärm, **Felix Maximilian Bauer**, Anja Klotzsche, Andrea Schnepf, Thomas Gaiser, Hubert Hüging, Frank Ewert (2024). Multi-year aboveground data of minirhizotron facilities in Selhausen. *Scientific Data* 11, 674. <https://doi.org/10.1038/s41597-024-03535-2>.

Thuy Huu Nguyen, Thomas Gaiser, Jan Vanderborght, Andrea Schnepf, **Felix Maximilian Bauer**, Anja Klotzsche, Lena Lärm, Hubert Hüging, Frank Ewert (2024). Responses of field-grown maize to different soil types, water regimes, and contrasting vapor pressure deficit. *Biogeoscience*. <https://doi.org/10.5194/egusphere-2023-2967>.

Peng Yu, Chunhui Li, Meng Li, Xiaoming He, Danning Wang, Hongjie Li, Caroline Marcon, Yu Li, Sergio Perez-Limón, Xinping Chen, Manuel Delgado-Baquerizo, Robert Koller, Ralf Metzner, Dagmar van Dusschoten, Daniel Pflugfelder, Ljudmilla Borisjuk, Iaroslav Plutenko, Audrey Mahon, Marcio F.R. Resende Jr., Silvio Salvi, Asegidew Akale, Mohammed Abdalla, Mutez Ali Ahmed, **Felix Maximilian Bauer**, Andrea Schnepf, Guillaume Lobet, Adrien Heymans, Kiran Suresh, Lukas Schreiber, Chloe M. McLaughlin, Chunjian Li, Manfred Mayer, Chris-Carolin Schön, Vivian Bernau, Nicolaus von Wirén, Ruairidh J. H. Sawers, Tianyu Wang, Frank Hochholdinger. Seedling root system adaptation to water availability during maize domestication and global expansion (2024). *Nature Genetics* 56, 1245–1256. <https://doi.org/10.1038/s41588-024-01761-3>.

Dirk Norbert Baker, **Felix Maximilian Bauer**, Mona Giraud, Andrea Schnepf, Jens Henrik Göbbert, Hanno Scharr, Ebba Pora Hvannberg, Morris Riedel (2024). A scalable pipeline to create synthetic datasets from functional–structural plant models for deep learning. *in silico Plants*, Volume 6, Issue 1, diad022. <https://doi.org/10.1093/insilicoplants/diad022>

Dirk Norbert Baker, **Felix Maximilian Bauer**, Andrea Schnepf, Hanno Scharr, Morris Riedel, Jens Henrik Göbbert, Ebba Pora Hvannberg (2024). Adapting agricultural virtual environments in game engines to improve HPC accessibility. *Communications in Computer and Information Science*. <https://doi.org/10.34734/FZJ-2024-03386>.

C-1 Linking horizontal crosshole GPR variability with root image information for maize crops

In minirhizotrones, our resolution in measuring root dynamics is limited by the capability of the optical sensors, such as the cameras applied in the rhizotubes. Taking camera images takes a lot of time and personal resources. Finding additional ways, ideally with already existing methods, to complement our need for root measurement tools would be beneficial to increase spatial and temporal resolutions while minimising measurement time. The non-invasive monitoring agrogeophysical technique "ground penetrating radar" (GPR) may help us to enhance the resolution and provide additional insights into the root system dynamics and their environmental responses. GPR is a geophysical method that uses electromagnetic wave propagation in the soil. From this, we can derive the relative dielectric permittivity (eq. 3-1) that can be directly linked to soil water content (SWC) with a high spatial resolution (Klotzsche et al., 2019). In the past, it has been shown that GPR can be used to detect coarse roots, such as tree roots applying a surface GPR (Guo et al., 2013). However, detecting finer root systems of important arable crops, such as *Zea mays*, using GPR, is still challenging. The Selhausen minirhizotrons, presented in Chapters 2 and 3, are ideal experimental platforms to explore the capabilities to quantify root presence and development using GPR. Here, Klotzsche et al. (2019) already showed that the GPR signal and hence the SWC distribution, especially under dry soil conditions, is affected by maize root presence. However, it still remains elusive how the GPR-derived permittivity is linked to the presence of finer root systems. The synthesis of camera and *in situ* horizontal crosshole GPR measurements between neighbouring rhizotubes of minirhizotrons provides a comprehensive view into the plant-soil continuum, enabling the exact quantification of roots and linking them to GPR data. In Lärm et al. (2024), we aimed to non-invasively monitor the crops rooting zone by investigating the relationship between the root volume fraction (RVF) (eq. 1) and the GPR-derived permittivity in *Zea mays* crops in the corresponding measurement depths.

Given the soil volume V_{soil} , the equations for calculating RVF are defined as follows:

$$RVF = \frac{RV}{V_{\text{soil}}} \quad (1)$$

while using

$$V_{\text{soil}} = L \cdot W \cdot r_{\text{rhizotube}} \quad (2)$$

where W is the width of the image, L is the length of the image and $r_{\text{rhizotube}}$ is the radius of a rhizotube.

We used the already processed time-lapse data of root images and GPR presented in Chapter 2 and Chapter 3, respectively. While linking root data to GPR

measurements, we had to consider the noises from static influences, such as soil heterogeneity and rhizotube deviations, and dynamic influences, which are mainly caused by seasonal moisture changes. We achieved this by adapting the permittivity values across different time points and reflecting only the variations related to root presence, which are referred to as "trend-corrected spatial permittivity deviations of vegetation field". These corrected data showed a clear, increasing trend during the vegetation period. This trend could be linked to a similar increase in RVF during the same time period (Figure S3.1). The results further showed that the variability in permittivity is strongly correlated with the presence of roots. We found that patterns in permittivity show a consistent increase in variability with higher root presence in soil. Furthermore, we could reveal that the history of water management also influences root development and, consequently, the permittivity. Interestingly the trends were not influenced by different soil types and compaction layers. One possible explanation for the observed correlation is that the roots in the soil cause a redistribution of the soil water and, thus, an increase in the variability of the soil water.

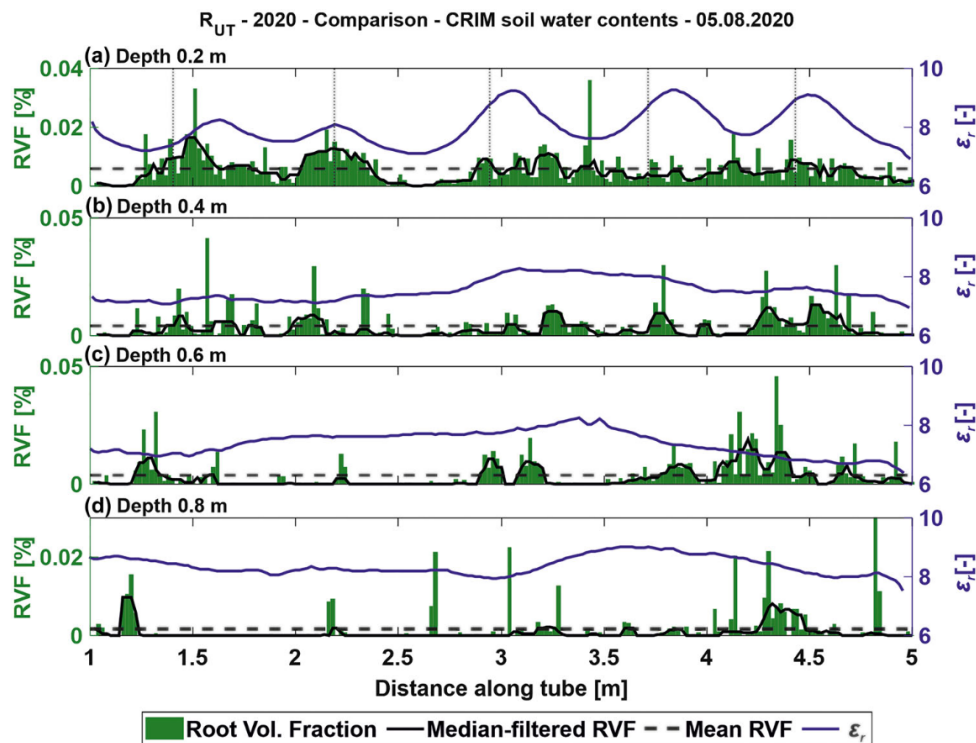


Figure S3.1: Exemplary comparison of the permittivity high-resolution root image dataset measured on August 5, 2020, and the respective root volume fraction (RVF). The different plots represent the different depths of 0.2–0.8 m, (a)–(d), respectively, for Plot 2 at R_{UT} . The solid blue line indicates the permittivity. The green bars indicate the RVF along the rhizotubes. The black solid line indicates the smoothed RVF along the rhizotube over five positions. The dashed black line represents the mean RVF along the rhizotubes (adapted from Lärm et al. (2024)).

Summarized, in Lärm et al. (2024), we showed that GPR-derived permittivity could be used as a proxy for assessing root presence, which may improve data acquisition for agronomic studies and crop modeling and shows the future potential of using GPR for precision agriculture.

C-2 Multi-year aboveground data of minirhizotron facilities in Selhausen

A better understanding of crop response to soil water stress is crucial for plant breeding, crop and cultivar selection, and management decisions to minimize adverse effects. Furthermore, these data are important for the development of soil-plant systems or crop models, which are the backbone for process understanding of crops and predictions for cropping systems. Studies on the ecophysiological properties of crops from leaf to canopy under different soil water conditions and crops are often carried out under controlled conditions. Measurements on plant water potential, together with CO₂ and H₂O gas fluxes and growth processes, performed under realistic field conditions, are rare.

This work presents a comprehensive dataset from leaf to the canopy using several sophisticated sensing techniques, including leaf chlorophyll, stomatal conductance and photosynthesis, canopy CO₂ exchange, sap flow, canopy temperature, and detailed plant growth traits, such as plant height, leaf area index, aboveground biomass, and yield measurements (FigureS3.2). The data was collected under field conditions with different soil types, water treatments, and different wheat and maize varieties analog to the experimental set-up presented in Lärm et al. (2023). The final data collection also covers the same time period, location, and treatments. The data were made available for studying soil/water-plant relations and improving soil-plant-atmospheric continuum models with this DOI: <https://doi.org/10.34731/1a9s-ax66>.

C-3 Responses of field-grown maize to different soil types, water regimes, and contrasting vapor pressure deficit

Scientific data are the foundation for all our analyses, interpretations, discussions, and conclusions. The data presented in Chapter 3 are a precious foundation for analyzing belowground crop behavior. Combining it with data from the aboveground part of the plant allows us to holistically tackle important agronomic questions, such as how crops react to different soil types, water regimes, and contracting vapor pressure deficits, as it was done in the study of Nguyen et al. (2024a).

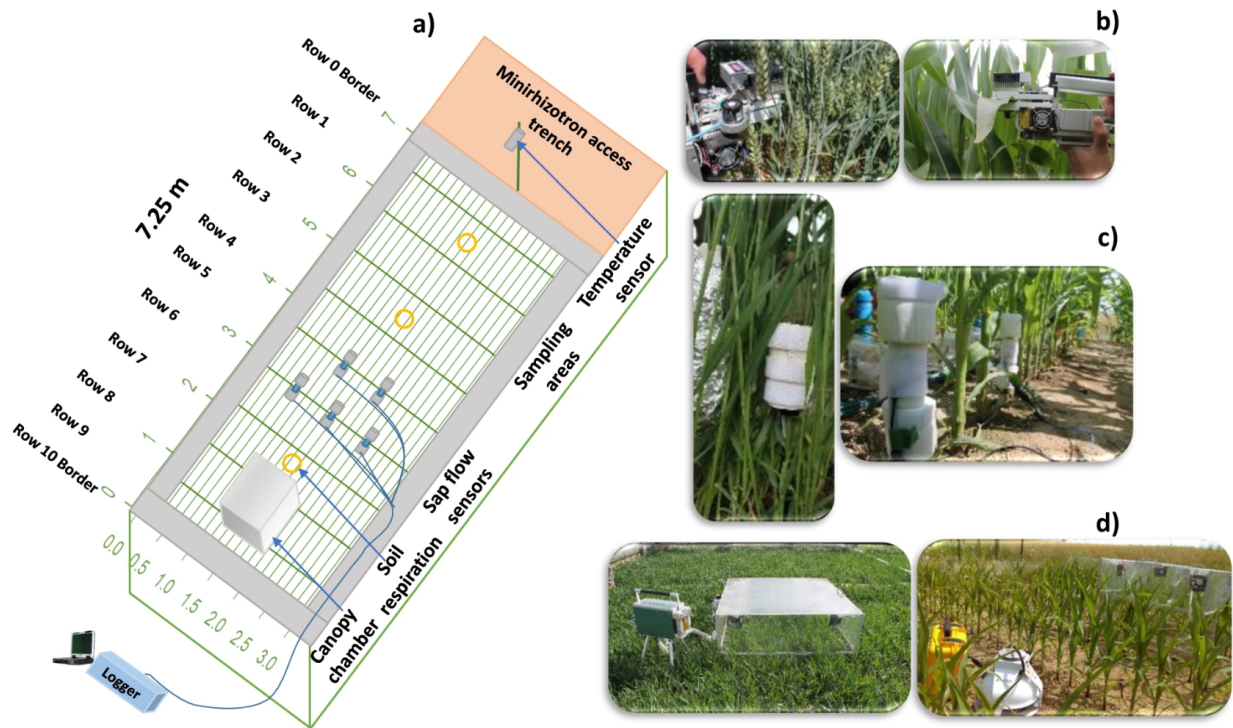


Figure S3.2: Overview of (a) above-ground measurement set-up in one exemplary plot (here for maize) within the minirhizotron facility, from the minirhizotron access trench: canopy temperature sensor, sampling area and leaf measurements, sap flow sensor installation with data logger, canopy chamber with LI-6400XT, and soil respiration chambers (b) leaf gas exchange measurement with LI-6400XT machines (c) sap flow measurements with the Dynamax sensors, and (d) canopy chamber measurements for winter wheat (left) and maize (right). (adapted from Nguyen et al. (2024b)).

We investigated the influences of the stony soil and the silty soil at the R_{UT} and R_{LT} minirhizotron facilities, different water regimes, namely irrigated and rainfed treatments on root to shoot growth characteristics and the hydraulic linkages between the soil and *Zea mays*. We used the data measured in the growing seasons of 2017 and 2018. These two years had very different climatic conditions, resulting in a low (2017) and high vapor pressure deficit (2018). In detail, we used the root growth data and soil moisture sensor data from (Bauer et al., 2022, Lärm et al., 2023, Lärm et al., 2023c,e) and combined them with crop growth measurements, leaf gas exchange, leaf water potential, and sap flow measurements to test two hypotheses.

We hypothesized that soil-plant hydraulic conductance, especially under dry soil conditions, depends on soil hydraulic properties. The minimum leaf water potential of maize does not significantly differ across the different soil types, water treatments, and climatic conditions represented by the two growing seasons. We tested this by checking the effects of soil types, water treatments, and climatic

conditions on root growth, stomatal conductance, leaf photosynthesis, transpiration, and leaf water potential. Furthermore, we analyzed the relative contribution of root growth and shoot development to the water uptake capacity of maize.

We found that generally, in the stony soil, more roots grew in the upper soil layer up to 20 cm, while in the silty soil, the highest root density could be observed in the subsoil from 60-80 cm depth. In the silty soil, the total root length was 2.5-6 times the total root length in the stony soil under the same water treatments. Interestingly, the ratio of root length to shoot biomass was even up to 3 times higher under rainfed conditions than in the irrigated treatments of silty soil, while the ratio did not differ between treatments in the stony soil. Comparing the soil with the same water treatments, the ratio of root length to shoot was always higher for the silty soil. Comparing the minimal leaf water potential (ψ_{leaf}), we observed a difference from -1 MPa between 2017 ($\psi_{leaf} = -1.5$ MPa) and 2018 ($\psi_{leaf} = -2.5$ MPa) on rainfed stony soil and thus lower than on silty soil ($\psi_{leaf} = -1.5$ to -2 MPa in 2017, $\psi_{leaf} = -2$ to -2.5 MPa in 2018).

Leaf water potential, water potential gradients from soil to plant roots, plant hydraulic conductance, stomatal conductance, transpiration, and photosynthesis were considerably influenced by soil water content. The stony soil generally had a lower soil water availability, and consequently, the plant's water stress levels were higher. Our results show that the plant's reaction to lower water availability on the stony soil resulted in fewer roots with a higher root tissue conductance compared to the silty soil. However, on the silty soil, we observed the opposite. Plants growing on the rainfed treatment, which had a lower water availability, resulted in more roots with a lower root tissue conductance than in irrigated treatments. Despite the root length reduction of plants in irrigated stony soil, the transpiration rate was not much lower than in the silty irrigated plots. This compensatory adaptation was reflected in higher root conductance per unit root length compared to plants in silty soil.

Additionally, we found that stomatal regulation maintains leaf water potential at certain thresholds, which depend on soil types, soil water availability, and seasonal atmospheric demand. The stomata conductance was lower and at a more negative leaf water potential in stony soil than in silty soil.

We concluded that the response of *Zea mays* to stress can be completely opposite depending on soil conditions. To cope with water deficit, *Zea mays* had a higher water uptake rate per unit root length and higher root segment conductance in the stony soil than in the silty soil, while at the same time, the crop reduced transpired water via reduced shoot size.

C-4 Seedling root system adaptation to water availability during maize domestication and global expansion

Although maize grows in a lot of climatic conditions all around the world, maize cropping can be challenging. Not only the absence of crucial nutrients such as phosphorus may inhibit the plant development, as shown in Chapter 4. As in most agricultural systems, sufficient water availability is also absolutely essential for the plants to grow and develop the highest possible yields. Already in the first days of growth, water scarcity leads to significant stress, which in turn affects plant development and influences the yield. Even a short drought spell can cause severe damage or death to young plants. Consequently, it is key that the seedling has optimal water availability. However, the amount of water that is considered optimal is highly dependent on the *Zea mays* variety. As we already know from Chapter 4, mainly the root systems account for the ease and the amount of water that can be taken up. Already in seedlings and young plants, root system architectural organization and, consequently, functional traits, such as root system conductance, differ between varieties. The root system itself has been reshaped indirectly during domestication. Climate and geographical conditions, such as water and nutrient availability and soil features, drive the root system's reshaping during the colonization of new sites. The domestication process of *Zea mays* started more than 9,000 years ago from teosinte (*Zea mays* ssp. *parviglumis*) from the lowlands of Mexico. Then, maize spread over Panama to Peru, South American lowlands in the Caribbean and Amazon, and back north to the Mexican highlands. From there, the domestication continued in the southwest US and, much later, northern territories of today's Canada and the US. Approximately 500 years ago, maize arrived in Europe and finally conquered almost the whole world (Figure S3.3). During this time, the domestication processes adapted the root system of the plant and, therefore, altered the water uptake capacity of the root system of maize seedlings. In the following results of the study of Yu et al. (2024) we will illuminate which changes in root system architecture occurred and how this relates to the water uptake functionality.

The maize seedling's root system mainly consists of a primary root and a variable amount of seminal roots (0-14, average: 3.3), Primary and seminal roots do have lateral roots (Figure 1-3). Crown roots and secondary lateral roots are rather not yet present in seedlings and can therefore be neglected (Hochholdinger, 2009). Seminal root number mainly form the root system architecture at this point. Consequently, this influences the depth and soil volume that roots can explore. So far, it is not well known how the root system changed form and function during global expansion. With our study, we aimed to understand how the seminal root number (SRN) was affected by environmental conditions, the underlying genetic foundation, and whether it is possible to use SRN as a potential adaptive function to develop maize crops that are resilient to effects of climate change, such as drought.

Within this study, over 9,000 *Zea* accessions were analyzed regarding SRN, representing traditional varieties, modern inbred lines, and wild teosinte from all around the globe. Since seminal roots are embryonic, seed size was often hypothesized to be important for the number of seminal roots. However, we could not find a significant correlation between seminal root number and seed size. Furthermore, we could show that SRN does not depend on the amount of carbohydrates available during seed development. We concluded that SRN depends on domestication but not on seed size. That posed the question of which environmental signals might influence the SRN. We found that mean diurnal temperature range ($r = -0.36$), temperature seasonality ($r = -0.29$) and precipitation seasonality ($r = -0.07$) are important climatic drivers, while soil organic carbon ($r = 0.11$) and soil sand content ($r = -0.16$) are the main influences originating from the location. Precipitation in the mid-Holocene also showed a positive correlation ($r = 0.3$), showing the importance of rain events and, consequently, water availability during maize evolution (Figure S3.4a). With a random forest model, it was identified that SRN decreased with increasing geographical latitude (Figure S3.4b). A genome-wide association study, combined with a phenotype mapping with eight founders Multi-parent Advanced Generation InterCross (MAGIC), which represent the latitudinal trend observed, identified several shared genomic regions. A specific already known gen locus (rootless concerning crown and seminal roots, *rtcs*) was prominent (Figure S3.4c). A genome-wide predictive model for SRN using the MAGIC families was applied to the eight founder haplotypes and successfully captured the latitudinal trend in SRN as well. The model was effective and robust since removing any single chromosome from the model did not change the prediction, also indicating that more than one genome locus is involved. Detailed analysis of the *rtcs* region revealed different allele effects from the eight founders,

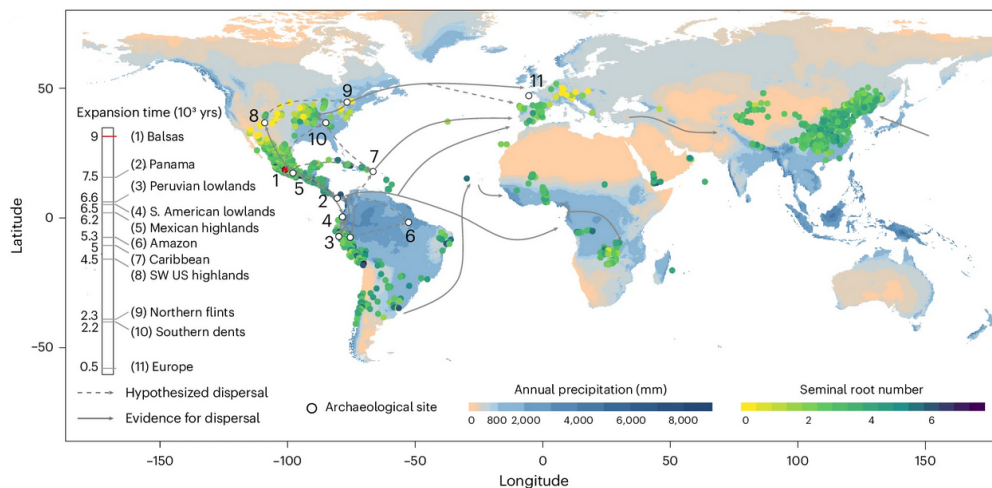


Figure S3.3: Geographical variability of SRN in traditional varieties of maize. SRN was determined in globally collected traditional varieties of indicated geographical origin. Domestication and expansion times for maize populations are indicated accordingly. (Figure is adapted from Yu et al. (2024)).

ranging from positive to negative, depending on the founder's geographical origin, but also following the latitudinal trend. The variation in SRN among different varieties is likely driven by indirect selection. The SRN changes are a byproduct of other adaptive changes to the environment. An additional driver for SRN is the Northern Flint alleles, a group from Southwest US. The proportion of alleles derived from Northern Flint germplasm was negatively correlated with SRN, indicating that cultivars with a higher share of the Northern Flint genome formed fewer seminal roots (Figure S3.4d).

Having identified the genomic and geographical drivers for SRN formation, we investigated the more precise morphological influences and functional implications. We did this with precise sub-organ phenotyping and functional-structural modeling. In a rhizobox set-up, we measured 218 representative traditional varieties using the pipeline described in Chapter 4 to access root architectural and morphological traits. We then created one FSPM with CPlantBox for each line, including statistical variation from several repetitions, for a 9-day-old seedling (Figure 5-2). We found that SRN negatively correlates with primary root length and lateral root density along the primary root (Figure S3.4f). Our simulation, which was performed in a simplified set-up used for the simulation procedure presented in Chapter 4, showed that SRN affects seedling vigor by modulating the root system conductance (K_{rs}) (Figure S3.4g). In field soil, we could see that in the absence of seminal roots, the *rtcs* mutant produced an increased number of lateral roots. Since lateral roots mainly drive water uptake in young maize plants, we suggest that the reduction of seminal root count favors seedling establishment in water-limited conditions. Variations in SRN may shape the size and branching of the entire root system, which in turn might determine the plant's water uptake capacity. Our CPlantBox realizations were then used to demonstrate that the relative contribution of lateral roots to total root water uptake decreases with increasing SRN by simulating the standard uptake fraction (SUF). A soil-hydraulic modeling approach further showed that the point at which a small increase in transpiration provokes a large drop in leaf water potential at a given soil water potential (stress onset limit) occurred at a less negative leaf water potential in the traditional varieties with lower SRNs. This implies that plants with a higher number of seminal roots require higher flow rates at the same root length for water uptake and, therefore, a higher plant water potential to maintain transpiration than cultivars with a low SRN. Cultivars with low SRNs are, hence, more tolerant to drought conditions. Additionally, we could show that the lignin accumulation along the tip of the primary roots is higher with lower SRN, facilitating root penetration in dry soils and adding an additional beneficial feature for drought tolerance.

To investigate genetic factors affecting SRN in inbred maize, a genome-wide association study helped to identify associated single-nucleotide polymorphisms associated with SRN, including the key gene *rtcs*. Further experiments with CRISPR-Cas9 knockouts of another important gene, *ZmHb77*, revealed that mutations in this gene reduced SRN but increased lateral root density. A drought stress experiment with re-watering showed that *ZmHb77* knockout mutants with lower SRN and higher lateral density had a significantly better performance under drought and better recovery after re-watering, while under optimal conditions, no sig-

nificant differences were detected (Figure S3.4h). This indicates that *ZmHb77* controls SRN and the depending architectural traits. In further experiments with maize inbreeds with high and low SRN and drought tolerance, RNA sequencing was conducted to explore the gene expression pattern in the embryo and root stele tissue. *ZmHb77* is mainly expressed in the root stele tissue at the point of lateral root initiation, suggesting that the major function of *ZmHb77* is linked with lateral root formation in a way that it potentially promotes the formation of seminal roots while inhibiting the density of lateral roots (Figure S3.4i).

Generally, we concluded that SRN variations impact maize seedlings' hydraulic properties. This has the genetic potential to modify root plasticity and offer insights into root responses to changes in water availability. Our findings highlight the historical impact of domestication and adaptation on maize roots. They also underscore the potential of genetic advancement to assess climate resilience in future *Zea mays* generations.

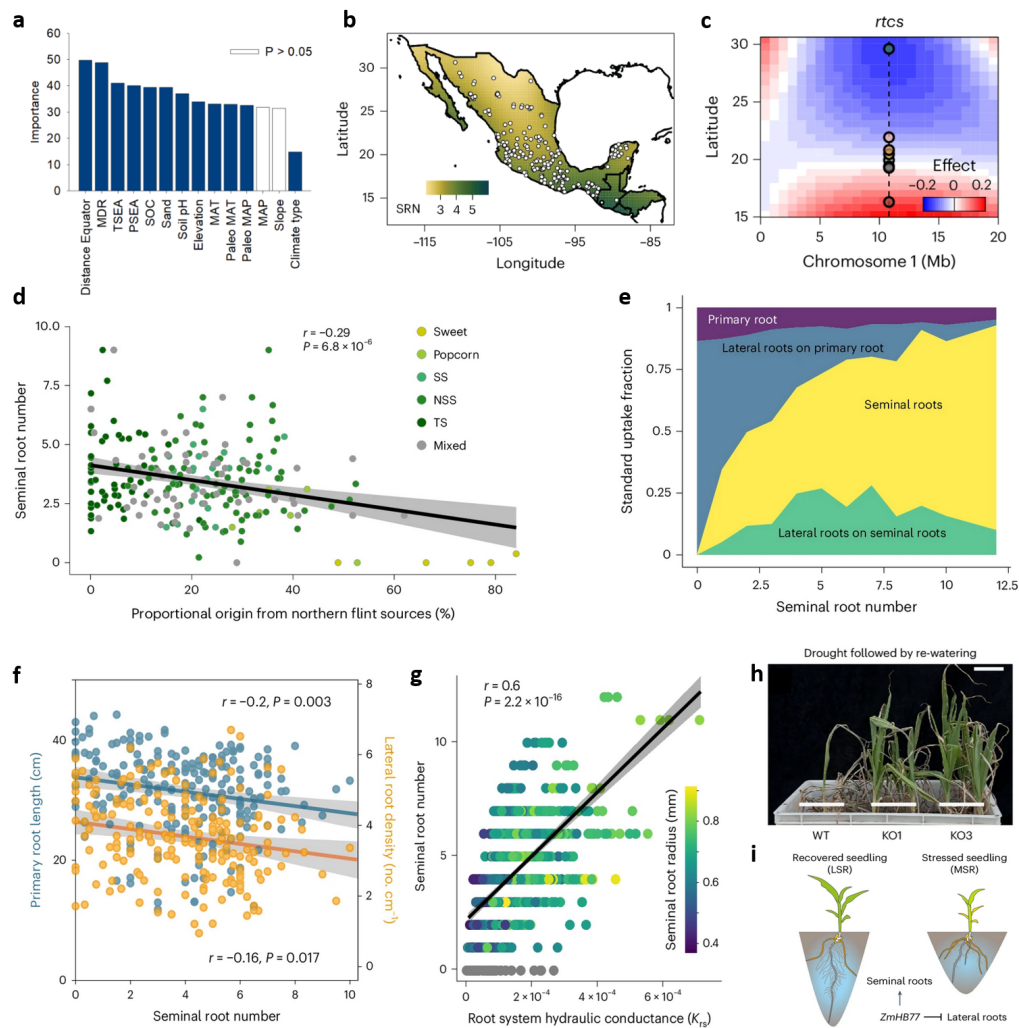


Figure S3.4: a) Comparison of seminal root numbers in maize lines originating from different climate groups according to the Köppen-Geiger climate classification maps. Significant differences were tested by one-way PERMANOVA with post-hoc test ($p < 0.05$); b) SRN decreases along a latitudinal gradient from south to north in Mexico. c) MAGIC founder allele effects in a 20 Mb window around *rtcs*; d) Correlation between SRN and the proportion of Northern Flint sources in the US Ames panel; e) SUF of seminal roots and lateral roots as a function of SRN. For each SRN, the average proportion of water uptake per root type is expressed as a ratio relative to overall water uptake; f) SRN is negatively correlated with rooting depth of the primary root and lateral root density in different maize traditional variety accessions; g) Seminal root variation affects K_{rs} ; h) Comparison of drought tolerance between WT and plants of the two *ZmHb77* CRISPR-knockout lines after drought conditions and re-watering; i) Model of a potential function of *ZmHb77* on the formation of seminal roots and lateral roots in contribution to maize seedling drought tolerance (figures are adapted from Yu et al. (2024)).

C-5 A scalable pipeline to create synthetic datasets from functional–structural plant models for deep learning.

Deep learning has expanded our ability to analyze new data and investigate structural plant responses beyond the limits of our already implemented mechanistic approaches. Image analysis, in particular, has been significantly improved by this technique, and the quantity and quality of structural plant parameters obtained in a much shorter time is an enormous gain (Pound et al., 2017). The current bottleneck of deep neural networks is the amount of data required to train them, as stated in Chapters 1 and 2. We follow a new approach to overcome these bottlenecks, as shown in Baker et al. (2023).

To train neural networks, we require sufficient data, e.g., images for CNNs (Bauer et al., 2022). However, these data require some kind of ground-truth, such as already known parameters or structures. Annotating images is time-intensive, as shown in Chapter 2. Consequently, annotated images are a scarce resource. Synthetic data are a promising way to cope with this limitation as long as they offer ground-truth and validation. The current challenge in creating synthetic data requires expert knowledge in Computer Graphics, Visualization, and High-Performance Computing (HPC) to generate data of sufficient quality. To facilitate this, a model that generates the ground truth, a visualization tool that displays a most realistic output, and a framework coupling these parts and enabling an interface for the neural network implementation are required.

In Baker et al. (2023), we present *SynavisUE*, a framework that enables synthetic data generation in real-time. The underlying pipeline integrates a CPlantBox (Giraud et al., 2023) realized plant structure with a newly implemented shoot geometry into the game graphic engine "Unreal Engine" to generate synthetic images that can be directly used for a user-defined neural network training. Due to the versatility of the Unreal Engine, which allows the modification of environmental parameters, such as light and shadows, it is possible to create heterogeneity while keeping the plant architectural ground-truth data. *SynavisUE* is ready to use and offers a user-friendly environment.

In order to evaluate the reliability and versatility of the *SynavisUE* pipeline, we created a synthetic copy of the greenhouse set-up we used in Chapter 4 to evaluate the precision. Then, we aimed to measure the performance on an HPC cluster with a virtual drone flight, producing synthetic drone images of a virtual maize field based on the FSPM parameterization we obtained with the study presented in Chapter 4. In the greenhouse scene, we could induce heterogeneity by changing camera properties and angle. To evaluate the results, we compared the leaf blade area from our *SynavisUE* generated synthetic greenhouse rhizotron set-up with the real measurement since this is a common agronomic research task. We found that the synthetic data were slightly but systematically underestimating blade area, however results were consistent. We used CPlantBox stochasticity and Unreal Engine's environmental altering functions to generate heterogeneity

in the field scenario. To minimize the warm-up time until the scene is loaded and maximize the frame rate, we parallelized Unreal Engine exclusively on the GPU and CPlantBox realizations on the CPU. The virtual drone scene was feasible and produced usable and comparable results as well. However, a lot of computational power was required to render the scene in real-time, and the frame rate dropped to a minimal $2.5 \text{ images s}^{-1}$.

Generally, we found that our coupling framework, together with a visualization of the FSPM CPlantBox, is a promising and practical way to generate synthetic data for neural network training. However, to access the full potential, the incorporation of more morphological features, the use of real agronomic research questions, and a performance improvement on the HPC side to distribute workload and increase speed are required in the future.

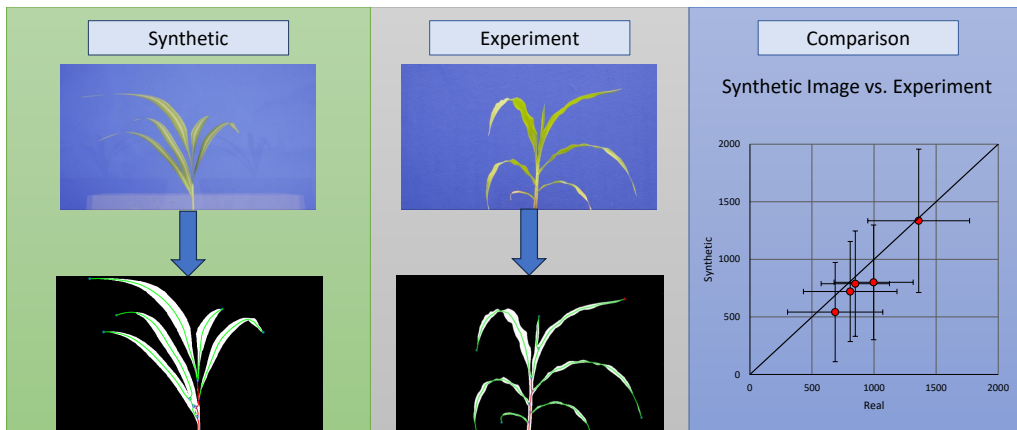


Figure S3.5: Comparison of parameter extraction pipeline between synthetic and real-world data. Real-world data, 23 plant images at this growth stage and angle, were acquired in controlled rhizotron experiments. Bottom: Analyzed skeletons of shoot organs, starting with the pseudo-stem. Right: Comparison of blade lengths in mm, compared across samples sorted by longest first. The error bars indicate the standard deviation on each axis (figure adapted from Baker et al. (2023)).

C-6 Adapting Agricultural Virtual Environments in Game Engines to Improve HPC Accessibility

As stated before, using *SynavisUE* to generate virtual data of fields with a high-density crop stand containing a lot of generated plant geometries is computationally demanding, even on HPC systems. These scenes typically cannot be rendered in real time without specialized techniques. Within the study of Baker et al. (2024a), we try to address this challenge since it is particularly relevant in agricultural science, where virtual fields may consist of numerous individual plant geometries.

As before we used the Unreal Engine as the primary rendering framework, integrated with the *Synavis* framework to facilitate data production and image analysis, based on CPlantBox realizations. To address the scalability problem, a technique to partition large-scale virtual fields across multiple GPU nodes was developed. This partitioning enables the generation of extensive datasets without overpowering individual nodes and thereby maintaining high performance and efficiency.

We conducted two virtual experiments to evaluate the effectiveness and feasibility of the newly integrated methods. In the first experiment, GPU performance was evaluated when rendering an increasing number of FSPM instances, and the scene was continuously updated as time progressed. We measured the frame time and GPU utilization. The results showed a superlinear increase in frame time as the number of plants increased, resulting in lower GPU efficiency. For example, with about 10,000 plant geometries, about 10.7 frames per second were provided, and GPU utilization decreased due to memory exhaustion. In the second experiment, the effects of rendering multiple instances simultaneously on the same GPU node were investigated. The results showed higher average frame times and greater variance when four instances were run simultaneously on a single node. This simultaneous rendering led to competition for resources, which affected overall performance. The results of this experiment showed the importance of optimal partitioning and distribution techniques to ensure high GPU utilization and efficiency. We therefore concluded that field partitioning, where large fields are divided into manageable sections, improves GPU efficiency and enables scalable data generation. This method ensures that virtual environments can replicate real-world farming conditions, supporting robust and scalable training models.

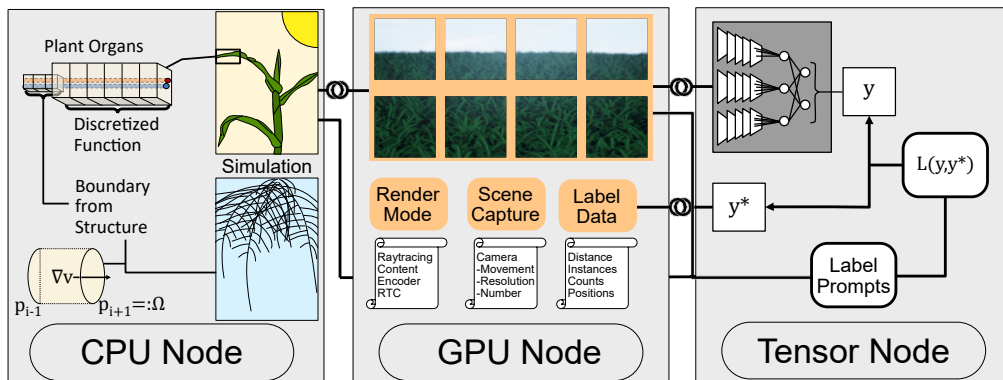


Figure S3.6: Overview of technical components and data flows. The illustrated assignment to specific nodes is a performance recommendation, though individual components can share resources. A linked line indicates concurrent coupling (figure adapted from Baker et al. (2024a)).

The results of this study and the findings of the study of (Baker et al., 2023) showed that distributed rendering of virtual agricultural fields using HPC systems represents a significant advance in data generation for crop science. By utilizing game engines such as Unreal Engine and frameworks such as *Synavis*, researchers can create dynamic, high-quality datasets that address the lack of annotated data in agriculture. The presented approach not only improves the efficiency of HPC resource use but also supports the development of more accurate and robust deep learning models. Most importantly, we presented the potential for large-scale use cases to benefit from these techniques.

Appendix D: *In silico* investigation on phosphorus efficiency of *Zea mays*: An experimental whole plant model parametrization approach.

From: **Felix Maximilian Bauer**, Guillaume Lobet, Dirk Norbert Helmrich, Anna Galisnki, Zamiga Kahlilova, Lisa Zander, Peng Yu, Gabriel Schaaf, Andrea Schnepf. *In silico* investigation on phosphorus efficiency of *Zea mays*: An experimental whole plant model parametrization approach. Poster at *10th International Conference on Functional-Structural Plant Models* (FSPM2023). <https://doi.org/10.34734/FZJ-2023-04032>.

D-1 Introduction

Phosphorus (P) is a crucial macronutrient for plant growth and essential for yield development. In 70 % of the globally cultivated land area, P is a limiting nutrient. Yield security is currently only obtained by regular application of plant available P fertilizer. However, the crops use-efficiency of the fertilized P is low. 70-80 % of this P is not utilized and eventually cause eutrophication of open water bodies. Therefore, it is important to increase the P use-efficiency of crops by improving breeding and agricultural management. The first step towards this is the prediction of the effects of P availability and deficiency to relevant crops. Significant changes in plant architecture, like reduced growth and rigid appearance of shoots, inhibition of primary root growth, or changes within lateral root growth have been associated with P deficiency. However, it is challenging to quantify the relevant processes that cause the detrimental effects of P limitation on crop and canopy development and the consequences on relevant physiological processes (Marschner, 2011). FSPMs are appropriate tools to approach this, since they integrate several processes based on (3D-)simulated plant structures (Schnepf et al., 2018). To parametrize these models for the evaluation of P deficiency effects on plant structure, times-series data of whole plants under P deficiency are required. Specific parameters, related to growth processes, like the elongation rate of stem, leaf, base and lateral roots are important, but often difficult to acquire. This project focuses on the creation of a dataset for the parameterization of a FSPM for *Zea mays* under various levels of P limitation. The data include time-series of photographs of shoot and root of maize until 28 days after sowing, growing at different P levels in soil. Our aim is to parametrize the FSPM CPlantBox to simulate crop structure development under P deficiency. Through the coupling of CPlantBox with water, carbon-flow and photosynthesis modules, we will enable the modelling of structure, water- and nutrient uptake and light-use efficiency of a maize crop with variable P limitation under field conditions (Zhou et al., 2020). This study introduces an easy to implement workflow to acquire dynamical data of root and shoot simultaneously for FSPM parameterization. We aim for a broader understanding of the influences of P deficiency on maize, by using a FSPM, to unravel the effects of P deficiency on plant structure and function.

D-2 Materials and Methods

Zea mays cv. B73 was grown in greenhouse-rhizotrons in a P deficient luvisol soil from a long time fertilization trial. The initial plant available P concentration was 2.0 mg P 100 g⁻¹ soil (CAL-Method). To obtain the different P treatments, the substrate was additionally fertilized with 2.0, 4.0 and 6.0 mg P 100 g⁻¹. P was the only limiting factor for plant growth. Images of shoot and root, starting with germination, were regularly taken on a fixed position. Image processing was done in several steps including segmentation, skeletonization and parameter extraction. Above- and below-ground organ segmentation differed. Shoot segmentation was performed by a background color filter algorithm. For root segmentation,

we implemented a combination of automated segmentation with convolutional neural networks and manual correction into the segmentation tool “RootPainter”, enabling the processing of time-series (Smith et al., 2022). The skeletonization was performed by RootSystemAnalyzer, a program originally designed for root parameter extraction, but also usable on shoot segments (Leitner et al., 2013a). It directly provided the shoot parameter and RSML-files from which the parameters for the root system were derived.

D-3 Results and Discussion

We established a pipeline to extract root and shoot parameters from 2D images, usable for the parametrization of the FSPM CPlantBox. With this, we obtained full parameter-sets for *Zea mays* with corresponding response-curves of key-parameters under various P limitations. First results show that the P level in the soil influences, e.g., leaf and basal root elongation. Diameter of basal roots raise with increasing P supply, while the seminal root count is decreasing. Our plant models indicates that the root system re-organize without a gain in total root length until a P threshold, while the leaf growth is increasing until the same P level. Only with P supply higher this threshold, total root system length increases, while leaf area stagnates. The coupling with photosynthesis, water- and carbon-flow modules will enable investigations on underlying mechanisms.

D-4 Conclusion

Our results will facilitate the *in silico* observation of functional and structural crop reaction to various P limitations and help to understand more detailed the architectural and physiological responses of maize to P deficiency. These insights will provide valuable information for breeders on trait selection and management decisions.

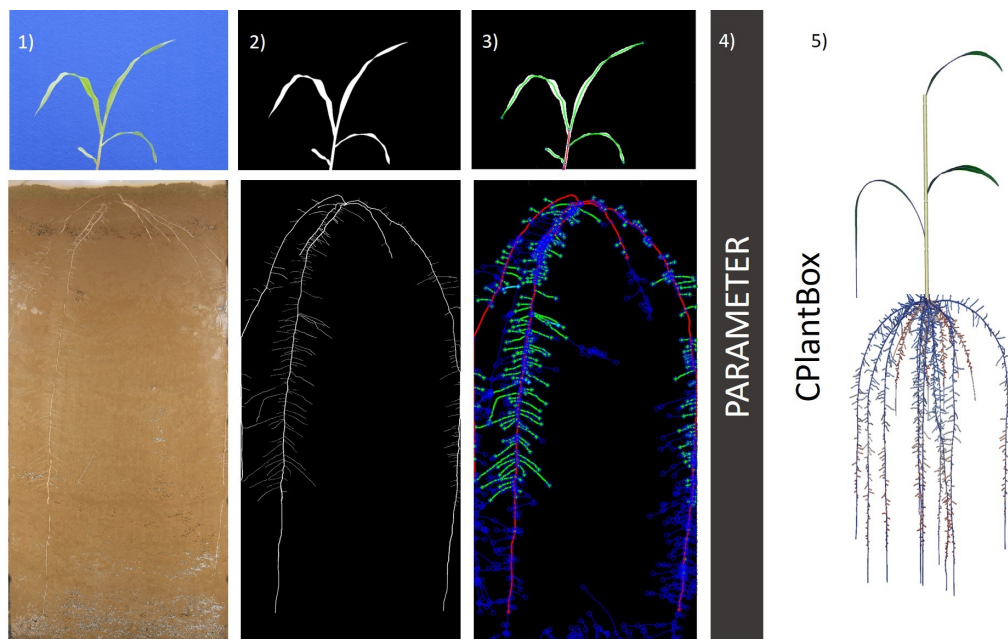


Figure S4.1: Workflow from 2D- images of shoot and roots to FSPM parametrization: 1) image acquisition, 2) segmentation, 3) feature detection and parameter extraction, 4) assemble parameter set, 5) plant structure from parameter.

Appendix E: Modeling architectural and functional response of *Zea mays* to phosphorus deficiency based on experimental data.

From: **Felix Maximilian Bauer**, Mona Giraud, Dirk Norbert Helmrich, Guillaume Lobet, Andrea Schnepf. Modelling architectural and functional response of *Zea mays* to phosphorus deficiency based on experimental data. Presentation at *Plant Biology*, Savannah, GA, USA, 5 Aug 2023 - 9 Aug 2023. <https://juser.fz-juelich.de/record/1017292>.

Agricultural practices often rely on the excessive use of mineral fertilizer. Phosphorus (P) is an essential macronutrient and is required for plant growth. Within the next years, the availability of rock phosphate, the current main P-fertilizer source, will decline. Especially for *Zea mays* it is known that yield declines and canopy development is inhibited by P-deficiency. However, it remains unclear how various P-limitation levels affect structural properties and the depending life-sustaining processes like water uptake. We conducted a greenhouse rhizotron experiment with *Zea mays* cv. B73 in agricultural soil at four P fertilization levels, from strongly to not P-deficient. 2D RGB-imaging of shoot and root-systems was conducted on a daily basis. The resulting timeline data were analyzed, using a neural network-supported and mostly automated analysis pipeline, to obtain architectural parameters of all plant organs. Our observations revealed that the leaf area was maintained for plants with higher P-supply and sharply decreased at the two lowest P-levels. Total root length sharply decreased when P was below the highest level and stagnated at the three lowest P-levels. We also observed a reorganization of the root systems resulting in more seminal roots and shorter and thinner basal roots at lower P-supply. We used the measured architectural and anatomical parameters to calibrate the functional-structural plant model CPlant-Box. We simulate empirically the growth of *Zea mays* at the four P-supply levels and mechanistically the resulting water flow. *Zea mays* with the highest P-supply had a significantly higher total root conductance (K_{rs}) compared with the K_{rs} for the three lower P-supply levels. In the next steps, we will evaluate how this affects the plant fitness and water flow in the soil-plant-atmosphere continuum.

Appendix F: The selhausen minirhizotron facilities: A unique set-up to investigate subsoil processes within the soil-plant continuum.

From: **Felix Maximilian Bauer**, Lena Lärm, Normen Hermes, Harry Vereecken, Jan Vanderborght, Andrea Schnepf, Anja Klotzsche. The selhausen minirhizotron facilities: A unique set-up to investigate subsoil processes within the soil-plant continuum. Poster at *TERENO-OZCAR Conference 2023*. <https://doi.org/10.34734/FZJ-2023-04033>.

Climate change raises new challenges for agriculture. A comprehensive understanding of whole plant responses to a changing environment is the key to maintain yield and improve sustainable crop production. Although there are many projects approaching this challenge, most studies focus on the acquisition and analysis of above-ground field data. The subsoil processes involved in plant root growth and resource acquisition are rarely in focus, since very complex set-ups are required to obtain these data on field scale. Therefore, detailed measurement of the plant roots and the corresponding soil conditions are required. The minirhizotron facilities in Selhausen (Germany) are located within the TERENO-Selhausen test site in the lower Rhine valley. They enable non-invasive longer-term studies of the soil–plant continuum on two different soils in the same climate by offering a unique set-up to record above- and belowground information over entire crop growing seasons under various field conditions and agronomic treatments. Detailed information about soil water content, soil water potential, soil temperature and root development are collected with a high spatial and temporal resolution. Above-ground measurements, such as biomass, transpiration fluxes and assimilation rates are performed additionally.

In recent years, continuous development and improvement of measurement technology and data analysis has facilitated the process, transfer and access to these data. Currently several dynamic and permanently installed sensors are used within the facilities. 7 m-long transparent tubes are horizontally located in several depths. An in-house developed RGB-camera system enables root imaging along the tubes in multiple directions. The images are analyzed with a deep neural network-based analysis pipeline that provides relevant root system traits, such as total root length and root length density. To obtain the spatial soil water content variations per depth, crosshole ground-penetrating radar (GPR) measurements are performed between the tubes. The derived permittivity and hence soil water content values show a clear spatial variation along the tubes and different behaviors for various plant and soil types. Recently, a novel analysis tool to derive the trend-corrected spatial permittivity deviation was introduced, allowing an investigation of the GPR variability independently of static and dynamic influences.

The ongoing measurements currently cover five years of wheat and maize trials, including water stress treatments, sowing density, planting time, and crop mixtures. Data collected in this study are available through the TERENO data portal and can be used to develop, calibrate, and validate models of the soil–plant continuum across different scales, including soil process, root development and root water uptake models, as well as model compilations, such as single-plant and multi-plant models. Further, the data can be of direct use for agronomists and ecologists.

Appendix G: Unrevealing subsoil processes in the selhausen minirhizotron facilities: Comprehensive insights into the soil-plant continuum with a new unique dataset.

From: **Felix Maximilian Bauer**, Lena Lärm, Normen Hermes, Harry Vereecken, Jan Vanderborght, Jan van der Kruk, Thuy Huu Nguyen, Gina Lopez, Sabine Julia Seidel, Frank Ewert, Anja Klotzsche, Andrea Schnepf. Unrevealing subsoil processes in the selhausen minirhizotron facilities: Comprehensive insights into the soil-plant continuum with a new unique dataset. Poster at *AGU Fall Meeting*, AGU23, San Francisco, USA, 11 Dec 2023 - 15 Dec 2023. <https://juser.fz-juelich.de/record/1020308>.

Agriculture faces enormous challenges due to climate change that require innovation in crop production. A comprehensive understanding of whole plant responses to a changing environment is the key to maintain yield and improve sustainable crop production. Many studies focus on shoot development and its response to environment, but due to its inaccessibility, little attention is paid to root system development and the subsoil processes and soil conditions that influence it. However, this information is indispensable to understand crop reactions to climate change. The minirhizotron facilities in Selhausen (Germany) were constructed within the TERENO test site Selhausen in the Lower Rhine valley, to enable non-invasive long-term studies of the soil-plant continuum on two different soils under the same climate conditions. A unique set-up of sensors provides detailed information about soil water content and potential, soil temperature and root development with a high spatial and temporal resolution over entire growing seasons and for various agronomic treatments. Vegetation measurements, such as biomass, transpiration fluxes and assimilation rates are performed additionally. A continuous development of technology and analysis has improved the processing, transfer and accessibility of this data. Static sensors are continuously monitoring the soil water status. Dynamic sensors enable the measurement of spatial soil water content variations and the observation of root growth through 7m long tubes installed at several depth. An in-house developed camera-system is used for acquiring images that are analyzed with a deep neural network integrated pipeline to extract root features.

The measurements cover five years of wheat and maize trials, including various treatments differing in the magnitude of water stress, sowing density, planting time, and crop mixture experiments. To our knowledge, this is the most comprehensive dataset including crop, water and soil related information over time. The data are freely available and can be used to develop, calibrate, and validate models of the soil-plant continuum across different scales, including soil processes, root development and root water uptake models. The data can be helpful for agronomists, ecologists or breeders to cope with the challenges of climate change.

Appendix H: Functional-structural plant modelling based on experimental data reveals that soil phosphorus status influences root system conductance.

From: **Felix Maximilian Bauer**, Mona Giraud, Dirk Norbert Helmrich, Guillaume Lobet, Andrea Schnepf. Functional-structural plant modelling based on experimental data reveals that soil phosphorus status influences root system conductance. Presentation at *International Society of Root Research 12th International Symposium* (ISRR 2024), Leipzig, Germany, 2 Jun 2024 - 7 Jun 2024.

Content Snapshot

Dynamic functional-structural modeling of *Zea mays* under phosphorus deficiency, parameterized from experimental data, showed that total root system conductance does not differ between low to mild phosphorus deficient plants, but between fully fertilized and deficient plants.

H-1 Background

The exploitation of natural resources and climate change pose new challenges to agriculture. The supply of phosphorus (P), a vital nutrient derived from finite mined resources, will decrease in the future. Climate change will also reduce water availability in most regions of the globe. It is therefore crucial to gain insight on how decreasing P availability influences crops architecture and thereby their functional traits, such as their root systems' water uptake capability.

H-2 Objective

We investigate the structural and functional responses of *Zea mays* to varying P fertilization levels with respect to the water uptake capability of the root system.

H-3 Material and Methods

We conducted a systematic investigation across a spectrum of P availability, from severe deficiency to full sufficiency with a greenhouse rhizotron setup. As basis we used a strongly P deficient field soil from a long-term fertilization experiment. Detailed architectural parameters of the plant's shoot and root system were obtained from a neural network analyzed image time series. We combined these data with anatomical root data to parameterize the CPlantBox model, enabling dynamic growth simulations and root system conductance (K_{rs}) calculation under the distinct P supply regimes.

H-4 Results and Discussion

Our analysis and structural modeling show a reorganization in root system architecture characterized by an increased seminal rooting and reduced basal root thickness with declining P availability, leading to a linear increase in root system volume. Interestingly, the modeling revealed that only plants with optimal P availability sustained a high K_{rs} , while all other P levels led to a significantly lower K_{rs} , regardless of whether it is a light or severe P deficiency. The model outcome also underscored that targeted root systems architectural and anatomical traits are more critical for estimating its function than merely considering the root system's total size.

Acknowledgements

The journey has come to an end, and now, as I promised in the beginning, it is time to express my gratitude to those who have supported me along the way. Their guidance, encouragement, and contributions have been instrumental in bringing this thesis to life, and I am genuinely grateful for the invaluable roles they have played in this endeavor.

My deepest gratitude goes to Prof. Dr. Andrea Schnepf and Prof. Dr. Guillaume Lobet, for making this doctoral project possible and for giving me the opportunity to complete it. I am very grateful for their guidance, support, motivation, persistent encouragement and professional and personal leadership. I would like to extend my gratitude to Prof. Dr. Gabriel Schaaf for his invaluable efforts in reading and examining this doctoral thesis.

Furthermore, I would like to thank Prof. Dr. Harry Vereecken and Prof. Dr. Jan Vanderborght for their scientific guidance and insights throughout this project.

This work was been funded by the German Research Foundation under Germany's Excellence Strategy, EXC-2070 - 390732324 - PhenoRob. I am very grateful to have been part of this Cluster of Excellence and the contribution it made to my doctoral project through the financial support of workshops, seminars, travel opportunities, and the building of a scientific community to exchange with peers and to make lasting connections.

I acknowledge the support of the German Federal Ministry of Education and Research (BMBF) in the framework of the funding initiative "Plant roots and soil ecosystems, significance of the rhizosphere for the bio-economy" (Rhizo4Bio), subproject CROP (ref. FKZ 031B0909A). Furthermore, I thank the Terrestrial Environmental Observatories (TERENO) for support.

I thank Prof. Dr. Xavier Draye for the early access to the Manneback-cluster of the UCLouvain, Dr. Abraham Smith for the help with RootPainter and Prof. Dr. Larry York for the help with RhizoVision Explorer. Further, I thank Prof. Dr. Kerstin Nagel for providing the greenhouse infrastructure, Anna Galinski for providing assistance with the experiments and Marion Deichmann and Matthias Claß for the help with the analysis of the soil samples. I thank Springer Nature and Prof. Dr. Frank Hochholdinger for the re-use permission of Figures.

I am very grateful for the time at the Forschungszentrum Jülich and the opportunity to meet other doctoral students and scientists. I would especially like to thank the ROSI team with Mona Giraud, Dirk Norbert Baker, Dr. Juan Carlos Baca Cabrera, Dr. Magdlena Landl, Dr. Tobias Selzner, Ullah Sibghat, Larissa Reineccius, Osman Mustafa, Dr. Sathyan Rao, and Dr. Daniel Leitner.

Furthermore, I thank Tim Spieker, Normen Hermes, Moritz Harings, Christoph Tempelmann, Anika Sommerfeld-Vreux, and Giulian Katzenstein for the cooperation, support and maintenance of the minirhizotron facilities and the student assistants Lisa Dollhäuble, Yannick Preim, Julia Schild, Nastasia Kramer, Neil Sommer, and Julia Hack for their tremendous effort. I want to express my sincere gratitude to Dr. Lena Lärm, Sophia Schiebel, and Prof. Dr. Anja Klotzsche for their invaluable support and collaboration.

An additional shoutout to my brother Tim, my grandparents, my friends, and my partner for their endless cheering, questionable advice, and ensuring I did not lose my sanity throughout this journey.

Finally, I would like to express my heartfelt gratitude to my parents, Susanne and Armin, for their unwavering support and for laying the foundation for my journey.

Jülich
30.08.2024

Felix Maximilian Bauer

Bibliography

- Ahmed, M. A., Zarebanadkouki, M., Meunier, F., Javaux, M., Kaestner, A., and Carminati, A. (2018). Root type matters: measurement of water uptake by seminal, crown, and lateral roots in maize. *Journal of Experimental Botany*, 69(5):1199–1206.
- Aidoo, M. K., Sherman, T., Ephrath, J. E., Fait, A., Rachmilevitch, S., and Lazarovitch, N. (2018). Grafting as a method to increase the tolerance response of bell pepper to extreme temperatures. *Vadose Zone Journal*, 17(1):170006.
- Ajmera, I., Henry, A., Radanielson, A. M., Klein, S. P., Ianevski, A., Bennett, M. J., Band, L. R., and Lynch, J. P. (2022). Integrated root phenotypes for improved rice performance under low nitrogen availability. *Plant, Cell & Environment*, 45(3):805–822.
- Alexandratos, N. and Bruinsma, J. (2012). World agriculture towards 2030/2050: the 2012 revision. *ESA Working Papers*.
- Alzubaidi, L., Zhang, J., Humaidi, A. J., Al-Dujaili, A., Duan, Y., Al-Shamma, O., Santamaría, J., Fadhel, M. A., Al-Amidie, M., and Farhan, L. (2021). Review of deep learning: concepts, CNN architectures, challenges, applications, future directions. *Journal of Big Data*, 8(1).
- Araus, J. L. and Cairns, J. E. (2014). Field high-throughput phenotyping: the new crop breeding frontier. *Trends in Plant Science*, 19(1):52–61.
- Armengaud, P., Zambaux, K., Hills, A., Sulpice, R., Pattison, R. J., Blatt, M. R., and Amtmann, A. (2009). Ez-rhizo: integrated software for the fast and accurate measurement of root system architecture. *The Plant Journal*, 57(5):945–956.
- Aroca, R., Porcel, R., and Ruiz-Lozano, J. M. (2011). Regulation of root water uptake under abiotic stress conditions. *Journal of Experimental Botany*, 63(1):43–57.

- Atkinson, D., Smit, A. L., Bengough, A. G., Engels, C., van Noordwijk, M., Pellerin, S., and van de Geijn, S. C. (2000). *Root Characteristics: Why and What to Measure*. Springer Berlin Heidelberg, Berlin, Heidelberg.
- Atkinson, J. A., Pound, M. P., Bennett, M. J., and Wells, D. M. (2019). Uncovering the hidden half of plants using new advances in root phenotyping. *Current Opinion in Biotechnology*, 55:1–8.
- Atta, A. A., Morgan, K. T., and Kadyampakeni, D. M. (2022). Spatial and temporal nutrient dynamics and water management of huanglongbing-affected mature citrus trees on florida sandy soils. *Sustainability*, 14(12).
- Baca Cabrera, J. C., Vanderborght, J., Couvreur, V., Behrend, D., Gaiser, T., Nguyen, T. H., and Lobet, G. (2024). Root hydraulic properties: An exploration of their variability across scales. *Plant Direct*, 8(4):e582.
- Baker, D., Bauer, F., Schnepf, A., Scharr, H., Riedel, M., Göbbert, J. H., and Hvannberg, E. (2024a). Adapting Agricultural Virtual Environments in Game Engines to Improve HPC Accessibility. In *Communications in Computer and Information Science*, pages 1–15. nordic e-Infrastructure Collaboration Conference, Tallinn (Estonia), 27 May 2024 - 29 May 2024, Springer. Preprint.
- Baker, D. N., Bauer, F. M., Giraud, M., Schnepf, A., Göbbert, J. H., Scharr, H., Hvannberg, E. P., and Riedel, M. (2023). A scalable pipeline to create synthetic datasets from functional–structural plant models for deep learning. *in silico Plants*, 6(1):diad022.
- Baker, D. N., Selzner, T., Göbbert, J. H., Scharr, H., Riedel, M., Hvannberg, E. P., Schnepf, A., and Zielasko, D. (2024b). Vroot: An xr-based application for manual root system architecture reconstruction. *bioRxiv*. Preprint.
- Balestrini, R., Sillo, F., Boussageon, R., Wipf, D., and Courty, P. E. (2024). The hidden side of interaction: microbes and roots get together to improve plant resilience. *Journal of Plant Interactions*, 19(1).
- Banet, T., Smith, A. G., McGrail, R., McNear Jr., D. H., and Poffenbarger, H. (2024). Toward improved image-based root phenotyping: Handling temporal and cross-site domain shifts in crop root segmentation models. *The Plant Phenome Journal*, 7(1):e20094.
- Bauer, F. M., Baker, D. N., Giraud, M., Baca Cabrera, J. C., Vanderborght, J., Lobet, G., and Schnepf, A. (2024). Root system architecture reorganization under decreasing soil phosphorus lowers root system conductance of zea mays. *bioRxiv*. Preprint.
- Bauer, F. M., Lärm, L., Morandage, S., Lobet, G., Vanderborght, J., Vereecken, H., and Schnepf, A. (2022). Development and validation of a deep learning based automated minirhizotron image analysis pipeline. *Plant Phenomics*, 2022.

- Bauer, J., Weihermüller, L., Huisman, J. A., Herbst, M., Graf, A., Séquaris, J. M., and Vereecken, H. (2011). Inverse determination of heterotrophic soil respiration response to temperature and water content under field conditions. *Biogeochemistry*, 108(1-3):119–134.
- Bechmann, M., Schneider, C., Carminati, A., Vetterlein, D., Attinger, S., and Hildebrandt, A. (2014). Parameterizing complex root water uptake models—the arrangement of root hydraulic properties within the root architecture affects dynamics and efficiency of root water uptake. *Hydrology & Earth System Sciences Discussions*, 11(1).
- Berrigan, E. M., Wang, L., Carrillo, H., Echevoyen, K., Kappes, M., Torres, J., Ai-Perreira, A., McCoy, E., Shane, E., Copeland, C. D., Ragel, L., Georgousakis, C., Lee, S., Reynolds, D., Talgo, A., Gonzalez, J., Zhang, L., Rajurkar, A. B., Ruiz, M., Daniels, E., Maree, L., Pariyar, S., Busch, W., and Pereira, T. D. (2024). Fast and efficient root phenotyping via pose estimation. *Plant Phenomics*, 6:0175.
- Beudez, N., Doussan, C., Lefeuvre-Mesgouez, G., and Mesgouez, A. (2013). Influence of three root spatial arrangement on soil water flow and uptake. results from an explicit and an equivalent, upscaled, model. *Procedia Environmental Sciences*, 19:37–46.
- Bianco, M. D. and Kepinski, S. (2018). Building a future with root architecture. *Journal of Experimental Botany*, 69(22):5319–5323.
- Binder, D., Sander, D. H., and Walters, D. (2000). Maize response to time of nitrogen application as affected by level of nitrogen deficiency. *Agronomy Journal*, 92:1228–1236.
- Blanchy, G., Deroo, W., De Swaef, T., Lootens, P., Quataert, P., Roldán-Ruíz, I., and Garré, S. (2024). Closing the phenotyping gap with non-invasive below-ground field phenotyping. *EGUsphere*, 2024:1–30.
- Boesch, D. F., Brinsfield, R. B., and Magnien, R. E. (2001). Chesapeake bay eutrophication: Scientific understanding, ecosystem restoration, and challenges for agriculture. *Journal of Environmental Quality*, 30(2):303–320.
- Bogena, H., Montzka, C., Huisman, J., Graf, A., Schmidt, M., Stockinger, M., von Hebel, C., Hendricks-Franssen, H., van der Kruk, J., Tappe, W., Lücke, A., Baatz, R., Bol, R., Groh, J., Pütz, T., Jakobi, J., Kunkel, R., Sorg, J., and Vereecken, H. (2018). The TERENO-rur hydrological observatory: A multiscale multi-compartment research platform for the advancement of hydrological science. *Vadose Zone Journal*, 17(1):180055.
- Boote, K. J., Jones, J. W., and Hoogenboom, G. (2021). Incorporating realistic trait physiology into crop growth models to support genetic improvement. *in silico Plants*, 3(1):diab002.

- Borch, K., Bouma, T., Lynch, J., and Brown, K. (1999). Ethylene: a regulator of root architectural responses to soil phosphorus availability. *Plant, Cell & Environment*, 22(4):425–431.
- Bot, J. L., Serra, V., Fabre, J., Draye, X., Adamowicz, S., and Pagès, L. (2009). DART: a software to analyse root system architecture and development from captured images. *Plant and Soil*, 326(1-2):261–273.
- Branding, J., von Hoersten, D., Wegener, J. K., Boeckmann, E., and Hartung, E. (2023). Towards noise robust acoustic insect detection: from the lab to the greenhouse. *Künstliche Intelligenz*, 37(2-4, SI):157–173.
- Broggi, C., Huisman, J., Pätzold, S., von Hebel, C., Weihermüller, L., Kaufmann, M., van der Kruk, J., and Vereecken, H. (2019). Large-scale soil mapping using multi-configuration EMI and supervised image classification. *Geoderma*, 335:133–148.
- Brunel-Muguet, S., Pellerin, S., and Mollie, A. B. (2014). Impact of early growth traits on further genotypic performance during the vegetative growth of maize (*zea mays* l.) in response to phosphorus (p) availability. *Australian Journal of Crop Science*, 8:402–412.
- Cai, G., Morandage, S., Vanderborght, J., Schnepf, A., and Vereecken, H. (2018a). Erratum to “construction of minirhizotron facilities for investigating root zone processes” and “parameterization of root water uptake models considering dynamic root distributions and water uptake compensation”. *Vadose Zone Journal*, 17(1):170201.
- Cai, G., Vanderborght, J., Couvreur, V., Mboh, C. M., and Vereecken, H. (2017). Parameterization of root water uptake models considering dynamic root distributions and water uptake compensation. *Vadose Zone Journal*.
- Cai, G., Vanderborght, J., Couvreur, V., Mboh, C. M., and Vereecken, H. (2018b). Parameterization of root water uptake models considering dynamic root distributions and water uptake compensation. *Vadose Zone Journal*, 17(1):160125.
- Cai, G., Vanderborght, J., Klotzsche, A., van der Kruk, J., Neumann, J., Hermes, N., and Vereecken, H. (2016a). Construction of minirhizotron facilities for investigating root zone processes. *Vadose Zone Journal*, 15(9):vzj2016.05.0043.
- Cai, G., Vanderborght, J., Klotzsche, A., van der Kruk, J., Neumann, J., Hermes, N., and Vereecken, H. (2016b). Construction of minirhizotron facilities for investigating root zone processes. *Vadose Zone Journal*, 15(9).
- Carpenter, S. R., Caraco, N. F., Correll, D. L., Howarth, R. W., Sharpley, A. N., and Smith, V. H. (1998). Nonpoint pollution of surface waters with phosphorus and nitrogen. *Ecological Applications*, 8:559.
- Chandrasoma, J. M., Masters, M. D., Allen, D., McCoy, S., Black, C. K., von Haden, A. C., Blanc-Betes, E., Kantola, I. B., Gomez-Casanovas, N., Yang,

- W. H., Leakey, A. D., and DeLucia, E. H. (2023). Root Demographics of Three Bioenergy Crops: How Energy Sorghum Compares to Maize and Miscanthus. In *AGU Fall Meeting Abstracts*, volume 2023, pages B43F–2619.
- Chaturvedi, V., Hejazi, M., Edmonds, J., Clarke, L., Kyle, P., Davies, E., and Wise, M. (2015). Climate mitigation policy implications for global irrigation water demand. *Mitigation and Adaptation Strategies for Global Change*, 20(3):389–407.
- Chenu, K., Chapman, S. C., Hammer, G. L., McLean, G., Salah, H. B. H., and Tardieu, F. (2008). Short-term responses of leaf growth rate to water deficit scale up to whole-plant and crop levels: an integrated modelling approach in maize. *Plant, Cell & Environment*, 31(3):378–391.
- Chimungu, J., Brown, K., and Lynch, J. (2014). Large root cortical cell size improves drought tolerance in maize. *Plant Physiology*, 166:2166 – 2178.
- Chun, L., Mi, G., Li, J., Chen, F., and Zhang, F. (2005). Genetic analysis of maize root characteristics in response to low nitrogen stress. *Plant and Soil*, 276:369–382.
- Cieslak, M., Seleznyova, A., Prusinkiewicz, P., and Hanan, J. (2011). Towards aspect-oriented functional–structural plant modelling. *Annals of Botany*, 108(6):1025–41.
- Clark, H. P., Smith, A. G., Fletcher, D. M., Larsson, A. I., Jaspars, M., and De Clippele, L. H. (2024). New interactive machine learning tool for marine image analysis. *Royal Society Open Science*, 11(5).
- Cordell, D., Drangert, J., and White, S. W. (2009). The story of phosphorus: global food security and food for thought. *Global Environmental Change*, 19:292–305.
- Cordell, D. and White, S. W. (2011). Peak phosphorus: clarifying the key issues of a vigorous debate about long-term phosphorus security. *Sustainability*, 3:2027–2049.
- Cordell, D. and White, S. W. (2013). Sustainable phosphorus measures: strategies and technologies for achieving phosphorus security. *Agronomy*, 3:86–116.
- Couvreur, V., Faget, M., Lobet, G., Javaux, M., Chaumont, F., and Draye, X. (2018). Going with the flow: multiscale insights into the composite nature of water transport in roots. *Plant Physiology*, 178(4):1689–1703.
- Couvreur, V., Vanderborght, J., and Javaux, M. (2012). A simple three-dimensional macroscopic root water uptake model based on the hydraulic architecture approach. *Hydrology and Earth System Sciences*, 16(8):2957–2971.
- Crawley, M. J. (2009). *Plant ecology*. John Wiley & Sons.

- Cseresnyés, I., Kelemen, B., Takács, T., Füzy, A., Kovács, R., Megyeri, M., Parádi, I., and Mikó, P. (2021). Electrical capacitance versus minirhizotron technique: A study of root dynamics in wheat–pea intercrops. *Plants*, 10(10).
- Das, A., Schneider, H., Burrige, J., Ascanio, A. K. M., Wojciechowski, T., Topp, C. N., Lynch, J. P., Weitz, J. S., and Bucksch, A. (2015). Digital imaging of root traits (DIRT): a high-throughput computing and collaboration platform for field-based root phenomics. *Plant Methods*, 11(1).
- De Bauw, P., Mai, T. H., Schnepf, A., Merckx, R., Smolders, E., and Vanderborght, J. (2020). A functional–structural model of upland rice systems reveals the importance of laterals and growing root tips for phosphate uptake from wet and dry soils. *Annals of Botany*, 126(4):789–806.
- de Moraes, M. T., Debiase, H., Franchini, J. C., Bonetti, J. d. A., Levien, R., Schnepf, A., and Leitner, D. (2019). Mechanical and hydric stress effects on maize root system development at different soil compaction levels. *Frontiers in Plant Science*, 10.
- Defrenne, C. E., Childs, J., Fernandez, C. W., Taggart, M., Nettles, W. R., Allen, M. F., Hanson, P. J., and Iversen, C. M. (2021). High-resolution minirhizotrons advance our understanding of root–fungal dynamics in an experimentally warmed peatland. *Plants, People, Planet*, 3(5):640–652.
- Dejong, T., Silva, D. D., Vos, J., and Escobar-Gutiérrez, A. (2011). Using functional–structural plant models to study, understand and integrate plant development and ecophysiology. *Annals of Botany*, 108(6):987–9.
- Delory, B. M., Weidlich, E. W., Meder, L., Lütje, A., van Duijnen, R., Weidlich, R., and Temperton, V. M. (2017). Accuracy and bias of methods used for root length measurements in functional root research. *Methods in Ecology and Evolution*, 8(11):1594–1606.
- Dorigo, W., Wagner, W., Albergel, C., Albrecht, F., Balsamo, G., Brocca, L., Chung, D., Ertl, M., Forkel, M., Gruber, A., Haas, E., Hamer, P. D., Hirschi, M., Ikonen, J., de Jeu, R., Kidd, R., Lahoz, W., Liu, Y. Y., Miralles, D., Mistelbauer, T., Nicolai-Shaw, N., Parinussa, R., Pratola, C., Reimer, C., van der Schalie, R., Seneviratne, S. I., Smolander, T., and Lecomte, P. (2017). Esa cci soil moisture for improved earth system understanding: State-of-the art and future directions. *Remote Sensing of Environment*, 203:185–215.
- Doussan, C., Pierret, A., Garrigues, E., and Pages, L. (2006). Water uptake by plant roots:: Ii -: Modelling of water transfer in the soil root-system with explicit account of flow within the root system -: Comparison with experiments. *Plant and Soil*, 283(1-2):99–117.
- Doussan, C., Vercambre, G., and Pagè, L. (1998). Modelling of the hydraulic architecture of root systems: An integrated approach to water absorption—distribution of axial and radial conductances in maize. *Annals of Botany*, 81(2):225–232.

- Dowdy, R., Smucker, A., Dolan, M., and Ferguson, J. (1998). Automated image analysis for separating plant roots from soil debris elutriated from soil core. *Plant and Soil*, 200(1):91–94.
- Drouet, J.-L. and Pagès, L. (2003). Graal: a model of growth, architecture and carbon allocation during the vegetative phase of the whole maize plant: Model description and parameterisation. *Ecological Modelling*, 165(2):147–173.
- Du, Q., Wang, K., Zou, C., Xu, C., and Li, W.-X. (2018). The PILNCR1-miR399 Regulatory Module Is Important for Low Phosphate Tolerance in Maize. *Plant Physiology*, 177(4):1743–1753.
- Essel, B., Abaidoo, R., Opoku, A., and Ewusi-Mensah, N. (2020). Economically optimal rate for nutrient application to maize in the semi-deciduous forest zone of Ghana. *Journal of Soil Science and Plant Nutrition*, 20:1703 – 1713.
- Falk, K. G., Jubery, T. Z., Mirnezami, V. S., Parmley, K. A., Sarkar, S., Singh, A., Ganapathysubramanian, B., and Singh, A. K. (2020). Computer vision and machine learning enabled soybean root phenotyping pipeline. *Plant Methods*, 16(1).
- Fan, M., Bai, R., Zhao, X., and Zhang, J. (2007). Aerenchyma formed under phosphorus deficiency contributes to the reduced root hydraulic conductivity in maize roots. *Journal of Integrative Plant Biology*, 49(5):598–604.
- FAO (2011). *Natural Capital Impacts in Agriculture*. Food and Agriculture Organization of the United Nations.
- FAO (2015). *Climate change, water and food security*. Food and Agriculture Organization of the United Nations.
- FAOSTAT (2024a). Land, inputs and sustainability / fertilizers by nutrient - metadata. <https://www.fao.org/faostat/en/data/QCL/metadata>.
- FAOSTAT (2024b). Production / crops and livestock products. <https://www.fao.org/faostat/en/data/QCL/metadata>.
- Fiorani, F. and Schurr, U. (2013). Future scenarios for plant phenotyping. *Annual review of plant biology*, 64:267–91.
- Fourcaud, T., Zhang, X., Stokes, A., Lambers, H., and Körner, C. (2008). Plant Growth Modelling and Applications: The Increasing Importance of Plant Architecture in Growth Models. *Annals of Botany*, 101(8):1053–1063.
- Frensch, J. and Steudle, E. (1989). Axial and radial hydraulic resistance to roots of maize (*Zea mays* L.). *Plant Physiology*, 91(2):719–726.
- Freundl, E., Steudle, E., and Hartung, W. (2000). Apoplastic transport of abscisic acid through roots of maize: effect of the exodermis. *Planta*, 210(2):222–231.

- Fry, E. L., Evans, A., Sturrock, C. J., Bullock, J. M., and Bardgett, R. D. (2018). Root architecture governs plasticity in response to drought. *Plant and Soil*, 433:189–200.
- Gaggion, N., Ariel, F., Daric, V., Lambert, E., Legendre, S., Roulé, T., Camoirano, A., Milone, D. H., Crespi, M., Blein, T., and Ferrante, E. (2021). ChronoRoot: High-throughput phenotyping by deep segmentation networks reveals novel temporal parameters of plant root system architecture. *GigaScience*, 10(7):giab052.
- Galkovskyi, T., Mileyko, Y., Bucksch, A., Moore, B., Symonova, O., Price, C. A., Topp, C. N., Iyer-Pascuzzi, A. S., Zurek, P. R., Fang, S., Harer, J., Benfey, P. N., and Weitz, J. S. (2012). GiA roots: software for the high throughput analysis of plant root system architecture. *BMC Plant Biology*, 12(1):116.
- Gao, K., Chen, F., Yuan, L., and Mi, G. (2014). Cell production and expansion in the primary root of maize in response to low-nitrogen stress. *Journal of Integrative Agriculture*, 13:2508–2517.
- Gao, Y. and Lynch, J. P. (2016). Reduced crown root number improves water acquisition under water deficit stress in maize (*Zea mays* L.). *Journal of Experimental Botany*, 67(15):4545–4557.
- Garré, S., Pagès, L., Laloy, E., Javaux, M., Vanderborght, J., and Vereecken, H. (2012). Parameterizing a dynamic architectural model of the root system of spring barley from minirhizotron data. *Vadose Zone Journal*, 11(4):vzj2011.0179.
- Gehan, M. A., Fahlgren, N., Abbasi, A., Berry, J. C., Callen, S. T., Chavez, L., Doust, A. N., Feldman, M. J., Gilbert, K. B., Hodge, J. G., et al. (2017). Plantcv v2: Image analysis software for high-throughput plant phenotyping. *PeerJ*, 5:e4088.
- Ghezzehei, T. A. (2008). Errors in determination of soil water content using time domain reflectometry caused by soil compaction around waveguides. *Water Resources Research*, 44(8).
- Gillert, A., Peters, B., von Lukas, U. F., Kreyling, J., and Blume-Werry, G. (2023). Tracking growth and decay of plant roots in minirhizotron images. In *2023 IEEE/CVF Winter Conference on Applications of Computer Vision (WACV)*, IEEE Winter Conference on Applications of Computer Vision, pages 3688–3697. IEEE; CVF; IEEE Comp Soc. 23rd IEEE/CVF Winter Conference on Applications of Computer Vision (WACV), Waikoloa, HI, JAN 03-07, 2023.
- Giraud, M., Gall, S. L., Harings, M., Javaux, M., Leitner, D., Meunier, F., Rothfuss, Y., van Dusschoten, D., Vanderborght, J., Vereecken, H., Lobet, G., and Schnepf, A. (2023). CPlantBox: a fully coupled modelling platform for the water and carbon fluxes in the soil–plant–atmosphere continuum. *in silico Plants*, 5(2):diad009.

- Godin, C. and Caraglio, Y. (1998). A multiscale model of plant topological structures. *Journal of Theoretical Biology*, 191(1):1–46.
- Godin, C. and Sinoquet, H. (2005). Functional–structural plant modelling. *New Phytologist*, 166(3):705–708.
- Gosling, S. N. and Arnell, N. W. (2013). A global assessment of the impact of climate change on water scarcity. *Climatic Change*, 134:371–385.
- Gruber, A., Scanlon, T., van der Schalie, R., Wagner, W., and Dorigo, W. (2019). Evolution of the esa cci soil moisture climate data records and their underlying merging methodology. *Earth System Science Data*, 11(2):717–739.
- Guo, L., Chen, J., Cui, X., Fan, B., and Lin, H. (2013). Application of ground penetrating radar for coarse root detection and quantification: a review. *Plant and Soil*, 362(1-2):1–23.
- Hampel, F. R. (1974). The influence curve and its role in robust estimation. *Journal of the American Statistical Association*, 69(346):383–393.
- Han, E., Smith, A. G., Kemper, R., White, R., Kirkegaard, J. A., Thorup-Kristensen, K., and Athmann, M. (2021). Digging roots is easier with AI. *Journal of Experimental Botany*, 72(13):4680–4690.
- Helin, J. and Weikard, H.-P. (2019). A model for estimating phosphorus requirements of world food production. *Agricultural Systems*, 176:102666.
- Heuer, S., Gaxiola, R., Schilling, R., Herrera-Estrella, L., Lopez-Arredondo, D., Wissuwa, M., Delhaize, E., and Rouached, H. (2017). Improving phosphorus use efficiency: a complex trait with emerging opportunities. *Plant Journal*, 90(5):868–885.
- Heydari, M. M., Brook, R. M., and Jones, D. L. (2019). The role of phosphorus sources on root diameter, root length and root dry matter of barley (*hordeum vulgare* l.). *Journal of Plant Nutrition*, 42(1):1–15.
- Heymans, A., Couvreur, V., LaRue, T., Paez-Garcia, A., and Lobet, G. (2020). Granar, a computational tool to better understand the functional importance of monocotyledon root anatomy. *Plant Physiology*, 182(2):707–720.
- Heymans, A., Couvreur, V., and Lobet, G. (2021). Combining cross-section images and modeling tools to create high-resolution root system hydraulic atlases in *zea mays*. *Plant Direct*, 5(7):e00290.
- Hochholdinger, F. (2009). *The Maize Root System: Morphology, Anatomy, and Genetics*, pages 145–160. Springer New York, New York, NY.
- Hose, E., Steudle, E., and Hartung, W. (2000). Abscisic acid and hydraulic conductivity of maize roots: a study using cell-and root-pressure probes. *Planta*, 211:874–882.

- Hu, T., Kang, S., Li, F., and Zhang, J. (2011). Effects of partial root-zone irrigation on hydraulic conductivity in the soil-root system of maize plants. *Journal of Experimental Botany*, 62(12):4163–4172.
- Huang, Y., Yan, J., Zhang, Y., Ye, W., Zhang, C., Gao, P., and Lv, X. (2023). Automatic segmentation of cotton roots in high-resolution minirhizotron images based on improved ocrnet. *Frontiers in Plant Science*, 14.
- Huisman, J., Hubbard, S., Redman, J., and Annan, A. (2003). Measuring soil water content with ground penetrating radar. *Vadose Zone Journal*, 2(4):476–491.
- Hunter, J. D. (2007). Matplotlib: A 2d graphics environment. *Computing in Science & Engineering*, 9(3):90–95.
- Hussain, M. Z., Hamilton, S. K., Robertson, G. P., and Basso, B. (2021). Phosphorus availability and leaching losses in annual and perennial cropping systems in an upper us midwest landscape. *Scientific Reports*, 11(1).
- Ingram, K. T. and Leers, G. A. (2001). Software for measuring root characters from digital images. *Agronomy Journal*, 93(4):918–922.
- Jadoon, K. Z., Weihermüller, L., Scharnagl, B., Kowalsky, M. B., Bechtold, M., Hubbard, S. S., Vereecken, H., and Lambot, S. (2012). Estimation of soil hydraulic parameters in the field by integrated hydrogeophysical inversion of time-lapse ground-penetrating radar data. *Vadose Zone Journal*, 11(4).
- Janiesch, C., Zschech, P., and Heinrich, K. (2021). Machine learning and deep learning. *Electronic Markets*.
- Janott, M., Gayler, S., Gessler, A., Javaux, M., Klier, C., and Priesack, E. (2011). A one-dimensional model of water flow in soil-plant systems based on plant architecture. *Plant and Soil*, 341(1-2):233–256.
- Javaux, M., Schröder, T., Vanderborght, J., and Vereecken, H. (2008). Use of a three-dimensional detailed modeling approach for predicting root water uptake. *Vadose Zone Journal*, 7(3):1079–1088.
- Johannsen, W. (1911). The genotype conception of heredity. *The American Naturalist*, 45(531):129–159.
- Johnson, M., Tingey, D., Phillips, D., and Storm, M. (2001). Advancing fine root research with minirhizotrons. *Environmental and Experimental Botany*, 45(3):263–289.
- Jol, H. M. (2008). *Ground penetrating radar theory and applications*. elsevier.
- Jorda, H., Huber, K., Kunkel, A., Vanderborght, J., Javaux, M., Oberdörster, C., Hammel, K., and Schnepf, A. (2021). Mechanistic modeling of pesticide uptake with a 3d plant architecture model. *Environmental Science and Pollution Research*, 28(39):55678–55689.

- Joslin, J. D., Gaudinski, J. B., Torn, M. S., Riley, W. J., and Hanson, P. J. (2006). Fine-root turnover patterns and their relationship to root diameter and soil depth in a 14c-labeled hardwood forest. *New Phytologist*, 172(3):523–535.
- Kaeppler, S. M., Parke, J. L., Mueller, S. M., Senior, L., Stuber, C., and Tracy, W. F. (2000). Variation among maize inbred lines and detection of quantitative trait loci for growth at low phosphorus and responsiveness to arbuscular mycorrhizal fungi. *Crop Science*, 40(2):358–364.
- Kamilaris, A. and Prenafeta-Boldú, F. X. (2018). A review of the use of convolutional neural networks in agriculture. *The Journal of Agricultural Science*, 156(3):312–322.
- Keller, K., Kirchgessner, N., Khanna, R., Siegwart, R., Walter, A., and Aasen, H. (2018). Soybean leaf coverage estimation with machine learning and thresholding algorithms for field phenotyping. In *Proceedings of the British Machine Vision Conference, Newcastle, UK*, pages 3–6.
- Khamis, S., Lamaze, T., Lemoine, Y., and Foyer, C. (1990). Adaptation of the photosynthetic apparatus in maize leaves as a result of nitrogen limitation : Relationships between electron transport and carbon assimilation. *Plant Physiology*, 94 3:1436–43.
- Khoroshevsky, F., Zhou, K., Chemweno, S., Edan, Y., Bar-Hillel, A., Hadar, O., Rewald, B., Baykalov, P., Ephrath, J. E., and Lazarovitch, N. (2024). Automatic root length estimation from images acquired in situ without segmentation. *Plant Phenomics*, 6.
- Klein, S. P., Schneider, H. M., Perkins, A. C., Brown, K. M., and Lynch, J. P. (2020). Multiple Integrated Root Phenotypes Are Associated with Improved Drought Tolerance. *Plant Physiology*, 183(3):1011–1025.
- Klotzsche, A., Lärm, L., Vanderborght, J., Cai, G., Morandage, S., Zörner, M., Vereecken, H., and Kruk, J. (2019). Monitoring soil water content using time-lapse horizontal borehole gpr data at the field-plot scale. *Vadose Zone Journal*, 18.
- Koch, T., Gläser, D., Weishaupt, K., Ackermann, S., Beck, M., Becker, B., Burbulla, S., Class, H., Coltman, E., Emmert, S., Fetzer, T., Grüninger, C., Heck, K., Hommel, J., Kurz, T., Lipp, M., Mohammadi, F., Scherrer, S., Schneider, M., Seitz, G., Stadler, L., Utz, M., Weinhardt, F., and Flemisch, B. (2021). Dumux 3 – an open-source simulator for solving flow and transport problems in porous media with a focus on model coupling. *Computers & Mathematics with Applications*, 81:423–443. Development and Application of Open-source Software for Problems with Numerical PDEs.
- Koppelaar, R. and Weikard, H. (2013). Assessing phosphate rock depletion and phosphorus recycling options. *Global Environmental Change*, 23(6):1454–1466.

- Krizhevsky, A., Sutskever, I., and Hinton, G. E. (2012). Imagenet classification with deep convolutional neural networks. *Advances in neural information processing systems*, 25:1097–1105.
- Kurth, W. (1994). Morphological models of plant growth: possibilities and ecological relevance. *Ecological Modelling*, 75:299–308.
- Landl, M., Phalempin, M., Schlüter, S., Vetterlein, D., Vanderborght, J., Kroener, E., and Schnepf, A. (2021). Modeling the impact of rhizosphere bulk density and mucilage gradients on root water uptake. *Frontiers in Agronomy*, 3.
- Landl, M., Schnepf, A., Uteau, D., Peth, S., Athmann, M., Kautz, T., Perkons, U., Vereecken, H., and Vanderborght, J. (2019). Modeling the impact of biopores on root growth and root water uptake. *Vadose Zone Journal*, 18(1):1–20.
- Lärm, L., Bauer, F. M., Hermes, N., van der Kruk, J., Vereecken, H., Vanderborght, J., Nguyen, T. H., Lopez, G., Seidel, S. J., Ewert, F., et al. (2023). Multi-year belowground data of minirhizotron facilities in selhausen. *Scientific Data*, 10(1):672.
- LaRue, T., Lindner, H., Srinivas, A., Exposito-Alonso, M., Lobet, G., and Dinnyen, J. R. (2022). Uncovering natural variation in root system architecture and growth dynamics using a robotics-assisted phenomics platform. *ELIFE*, 11.
- Le, S., Josse, J., and Husson, F. (2008). Factominer: An r package for multivariate analysis. *Journal of Statistical Software*, 25(1):1–18.
- LeCun, Y., Bengio, Y., and Hinton, G. (2015). Deep learning. *Nature*, 521(7553):436–444.
- Leitner, D., Felderer, B., Vontobel, P., and Schnepf, A. (2013a). Recovering Root System Traits Using Image Analysis Exemplified by Two-Dimensional Neutron Radiography Images of Lupine. *Plant Physiology*, 164(1):24–35.
- Leitner, D., Felderer, B., Vontobel, P., and Schnepf, A. (2013b). Recovering root system traits using image analysis exemplified by two-dimensional neutron radiography images of lupine . *Plant Physiology*, 164(1):24–35.
- Li, L., Zhang, Q., and Huang, D. (2014). A review of imaging techniques for plant phenotyping. *Sensors*, 14(11):20078–20111.
- Li, Y., Sperry, J. S., and Shao, M. (2009). Hydraulic conductance and vulnerability to cavitation in corn (*zea mays* l.) hybrids of differing drought resistance. *Environmental and Experimental Botany*, 66(2):341–346.
- Liedgens, M. and Richner, W. (2001). Minirhizotron observations of the spatial distribution of the maize root system. *Agronomy Journal*, 93:1097–1104.
- Lin, L., He, Y., and Chen, J. (2016). The influence of soil drying- and tillage-induced penetration resistance on maize root growth in a clayey soil. *Journal of Integrative Agriculture*, 15:1112–1120.

- Lindenmayer, A. (1968). Mathematical models for cellular interactions in development i. filaments with one-sided inputs. *Journal of Theoretical Biology*, 18(3):280–299.
- Lizbeth Lopez-Arredondo, D., Antonio Leyva-Gonzalez, M., Isabel Gonzalez-Morales, S., Lopez-Bucio, J., and Herrera-Estrella, L. (2014). Phosphate nutrition: Improving low-phosphate tolerance in crops. In Merchant, S., editor, *Annual Review of Plant Biology*, volume 65 of *Annual Review of Plant Biology*, pages 95–123. Annual Reviews.
- Lobet, G., Draye, X., and Périlleux, C. (2013). An online database for plant image analysis software tools. *Plant Methods*, 9(1):1–8.
- Lobet, G., Pagès, L., and Draye, X. (2014). A modeling approach to determine the importance of dynamic regulation of plant hydraulic conductivities on the water uptake dynamics in the soil-plant-atmosphere system. *Ecological Modelling*, 290:65–75.
- Lobet, G., Pagès, L., and Draye, X. (2011). A Novel Image-Analysis Toolbox Enabling Quantitative Analysis of Root System Architecture. *Plant Physiology*, 157(1):29–39.
- Lobet, G., Pound, M. P., Diener, J., Pradal, C., Draye, X., Godin, C., Javaux, M., Leitner, D., Meunier, F., Nacry, P., Pridmore, T. P., and Schnepf, A. (2015). Root System Markup Language: Toward a Unified Root Architecture Description Language. *Plant Physiology*, 167(3):617–627.
- Lopez, G., Ahmadi, S. H., Amelung, W., Athmann, M., Ewert, F., Gaiser, T., Gocke, M. I., Kautz, T., Postma, J., Rachmilevitch, S., Schaaf, G., Schnepf, A., Stoschus, A., Watt, M., Yu, P., and Seidel, S. J. (2023). Nutrient deficiency effects on root architecture and root-to-shoot ratio in arable crops. *Frontiers in Plant Science*, 13.
- Louarn, G. and Song, Y. (2020). Two decades of functional–structural plant modelling: now addressing fundamental questions in systems biology and predictive ecology. *Annals of Botany*, 126:501–509.
- Ludbrook, J. (1997). Comparing methods of measurement. *Clinical and Experimental Pharmacology and Physiology*, 24(2):198–203.
- Lynch, J. P. (2007). Roots of the second green revolution. *Australian Journal of Botany*, 55(5):493.
- Lynch, J. P. (2011). Root Phenotypes for Enhanced Soil Exploration and Phosphorus Acquisition: Tools for Future Crops. *Plant Physiology*, 156(3):1041–1049.
- Lynch, J. P. (2013). Steep, cheap and deep: an ideotype to optimize water and n acquisition by maize root systems. *Annals of Botany*, 112(2):347–357.
- Lynch, J. P. (2019). Root phenotypes for improved nutrient capture: an under-exploited opportunity for global agriculture. *New Phytologist*, 223(2):548–564.

- Lynch, J. P., Galindo-Castaneda, T., Schneider, H. M., Sidhu, J. S., Rangarajan, H., and York, L. M. (2023). Root phenotypes for improved nitrogen capture. *Plant and Soil*.
- Lynch, J. P., Ho, M. D., and Phosphorus, L. (2005). Rhizoeconomics: carbon costs of phosphorus acquisition. *Plant and soil*, 269:45–56.
- Lynch, J. P., Nielsen, K. L., Davis, R. D., and Jablokow, A. G. (1997). Simroot: Modelling and visualization of root systems. *Plant and Soil*, 188(1):139–151.
- Lärm, L., Bauer, F., Hermes, N., van der Kruk, J., Vereecken, H., Vanderborght, J., Nguyen, T. H., Lopez, G., Seidel, S. J., Ewert, F., Schnepf, A., and Klotzsche, A. (2023a). Multi-year belowground data of minirhizotron facilities in selhausen: Additional information. *TERENO Database*.
- Lärm, L., Bauer, F., Hermes, N., van der Kruk, J., Vereecken, H., Vanderborght, J., Nguyen, T. H., Lopez, G., Seidel, S. J., Ewert, F., Schnepf, A., and Klotzsche, A. (2023b). Multi-year belowground data of minirhizotron facilities in selhausen: Gpr data. *TERENO Database*.
- Lärm, L., Bauer, F., Hermes, N., van der Kruk, J., Vereecken, H., Vanderborght, J., Nguyen, T. H., Lopez, G., Seidel, S. J., Ewert, F., Schnepf, A., and Klotzsche, A. (2023c). Multi-year belowground data of minirhizotron facilities in selhausen: Root data. *TERENO Database*.
- Lärm, L., Bauer, F., Hermes, N., van der Kruk, J., Vereecken, H., Vanderborght, J., Nguyen, T. H., Lopez, G., Seidel, S. J., Ewert, F., Schnepf, A., and Klotzsche, A. (2023d). Multi-year belowground data of minirhizotron facilities in selhausen: Root images. *TERENO Database*.
- Lärm, L., Bauer, F., Hermes, N., van der Kruk, J., Vereecken, H., Vanderborght, J., Nguyen, T. H., Lopez, G., Seidel, S. J., Ewert, F., Schnepf, A., and Klotzsche, A. (2023e). Multi-year belowground data of minirhizotron facilities in selhausen: Soil sensor data. *TERENO Database*.
- Lärm, L., Bauer, F. M., van der Kruk, J., Vanderborght, J., Morandage, S., Vereecken, H., Schnepf, A., and Klotzsche, A. (2024). Linking horizontal cross-hole gpr variability with root image information for maize crops. *Vadose Zone Journal*, 23(1):e20293.
- Mai, T. H., Schnepf, A., Vereecken, H., and Vanderborght, J. (2019). Continuum multiscale model of root water and nutrient uptake from soil with explicit consideration of the 3d root architecture and the rhizosphere gradients. *Plant and Soil*, 439(1-2, SI):273–292.
- Marschner, H. (2011). *Marschner's mineral nutrition of higher plants*. Academic press.
- Mercado, J. A. V. and Engel, B. A. (2021). Multi-scale analysis of the dependence of water quality on land use using linear and mixed models. *Water*, 13:2618.

- Meunier, F., Couvreur, V., Draye, X., Lobet, G., Huber, K., Schroeder, N., Jorda, H., Koch, A., Landl, M., Schnepf, A., Vanderborght, J., Vereecken, H., and Javaux, M. (2022). *Investigating Soil–Root Interactions with the Numerical Model R-SWMS*, pages 259–283. Springer New York, New York, NY.
- Meunier, F., Draye, X., Vanderborght, J., Javaux, M., and Couvreur, V. (2017). A hybrid analytical-numerical method for solving water flow equations in root hydraulic architectures. *Applied Mathematical Modelling*, 52:648–663.
- Meunier, F., Heymans, A., Draye, X., Couvreur, V., Javaux, M., and Lobet, G. (2020). Marshal, a novel tool for virtual phenotyping of maize root system hydraulic architectures. *in silico Plants*, 2(1):diz012.
- Meunier, F., Zarebanadkouki, M., Ahmed, M. A., Carminati, A., Couvreur, V., and Javaux, M. (2018). Hydraulic conductivity of soil-grown lupine and maize unbranched roots and maize root-shoot junctions. *Journal of Plant Physiology*, 227:31–44.
- Michels, V., Chou, C., Weigand, M., Wu, Y., and Kemna, A. (2024). Quantitative phenotyping of crop roots with spectral electrical impedance tomography: a rhizotron study with optimized measurement design. *Plant Methods*, 20(1).
- Minervini, M., Scharr, H., and Tsiftaris, S. A. (2015). Image analysis: the new bottleneck in plant phenotyping. *IEEE signal processing magazine*, 32(4):126–131.
- Möller, B., Chen, H., Schmidt, T., Zieschank, A., Patzak, R., Türke, M., Weigelt, A., and Posch, S. (2019). rhizotrak: A flexible open source fiji plugin for user-friendly manual annotation of time-series images from minirhizotrons. *Plant and Soil*, 444(1):519–534.
- Morandage, S. (2020). *Characterization of Root System Architectures from Field Root Sampling Methods*. PhD thesis, Rheinische Friedrich-Wilhelms-Universität Bonn.
- Morandage, S., Schnepf, A., Leitner, D., Javaux, M., Vereecken, H., and Vanderborght, J. (2019). Parameter sensitivity analysis of a root system architecture model based on virtual field sampling. *Plant and Soil*, 438(1-2):101–126.
- Morandage, S., Vanderborght, J., Zörner, M., Cai, G., Leitner, D., Vereecken, H., and Schnepf, A. (2021). Root architecture development in stony soils. *Vadose Zone Journal*, 20(4).
- Mu, Z., Zhang, S., Zhang, L., Liang, A., and Liang, Z. (2006). Hydraulic conductivity of whole root system is better than hydraulic conductivity of single root in correlation with the leaf water status of maize. *Botanical Studies*, 47(2):145–151.
- Murphy, S. L. and Smucker, A. J. M. (1995). Evaluation of video image analysis and line-intercept methods for measuring root systems of alfalfa and ryegrass. *Agronomy Journal*, 87(5):865–868.

- Müller, H.-W., Dohrmann, R., Klosa, D., Rehder, S., and Eckelmann, W. (2009). Comparison of two procedures for particle-size analysis: Köhn pipette and x-ray granulometry. *Journal of Plant Nutrition and Soil Science*, 172(2):172–179.
- Nagel, K. A., Putz, A., Gilmer, F., Heinz, K., Fischbach, A., Pfeifer, J., Faget, M., Blossfeld, S., Ernst, M., Dimaki, C., et al. (2012). Growscreen-rhizo is a novel phenotyping robot enabling simultaneous measurements of root and shoot growth for plants grown in soil-filled rhizotrons. *Functional Plant Biology*, 39(11):891–904.
- Nair, R., Strube, M., Hertel, M., Kolle, O., Rolo, V., and Migliavacca, M. (2023). High frequency root dynamics: sampling and interpretation using replicated robotic minirhizotrons. *Journal of Experimental Botany*, 74(3):769–786.
- Narisetti, N., Henke, M., Seiler, C., Junker, A., Ostermann, J., Altmann, T., and Gladilin, E. (2021). Fully-automated root image analysis (faRIA). *Scientific Reports*, 11(1).
- Nguyen, T. H., Gaiser, T., Vanderborcht, J., Schnepf, A., Bauer, F. M., Klotzsche, A., Lärm, L., Hüging, H., and Ewert, F. (2024a). Responses of field-grown maize to different soil types, water regimes, and contrasting vapor pressure deficit. *Biogeoscience*. Preprint.
- Nguyen, T. H., Langensiepen, M., Gaiser, T., Webber, H., Ahrends, H., Hueging, H., and Ewert, F. (2022a). Responses of winter wheat and maize to varying soil moisture: From leaf to canopy. *Agricultural and Forest Meteorology*, 314.
- Nguyen, T. H., Langensiepen, M., Hueging, H., Gaiser, T., Seidel, S. J., and Ewert, F. (2022b). Expansion and evaluation of two coupled root–shoot models in simulating co₂ and h₂o fluxes and growth of maize. *Vadose Zone Journal*, 21(3).
- Nguyen, T. H., Langensiepen, M., Vanderborcht, J., Hüging, H., Mboh, C. M., and Ewert, F. (2020). Comparison of root water uptake models in simulating co₂ and h₂o fluxes and growth of wheat. *Hydrology and Earth System Sciences*, 24(10):4943–4969.
- Nguyen, T. H., Lopez, G., Seidel, S. J., Lärm, L., Bauer, F. M., Klotzsche, A., Schnepf, A., Gaiser, T., Hüging, H., and Ewert, F. (2024b). Multi-year aboveground data of minirhizotron facilities in selhausen. *Scientific Data*, 10(1).
- Niu, X., Hu, T., Zhang, F., and Feng, P. (2016). Severity and duration of osmotic stress on partial root system: effects on root hydraulic conductance and root growth. *Plant Growth Regulation*, 79(2):177–186.
- Niu, Y. F., Chai, R. S., Jin, G. L., Wang, H., Tang, C. X., and Zhang, Y. S. (2013). Responses of root architecture development to low phosphorus availability: a review. *Annals of Botany*, 112(2):391–408.

- Ordóñez, R. A., Castellano, M. J., Hatfield, J. L., Helmers, M. J., Licht, M. A., Liebman, M., Dietzel, R., Martinez-Feria, R., Iqbal, J., Puntel, L. A., Córdova, S., Togliatti, K., Wright, E. E., and Archontoulis, S. V. (2018). Maize and soybean root front velocity and maximum depth in iowa, usa. *Field Crops Research*, 215:122–131.
- Pandey, R., Maranville, J., and Chetima, M. M. (2000). Deficit irrigation and nitrogen effects on maize in a sahelian environment: Ii. shoot growth, nitrogen uptake and water extraction. *Agricultural Water Management*, 46:15–27.
- Parent, B., Hachez, C., Redondo, E., Simonneau, T., Chaumont, F., and Tardieu, F. (2009). Drought and Abscisic Acid Effects on Aquaporin Content Translate into Changes in Hydraulic Conductivity and Leaf Growth Rate: A Trans-Scale Approach. *Plant Physiology*, 149(4):2000–2012.
- Passot, S., Couvreur, V., Meunier, F., Draye, X., Javaux, M., Leitner, D., Pagès, L., Schnepf, A., Vanderborght, J., and Lobet, G. (2019). Connecting the dots between computational tools to analyse soil–root water relations. *Journal of Experimental Botany*, 70(9):2345–2357.
- Paulus, S. (2019). Measuring crops in 3d: using geometry for plant phenotyping. *Plant Methods*, 15(1).
- Pedregosa, F., Varoquaux, G., Gramfort, A., Michel, V., Thirion, B., Grisel, O., Blondel, M., Prettenhofer, P., Weiss, R., Dubourg, V., Vanderplas, J., Passos, A., Cournapeau, D., Brucher, M., Perrot, M., and Duchesnay, E. (2011). Scikit-learn: Machine learning in python. *Journal of Machine Learning Research*, 12:2825–2830.
- Pereira, S., Abreu, D., Moreira, H., Vega, A., and Castro, P. (2020). Plant growth-promoting rhizobacteria (pgpr) improve the growth and nutrient use efficiency in maize (*zea mays* l.) under water deficit conditions. *Heliyon*, 6(10):e05106.
- Perkins, A. C. and Lynch, J. P. (2021). Increased seminal root number associated with domestication improves nitrogen and phosphorus acquisition in maize seedlings. *Annals of Botany*, 128(4):453–468.
- Peters, B., Blume-Werry, G., Gillert, A., Schwieger, S., von Lukas, U. F., and Kreyling, J. (2023). As good as human experts in detecting plant roots in minirhizotron images but efficient and reproducible: the convolutional neural network “rootdetector”. *Scientific Reports*, 13(1).
- Pfeifer, J., Faget, M., Walter, A., Blossfeld, S., Fiorani, F., Schurr, U., and Nagel, K. A. (2014). Spring barley shows dynamic compensatory root and shoot growth responses when exposed to localised soil compaction and fertilisation. *Functional Plant Biology*, 41(6):581–597.
- Pierret, A., Gonkhamdee, S., Jourdan, C., and Maeght, J.-L. (2013). IJ_rhizo: an open-source software to measure scanned images of root samples. *Plant and Soil*, 373(1-2):531–539.

- Plénet, D., Mollier, A., and Pellerin, S. (2000). Growth analysis of maize field crops under phosphorus deficiency. ii. radiation-use efficiency, biomass accumulation and yield components. *Plant and Soil*, 224(2):259–272.
- Plénet, D., Etchebest, S., Mollier, A., and Pellerin, S. (2000). Growth analysis of maize field crops under phosphorus deficiency. *Plant and Soil*, 223(1-2):119–132.
- Postma, J. A., Dathe, A., and Lynch, J. P. (2014). The Optimal Lateral Root Branching Density for Maize Depends on Nitrogen and Phosphorus Availability. *Plant Physiology*, 166(2):590–602.
- Postma, J. A., Kuppe, C., Owen, M. R., Mellor, N., Griffiths, M., Bennett, M. J., Lynch, J. P., and Watt, M. (2017). Opensimroot: widening the scope and application of root architectural models. *New Phytologist*, 215(3):1274–1286.
- Postma, J. A. and Lynch, J. P. (2011). Root Cortical Aerenchyma Enhances the Growth of Maize on Soils with Suboptimal Availability of Nitrogen, Phosphorus, and Potassium. *Plant Physiology*, 156(3):1190–1201.
- Pound, M. P., Atkinson, J. A., Townsend, A. J., Wilson, M. H., Griffiths, M., Jackson, A. S., Bulat, A., Tzimiropoulos, G., Wells, D. M., Murchie, E. H., Pridmore, T. P., and French, A. P. (2017). Deep machine learning provides state-of-the-art performance in image-based plant phenotyping. *GigaScience*, 6(10).
- Pritchard, S. G., Strand, A. E., McCormack, M. L., Davis, M. A., and Oren, R. (2008). Mycorrhizal and rhizomorph dynamics in a loblolly pine forest during 5 years of free-air-co₂-enrichment. *Global Change Biology*, 14(6):1252–1264.
- Proctor, J., Rigden, A., Chan, D., and Huybers, P. (2022). More accurate specification of water supply shows its importance for global crop production. *Nature Food*, 3(9):753–763.
- Prusinkiewicz, P. and Lindenmayer, A. (1990). *The algorithmic beauty of plants*. Springer Science & Business Media.
- Punyasu, N., Thaiprasit, J., Kalapanulak, S., Saithong, T., and Postma, J. A. (2024). Modeling cassava root system architecture and the underlying dynamics in shoot-root carbon allocation during the early storage root bulking stage. *Plant and Soil*.
- Pütz, T., Kiese, R., Wollschläger, U., Groh, J., Rupp, H., Zacharias, S., Priesack, E., Gerke, H. H., Gasche, R., Bens, O., Borg, E., Baessler, C., Kaiser, K., Herbrich, M., Munch, J.-C., Sommer, M., Vogel, H.-J., Vanderborght, J., and Vereecken, H. (2016). TERENO-SOILCan: a lysimeter-network in germany observing soil processes and plant diversity influenced by climate change. *Environmental Earth Sciences*, 75(18).

- Qian, L., Huang, T., Zeng, W., Chen, X., and Wang, X. (2023). Determining the dynamic responses of cotton root morphological characteristics under waterlogging stress using the minirhizotron technique. *Irrigation and Drainage*, 72(1):60–74.
- Qiao, S., Fang, Y., Wu, A., Xu, B., Zhang, S., Deng, X., Djalovic, I., Siddique, K. H. M., and Chen, Y. (2019). Dissecting root trait variability in maize genotypes using the semi-hydroponic phenotyping platform. *Plant and Soil*, 439(1-2, SI):75–90.
- Rajurkar, A. B., McCoy, S. M., Ruhter, J., Mulcrone, J., Freyfogle, L., and Leakey, A. D. B. (2022). Installation and imaging of thousands of minirhizotrons to phenotype root systems of field-grown plants. *Plant Methods*, 18(1).
- Randall, J. R. (2003). Watershed abatement costs for agricultural phosphorus. *Water Resources Research*, 39.
- Ranum, P., Peña-Rosas, J. P., and Garcia-Casal, M. N. (2014). Global maize production, utilization, and consumption. *Annals of the New York Academy of Sciences*, 1312(1):105–112.
- Rasmussen, C. R., Thorup-Kristensen, K., and Dresbøll, D. B. (2020). Uptake of subsoil water below 2 m fails to alleviate drought response in deep-rooted chicory (*cichorium intybus* l.). *Plant and Soil*, 446:275–290.
- Ray, D. K., Mueller, N. D., West, P. C., and Foley, J. A. (2013). Yield trends are insufficient to double global crop production by 2050. *PLOS ONE*, 8(6):1–8.
- Reidinger, R. B. (1976). World fertilizer review and prospects to 1980/81. *Foreign Agricultural Economic Report*, 115.
- Reijnders, L. (2014). Phosphorus resources, their depletion and conservation, a review. *Resources, Conservation and Recycling*, 93:32–49.
- Ribaut, J.-M., Betran, J., Monneveux, P., and Setter, T. (2009). *Drought Tolerance in Maize*, pages 311–344. Springer New York, New York, NY.
- Richardson, K., Steffen, W., Lucht, W., Bendtsen, J., Cornell, S. E., Donges, J. F., Drüke, M., Fetzer, I., Bala, G., von Bloh, W., Feulner, G., Fiedler, S., Gerten, D., Gleeson, T., Hofmann, M., Huiskamp, W., Kummu, M., Mohan, C., Nogués-Bravo, D., Petri, S., Porkka, M., Rahmstorf, S., Schaphoff, S., Thonicke, K., Tobian, A., Virkki, V., Wang-Erlandsson, L., Weber, L., and Rockström, J. (2023). Earth beyond six of nine planetary boundaries. *Science Advances*, 9(37):eadh2458.
- Riedell, W. (2010). Mineral-nutrient synergism and dilution responses to nitrogen fertilizer in field-grown maize. *Journal of Plant Nutrition and Soil Science*, 173:869–874.

- Rishmawi, L., Bauget, F., Protto, V., Bauland, C., Nacry, P., and Maurel, C. (2023). Natural variation of maize root hydraulic architecture underlies highly diverse water uptake capacities. *Plant Physiology*, 192(3):2404–2418.
- Robinson, D. A., Jones, S. B., Blonquist, J. M., and Friedman, S. P. (2005). A physically derived water content/permittivity calibration model for coarse-textured, layered soils. *Soil Science Society of America Journal*, 69(5):1372–1378.
- Ronneberger, O., Fischer, P., and Brox, T. (2015). U-net: Convolutional networks for biomedical image segmentation. In Navab, N., Hornegger, J., Wells, W. M., and Frangi, A. F., editors, *Medical Image Computing and Computer-Assisted Intervention – MICCAI 2015*, pages 234–241, Cham. Springer International Publishing.
- Saengwilai, P., Strock, C., Rangarajan, H., Chimungu, J., Salungyu, J., and Lynch, J. P. (2021). Root hair phenotypes influence nitrogen acquisition in maize. *Annals of Botany*, 128(7):849–858.
- Saengwilai, P., Tian, X., and Lynch, J. P. (2014). Low Crown Root Number Enhances Nitrogen Acquisition from Low-Nitrogen Soils in Maize. *Plant Physiology*, 166(2):581–589.
- Salman, S. and Liu, X. (2019). Overfitting mechanism and avoidance in deep neural networks. *CoRR*, abs/1901.06566.
- Santos, L., Santos, F. N., Oliveira, P. M., and Shinde, P. (2020). Deep learning applications in agriculture: A short review. In Silva, M. F., Luís Lima, J., Reis, L. P., Sanfeliu, A., and Tardioli, D., editors, *Robot 2019: Fourth Iberian Robotics Conference*, pages 139–151, Cham. Springer International Publishing.
- Schaal, B. (2019). Plants and people: Our shared history and future. *Plants, People, Planet*, 1(1):14–19.
- Schaap, M. G., Leij, F. J., and van Genuchten, M. T. (2001). rosetta: a computer program for estimating soil hydraulic parameters with hierarchical pedotransfer functions. *Journal of Hydrology*, 251(3):163–176.
- Schellberg, J. and Hüging, H. (1997). Die entwicklung der erträge von getreide, hackfrüchten und klee im dauerdüngungsversuch dikopshof von 1906 bis 1996. *Archives of Agronomy and Soil Science*, 42(3-4):303–318.
- Schindler, U., Durner, W., von Unold, G., and Müller, L. (2010). Evaporation method for measuring unsaturated hydraulic properties of soils: Extending the measurement range. *Soil Science Society of America Journal*, 74(4):1071–1083.
- Schneider, H. M., Yang, J. T., Brown, K. M., and Lynch, J. P. (2021). Nodal root diameter and node number in maize (*zea mays* l.) interact to influence plant growth under nitrogen stress. *Plant Direct*, 5(3):e00310.

- Schnepf, A., Black, C. K., Couvreur, V., Delory, B. M., Doussan, C., Heymans, A., Javaux, M., Khare, D., Koch, A., Koch, T., Kuppe, C. W., Landl, M., Leitner, D., Lobet, G., Meunier, F., Postma, J. A., Schäfer, E. D., Selzner, T., Vanderborght, J., and Vereecken, H. (2023). Collaborative benchmarking of functional-structural root architecture models: Quantitative comparison of simulated root water uptake. *in silico Plants*, 5(1):diad005.
- Schnepf, A., Carminati, A., Ahmed, M. A., Ani, M., Benard, P., Bentz, J., Bonkowski, M., Knott, M., Diehl, D., Duddek, P., Kröner, E., Javaux, M., Landl, M., Lehndorff, E., Lippold, E., Lieu, A., Mueller, C. W., Oburger, E., Otten, W., Portell, X., Phalempin, M., Prechtel, A., Schulz, R., Vanderborght, J., and Vetterlein, D. (2022a). Linking rhizosphere processes across scales: Opinion. *Plant and Soil*.
- Schnepf, A., Leitner, D., Bodner, G., and Javaux, M. (2022b). Editorial: Benchmarking 3d-models of root growth, architecture and functioning. *Frontiers in Plant Science*, 13.
- Schnepf, A., Leitner, D., Landl, M., Lobet, G., Mai, T. H., Morandage, S., Sheng, C., Zörner, M., Vanderborght, J., and Vereecken, H. (2018). Crootbox: a structural-functional modelling framework for root systems. *Annals of Botany*, 121(5):1033–1053.
- Schüller, H. (1969). Die cal-methode, eine neue methode zur bestimmung des pflanzenverfügbaren phosphates in böden. *Zeitschrift für Pflanzenernährung und Bodenkunde*, 123(1):48–63.
- Seethepalli, A., Dhakal, K., Griffiths, M., Guo, H., Freschet, G. T., and York, L. M. (2021). RhizoVision Explorer: open-source software for root image analysis and measurement standardization. *AoB PLANTS*, 13(6):plab056.
- Seethepalli, A., Ottley, C., Childs, J., Cope, K., Fine, A. K., Lagergren, J., Iversen, C. M., Kalluri, U., and York, L. M. (2024). Divide and conquer: Using rhizovision explorer to aggregate data from multiple root scans using image concatenation and statistical methods. *bioRxiv*. Preprint.
- Seethepalli, A. and York, L. M. (2020). Rhizovision explorer - interactive software for generalized root image analysis designed for everyone.
- Seidel, S. J., Gaiser, T., Srivastava, A. K., Leitner, D., Schmittmann, O., Athmann, M., Kautz, T., Guigue, J., Ewert, F., and Schnepf, A. (2022). Simulating root growth as a function of soil strength and yield with a field-scale crop model coupled with a 3d architectural root model. *Frontiers in Plant Science*, 13.
- Selzner, T., Horn, J., Landl, M., Pohlmeier, A., Helmrich, D., Huber, K., Vanderborght, J., Vereecken, H., Behnke, S., and Schnepf, A. (2023). 3d u-net segmentation improves root system reconstruction from 3d mri images in automated and manual virtual reality work flows. *Plant Phenomics*, 5:0076.

- Shalhevet, J., Huck, M. G., and Schroeder, B. P. (1995). Root and shoot growth responses to salinity in maize and soybean. *Agronomy Journal*, 87:512–516.
- Shangguan, Z.-P., Lei, T.-W., Shao, M.-A., and Xue, Q.-W. (2005). Effects of phosphorus nutrient on the hydraulic conductivity of sorghum (*sorghum vulgare pers.*) seedling roots under water deficiency. *Journal of Integrative Plant Biology*, 47(4):421–427.
- Shen, C., Liu, L., Zhu, L., Kang, J., Wang, N., and Shao, L. (2020). High-throughput in situ root image segmentation based on the improved DeepLabv3+ method. *Frontiers in Plant Science*, 11.
- Sheng, M., Lalande, R., Hamel, C., Ziadi, N., and Shi, Y. (2012). Growth of corn roots and associated arbuscular mycorrhizae are affected by long-term tillage and phosphorus fertilization. *Agronomy Journal*, 104(6):1672–1678.
- Silva, D. D. and Beeson, R. C. (2011). A large-volume rhizotron for evaluating root growth under natural-like soil moisture conditions. *HortScience*, 46(12):1677 – 1682.
- Smith, A. G., Han, E., Petersen, J., Olsen, N. A. F., Giese, C., Athmann, M., Dresbøll, D. B., and Thorup-Kristensen, K. (2020a). Rootpainter: deep learning segmentation of biological images with corrective annotation. *Bioarxiv*.
- Smith, A. G., Han, E., Petersen, J., Olsen, N. A. F., Giese, C., Athmann, M., Dresbøll, D. B., and Thorup-Kristensen, K. (2022). Rootpainter: deep learning segmentation of biological images with corrective annotation. *New Phytologist*, 236(2):774–791.
- Smith, A. G., Malinowska, M., Janss, L., Ruud, A. K., Krusell, L., Jensen, J. D., and Asp, T. (2024). Automated seminal root angle measurement with corrective annotation. *bioRxiv*. Preprint.
- Smith, A. G., Petersen, J., Selvan, R., and Rasmussen, C. R. (2020b). Segmentation of roots in soil with u-net. *Plant Methods*, 16(1).
- Smith, L. N. (2018). A disciplined approach to neural network hyper-parameters: Part 1—learning rate, batch size, momentum, and weight decay. *arXiv preprint arXiv:1803.09820*.
- Solaimalai, A., Anantharaju, P., Irulandi, S., and Theradimani, M. (2020). 6. growth and development stages. In *Maize Crop: Improvement, Production, Protection and Post Harvest Technology*, chapter 6. CRC Press.
- Solimani, F., Cardellicchio, A., Nitti, M., Lako, A., Dimauro, G., and Reno, V. (2023). A systematic review of effective hardware and software factors affecting high-throughput plant phenotyping. *Information*, 14(4).
- Song, P., Wang, J., Guo, X., Yang, W., and Zhao, C. (2021). High-throughput phenotyping: Breaking through the bottleneck in future crop breeding. *The Crop Journal*, 9(3):633–645.

- Srivastav, A., Dhyani, R., Ranjan, M., Madhav, S., and Sillanpää, M. (2021). Climate-resilient strategies for sustainable management of water resources and agriculture. *Environmental Science and Pollution Research*, 28:41576 – 41595.
- Steelman, C. M. and Endres, A. L. (2011). Comparison of petrophysical relationships for soil moisture estimation using gpr ground waves. *Zone Journal*, 10(1):270–285.
- Steudle, E. (2001). Water uptake by plant roots: an integration of views. *Recent Advances of Plant Root Structure and Function*, pages 71–82.
- Sun, B., Gao, Y., and Lynch, J. P. (2018). Large Crown Root Number Improves Topsoil Foraging and Phosphorus Acquisition. *Plant Physiology*, 177(1):90–104.
- Svane, S. F., Jensen, C. S., and Thorup-Kristensen, K. (2019). Construction of a large-scale semi-field facility to study genotypic differences in deep root growth and resources acquisition. *Plant Methods*, 15(1).
- Tanno, K. and Willcox, G. (2006). How fast was wild wheat domesticated? *Science*, 311:1886 – 1886.
- Taylor, H., Upchurch, D., and McMichael, B. (1990). Applications and limitations of rhizotrons and minirhizotrons for root studies. *Plant and Soil*, 129:29–35.
- Thorup-Kristensen, K., Halberg, N., Nicolaisen, M. H., Olesen, J. E., and Dresbøll, D. B. (2020). Exposing deep roots: A rhizobox laboratory. *Trends in Plant Science*, 25(4):418–419.
- Topp, G. C., Davis, J. L., and Annan, A. P. (1980). Electromagnetic determination of soil water content: Measurements in coaxial transmission lines. *Water Resources Research*, 16(3):574–582.
- Trachsel, S., Kaeppler, S., Brown, K., and Lynch, J. (2013). Maize root growth angles become steeper under low n conditions. *Field Crops Research*, 140:18–31.
- Tyree, M. T., Yang, S., Cruiziat, P., and Sinclair, B. (1994). Novel methods of measuring hydraulic conductivity of tree root systems and interpretation using amaized (a maize-root dynamic model for water and solute transport). *Plant Physiology*, 104(1):189–199.
- Ubbens, J. R. and Stavness, I. (2017). Deep plant phenomics: a deep learning platform for complex plant phenotyping tasks. *Frontiers in Plant Science*, 8.
- UN (2023). Global sustainable development report 2023: Times of crisis, times of change: Science for accelerating transformations to sustainable development. *United Nations*.
- Vadas, P., Busch, D., Powell, J. M., and Brink, G. E. (2015). Monitoring runoff from cattle-grazed pastures for a phosphorus loss quantification tool. *Agriculture, Ecosystems & Environment*, 199:124–131.

- Vamerali, T., Bandiera, M., and Mosca, G. (2011). Minirhizotrons in modern root studies. In *Measuring Roots*, pages 341–361. Springer Berlin Heidelberg.
- Vamerali, T., Bandiera, M., and Mosca, G. (2012). *Minirhizotrons in Modern Root Studies*, pages 341–361. Springer Berlin Heidelberg, Berlin, Heidelberg.
- Van de Geijn, S., Vos, J., Groenwold, J., Goudriaan, J., and Leffelaar, P. (1994). The wageningen rhizolab—a facility to study soil-root-shoot-atmosphere interactions in crops: I. description of main functions. *Plant and Soil*, 161:275–287.
- Van Genuchten, M. T. (1980). A closed-form equation for predicting the hydraulic conductivity of unsaturated soils. *Soil Science Society of America Journal*, 44(5):892–898.
- Vanderborght, J., Leitner, D., Schnepf, A., Couvreur, V., Vereecken, H., and Javaux, M. (2024). Combining root and soil hydraulics in macroscopic representations of root water uptake. *Vadose Zone Journal*, 23(3):e20273.
- Vargas Zeppetello, L. R., Trevino, A. M., and Huybers, P. (2024). Disentangling contributions to past and future trends in us surface soil moisture. *Nature Water*, 2(2):127–138.
- Vereecken, H., Schnepf, A., Hopmans, J., Javaux, M., Or, D., Roose, T., Vanderborght, J., Young, M., Amelung, W., Aitkenhead, M., Allison, S., Assouline, S., Baveye, P., Berli, M., Brüggemann, N., Finke, P., Flury, M., Gaiser, T., Govers, G., Ghezzehei, T., Hallett, P., Franssen, H. H., Heppell, J., Horn, R., Huisman, J., Jacques, D., Jonard, F., Kollet, S., Lafolie, F., Lamorski, K., Leitner, D., McBratney, A., Minasny, B., Montzka, C., Nowak, W., Pachepsky, Y., Padarian, J., Romano, N., Roth, K., Rothfuss, Y., Rowe, E., Schwen, A., Šimůnek, J., Tiktak, A., Dam, J. V., van der Zee, S., Vogel, H., Vrugt, J., Wöhling, T., and Young, I. (2016). Modeling soil processes: Review, key challenges, and new perspectives. *Vadose Zone Journal*, 15(5).
- Virtanen, P., Gommers, R., Oliphant, T. E., Haberland, M., Reddy, T., Cournapeau, D., Burovski, E., Peterson, P., Weckesser, W., Bright, J., van der Walt, S. J., Brett, M., Wilson, J., Millman, K. J., Mayorov, N., Nelson, A. R. J., Jones, E., Kern, R., Larson, E., Carey, C. J., Polat, I., Feng, Y., Moore, E. W., VanderPlas, J., Laxalde, D., Perktold, J., Cimrman, R., Henriksen, I., Quintero, E. A., Harris, C. R., Archibald, A. M., Ribeiro, A. H., Pedregosa, F., van Mulbregt, P., and Contributors, S. . . (2020). Scipy 1.0: fundamental algorithms for scientific computing in python. *Nature Methods*, 17(3):261–272.
- von Arx, G. and Carrer, M. (2014). Roxas – a new tool to build centuries-long tracheid-lumen chronologies in conifers. *Dendrochronologia*, 32(3):290–293.
- Vos, J., Evers, J. B., Buck-Sorlin, G., Andrieu, B., Chelle, M., and Visser, P. d. (2009). Functional–structural plant modelling: A new versatile tool in crop science. *Journal of Experimental Botany*.

- Vos, J., Marcelis, L., and Evers, J. (2007). Functional-structural plant modelling in crop production. In *Functional-structural plant modelling in crop production*, pages 1–12. Springer.
- Wacker, T. S., Popovic, O., Olsen, N. A. F., Markussen, B., Smith, A. G., Svane, S. F., and Thorup-Kristensen, K. (2022). Semifield root phenotyping: Root traits for deep nitrate uptake. *Plant, Cell & Environment*, 45(3):823–836.
- Wagena, M. B. and Easton, Z. M. (2018). Agricultural conservation practices can help mitigate the impact of climate change. *Science of The Total Environment*, 635:132–143.
- Wang, M., White, N., Hanan, J., He, D., Wang, E., Cribb, B., Kriticos, D., Paini, D., and Grimm, V. (2020). Parameter estimation for functional-structural plant models when data are scarce: using multiple patterns for rejecting unsuitable parameter sets. *Annals of Botany*.
- Wang, T., Rostamza, M., Song, Z., Wang, L., McNickle, G., Iyer-Pascuzzi, A. S., Qiu, Z., and Jin, J. (2019). Segroot: A high throughput segmentation method for root image analysis. *Computers and Electronics in Agriculture*, 162:845–854.
- Wang, Y.-H. and Su, W.-H. (2022). Convolutional neural networks in computer vision for grain crop phenotyping: A review. *Agronomy*, 12(11).
- Wang, Z., Qi, Z., Xue, L., Bukovsky, M., and Helmers, M. (2015). Modeling the impacts of climate change on nitrogen losses and crop yield in a subsurface drained field. *Climatic Change*, 129:323–335.
- Wasson, A. P., Nagel, K. A., Tracy, S., and Watt, M. (2020). Beyond digging: Noninvasive root and rhizosphere phenotyping. *Trends in Plant Science*, 25(1):119–120.
- Watson, K. K. (1966). An instantaneous profile method for determining the hydraulic conductivity of unsaturated porous materials. *Water Resources Research*, 2(4):709–715.
- Watt, M., Fiorani, F., Usadel, B., Rascher, U., Muller, O., and Schurr, U. (2020). Phenotyping: New windows into the plant for breeders. *Annual Review of Plant Biology*, 71:689–712.
- Weigand, M., Zimmermann, E., Michels, V., Huisman, J. A., and Kemna, A. (2022). Design and operation of a long-term monitoring system for spectral electrical impedance tomography (seit). *Geoscientific Instrumentation, Methods and Data Systems*, 11(2):413–433.
- Weihermüller, L., Huisman, J., Hermes, N., Pickel, S., and Vereecken, H. (2013). A new tdr multiplexing system for reliable electrical conductivity and soil water content measurements. *Vadose Zone Journal*, 12(2).

- Weihermüller, L., Huisman, J., Lambot, S., Herbst, M., and Vereecken, H. (2007). Mapping the spatial variation of soil water content at the field scale with different ground penetrating radar techniques. *Journal of Hydrology*, 340(3-4):205–216.
- Weih, B. J., Heuschele, D.-J., Tang, Z., York, L. M., Zhang, Z., and Xu, Z. (2024). The state of the art in root system architecture image analysis using artificial intelligence: A review. *Plant Phenomics*, 6:0178.
- Wen, Z., Li, H., Shen, J., and Rengel, Z. (2017). Maize responds to low shoot p concentration by altering root morphology rather than increasing root exudation. *Plant and Soil*, 416:377–389.
- Wiesler, Appel, Dittert, Ebertseder, Müller, Nätscher, Olfs, Rex, Schweitzer, Stefens, Taube, and Zorn (2018). Phosphordüngung nach bodenuntersuchung und pflanzenbedarf. *VDLUFA*.
- Xu, W., Yu, G., Cui, Y., Gloaguen, R., Zare, A., Bonnette, J., Reyes-Cabrera, J., Rajurkar, A., Rowland, D., Matamala, R., et al. (2022). Prmi: A dataset of minirhizotron images for diverse plant root study. *arXiv preprint arXiv:2201.08002*.
- Yang, W., Feng, H., Zhang, X., Zhang, J., Doonan, J. H., Batchelor, W. D., Xiong, L., and Yan, J. (2020). Crop phenomics and high-throughput phenotyping: past decades, current challenges, and future perspectives. *Molecular Plant*, 13(2):187–214.
- Yasrab, R., Atkinson, J. A., Wells, D. M., French, A. P., Pridmore, T. P., and Pound, M. P. (2019). RootNav 2.0: Deep learning for automatic navigation of complex plant root architectures. *GigaScience*, 8(11).
- York, L., Nord, E., and Lynch, J. P. (2013). Integration of root phenes for soil resource acquisition. *Frontiers in Plant Science*, 4.
- York, L. M. (2021). *Phenotyping Root System Architecture, Anatomy, and Physiology to Understand Soil Foraging*, pages 209–221. Springer International Publishing, Cham.
- Ytting, N. K., Andersen, S. B., and Thorup-Kristensen, K. (2014). Using tube rhizotrons to measure variation in depth penetration rate among modern north-european winter wheat (*triticum aestivum* l.) cultivars. *Euphytica*, 199(1-2):233–245.
- Yu, P., Li, C., Li, M., He, X., Wang, D., Li, H., Marcon, C., Li, Y., Perez-Limón, S., Chen, X., Delgado-Baquerizo, M., Koller, R., Metzner, R., van Dusschoten, D., Pflugfelder, D., Borisjuk, L., Plutenko, I., Mahon, A., Jr., M. F. R., Salvi, S., Akale, A., Abdalla, M., Ahmed, M. A., Bauer, F. M., Schnepf, A., Lobet, G., Heymans, A., Suresh, K., Schreiber, L., McLaughlin, C. M., Li, C., Mayer, M., Schön, C.-C., Bernau, V., von Wirén, N., Sawers, R. J. H., Wang, T., and Hochholdinger, F. (2024). Seedling root system adaptation to water availability during maize domestication and global expansion. *Nature Genetics*, 56(6).

- Yu, Y., Klotzsche, A., Weihermüller, L., Huisman, J. A., Vanderborght, J., Vereecken, H., and der Kruk, J. (2020). Measuring vertical soil water content profiles by combining horizontal borehole and dispersive surface ground penetrating radar data. *Near Surface Geophysics*, 18(3):275–294.
- Zarebanadkouki, M., Meunier, F., Couvreur, V., Cesar, J., Javaux, M., and Carminati, A. (2016). Estimation of the hydraulic conductivities of lupine roots by inverse modelling of high-resolution measurements of root water uptake. *Annals of Botany*, 118(4):853–864.
- Zeng, G., Birchfield, S. T., and Wells, C. E. (2008). Automatic discrimination of fine roots in minirhizotron images. *New Phytologist*.
- Zeng, G., Birchfield, S. T., and Wells, C. E. (2010). Rapid automated detection of roots in minirhizotron images. *Machine Vision and Applications*, 21(3):309–317.
- Zhan, A., Schneider, H., and Lynch, J. (2015). Reduced lateral root branching density improves drought tolerance in maize. *Plant Physiology*, 168:1603 – 1615.
- Zhang, W., Chen, X., Liu, Y., Liu, D., Du, Y.-F., ping Chen, X., and Zou, C. (2018). The role of phosphorus supply in maximizing the leaf area, photosynthetic rate, coordinated to grain yield of summer maize. *Field Crops Research*, 219:113–119.
- Zhang, Y., Yu, P., Peng, Y.-F., Li, X.-X., Chen, F.-J., and Li, C.-J. (2012). Fine root patterning and balanced inorganic phosphorus distribution in the soil indicate distinctive adaptation of maize plants to phosphorus deficiency. *Pedosphere*, 22(6):870–877.
- Zhou, K., Jerszurki, D., Sadka, A., Shlizerman, L., Rachmilevitch, S., and Ephrath, J. (2018). Effects of photoselective netting on root growth and development of young grafted orange trees under semi-arid climate. *Scientia Horticulturae*, 238:272–280.
- Zhou, X.-R., Schnepf, A., Vanderborght, J., Leitner, D., Lacoïnte, A., Vereecken, H., and Lobet, G. (2020). Cplantbox, a whole-plant modelling framework for the simulation of water-and carbon-related processes. *in silico Plants*, 2(1).
- Zhou, X.-R., Schnepf, A., Vanderborght, J., Leitner, D., Vereecken, H., and Lobet, G. (2023). Phloem anatomy restricts root system architecture development: theoretical clues from in silico experiments. *in silico Plants*, 5(2):diad012.
- Zhu, C., Yu, H., Lu, T., Li, Y., Jiang, W., and Li, Q. (2024). Deep learning-based association analysis of root image data and cucumber yield. *Plant Journal*, 118(3):696–716.
- Zhu, J., Kaeppler, S. M., and Lynch, J. P. (2005a). Mapping of qtls for lateral root branching and length in maize (*zea mays* l.) under differential phosphorus supply. *Theoretical and Applied Genetics*, 111:688–695.

- Zhu, J., Kaeppler, S. M., and Lynch, J. P. (2005b). Topsoil foraging and phosphorus acquisition efficiency in maize (*zea mays*). *Functional Plant Biology*, 32(8):749–762.
- Zhu, J. and Lynch, J. P. (2004). The contribution of lateral rooting to phosphorus acquisition efficiency in maize (*zea mays*) seedlings. *Functional Plant Biology*, 31(10):949–958.
- Zhu, J., Mickelson, S. M., Kaeppler, S. M., and Lynch, J. P. (2006). Detection of quantitative trait loci for seminal root traits in maize (*zea mays* l.) seedlings grown under differential phosphorus levels. *Theoretical and Applied Genetics*, 113:1–10.
- Zimmermann, H., Hartmann, K., Schreiber, L., and Steudle, E. (2000). Chemical composition of apoplastic transport barriers in relation to radial hydraulic conductivity of corn roots (*zea mays*). *Planta*, 210(2):302–311.
- Zuo, Q., Jie, F., Zhang, R., and Meng, L. (2004). A generalized function of wheat's root length density distributions. *Vadose Zone Journal*, 3(1):271–277.
- Zwieniecki, M. A., Thompson, M. V., and Holbrook, N. M. (2002). Understanding the hydraulics of porous pipes: tradeoffs between water uptake and root length utilization. *Journal of Plant Growth Regulation*, 21:315–323.

